THE UNIVERSITY
of EDINBURGH

Investigating the role of TREM2 and neuroinflammation in an experimental model of chronic cerebral hypoperfusion

THE UNIVERSITY *of* EDINBURGH

Stefan Robert Szymkowiak Bsc (Hons)

Doctor of Philosophy

University of Edinburgh, 2019

Contents

Acknowledgements

First and foremost I have to thank **Liz Rowley** for persuading me to pursue a career in science 10 years ago. If it wasn't for you I wouldn't be here so I cannot thank you enough.

I would also like to say a massive thank you to my supervisors **Dr. Barry McColl** and **Professor Karen Horsburgh** for their guidance and direction throughout this project. I've learnt and gained so much experience (and resilience) in the last three years. Thank you for the opportunities and your continuous encouragement and enthusiasm. I promise I'll stop losing my worldly possessions at every conference!

I also want to say a huge huge thank you to all previous and current McColl and Horsburgh lab members, particularly **Clare Latta** for assisting with the many 7 am perfusions and flow preps. I also have to say a big thanks to **Laura McColloch.** Your continuous optimism and wisdom on everything lab and non-lab related (particularly restaurants, cocktails and my favourite, the Grinch) made my PhD experience so enjoyable. You are a brilliant scientist and it's been great working alongside you! Lastly, I have to say a huge thank you to **Jess Duncombe** for teaching me laser speckle imaging and most importantly, how to survive in LF2.

I would also like to thank my family and dedicate this thesis to my wonderful parents **Lucy** and **Andrew Szymkowiak**. I really could not have done this without your continuous encouragement and support. I'm so proud to call you my parents and a thesis acknowledgement expresses only a fraction of my gratitude. Thank you for everything! I must also thank **Peter Szymkowiak, Jana Šindelařová, Vladimir Šindelařová and Jakub Szymkowiak** for keeping me sane when everything was blowing up in the lab. Thank you for keeping my glass topped up and supplying excellent scran whenever I come back to Manchester. Last but certainly not least, I have to thank **Thomas Szymkowiak** for the many nights playing GTA V and rocket league (I promise I'll get better eventually). Thank you for always being there when I needed help and for pushing me when I felt like I couldn't do it. I've said it once and I'll keep saying it thank you all so much I really could not have done it without you.

From the Roslin Institute I thank the **biological resource facility staff** particularly **Dave Davies, Christine Marsh, Lorraine Blackwood, Darren Smith and Tricia Mattheason** for assistance with training and animal husbandry. I also would like to thank **Graeme Robertson** and **Bob Fleming** for aiding with microscopy and FACS sorting of microglia.

From QMRI, I thank **Pamela Brown** within the Biomolecular Core and **Mike Millar** and **Fiona Inglis** for assistance with setting up Axio Slide Scanner profiles. I would also like to thank **Larraine Jackson** in LF2 for assistance with animal husbandry. Lastly, I would like to thank **Shonna Johnstone**, **Mari Pattison** and **Will Ramsay** for aiding with flow cytometry and FACS isolation of microglia.

Finally, a huge shout out to my brilliant Edinburgh and Manchester friends especially **Greg Wilson** and **Becky Sutton** for being so supportive and always making me laugh. I also have to thank **Ross Culling, Katrina Hemingway, Fraser McMurdo, Kyle McDowall, Connor O'Halloran, Isobel MacGregor, Laura Kinghorn, Craig Wynn, Lloyd Peter, Mark Harmon, Chess De Munnich, Fergus Mutch, Chris Rennie, Jaclyn Otto, Rachel Loinsigh, Roy Shankland, Katy Cooper, Alicia Edmenson Cook, Philip Hope and Greg Hull.** Thank you for all laughs and memories. Here's to many more!

Declaration

I declare that this thesis has been composed solely by myself, that it has not been submitted for any previous degree or qualification, and that the work described within this thesis comprises my own original work except where stated otherwise in the text.

Date: _____29.07.2019_____

List of figures

List of tables

List of abbreviations

ABC transporters: ATP binding cassette transporters
ACAS: Asymmetric common carotid artery stenosis
AD: Alzheimer's disease
ALS: Amyotrophic lateral sclerosis
ANOVA: Analysis of variance
APOE4: Apolipoprotein E4
ATP: Adenosine triphosphate
Aβ: Amyloid beta
BBB: Blood brain barrier
BCAS: Bilateral common carotid artery stenosis
BCCAO: Bilateral common carotid artery occlusion
BDNF: Brain-derived neurotrophic factor
BMDM: Bone marrow derived macrophages
BrdU: Bromodeoxyuridine
BSA: Bovine serum albumin
CAA: Cerebral amyloid angiopathy
CADASIL: Cerebral autosomal dominant arteriopathy with subcortical infarcts and leukoencephalopathy
CARASIL: Cerebral autosomal recessive arteriopathy with subcortical infarcts and leukoencephalopathy
cDNA: Complementary deoxyribonucleic acid
CNS: Central nervous system
COL4A1: Collagen-alpha-1 IV chain
COL4A2: Collagen alpha-2 (IV) chain
CR3: Complement receptor 3
CSF1: Colony stimulating factor 1
CSF1R: Colony stimulating factor 1 receptor
cSVD: Cerebral small vessel disease
Ct: Cycle threshold
CTF: C terminal fragment
DAM: Disease associated microglia
DAMP: Damage associated molecular patterns
DAP12: DNAX-Activation Protein 12
DEPC: Diethyl Polycarbonate
DNA: Deoxyribonucleic acid
DTI: Diffusion tensor imaging
EAE: Experimental autoimmune encephalitis
FACS: Fluorescence activated cell sorting

FTD: Frontotemporal dementia
FTLD: Frontotemporal lobar dementia
GCAS: Gradual common carotid artery stenosis
GDNF: Glial cell derived neurotrophic factor
GFAP: Glial fibrillary acidic protein
GLUT1: Glucose transporter 1
GM-CSF: Granulocyte macrophage colony stimulating factor
GWAS: Genome wide association studies
H & E: Haematoxylin and eosin
HBSS: Hank's buffered saline solution
HIF: Hypoxia inducible factor
HTRA1: High temperature requirement A serine protease 1
IBA1: Ionised calcium binding adaptor protein 1
ICAM1: Intercellular adhesion molecule 1
IFN-γ: Interferon gamma
IGF-1: Insulin growth factor 1
IHC: Immunohistochemistry
IL: Interleukin
IRF: Interferon regulatory factor
ITAM: Immunoreceptor tyrosine based activation motif
LDL: Low density lipoprotein
LIF: Leukaemia inhibitory factor
LPS: Lipopolysaccharide
MAG: Myelin associated glycoprotein
MCAO: Middle cerebral artery occlusion
MFI: Mean fluorescence intensity
MHCII: Major histocompatibility complex class II
MMP: Matrix metalloproteinase
MRI: Magnetic resonance imaging
MS: Multiple sclerosis
mTOR: mammalian target of rapamycin
NFκB: Nuclear factor kappa light chain enhancer of activated B cells
NHD: Nasu Hakola Disease
NOTCH3: Neurogenic locus notch homolog protein 3
NVU: Neurovascular unit
OPC: Oligodendrocyte precursor cell
PAMP: Pathogen associated molecular patterns
PBS: Phosphate buffered saline
PCR: Polymerase chain reaction
PDGFβ: Platelet derived growth factor beta

PDGFβR: Platelet derived growth factor beta receptor

PVM: Perivascular macrophage

RNA: Ribonucleic acid

ROS: Reactive oxygen species

RT-QPCR: Real time quantitative polymerase chain reaction

SHRSP: Spontaneously hypertensive stroke prone rats

TGFβ: Transforming growth factor beta

TLR: Toll like receptors

TNFα: Tumour necrosis factor alpha

TREM1: Triggering receptor expressed on myeloid cells 1

TREM2: Triggering receptor expressed on myeloid cells 2

TREX1: Three prime repair exonuclease 1

VCAM1: Vascular cell adhesion molecule 1

VCI: Vascular cognitive impairment

VEGF: Vascular endothelial growth factor

VSMC: Vascular smooth muscle cell

WT: Wild type

Abstract

Chronic cerebral hypoperfusion resulting from cerebrovascular disease is associated with the development of white matter damage, cognitive impairment and dementia. Although incompletely understood, recent studies suggest neuroinflammation is a key mechanism driving vascular pathology, white matter damage and cognitive decline.

receptor expressed on myeloid cells 2 (TREM2) increase susceptibility to neurodegenerative conditions and dementia providing key evidence for the role of microglial dysfunction in dementia pathogenesis. Precisely how TREM2 dysfunction contributes to neurodegeneration and dementia remains to be established, particularly in relation to cerebrovascular causes of degeneration.

To investigate the contribution of TREM2 to cerebrovascular-mediated white matter damage, the bilateral common carotid artery stenosis (BCAS) model of chronic cerebral hypoperfusion was implemented in wild type (WT) and TREM2-/- C57BL/6Ntac mice. Initial studies demonstrated 0.18 mm internal diameter microcoils failed to induce sufficient white matter pathology or neuroinflammatory changes in WT C57BL/6Ntac mice. However, implementation of microcoils with smaller internal diameters (0.16 mm) precipitated robust myelin damage associated with neuroinflammation. In the absence of TREM2 expression, myelin damage was exacerbated and microglial responses to BCAS were blunted as assessed by immunohistochemistry and flow cytometric analysis.

Collectively, the data presented in this thesis suggest TREM2 plays a key role in regulating microglial responses to chronic cerebral hypoperfusion. Given that TREM2 deficiency exacerbated myelin damage, it appears TREM2 confers protection to cerebrovascular dysfunction. However, the precise mechanisms remain unclear. Furthermore, the effects of TREM2 deficiency on white matter function and cognition remain unknown. Future studies investigating the impact of chronic cerebral hypoperfusion on the microglial transcriptome will advance our understanding of microglial function and neuroinflammation in the context of

vascular cognitive impairment (VCI) and dementia. Such studies may reveal novel TREM2-regulated pathways that attenuate neurodegenerative processes and ameliorate cognitive impairment.

Lay Summary

Despite constituting only 2 % of total body mass, the brain requires 20 % of energy intake. As the brain has a high energy demand, efficient delivery of oxygen and other nutrients via the blood stream is crucial to maintain normal brain function. Ageing as well as vascular risk factors such as high blood pressure and diabetes cause damage to the brain's blood vessels over time impairing blood flow to the brain, also known as chronic cerebral hypoperfusion. If blood flow to the brain is compromised, brain cells are starved of nutrients and this can result in tissue damage and lead to memory loss and dementia.

The term 'vascular cognitive impairment' (VCI) is used to describe a loss of memory and thinking skills caused by damage to the brain's blood vessels. VCI is the second most common cause of dementia and as yet, no effective treatment exists. Given that the number of people suffering from dementia is rising, it is crucial to gain a better understanding of the disease mechanisms to identify potential drug treatments.

Recent experimental studies suggest brain inflammation, also known as neuroinflammation, may play a role in vascular-mediated brain damage and dementia. Within the brain, immune cells called microglia are primary drivers of neuroinflammation through the release of inflammatory molecules. Although neuroinflammation is usually initiated to protect the brain from damage or infection, if prolonged or dysregulated it can do more harm than good.

Mutations in immune genes expressed by microglia such as triggering receptor expressed on myeloid cells 2 (TREM2) increase the risk of developing dementia providing key evidence that microglial dysfunction can contribute to dementia. Increased numbers of microglia are observed in areas of vascular-mediated brain damage. However, the precise function of microglia and whether they contribute to or protect from brain damage remains unclear. Furthermore, the role of TREM2 in vascular-mediated brain damage remains unknown.

To understand how neuroinflammation and TREM2 contribute to vascular-mediated brain damage, chronic cerebral hypoperfusion was induced in mice which lack the TREM2 gene and resultant microglial responses and brain damage were investigated. Chronically reducing blood flow to the brain resulted in widespread damage associated with increased numbers of microglia. Interestingly, brain damage was worsened and microglial responses were dampened in mice which did not have the TREM2 gene.

The results suggest TREM2 plays an important role in regulating microglial responses to chronically reduced brain blood flow and vascular-mediated brain damage. As mice lacking TREM2 had increased brain damage this suggests TREM2 regulates protective microglial processes. However, it remains unclear precisely what processes TREM2 may regulate to prevent brain damage. Furthermore, although mice without the TREM2 gene had increased brain damage, the impact on memory function has not yet been measured. Overall, this research demonstrates TREM2 regulated microglial functions play a key role in vascular mediated brain damage, however further work is necessary as understanding of these processes may point to potential therapeutic treatments for dementia.

Chapter 1:

Introduction

1.1 The cerebrovasculature

Although the brain constitutes just 2 % of total body mass, 20-25 % of total oxygen and glucose intake is required for normal brain function (Clarke & Sokoloff, 1999). The cerebrovasculature is therefore crucial for the delivery of nutrients and removal of waste products to support normal brain function. The cerebrovasculature originates from the carotid and vertebral arteries in the neck joining the circle of Willis at the base of the brain (fig.1.1A). From the circle of Willis, the posterior, middle and anterior cerebral arteries extend across the brain surface providing a rich anastomotic network of pial arteries and arterioles. Pial vessels penetrating the cortical surface give rise to smaller penetrating arterioles and capillaries before reaching deeper subcortical white matter regions (fig.1.1B). Given that the brain is critically dependant on cerebral blood flow, the correct regulation of cerebral blood flow by cells of the neurogliovascular unit is essential to ensure metabolic need is met by sufficient blood flow.

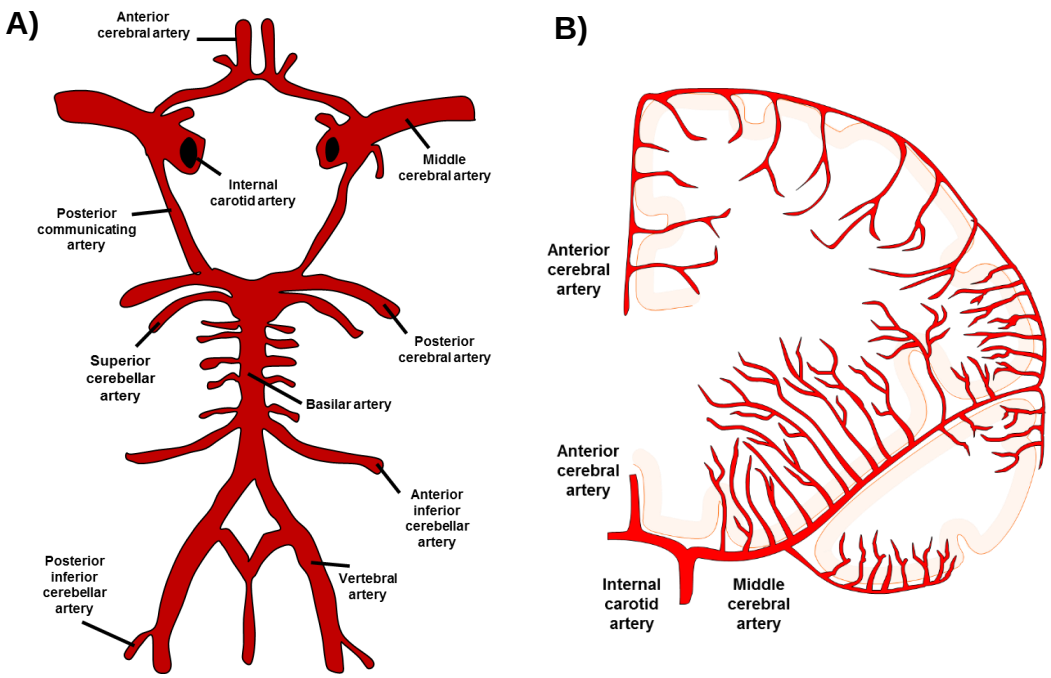

Figure 1.1: The human cerebrovasculature. (A) The circle of Willis. (B) The cerebrovascular supply of the deep subcortical white matter. The middle and anterior cerebral arteries arise from the internal carotid at the circle of Willis and supply the cortical surface before penetrating the brain parenchyma and supplying deep subcortical structures. Adapted from: Iadecola, 2013.

1.2 The neurogliovascular unit

Within the brain, endothelial cells, pericytes, vascular smooth muscle cells (VSMCs), glia and neurons form the neurogliovascular unit (fig. 1.2A). Together these cells orchestrate coordinated responses to ensure cerebral blood flow is sufficient for the brain's metabolic needs (Iadecola, 2010). Endothelial cells, astrocytes and mural cells (VSMCs and pericytes) form the blood brain barrier (BBB). Endothelial cells lacking fenestrae form the blood vessel wall providing a unique physical barrier limiting paracellular movement of solutes from the blood stream into the brain parenchyma and vice versa due to interconnecting tight junctions and adherens junctions. Low rates of endothelial transcytosis limits vesicle-mediated transcellular movement of solutes and expression of specialised transporters on luminal and abluminal membranes enables the selective influx or efflux of solutes across the endothelium. Whilst transporters such as glucose transport 1 (GLUT1) and amino acid transporters on the luminal membrane enable the influx of glucose and amino acids from the blood stream into the brain parenchyma, efflux transporters on the abluminal surface such as adenosine triphosphate (ATP) binding cassette transporters (ABC transporters) play a key role in the removal of waste or metabolic bi-products (Abbott et al., 2010). Endothelial cells also regulate vascular tone through the release of vasoactive factors in response to mechanical or chemical stimuli (Iadecola, 2010).

Mural cells including VSMCs and pericytes envelop the abluminal portion of endothelial cells. While VSMCs surround the endothelium in larger arteries and arterioles, these are replaced by pericytes at the capillary level (fig. 1.2B). VSMCs react to a range of vasoactive agents and mediate blood vessel constriction or dilation via contractile proteins to ensure cerebral blood flow is maintained at 50 ml per 100 g of brain tissue per minute within a range of pressures (60-160 mmHg) (van Beek et al., 2008). This protective mechanism, known as cerebral autoregulation, minimises potentially damaging perfusion pressure fluctuations associated with daily living. In response to low perfusion pressure, VSMCs trigger arterial dilation resulting in reduced vascular resistance, increased cerebral blood flow and vice versa.

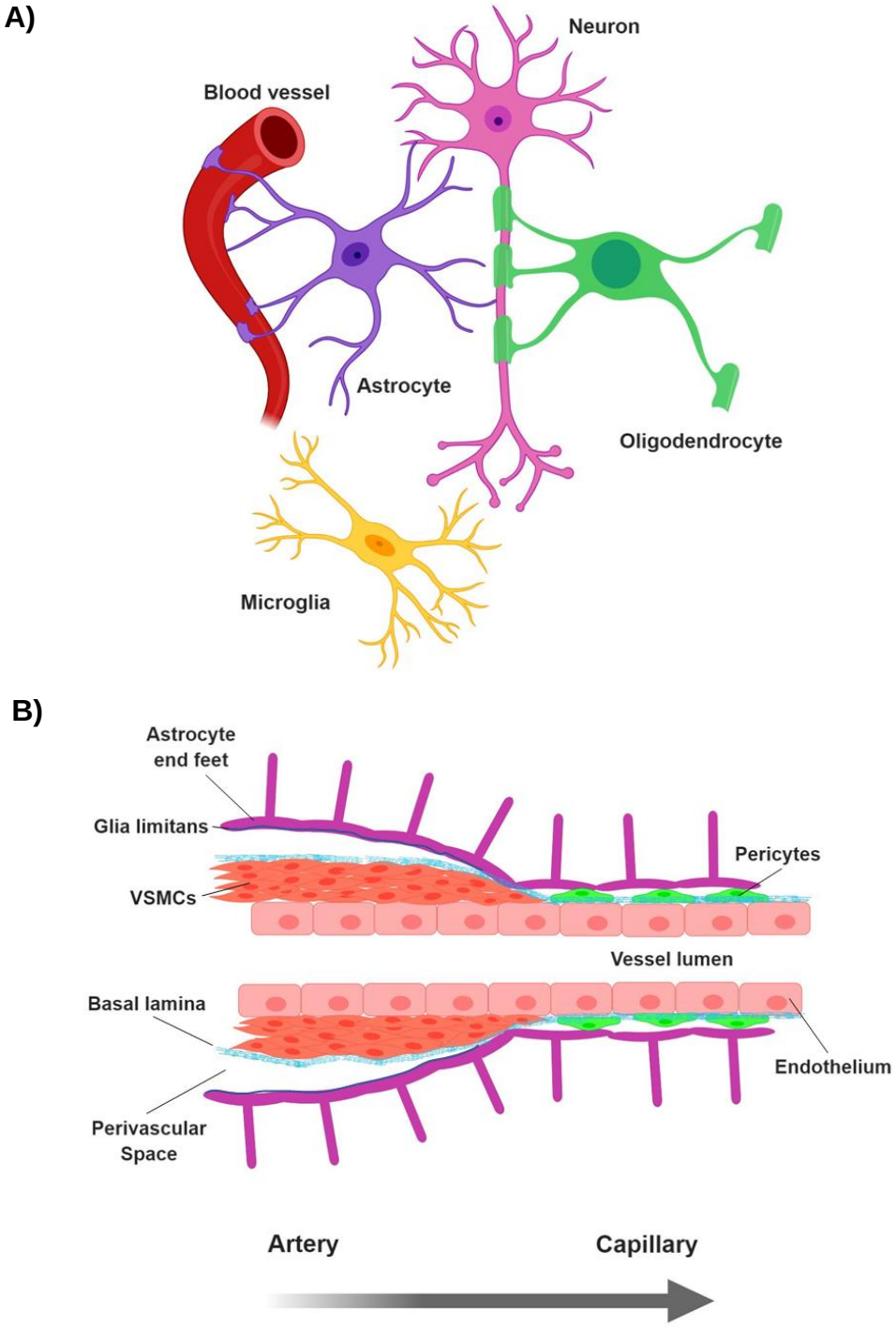

Figure 1.2: The neurogliovascular unit. A) The neurogliovascular unit consisting of the cerebrovasculature, glia (astrocytes, microglia and oligodendrocytes) and neurons. (B) Anatomy of the cerebrovasculature wall from artery to capillary.

At the level of the capillary, platelet derived growth factor β (PDGFβ) secreted by endothelial cells recruits pericytes to the vascular wall via platelet derived growth factor β receptor (PDGFβR). PDGFβ null mice demonstrate reduced pericyte coverage, microvessel abnormalities, microaneurysm and embryonic lethality (Lindahl et al., 1997). Pericyte deficient mice similarly demonstrate impaired capillary perfusion associated with BBB breakdown (Bell et al., 2010). In addition to maintenance of the BBB and cerebral blood flow, pericytes are also implicated in clearance of debris via phagocytosis, angiogenesis and regulation of leucocyte recruitment (Proebstl et al., 2012, Winkler, Sagare and Zlokovic, 2014).

Astrocyte end feet contacting nodes of Ranvier and neuronal synapses detect neuronal activity and ensure metabolic need is matched with sufficient blood flow by releasing vasoactive factors at end feet contacting blood vessels, a process known as neurovascular coupling (Gordon, Howarth and MacVicar, 2016). Astrocytic end feet contacting the cerebrovasculature also play key roles in development and maintenance of the BBB (Cabezas et al. 2014). Neurons also directly contact blood vessels and regulate vascular tone through release of vasoactive factors (Hamel, 2006).

Through the release of inflammatory mediators, microglia, the resident immune cells of the central nervous system (CNS), impact on neurovascular function by modulating BBB integrity, endothelial function and leucocyte recruitment (Thurgur and Pinteaux, 2019). Perivascular macrophage (PVMs) located within the perivascular space surrounding the basement membrane of penetrating arterioles also regulate neurovascular unit (NVU) integrity with suggested roles in waste clearance, antigen presentation and inflammatory cell recruitment in response to damage or infection (Polfliet et al., 2001, Hawkes and McLaurin, 2009, Zhang et al., 2011b). Given that the orchestrated interaction between multiple cell types of the NVU is crucial for the maintenance of cerebral blood flow and CNS homeostasis, damage to individual components can functionally impair the NVU and cerebrovascular integrity. If cerebral blood flow is compromised and autoregulation fails the brain attempts to compensate by increasing blood oxygen extraction (Cipolla, 2009). However, if the brain's metabolic need continues to

exceed the ability to extract oxygen from the bloodstream ischaemia ensues leading to cell loss and tissue damage

1.3 Vascular cognitive impairment

The term vascular cognitive impairment (VCI) was devised to encompass all forms of cognitive impairment primarily resulting from cerebrovascular dysfunction and accounts for 20 % of dementia cases (Farooq and Gorelick, 2013). Pathologies associated with VCI are highly heterogeneous and manifest as a spectrum of vascular lesions predominantly affecting the white matter. These pathologies include single (strategic) or multiple infarcts, lacunar infarcts, microinfarcts, white matter lesions, haemorrhage, microbleeds, enlarged perivascular spaces and brain atrophy (fig. 1.3) (Dichgans and Leys, 2017).

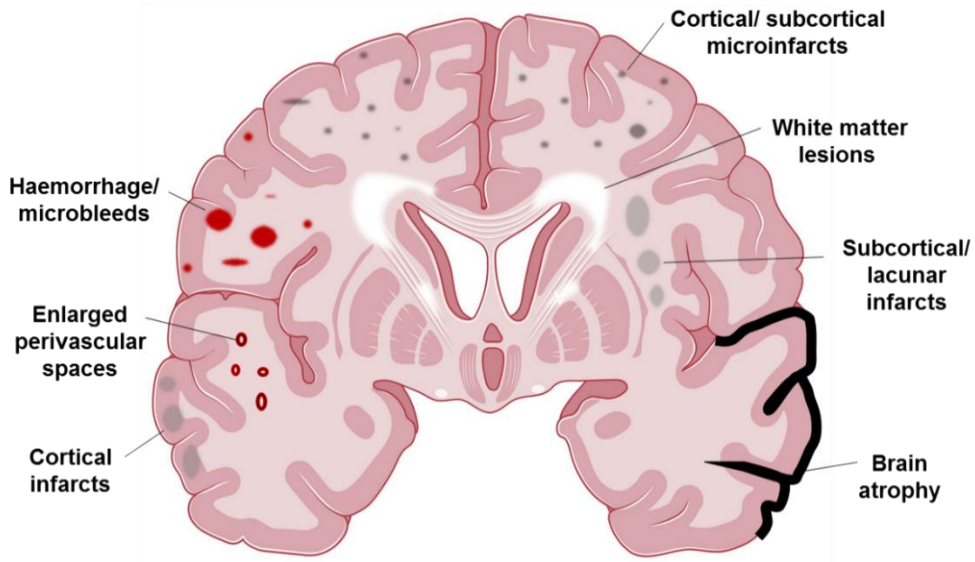

Figure 1.3: Pathological features of VCI. Pathologies associated with VCI are highly hetereogenous predominantly affecting the white matter of the brain consisting of cortical and subcortical infarcts, microinfarcts, enlarged perivascular spaces, haemorrhage and white matter lesions. In addition to local tissue damage, vascular injury can cause secondary neurodegeneration and cortical thinning resulting in brain atrophy.

Cerebral small vessel disease (cSVD), in which the small arteries, arterioles, capillaries and venules of the brain are damaged, is a primary cause of VCI. Whilst *in vivo* imaging of the brain's microvasculature is not yet possible, detection of damage to the surrounding parenchyma enables diagnosis of cSVD. White matter hyperintensities, characterised pathologically by demyelination and axonal damage, in addition to lacunar infarcts, microbleeds, enlarged perivascular spaces and brain atrophy are common radiological features of cSVD (ter Telgte et al., 2018). Post-mortem studies demonstrate vascular pathologies including deposition of hyaline in vessel walls, arteriosclerosis, atherosclerosis, fibrinoid necrosis and venous collagenosis (Iadecola, 2013). The progressive accumulation of amyloid β (Aβ) in cerebrovasculature, known as cerebral amyloid angiopathy (CAA) is also associated with cSVD. Although highly prevalent in Alzheimer's disease (AD) patients, CAA is frequently observed in the elderly in the absence of AD pathology (Vinters and Gilbert, 1983).

The white matter of the brain is particularly susceptible to cerebrovascular dysfunction due to lack of collateral vessels and non-overlapping vascular territories (Iadecola, 2013). The brain's white matter constitutes 50 % of total human brain volume containing glial cells including oligodendrocytes, astrocytes and microglia in addition to myelinated axons and blood vessels. Lipid rich oligodendrocyte processes extend and wrap around surrounding axons to form an insulating myelin sheath enabling saltatory conduction of action potentials limiting energy expenditure by restricting membrane depolarisation to nodes of Ranvier. Oligodendrocytes also provide support to axons through the release of trophic factors including insulin growth factor 1 (IGF-1) and glial cell derived neurotrophic factor (GDNF) (Wilkins et al., 2003). If myelin integrity is compromised, trophic support is lost impairing axon health.

As myelin is lost, the axon surface is increasingly exposed to neurotoxic stimuli in the surrounding microenvironment exacerbating damage. It is theorised damage to the white matter impairs cortical-cortical and cortical-subcortical connections within the brain leading to disruption of brain networks associated with VCI including processing speed and executive function (Lawrence et al., 2014). Studies have demonstrated key radiological features of cSVD including brain atrophy, lacunar infarction and white matter ultrastructural damage detected

by diffusion tensor imaging (DTI) are associated with poorer processing speed and executive function (Lawrence et al., 2013, Nitkunan et al., 2008, Nitkunan et al., 2011). Furthermore, white matter damage on DTI predicts cognitive decline and progression to dementia (Zeestraten et al., 2017). As the lesions associated with VCI are highly diverse and often coexist in the same brain the extent of cognitive impairment can vary. This is particularly true in patients exhibiting strategic or multiple infarcts in which the degree of cognitive impairment can depend on lesion size and location.

The incidence of cSVD is strongly influenced by aging and vascular risk factors including hypercholesterolaemia, smoking, hyperhomocysteinaemia, hypertension and diabetes (Dichgans and Leys, 2017). Importantly, many risk factors associated with cSVD can be treated or modified offering a potential strategy to reduce disease prevalence. Hereditary forms of cSVD include cerebral autosomal-dominant arteriopathy with subcortical infarcts and leukoencephalopathy (CADASIL), caused by mutations in the neurogenic locus notch homolog protein 3 (*NOTCH3*) gene. Post-mortem studies demonstrate accumulation of granular osmiophilic deposits containing NOTCH3 protein in the cerebrovascular wall and vessel wall thickening in addition to VSMC loss (Sondergaard et al., 2017).

On the other hand, cerebral autosomal-recessive arteriopathy with subcortical infarcts and leukoencephalopathy (CARASIL) is caused by mutations in the high temperature requirement A serine protease 1 (*HTRA1)* gene leading to defective transforming growth factor β (TGFβ) signalling and VSMC loss (Oide et al., 2008). Additional genetic causes of cSVD are caused by collagen alpha-1 (IV) chain (*COL4A1*) and collagen alpha-2 (IV) chain (*COL4A2*) gene mutations resulting in basement membrane defects and vessel wall thickening in addition to three prime repair exonuclease 1 (*TREX1*) gene mutations which cause autosomal dominant retinal vasculopathy with cerebral leukodystrophy (DiFrancesco et al., 2015).

Although VCI is suggested to account for 20 % of dementia cases it is now recognised there is substantial overlap with other dementias including AD. Neuropathological studies demonstrate up to 80 % of AD patients have cerebrovascular pathology (Toledo et al., 2013). The presence of vascular pathology lowers the threshold for cognitive impairment and dementia in AD (Esiri et al., 1999, Riekse et al., 2004, Snowdon et al., 1997). CSVD risk factors including hypertension, diabetes and hyperlipidaemia are similarly associated with AD and increase amyloid β (Aβ) and tau burden (Langbaum et al., 2012, Vemuri et al., 2017). Furthermore, VCI risk factors have been suggested to act synergistically with Aβ to induce tau deposition and cognitive impairment (Rabin et al., 2018, Rabin et al., 2019). Neuroimaging studies demonstrate cerebrovascular dysfunction occurs early during disease trajectory prior to Aβ deposition and may predict disease progression (Iturria-Medina et al., 2016, Yew, Nation and Alzheimer's Dis, 2017). White matter changes are also observed years prior to symptom onset in familial forms of AD suggesting that vascular dysfunction and white matter injury has a causal role in AD pathogenesis (Lee et al., 2016, Caballero et al., 2018).

Although cerebrovascular dysfunction plays a key role in cognitive impairment and dementia, the precise pathological mechanisms remain unclear. It is suggested that aging and vascular risk factors cause damage to the cerebrovasculature through several mechanisms including BBB breakdown, oxidative stress and neuroinflammation leading to the development of pathological lesions. Determining the mechanisms by which cSVD contributes to white matter damage and VCI in humans is difficult due to the presence of several confounding variables including age, gender and vascular risk factors. Numerous animal models have therefore been developed to recapitulate aspects of cSVD to investigate potential pathogenic mechanisms which contribute to white matter damage and cognitive decline. In addition to models which manipulate cerebral blood flow, several models have been developed which investigate how environmental and genetic risk factors contribute to white matter damage and cognitive impairment.

1.4 Animal models of VCI

1.4.1 Bilateral common carotid artery occlusion

Bilateral common carotid artery occlusion (BCCAO) by permanent occlusion or ligation of the carotid arteries was originally developed in rats to induce chronic cerebral hypoperfusion and precipitate white matter damage and cognitive impairment. Following vessel occlusion, animals demonstrate a 70 % reduction in cerebral blood flow immediately following surgery which gradually recovers to 40-50 % after 28 d (Tomimoto et al., 2003). Animals demonstrate disruption of the optic tract within the first 3 d with damage extending to other white matter regions such as the corpus callosum and internal capsule with longer durations of hypoperfusion (Otori et al., 2003, Wakita et al., 2002). Animals also demonstrate progressive hippocampal degeneration from as early as 2 w following surgery (Bennett et al., 1998, Farkas et al., 2006, Ohtaki et al., 2006). In addition to this, behavioural studies demonstrate increased escape latencies in the Morris water maze and increased errors in the radial arm maze compared to sham animals (Pappas et al., 1996, Bennett et al., 1998, Sopala and Danysz, 2001).

Although this model precipitates white matter damage and cognitive impairment, occlusion or ligation of the carotid arteries induces severe hypoperfusion associated with hippocampal neurodegeneration. Furthermore, the optic tract is highly susceptible to hypoperfusion-mediated damage which may impact on cognitive assessments utilising visual cues. BCCAO is also limited to rats as they have a fully developed circle of Willis whilst certain mouse strains have under-developed posterior communicating arteries (Yang et al., 1997). Therefore, whilst carotid occlusion is compensated by the vertebral circulation in rats, carotid occlusion induces extensive ischaemic damage in mice (Kitagawa et al., 1998, Yang et al., 1997).

1.4.2 Bilateral common carotid artery stenosis

The BCCAO model was therefore refined leading to development of the bilateral common carotid artery stenosis (BCAS) model. Placement of microcoils on the carotid arteries leads to partial, rather than complete occlusion of the carotid arteries meaning this model can be

implemented in mouse strains with underdeveloped posterior communicating arteries (Shibata, et al. 2004). Furthermore, the acute reduction in cerebral blood flow following microcoil placement is less severe than that caused by BCCAO. Application of 0.18 mm internal diameter microcoils induces an initial 30 - 40 % reduction in cerebral blood flow which gradually recovers to 15- 30 % of baseline 1 – 3 months following surgery in young mice. (Shibata et al., 2004, Nishio et al., 2010, McQueen et al., 2014).

Myelin disruption characterised by nodal/ paranodal breakdown is observed 3 d after BCAS and microarray analysis of white matter demonstrates alterations in various cell processes including cell proliferation, angiogenesis and inflammation (Reimer et al., 2011). Diffuse white matter damage coinciding with astrocyte and microglial activation is observed 1 m after BCAS associated with working memory impairment in the absence of grey matter damage (Coltman et al., 2011, Reimer et al., 2011, Shibata et al., 2007, Shibata et al., 2004). With prolonged BCAS (6 - 8 m), further loss of white matter integrity is accompanied by BBB disruption, development of cortical and subcortical ischaemic and haemorrhagic lesions and additional spatial reference memory impairment coinciding with hippocampal atrophy (Holland et al., 2015, Nishio et al., 2010).

In addition to recapitulating various pathological features of cSVD, the BCAS model provides a platform to investigate how loss of white matter integrity contributes to cognitive impairment in the absence of neuronal perikarya damage. An additional advantage of the BCAS model is that the extent of hypoperfusion can be manipulated by using microcoils with different internal diameters ranging from 0.16 mm – 0.22 mm (Shibata et al., 2004).

While use of 0.18 mm internal diameter microcoils induces diffuse white matter damage without overt neuronal perikaryal damage after 28 d, 0.16 mm internal diameter microcoils cause extensive white and grey matter damage associated with high mortality (75 %). To circumvent this, the BCAS model was modified so that a 0.18 mm microcoils is applied to the right carotid artery whilst a 0.16 mm microcoil is applied to the left carotid artery to induce greater cerebrovascular insufficiency and more definite white matter damage associated with reduced mortality (Miki et al., 2009). After 1 m, animals demonstrate widespread white matter

damage and neuronal perikarya damage in the hippocampus associated with neuroinflammation and spatial reference memory dysfunction (Miki et al., 2009). A more recent study similarly demonstrated robust white matter pathology and neuroinflammation after 1 w associated with impaired white matter conduction velocity (Fowler et al., 2018).

However, a limitation of the BCAS model is that placement of microcoils causes an acute reduction in cerebral blood flow that does not mimic the gradual onset of hypoperfusion seen with aging. To address this, the gradual common carotid artery stenosis model (GCAS) was developed for use in rodents in which ameroid constrictors containing casein are placed around the carotid arteries (Kitamura et al., 2012, Hattori et al., 2016a). The casein within the devices absorb extracellular fluid over time and swell, gradually reducing cerebral blood flow. In rats, a gradual 30 % reduction in cerebral blood flow is observed after 3 d recovering to 15 % after 28 d (Kitamura et al., 2012). In mice however, cerebral blood flow gradually decreases by 30 % without recovery up to 28 d following surgery (Hattori et al., 2016a).

Similar to the BCAS model, GCAS causes diffuse white matter damage associated with neuroinflammation without hippocampal neurodegeneration (Hattori et al., 2016a). GCAS mice also demonstrate spatial working memory and motor coordination deficits in the absence of spatial reference memory impairment (Hattori et al., 2016a). Although the GCAS model circumvents acute reductions in cerebral blood flow caused by microcoil placement it remains unclear if devices can be left on for longer durations without causing complete occlusion of the carotid arteries.

The GCAS model has also been adapted to induce greater cerebral hypoperfusion associated with more severe white matter pathology. In the asymmetric common carotid artery stenosis (ACAS) model, an ameroid constrictor is placed on the right carotid artery whilst a 0.16 mm internal diameter microcoil is placed on the left carotid artery (Hattori et al., 2015). While the right carotid artery becomes completely occluded 28 d after surgery, cerebral blood flow is reduced by 50 % in the left carotid. Mice develop numerous white matter infarcts in addition to frequent hippocampal damage associated with spatial working and reference impairment as well as impaired motor coordination (Hattori et al., 2015).

Although the above models enable investigation of how hypoperfusion contributes to CNS pathology, it must be noted that the above surgical models may directly impact autoregulation, vessel pulsatility or vessel stiffness independant of hypoperfusion. Furthermore, local inflammation resulting from surgery and application of devices may contribute to pathological or behavioural outcomes. Given that the above factors all contribute VCI pathogenesis it will be important characterise whether these factors are altered in hypoperfusion models.

1.4.3 Additional models of VCI

In addition to models that manipulate cerebral blood flow, models have been developed which investigate the contribution of environmental or genetic risk factors to VCI pathogenesis. Spontaneously hypertensive stroke prone (SHRSP) rats demonstrate spontaneous and progressive increases in mean arterial blood pressure from 4 w of age reaching 220 mmHg by early adulthood (Yamori et al., 1976). Neuropathological studies identify a range of vascular pathologies including vessel wall thickening, loss of BBB integrity and enlarged perivascular spaces which progress over time affecting 80 % by 30 w of age (Okamoto, Yamori and Nagaoka, 1974, HartHeistad and Brody, 1980, Fredriksson et al., 1985). Early endothelial dysfunction has recently been suggested as a key mechanism contributing to impaired oligodendrocyte maturation and white matter vulnerability (Rajani et al., 2018). By 9-12 m of age SHRSP rats exhibit stroke lesions varying in severity and location and 90 % mortality by 12 m of age (Madigan, Wilcock and Hainsworth, 2016). As the severity and location of cerebrovascular pathology can vary, the impact on cognitive function is unpredictable (Madigan et al., 2016).

Hyperhomocysteinaemia, a risk factor for VCI, can be induced by providing rodents a diet lacking vitamin B6, B9-folate and B12 with or without homocysteine precursor methionine supplementation (Sudduth et al., 2013). Hyperhomocysteinaemia leads to cerebrovascular abnormalities including reduced capillary density and microhaemorrhage associated with neuroinflammation in addition to impaired performance on the Morris water maze (Sudduth et al. 2013).

Transgenic mice harbouring mutations in NOTCH3 have also been utilised to investigate the pathological mechanisms of CADASIL, the most common genetic cause of VCI. Notch3^{R169C} mice exhibit increased Notch3 aggregation in the cerebrovasculature and demonstrate cerebrovascular abnormalities with increasing age including loss of BBB integrity, reduced pericyte coverage and impaired cerebrovascular reactivity (Ghosh, et al. 2015). At older ages Notch3^{R169C} mice demonstrate reduced cerebral blood flow and white matter damage associated with reactive gliosis and impaired myelin clearance (Joutel et al., 2010, Cognat et al., 2014, Ghosh et al., 2015). Although the precise mechanisms remain unclear, abnormal accumulation of vitronectin and TIMP3 is suggested to contribute to loss of cerebrovascular reactivity and subsequent white matter damage downstream of Notch3 deposition. While *Timp3* haploinsufficiency ameliorates impairments in functional hyperaemia and autoregulation, *Vtn* haploinsufficiency reduces white matter damage without impacting cerebral blood flow responses in notch3^{R169C} mice (Capone et al., 2015). Although notch3^{R169C} mice develop various pathological features of cSVD the impact on cognition remains unclear.

Whilst a model does not exist which fully recapitulates the heterogeneity of pathology observed in cSVD, utilisation of these models has led to the identification of several mechanisms which contribute to loss of white matter integrity and cognitive decline including chronic cerebral hypoperfusion, BBB breakdown, neuroinflammation and oxidative stress.

1.5 Mechanisms contributing to VCI

1.5.1 Chronic cerebral hypoperfusion

Chronic cerebral hypoperfusion, defined as a chronic reduction in cerebral blood flow, is increasingly implicated as a key mechanism contributing to white matter damage and cognitive impairment in the elderly. Lower cerebral blood flow is associated with greater prevalence of cognitive impairment and dementia (Ruitenberg et al., 2005, Chao et al., 2010). Furthermore, individuals with severe carotid stenosis demonstrate greater cognitive deterioration and faster transition from mild cognitive impairment to dementia (Balestrini et al., 2013, Buratti et al., 2014).

Aging, one of the biggest risk factors for cSVD, is associated with reduced cerebral blood flow and increased capillary loss (Brown and Thore, 2011). Indeed, between 20 – 80 years of age cerebral blood flow is reduced by 0.5 % a year (Leenders et al., 1990). Individuals with vascular diseases such hypertension and diabetes also have reduced cerebral blood flow associated with worsened cerebrovascular reactivity compared to healthy controls (Kim et al., 2008, Beason-Held et al., 2007). Hypertension is associated with vascular remodelling resulting in vessel wall thickening, lumen narrowing and reduced cerebral blood flow. Damage to the NVU, loss of BBB integrity and impaired vessel elasticity also disrupts neurovascular coupling thus contributing to cerebral hypoperfusion.

As stated earlier, the white matter of the brain is more susceptible to damage caused by cerebral hypoperfusion. Although larger arteries and arterioles provide a rich anastomotic network on the cortical surface, penetrating arterioles supplying subcortical structures lack collateral vessels. In addition to this, the subcortical white matter is supplied by non-overlapping distal branches of the middle and anterior cerebral arteries, known as watershed regions. Therefore, reductions in cerebral blood flow cannot be effectively compensated in deeper subcortical white matter regions increasing susceptibility to damage.

Preclinical animal models have demonstrated chronic cerebral hypoperfusion is a key driver of white matter damage and cognitive impairment. However, the precise contribution in humans remains unclear. White matter hyperintensities are associated with reduced cerebral blood flow and cerebrovascular reactivity and elderly individuals with lower cerebral blood flow demonstrate increased white matter burden (O'Sullivan et al., 2002, Schuff et al., 2009, Promjunyakul et al., 2015, van Dalen et al., 2016, Sam et al., 2016). Neuropathological studies have also demonstrated areas of white matter damage are associated with upregulation of hypoxia-related proteins including hypoxia inducible factor (HIF) 1 and 2 and matrix metalloproteinase (MMP) 7 suggestive of an ischaemic environment (Fernando et al., 2006). Furthermore, neuroimaging studies suggest reduced cerebral blood flow or cerebrovascular reactivity precedes the development of white matter hyperintensities suggesting chronic

cerebral hypoperfusion plays a causal role in white matter damage (O'Sullivan et al., 2002, Bernbaum et al., 2015, Sam et al., 2016).

However, a longitudinal study investigating the relationship between cerebral blood flow and white matter hyperintensities in patients with arterial disease demonstrated changes in parenchymal cerebral blood flow were not associated with progression of white matter damage (van der Veen et al., 2015). Furthermore, a recent meta-analysis of longitudinal studies demonstrated individuals with lower cerebral blood flow have greater white matter burden. However, evidence was insufficient to support chronic cerebral hypoperfusion occurs prior to development of white matter damage (Shi et al., 2016). It is therefore suggested hypoperfusion reflects reduced activity and metabolic requirement of damaged white matter and that factors other than chronic cerebral hypoperfusion such as impaired vessel pulsation and vessel stiffness contribute white matter damage.

1.5.2 Loss of blood brain barrier integrity

Endothelial dysfunction and loss of BBB integrity are also considered as key early mechanisms contributing to VCI. CSVD patients demonstrate increased albumin in cerebrospinal fluid (CSF) and neuropathological studies demonstrate extravasation of plasma proteins in areas of vascular pathology (Alafuzoff et al., 1985, Tomimoto et al., 2003, Akiguchi et al., 1998, Candelario-Jalil et al., 2011). Neuroimaging studies have also demonstrated increased BBB permeability with aging which is further exacerbated in patients with VCI or AD (Farrall and Wardlaw, 2009, Topakian et al., 2010, Maniega et al., 2017). A recent neuroimaging study also demonstrated white matter hyperintensities are associated with increased BBB permeability (Wardlaw et al., 2017). Furthermore, such areas predicted subsequent cognitive impairment suggesting loss of BBB integrity is an early pathological event which contributes to white matter damage and cognitive decline (Wardlaw et al., 2017).

Endothelial dysfunction and loss of BBB integrity are also frequently observed in preclinical models of VCI. Kitamura et al. (2017) reported gradual upregulation of endothelial adhesion molecules intercellular adhesion molecule 1 (ICAM-1) and vascular cell adhesion molecule 1

(VCAM1) 3 months after BCAS thus promoting immune cell attachment to the endothelial wall (Kitamura et al., 2017). In support of this, recent *in vivo* two photon imaging demonstrated leucocyte attachment and rolling across the cerebrovascular wall in response to BCAS (Yata et al., 2014).

In contrast, Liu et al. (2019) demonstrated a much more rapid loss of BBB integrity 3 days after BCAS concomitant with reduced pericyte coverage prior to onset of white matter injury (Liu et al., 2019). Rajani et al. (2018) similarly demonstrated early endothelial dysfunction and impaired oligodendrocyte precursor cell (OPC) maturation in SHRSP rats. Importantly, such findings were also observed in pre-symptomatic cSVD patient post-mortem tissue suggesting loss of BBB integrity is an early mechanism contributing to white matter damage and cognitive impairment (Rajani et al., 2018).

In addition to promoting infiltration of immune cells into the brain parenchyma, BBB breakdown also permits entry of plasma proteins including fibrinogen, complement and immunoglobulins all of which activate microglia contributing to neuroinflammation. In addition to this, endothelial dysfunction and BBB leakiness impair neurovascular coupling contributing to cerebral hypoperfusion. Importantly, therapeutic reversal of endothelial dysfunction ameliorates white matter vulnerability suggesting targeting endothelial dysfunction and BBB integrity may provide a potential therapeutic strategy for cSVD (Kitamura et al., 2017, Rajani et al., 2018).

1.5.3 Neuroinflammation

Neuropathological studies in the elderly demonstrate areas of white matter damage are associated with activated microglia in addition to markers of oxidative stress and inflammation (Akiguchi et al., 1998, Rosenberg, Sullivan and Esiri, 2001, Simpson et al., 2007, Back et al., 2011). Neuroinflammation coinciding with areas of white matter damage has also been demonstrated in preclinical models of VCI. Microarray analysis of white matter demonstrates alterations in biological pathways associated with cytokine-cytokine receptor interactions and inflammatory responses 72 h after BCAS (Reimer et al., 2011). Furthermore, microglial number closely correlates with loss of white matter structure and function (Manso et al., 2018).

Importantly, various studies have suggested immunomodulatory drugs reduce microglial activation and improve white matter structure and function (Wakita et al., 1995, Cho et al., 2006, Manso et al., 2018, Fowler et al., 2018). Genetic manipulation of inflammatory genes similarly alters disease trajectory further supporting the role of neuroinflammation in VCI (Liu et al., 2015, Miyanohara et al., 2018). In addition to microglia, reactive astrocytes are observed surrounding areas of white matter damage. Specific inhibition of astrocyte nuclear factor kappa-light-chain-enhancer of activated B cells (NFκB) attenuates reactive gliosis, white matter pathology and cognitive deficits suggesting astrocytes also contribute to neuroinflammation (Saggu et al., 2016).

Precisely how neuroinflammation contributes to white matter injury and VCI remains unclear. Upregulation of various cytokines including interleukin (IL)-1β, IL-6 and tumour necrosis factor α (TNF-α) is observed in preclinical modes of cSVD (Tsai et al., 2015, Lee et al., 2015). Cytokines themselves can further activate microglia resulting in a feed forward loop of microglial activation and production of inflammatory mediators which in excess may cause damage to surrounding cells.

In vitro stimulation of microglia and subsequent cytokine release impairs OPC maturation and promotes death (Sherwin and Fern, 2005). IL-1β upregulation following intracerebral injection of lipopolysaccharide (LPS) and is also associated with impaired oligodendrocyte maturation and hypomyelination in neonatal rats (Xie et al., 2016). Furthermore, exposure of primary OPCs to IL-1β impairs proliferation and maturation (Xie, et al., 2016). TNF-α overexpression also causes a chronic inflammatory demyelinating disease and early mortality in mice (Probert et al., 1995). Interferon-γ (IFN-γ) has also been demonstrated to suppress remyelination and delay functional recovery in cuprizone and experimental autoimmune encephalomyelitis (EAE) models of multiple sclerosis (MS) (Lin et al., 2006). IL-1β and TNF-α also influence BBB permeability and expression of endothelial adhesion molecules promoting infiltration of plasma proteins and attachment of circulating leucocytes thus amplifying inflammation (Wu et al., 2010, Yamagata et al., 2004, Mark and Miller, 1999, Wong, Prameya and Dorovini-Zis, 2007).

Activated microglia also secrete MMPs which degrade endothelial tight junctions, extracellular matrix and myelin thus contributing to BBB breakdown and white matter damage. In response to chronic cerebral hypoperfusion, increased MMP-2 expression is associated with BBB breakdown prior to the onset of white matter damage (Ihara et al., 2001). Furthermore, MMP-2 inhibition or genetic depletion attenuates BBB breakdown and white matter damage (Nakaji et al., 2006). MMP inhibition also reverses myelin loss following ischaemic reperfusion injury suggesting MMPs play a key role in mediating white matter damage (Walker and Rosenberg, 2010).

Microglia are also a key source of reactive oxygen species (ROS) thus contributing to oxidative stress. ROS also activate microglia perpetuating further microglial activation. ROS generation also impairs endothelial function and cerebral blood flow regulation by reducing nitric oxide availability thus contributing to cerebral hypoperfusion. Oligodendrocytes are suggested to be particularly susceptible to oxidative stress due to having a high metabolic rate and iron content coupled with low expression of antioxidants such as glutathione (Thorburne and Juurlink, 1996). Oxidative stress is observed in areas of white matter damage in the elderly and preclinical models of chronic cerebral hypoperfusion (Ueno et al., 2009, Washida et al., 2010, Back et al., 2011, Zhang et al., 2011a). Furthermore, use of the free radical scavenger edaravone reduces oligodendrocyte loss *in vitro* and *in vivo* and ameliorates cognitive deficits caused by chronic cerebral hypoperfusion (Miyamoto et al., 2013). Dong, et al. (2014) similarly demonstrated use of the superoxide scavenger tempol ameliorates oxidative stress, white matter damage and cognitive deficits resulting from chronic cerebral hypoperfusion (Dong et al., 2011). Overexpression of the anti-oxidant Nrf2 in astrocytes also protects white matter structure and function in response to chronic cerebral hypoperfusion through repression of inflammatory genes (Sigfridsson et al., 2018).

Vascular risk factors associated with cSVD such as hypertension and diabetes are also associated with chronic inflammation and increased expression of circulating pro-inflammatory cytokines (Lee et al., 2013, Krishnan et al., 2014). Furthermore, ageing, a major risk factor for cSVD and other neurodegenerative diseases, is associated with increased expression of

inflammatory genes and microglial dysfunction (Primiani et al., 2014). Recent analysis of the microglial transcriptome revealed upregulation of immune amplifying genes in aged mice compared to young mice (Grabert et al., 2016). Microglia derived from aged mice demonstrate a dystrophic-like morphology, impaired phagocytosis and exaggerated inflammatory responses to stimuli characterised by increased ROS and pro-inflammatory cytokine release (Matt and Johnson, 2016). In response to chronic cerebral hypoperfusion, aged mice demonstrate greater microglial activation, white matter damage and cognitive impairment compared to young mice (Wolf et al., 2017). Safaiyan et al. (2016) recently demonstrated myelin uptake leads to the accumulation of undegradable lysosomal aggregates contributing to microglial senescence and immune dysfunction (Safaiyan et al., 2016). It could therefore be postulated chronic non-resolving injury such as hypoxia, inflammation and white matter damage may overwhelm microglia leading to functional impairment, neuroimmune dysfunction and exacerbation of damage.

Additonal evidence for the contribution of microglia in dementia causing white matter disease derives from the identification of microgliopathies caused by mutations in microglial-enriched genes. Nasu Hakola disease (NHD) (*TREM2*) and adult-onset leukoencephalopathy with axonal spheroids and pigmented glia (*CSF1R*) are characterised by extensive demyelination, axonal loss and the development of pre-senile dementia during mid-life (Schuburth,Bianchin et al., 2004). Although the pathophysiological mechanisms remain unknown, these diseases demonstrate microglial dysfunction actively contributes to white matter degeneration and dementia.

However, microglia play a key role in various homeostatic processes throughout development and adult life including synaptic pruning, synaptic plasticity, neurogenesis and myelogenesis. Whilst inflammatory mediators released by microglia may contribute to neurodegenerative process such factors are also required for homeostatic or regenerative processes. For example, mice lacking TNF-α or IL-1β demonstrate decreased differentiation of OPCs into mature oligodendrocytes and delayed remyelination in the cuprizone model of demyelination (Arnett et al., 2001, Mason et al., 2001). Microglia are also a source of various trophic

mediators including brain derived neurotrophic factor (BDNF), IGF-1 and leukaemia inhibitory factor (LIF) (Goldstein et al., 2016). Lastly, microglial mediated clearance of debris is necessary to initiate regenerative processes such as remyelination (Lampron et al., 2015). Therefore, fine tuning of microglial function to amplify neuroprotective mechanisms whilst limiting potentially neurotoxic neuroinflammation may provide a promising therapeutic strategy for the treatment of VCI and other dementia causing diseases.

1.6 Microglia

Microglia are tissue resident macrophages of the CNS constituting 5-12 % of cells in the adult brain (Lawson et al., 1990). As innate immune cells of the CNS, microglia rapidly respond to CNS perturbation so to resolve damage and maintain CNS homeostasis. Under steady state conditions, microglia have small cell somas with thin branching processes which continuously survey the local microenvironment. Microglia mediate host defence against CNS injury and infectious agents through a range of receptors including Fc receptors, viral receptors and toll-like receptors (TLR). These receptors recognise a broad range of pathogen associated molecular patterns (PAMPS) such as LPS or damage associated molecular patterns (DAMPS) associated with cell damage or death (Olson and Miller, 2004). In response to CNS perturbation, microglial activation ensues during which microglia increase in size and retract processes adopting an amoeboid morphology (Ransohoff and Perry, 2009). Activated microglia migrate to the area of interest, proliferate, secrete pro-inflammatory mediators and increase their phagocytic ability in an attempt to remove pathogen, debris and dead cells to protect the CNS.

In addition to demonstrating robust morphological adaptations in response to CNS perturbation, microglia also exhibit functionally diverse phenotypes influenced by type and duration of stimuli. Previously, attempts were made to categorise microglial activation as pro- or anti-inflammatory based on *in vitro* classification devised for macrophages (Mantovani et al., 2004). It was initially hypothesised that macrophage activation could be categorised and and distinguished as classical (M1) or alternative (M2) based on expression of cytokines and other inflammatory molecules. Inflammatory mediators including TNF-α, IFN-γ, LPS or

granulocyte macrophage colony stimulating factor (GM-CSF) trigger M1 activation. This results in the upregulation of various pro-inflammatory mediators including IL-1β, TNF-α, IL-12, IL-23, chemokines, ROS and various immunoreceptors (Zhang et al., 2017).

In contrast, M2 activation is triggered by IL-4, IL-13, IL-10, TGF-β or glucocorticoids resulting in the release of anti-inflammatory mediators such as TGF-β, IL-10 and trophic factors promoting wound repair and resolution of inflammation (Zhang et al., 2017). Whilst this may be observed *in vitro*, various *in vivo* studies investigating macrophage and microglial phenotype fail to definitively characterise microglia as M1 or M2 (Mabbott et al., 2010, Chiu et al., 2013, Kim, Nakamura and Hsieh, 2016). Therefore, the M1/ M2 characterisation of microglial phenotype is deemed too simplistic and microglial phenotypes are suggested to be 'multi-dimensional' (Ransohoff, 2016). This concept is supported by recent single cell sequencing studies identifying diverse microglia activation states distinct from those induced by polarising stimuli including LPS and IL4 throughout development and disease (Hammond et al., 2019, Masuda et al., 2019).

1.7 Microglia origin

Although the precise origin of microglia remained enigmatic for many years, recent lineage tracing and parabiosis studies suggest microglia derive from RUNX1+, CD45-, c-kit+ erythromyeloid progenitors of the yolk sac (Kierdorf et al., 2013, Ginhoux et al., 2010). These cells colonise the developing CNS on embryonic day 9.5 via the bloodstream and mature into microglia via a Myb independent, PU.1, interferon regulatory factor (IRF) 8 dependant mechanism (Kierdorf et al., 2013, Ginhoux et al., 2010). Microglia continue to colonise the CNS until formation of the BBB on embryonic day 13.5. Whilst initially amoeboid, microglia adopt a ramified morphology on embryonic day 14.5 and remain highly proliferative until birth at which point they acquire a unique microglial TGF-β-dependant gene signature (Kierdorf et al., 2013, Butovsky et al., 2014). Tightly coupled apoptosis and proliferation maintain microglial populations throughout life (Askew et al., 2017). Recent single cell imaging also suggests microglia have a slow turnover with a median lifespan of over 15 months (Fueger et al., 2017).

Microglial differentiation and post-natal survival are critically dependant on colony stimulatory factor 1 receptor (CSF1R) function. Microglia are absent in *Csf1r-/-* mice and antibodies blocking CSF1R activity deplete developing microglia and macrophages (Ginhoux et al., 2010, Erblich et al., 2011, Hoeffel et al., 2015). *Csf1r-/-* mice also demonstrate brain abnormalities including ventricle enlargement, cortical thinning and olfactory hollowing (Erblich et al., 2011). Furthermore, mice carrying a mutation in colony stimulatory factor 1 (CSF1) (*Csf1*$^{op/op}$), a key ligand for CSF1R also demonstrate microglial depletion although less profound (Wegiel et al., 1998, Kondo, Lemere and Seabrook, 2007). This observation led to the suggestion that another CSF1R ligand exists resulting in the identification of IL-34. *Il-34-/-* mice similarly demonstrate less microglia however the impact of *Il-34* deficiency is region dependant suggesting IL-34 expression may differ spatially (Wang and Colonna, 2014).

In addition to CSF1 and IL-34, recent studies suggest TGF-β also plays a crucial role in microglial development. CNS TGFβ-/- mice demonstrate impaired microglial development from embryonic day 14.5 onwards with adult mice exhibiting reduced numbers of microglia with an amoeboid morphology (Butovsky et al., 2014). More recently, Buttgereit et al. (2016) demonstrated targeted deletion of microglial TGF-βR did not impact on microglial number but enhanced microglial reactivity suggesting TGF β signalling plays a key role in maintaining a microglial homeostatic phenotype rather than survival (Buttgereit et al., 2016). The transcription factor SALL1 is similarly suggested to be important for maintenance of homeostatic microglia as ablation of the *Sall1* gene locus induces an inflammatory phenotype associated with disturbed neurogenesis (Buttgereit et al., 2016).

1.8 Microglia in health and disease

It is becoming increasingly clear microglia play key roles in various homeostatic processes throughout development and adult life. Even though microglia are described as ‘resting’ under steady state conditions, *in vivo* two photon microscopy demonstrates microglia have highly motile processes which continuously contact astrocytes, blood vessels, axons, dendritic spines and neuronal cell bodies (Nimmerjahn, Kirchhoff and Helmchen, 2005, Wake et al., 2009, Tremblay, Lowery and Majewska, 2010).

Within the developing brain, microglia are suggested to play key roles in modelling of neuronal circuitry via synaptic pruning, a process in which synaptic structures are cleared by microglial phagocytosis. Using electron microscopy and two-photon imaging, Trembley et al. (2010) demonstrated microglial processes dynamically interact with synapses in the visual cortex in an activity dependent manner (Tremblay et al., 2010). Furthermore, microglia demonstrated increased cellular inclusions and phagocytosis of synaptic elements in response to sensory deprivation (Tremblay et al., 2010). Paolicelli et al. (2011) also demonstrated microglial mediated synapse engulfment and elimination in the hippocampus during development via STED and electron microscopy (Paolicelli et al., 2011). Furthermore, mice lacking *Cx3cr1* expression demonstrate defective synaptic pruning, excess excitatory synapses, impaired neural circuit maturation in addition to defective brain connectivity and behavioural abnormalities (Zhan et al., 2014, Paolicelli et al., 2011).

The classical complement cascade plays a key role in microglial-mediated synaptic pruning. Post-natal mice exhibit C1q and C3 deposition at synapses in the developing CNS and attenuated synapse elimination in the absence of C1q or C3 expression (Stevens, 2008). Signalling via microglial complement receptor 3 (CR3) is a key mechanism mediating synapse elimination during development as CR3 deficient mice demonstrate defective synaptic remodelling (Schafer et al., 2012). In addition to synapse elimination, microglia are also suggested to be crucial for learning- dependant synapse formation via release of BDNF (Parkhurst et al., 2013).

Microglia also regulate neuronal apoptosis and clearance throughout development. Microglial-derived ROS triggers neuronal apoptosis via a CD11B, DNAX activation protein of 12kD (DAP12) dependant pathway in the developing hippocampus (Wakselman et al., 2008). Marin-Teva et al. (2004) similarly demonstrated microglia actively induce Purkinje cell apoptosis in the developing cerebellum via ROS release (Marin-Teva et al., 2004). Furthermore, liposome and tetracycline- mediated depletion of fetal microglia *in utero* enhances the number of neural precursor cells in the developing cortex whilst maternal immune challenge and subsequent microglial activation attenuates the number of neural precursor cells providing key evidence

for microglia-mediated regulation of the neural precursor pool during neurogenesis (Cunningham, Martinez-Cerdeno and Noctor, 2013). Microglia also regulate adult neurogenesis via apoptosis coupled phagocytosis in the subgranular zone of the hippocampus (Sierra et al., 2010).

Recent studies suggest microglia are also important for myelogenesis. Following pharmacological depletion of microglia, OPCs are substantially reduced impacting subsequent myelogenesis during early postnatal development (Hagemeyer et al., 2017). Microglial depletion in the adult brain similarly reduces OPC number suggesting microglia also play a key role in OPC maintenance throughout development and adult life (Hagemeyer et al., 2017).

Given that microglia play numerous roles in maintenance of CNS homeostasis their dysfunction is suggested to contribute to a range of neurological conditions. Activated microglia are observed across all neurodegenerative diseases. However, it remains unclear whether neuroinflammation is a cause or consequence of neurodegenerative processes. Although it was originally believed neuroinflammation was mainly secondary to neurodegeneration, recent genome wide association studies (GWAS) identifying variants in several innate immune genes which increase susceptibility to neurodegenerative diseases provides key evidence for the role of neuroimmune dysfunction as a driver of neurodegenerative disease and dementia.

Amongst identified genes, mutations in triggering receptor expressed on myeloid cells 2 (TREM2) significantly increases the risk of developing AD similar to having one apolipoproteinE4 (APOE4) allele (Karch and Goate, 2015). In addition to increasing susceptibility to AD, TREM2 variants are also suggested to increase susceptibility to Parkinson's, frontotemporal dementia (FTD) and amyotrophic lateral sclerosis (ALS) (Guerreiro et al., 2013a, Rayaprolu et al., 2013, Cady et al., 2014). Furthermore, microgliopathies caused by homozygous loss of function mutations in microglial-enriched genes such as *CSF1R* in addition to *TREM2* cause leukodystrophies associated with demyelination, axonal pathology and pre-senile dementia providing key evidence that microglial dysfunction and neuroinflammation actively contribute to dementia pathogenesis.

1.9 TREM2

The importance of TREM2 in CNS homeostasis was first demonstrated by studies identifying homozygous loss of function mutations in TREM2 or its adaptor protein DAP12 causing NHD in which patients develop bone abnormalities and pre-senile dementia (Nasu, Tsukahara and Terayama, 1973, Kaneko et al., 2010, Hakola, 1972). Post-mortem studies report severe white matter degeneration characterised by extensive demyelination and axonal loss in addition to cortical atrophy associated with reactive gliosis. Mutations in TREM2 were first linked to NHD by Paloneva et al. (2003) and have since been replicated in several genetic studies (Paloneva, 2003, Soragna et al., 2003, Klunemann et al., 2006, Bock et al., 2013). NHD can also develop in the absence of bone abnormalities (Yamazaki et al., 2015). Furthermore, homozygous or heterozygous mutations associated with NHD can also cause FTD or frontotemporal lobar dementia (FTLD) (Le Ber et al., 2014, Guerreiro et al., 2013b, Giraldo et al., 2013).

Following this, genetic studies identified several rare TREM2 variants which increase the risk of developing AD. The R47H TREM2 variant has been repeatedly associated with increased AD risk and other variants have also been identified including R62H, D87N and H157Y (Guerreiro et al., 2013a, Jin et al., 2014, Jiang et al., 2016a, Ghani et al., 2016). Although the R47H TREM2 variant is consistently associated with AD risk it remains unclear how this contributes to clinical phenotype. While some studies suggest TREM2 R47H carriers demonstrate accelerated disease progression this has not always been replicated (Korvatska et al., 2015, Rajagopalan, Hibar and Thompson, 2013, Slattery et al., 2014). Similarly, studies have suggested TREM2 R47H is associated with premature disease onset whilst others have reported no association (Ruiz et al., 2014, Rosenthal et al., 2015). As the TREM2 R47H variant only occurs in a very small percentage of the population such studies are limited by small sample size. Therefore, a distinct clinical phenotype is yet to be identified in TREM2 R47H carriers.

TREM2 is located on human chromosome 6p21 and mouse chromosome 17C3 as part of a gene locus containing various TREM and TREM-like genes (Ford and McVicar, 2009). Although some genes within the TREM locus are highly conserved between humans and mice (e.g. *Trem1/TREM1* and *Trem2/ TREM2)*, others including *Trem3, Trem5* and *Treml6* are exclusively expressed by mice whilst expression of *TREML3* is limited to humans. Of the many genes within the TREM gene locus, triggering receptor expressed on myeloid cells 1 (TREM1) and TREM2 are best characterised. Whilst TREM1 is expressed by neutrophils, monocytes and microglia*,* TREM2 is expressed by dendritic cells, macrophages, microglia and osteoclasts (Bouchon, Dietrich and Colonna, 2000, Bouchon et al., 2001, Schmid et al., 2002, Turnbull et al., 2006).

Within the CNS, TREM2 expression is highly enriched on microglia. During development, TREM2 is detected as early as embryonic day 14 and continues to be expressed throughout adulthood. TREM2 expression fluctuates during early postnatal development in an age and region dependant manner (Chertoff et al., 2013). Furthermore, regional heterogeneity has also been detected in the adult CNS in both mice and humans with highest expression reported in the white matter and hippocampus (Chertoff et al., 2013, Forabosco et al., 2013).

Under steady state conditions, TREM2 is localised intracellularly on exocytotic vesicles and membranes of the Golgi network continuously shuttling between the cell membrane and cytoplasm in a beclin-1, Vps35 dependant manner (Prada et al., 2006, Lucin et al., 2013, Yin et al., 2016). Ionomycin stimulation and subsequent intracellular Ca2+ accumulation mimicking cell activation results in rapid redistribution of TREM2 to the cell membrane. TREM2 gene expression is also tightly modulated by inflammatory stimuli or damage. Treatment of human or murine microglia with inflammatory mediators such as LPS downregulates TREM2 expression whilst anti-inflammatory mediators such as IL-4 increase TREM2 expression (Owens et al., 2017). *In vivo,* TREM2 is downregulated in response to acute cerebral inflammatory challenges, whilst increased expression is observed in response to chronic CNS damage, inflammation and aging (Forabosco et al., 2013, Jiang et al., 2014b, Owens et al., 2017, Raha et al., 2017).

1.10 TREM2 protein structure and signalling

TREM2 exists as a single pass transmembrane protein with an extracellular V-type immunoglobulin (Ig) domain containing N-linked glycosylation sites followed by a short stork leading to a transmembrane helix and short cytoplasmic domain. A lysine residue in the transmembrane region of TREM2 associates with an aspartate residue on adaptor protein DAP12 via electrostatic interaction. DAP12 exists as a homodimer and contains an immunoreceptor tyrosine-based activation motif (ITAM) in its intracellular domain enabling downstream signalling upon receptor activation (Bouchon et al., 2000). In response to ligand binding, tyrosine residues in the ITAM motif of DAP12 are phosphorylated by Src kinases enabling binding of spleen tyrosine kinase (SYK) via SH2 domains. This initiates various downstream signalling cascades including mitogen-activated protein kinase (MAPK) activation, protein tyrosine phosphorylation, Ca2+ mobilisation and phosphoinositide 3 – kinase (PI3K) activation contributing to various cell processes including actin remodelling, proliferation, survival, phagocytosis and release of inflammatory mediators (fig. 1.4) (Colonna and Wang, 2016).

In addition to the membrane-bound form, a soluble form of TREM2 (sTREM2) is generated by proteolytic cleavage or alternative splicing. Membrane bound TREM2 is proteolytically cleaved in a sequential two step event. The ectodomain is first shed by a disintegrin and metalloproteinase domain-containing protein 17 (ADAM17) or ADAM10 producing sTREM2 and the remaining intracellular domain is subsequently cleaved by γ-secretase to produce C-terminal fragments (CTF) (Feuerbach et al., 2017). The precise role of sTREM2 remains controversial. It was originally suggested sTREM2 may act as a decoy receptor to attenuate TREM2 signalling. In support of this, Kim et al. (2005) demonstrated use of a chimeric TREM-Fc protein to model sTREM2 inhibited TREM2 mediated osteoclastogenesis (Kim et al., 2005). sTREM2 is also suggested to regulate additional biological functions including immunomodulation and microglial survival (Wu et al., 2015, Zhong et al., 2017).

In addition to sTREM2, recent studies propose TREM2 CTF may also regulate microglial function. In the absence of γ-secretase-mediated cleavage of TREM2, TREM2 CTF accumulates at the plasma membrane and sequesters DAP12 preventing interaction with full length TREM2 leading to reduced DAP12 phosphorylation and phospholipase Cγ (PLCγ) signalling (Wunderlich et al., 2013, Glebov et al., 2016). Glebov et al. (2016) subsequently demonstrated this was also associated with reduced microglial phagocytosis (Glebov, et al., 2016). Overexpressing TREM2 CTF in BV2 cells also reduces pro-inflammatory cytokine release following LPS stimulation suggesting TREM2 CTF contributes to immunomodulation (Zhong et al., 2015).

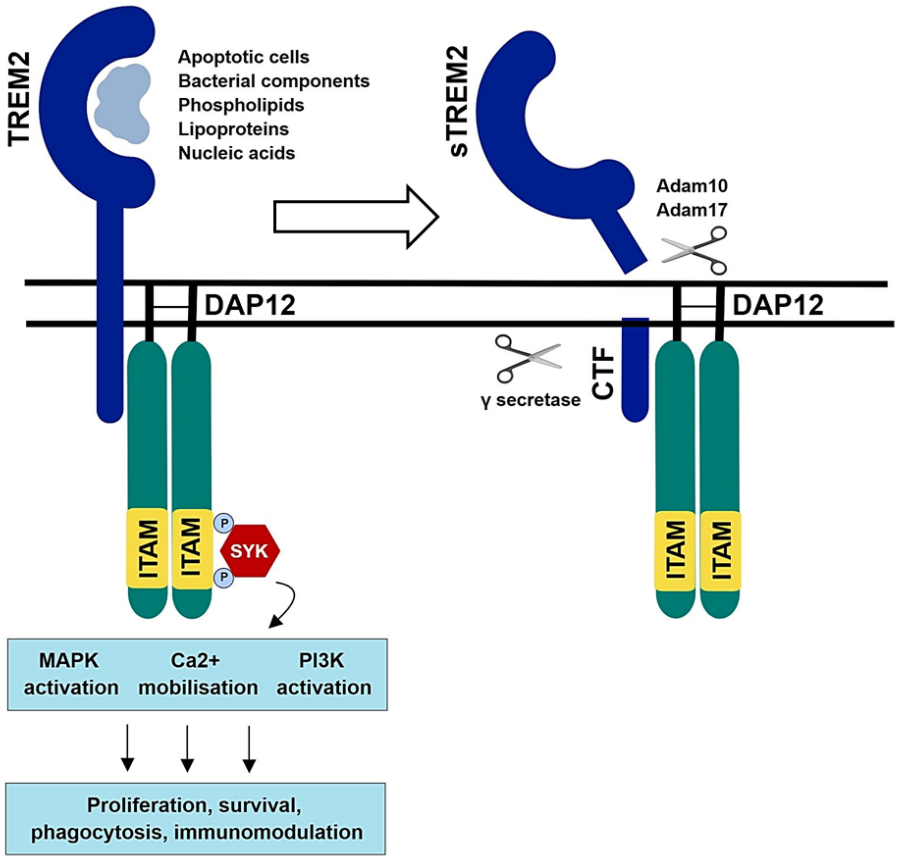

Figure 1.4: TREM2 signalling and cleavage. Upon ligand binding, DAP12 immunoreceptor tyrosine based activation motifs (ITAMs) are phosphorylated by Src kinases provided a binding site for SH2 domains of SYK resulting in various downstream signalling cascades (PI3K activation, Ca2+ mobilisation, MAPK activation) which regulate various cell processes including migration, proliferation, survival, phagocytosis and immunomodulation. sTREM2 is generated by ADAM10/ ADAM17 cleavage of the ectodomain while TREM2 CTF is generated by γ secretase-mediated cleavage of the transmembrane domain.

1.11 TREM2 ligands

TREM2 binds to a range of lipoproteins including ApoE, ApoA, low density lipoprotein (LDL) and clusterin. Bailey et al. (2015) first demonstrated TREM2 Ig fusion protein precipitates ApoE and ApoA from serum and cerebrospinal fluid (Bailey De Vaux and Farzan, 2015). ApoE was also shown to induce TREM2 signalling in a reporter cell line (Jendresen et al., 2017). Since discovering the interaction between ApoE and TREM2 it is suggested ApoE enables indirect TREM2-mediated recognition of CNS damage as ApoE binds to apoptotic cells and Aβ plaques. Subsequently, Yeh et al. (2016) demonstrated TREM2 also binds clusterin, ApoA, ApoB as well as low density lipoprotein via protein microarray (Yeh et al., 2016).

TREM2 is also suggested to bind a range of anionic molecules including phosphatidic acid, phosphatidylserine and cardiolipin (Cannon O'Driscoll and Litman, 2012, Kober et al., 2016). Studies utilising reporter cells also demonstrated lipids including sulfatide, sphingomyelin, phosphatidic acid, phosphatidylinositol, phosphatidylcholine and phosphatidyl stimulate TREM2 signalling (Wang et al., 2015, Poliani et al., 2015). Kawabori et al. (2015) also demonstrated TREM2 fusion protein binds to high molecular weight nucleic acids in the ischaemic brain via chromatin immunoprecipitation (Kawabori et al., 2015). Furthermore, treatment of reporter cells with purified deoxyribonucleic acid (DNA) induces TREM2 signalling (Kawabori, et al., 2015).

Mammalian cells and bacteria are also sources of TREM2 ligands. Initial studies demonstrated TREM2 fusion protein binds to a range of Gram-negative (*Staphylococcus aureus, Proteus mirabilis*) and Gram-positive (*Escherichia coli, Streptococcus pyogenes*) bacteria (Daws et al., 2003). Such binding was disrupted in the presence of LPS, dextran sulfate, peptidoglycan and lipoteichoic acid demonstrating TREM2 binds to a range of bacterial products (Daws et al., 2003, Phongsisay et al., 2015). Furthermore, TREM2 has also shown to bind to Pertussis toxin and cholera toxin (Phongsisay et al., 2015, Phongsisay et al., 2017).

Various mammalian cells including macrophages, THP-1 monocytes, dendritic cells, astrocytes and neurons are suggested to express endogenous TREM2 ligands (Hamerman et al., 2006, Hsieh et al., 2009, Ito and Hamerman, 2012, Kober et al., 2016, Daws et al., 2003). It was additionally shown induction of apoptosis increased TREM2 ligand expression on neuronal and non-neuronal cells. In response to apoptosis, TREM2 signalling and microglial phagocytosis were enhanced while this response was attenuated following treatment with an anti-TREM2 monoclonal antibody (Hsieh et al., 2009).

1.12 TREM2 function

1.12.1 Cell survival and proliferation

Various studies suggest TREM2 plays a key role in promoting cell survival and proliferation. Wang et al. (2016) demonstrated TREM2 knockdown induces S-phase cell cycle arrest and increased apoptosis in glioma cell lines and suppressed tumorigenesis *in vivo* (Wang et al., 2016a). Similar findings were also observed in a liver cancer cell line (Zhang et al., 2016). TREM2-/- cells also demonstrate reduced invasive and migratory ability suggesting TREM2 may regulate migration (Wang et al., 2016a). Otero et al. (2012) demonstrated TREM2 deficiency impairs CSF1-mediated activation and proliferation of osteoclast precursors via defective β-catenin signalling suggesting CSF1R and TREM2 signalling synergise to promote cell proliferation and survival (Otero et al., 2012). Otero, et al (2009) also showed that DAP12-/- macrophages demonstrate defective CSF1-mediated activation and proliferation *in vitro* associated with reduced β-catenin stabilisation (Otero et al., 2009). More recently, Zheng at al. (2017) demonstrated TREM2 deficiency prevents β-catenin stabilisation resulting in its degradation via RAC-alpha serine/threonine-protein kinase (AKT)/ glycogen synthase kinase 3 β (GSK3β) signalling leading to microglial cell cycle arrest, reduced proliferation and survival *in vitro* and *in vivo* (Zheng et al., 2017).

Reduced proliferation has also been demonstrated in animal models of demyelination and AD (Cantoni et al., 2015, Jay et al., 2017, Wang et al., 2016b). Furthermore, TREM2-/- microglia surrounding Aβ plaques demonstrate increased apoptosis (Wang et al., 2015). Decreased microglial clustering in areas of pathology is commonly observed in many TREM2-/- models of neurodegeneration highlighting the importance of TREM2 in maintaining microglial responses to noxious stimuli. However, it remains unclear if reduced microglial number is predominantly due to increased apoptosis or reduced survival.

1.12.2 Phagocytosis

Numerous studies suggest TREM2 plays a key role in modulating phagocytic capacity. Impaired phagocytosis of a wide range of substrates including apoptotic cells, pathogens and lipids has been demonstrated in the absence of TREM2 expression *in vitro* (Takahashi, Rochford and Neumann, 2005, Hsieh et al., 2009, Kleinberger et al., 2014, Yeh et al., 2016). Similarly, TREM2 is suggested to be important for clearance of myelin debris in response to demyelination and tissue resorption following middle cerebral artery occlusion (MCAO) *in vivo* (Takahashi et al., 2007, Kawabori et al., 2015, Poliani et al., 2015). TREM2 is also implicated in the uptake of Aβ as TREM2 knockdown or overexpression correlates with Aβ phagocytosis *in vitro* (Melchior et al., 2010, Jiang et al., 2014a). Similar findings have also been observed *in vivo* as TREM2-/- AD microglia demonstrate worsened Aβ burden (Wang et al., 2016b, Yuan et al., 2016). However, studies have also demonstrated no effect or reduced Aβ burden in the absence of TREM2 expression (Ulrich et al., 2014, Jay et al., 2015). Therefore, the precise role of TREM2 regulation of Aβ uptake remains unclear.

Interestingly, the impact of TREM2-mediated phagocytosis may be cell type specific. TREM2-/- bone marrow derived macrophages (BMDMs) demonstrated impaired uptake of *S. pneumoniae*, yet TREM2-/- alveolar macrophages demonstrated increased phagocytosis both *in vitro* and *in vivo* (Sharif et al., 2014). Furthermore, TREM2-mediated clearance may be influenced by mediators within the local microenvironment. While injection of BMDMs overexpressing TREM2 reduced mortality in response to polymicrobial sepsis, no such effect was observed in response to LPS challenge *in vitro* (Chen et al., 2013). Similarly, a similar

study showed that TREM2 expression positively correlates to Aβ phagocytosis and that this was greatly reduced by pre-treating TREM2 overexpressing microglia with LPS (Melchior et al., 2010).

Studies have also demonstrated TREM2 variants impact microglial phagocytosis. R47H impairs phagocytosis of fluorescent beads by BV2s (Yin et al., 2016). Furthermore, monocyte-derived macrophages expressing the R62H variant demonstrate reduced Aβ-LDL uptake *in vitro* (Yeh et al., 2016). Interestingly, it is suggested TREM2 variants may differentially impact recognition of different substrates. Although Y38C, R47H and T66M variants all impair phagocytosis of latex beads, R47H does not impair *E.coli* clearance (Kleinberger et al., 2014).

In addition to phagocytosis recent studies suggest TREM2 may also regulate lysosomal function. Cantoni et al. (2015) reported TREM2-/- microglia do not show defects in myelin uptake but instead demonstrate impaired degradation of internalised myelin (Cantoni et al., 2015). Similarly, Zhu et al. (2014) showed TREM2 deficiency did not impact internalisation of *Pseudomonas aeruginosa* but impaired bacterial killing via ROS release (Zhu et al., 2014). More recently, single cell sequencing of microglia from various disease models identified that TREM2 is required for the upregulation of lysosomal genes. Separate gene network analysis also demonstrated lysosome activity is associated with TREM2 in all human brain regions (Forabosco et al., 2013).

1.12.3 Immunomodulation

TREM2 is suggested to play a key role in modulation of inflammatory pathways in response to injury or infection. Although TREM2 is regularly described as ‘anti-inflammatory’ this is not always the case as both pro- and anti-inflammatory effect have been described. *In vitro* TREM2 knockdown generally enhances pro-inflammatory cytokine in response to a range of stimuli including Aβ, apoptotic cells, LPS and other TLR ligands such as zymosan and CpG (Turnbull et al., 2006). Furthermore, BV2 cells expressing the R47H variant demonstrate increased expression of pro inflammatory cytokines including IL-6 and TNF-α. In contrast,

overexpressing TREM2 reduces transcription of pro-inflammatory mediators (Jiang et al., 2016b, Jiang et al., 2014a).

In vivo studies also suggested TREM2 attenuates neuroinflammation however several studies suggest TREM2 actually amplifies neuroinflammation (Takahashi et al., 2007, Seno et al., 2009, Jiang et al., 2014b, Jiang et al., 2014a, Ren et al., 2018). TREM2-/- AD mice demonstrate reduced pro-inflammatory gene expression in the brain (Jay et al., 2017, Jay et al., 2015). Transcriptional analysis of TREM2-/- microglia demonstrate reduced transcription of several proinflammatory cytokines (Wang et al., 2015). Similar reductions in pro-inflammatory cytokine production have also been reported in models of stroke, MS, traumatic brain injury, lung infection and colonic mucosal injury (Sieber et al., 2013, Correale et al., 2013, Poliani et al., 2015, Sharif et al., 2014, Wu et al., 2015, Saber et al., 2017). In addition to gene expression, *in vivo* and *in vitro* studies have demonstrated TREM2-/- microglia exhibit an altered morphology with reduced cell somas and increased process length characteristic of microglia in their resting state (Kawabori et al., 2015, Wang et al., 2015).

In addition to modulation of microglia and macrophage responses, studies have demonstrated TREM2 also appears to modulate responses of other inflammatory cell types including T cells and astrocytes. TREM2-/- animals demonstrate reduced astrocyte coverage as assessed by glial fibrillary acid protein (GFAP) in models of AD and demyelination (Cantoni et al., 2015, Jay et al., 2017, Jay et al., 2015, Leyns et al., 2017). In contrast, Saber et al.(2017) found TREM2 deficiency did not impact GFAP coverage in a model of traumatic brain injury (Saber et al., 2017). Similarly, Kawabori et al. (2015) demonstrated a modest reduction in GFAP coverage in TREM2-/- mice in response to MCAO suggesting TREM2-mediated regulation of astrocytes may be context dependant (Kawabori et al., 2015).

A separate study investigating the impact of TREM2 deficiency on neuroinflammatory responses after MCAO demonstrated reduced infiltration of peripheral T cells suggesting TREM2 may regulate leucocyte recruitment to the CNS (Sieber et al., 2013). Although unclear, TREM2 may also regulate microglial antigen presentation. Bouchon et al. (2001) demonstrated TREM2 activation upregulates expression of various antigen presentation

molecules on immature dendritic cells required for T cell activation following LPS stimulation including major histocompability complex class II (MHCII), CD40, B7.1, B7.2 CCR7 (Bouchon et al., 2001). Microglia demonstrate upregulation of MHCII but no other antigen presentation molecules upon TREM2 stimulation *in vitro* suggesting TREM2 may initiate distinct antigen presenting functions in microglia compared to peripherally derived myeloid cells (Melchior, Puntambekar and Carson, 2006). By coculturing BV2 cells with CD4+ T cells, Melchior et al. (2010) also demonstrated TREM2 expression correlated with enhanced T cell proliferation and cytokine production *in vitro* suggesting TREM2 may play a key role in initiating adaptive responses (Melchior et al., 2010). However, whether this is observed *in vivo* is yet to be established.

1.12.4 Metabolic adaptation

In addition to immunomodulation, TREM2 was recently shown to play a key role in metabolic adaption. Using a combination of ribonucleic acid (RNA) sequencing and metabolomics, Ulland et al. (2017) demonstrated TREM2 deficiency impairs BMDM ATP generation, glycolysis and anabolic metabolism particularly following growth factor withdrawal via attenuated mammalian target of rapamycin (mTOR) signalling resulting in increased autophagy (Ulland et al., 2017). Confocal and electron microscopy also demonstrated increased autophagic vesicles in microglia surrounding Aβ plaques in TREM2-/- AD mice as well as AD patients with R47H or R62H variants characteristic of metabolic stress (Ulland et al., 2017). It is therefore postulated TREM2-mediated mTOR activation is required for maintenance of microglia in a high metabolic state following cell activation. In its absence, microglia cannot initiate an appropriate response to stimuli due to impaired energy production. TREM2 regulation of metabolism is further supported from neuroimaging studies demonstrating NHD patients exhibit reduced glucose metabolism (Ueki et al., 2000). Furthermore, TREM2 T66M mice lacking cell surface TREM2 expression demonstrate fewer microglia compared to wild type (WT) controls associated with reduced glucose metabolism (Kleinberger et al., 2017).

1.12.5 TREM2 during basal conditions

Given that TREM2 causes NHD in humans, characterised by bone abnormalities, severe demyelination and pre-senile dementia, TREM2-mediated microglial reactivity clearly plays an important role in maintenance of CNS homeostasis. Although few studies have been conducted investigating the impact of TREM2 deficiency in the brain during basal conditions, current data suggests TREM2 deficient mice do not develop CNS pathology akin to humans with NHD.

Unpublished data from the McColl lab has demonstrated TREM2 deficient mice show no overt difference in gross white or grey matter integrity or differences in microglial/ astrocyte number across several brain regions compared to WT mice. In addition, Kang et al. (2018) demonstrated TREM2 deficiency does not alter behavioural or cognitive performance in 6 month old mice during basal conditions. However, RNA sequencing of hippocampal tissue demonstrated alterations in pathways relating to inflammation and chemotaxis of immune cells (Kang, et al., 2018). In a separate study, Filipello, et al. (2018) demonstrated TREM2 appears to play an important role in early brain development. Young TREM2-/- mice exhibit reduced ionised calcium binding adaptor protein 1 (IBA1)+ cell density in the hippocampus associated with impaired synapse elimination. Interestingly, this was associated with impaired functional connectivity between brain regions and decreased sociability in the absense of cognitive deficits (Filipello, et al., 2018). Therefore, whilst TREM2 deficiency appears to alter impact synaptic elimination during development and alter inflammatory pathways at the transcriptomic level, this is not associated with overt CNS pathology comparable to that observed in Nasu Hakola disease.

Given that the mouse life span is much shorter than that of humans it could be postulated mice do not live long enough to develop pathology comparable to that observed in NHD. Furthermore, as mice used in the above studies were relatively young, it could be argued pathology develops at much later stages. Therefore, future studies phenotyping TREM2 deficient aged mice are required.

1.13 TREM2 in neurodegenerative disease

As TREM2 variants have been demonstrated to increase the risk of dementia, various models of neurodegenerative disease have been implemented in animals in which TREM2 expression has been manipulated to understand how TREM2 regulates microglial function in the context of disease.

1.13.1 Alzheimer's disease

The role of TREM2 in neurodegenerative disease has most frequently been investigated in animal models which develop amyloid or tau pathology mimicking AD. Studies investigating the impact of TREM2 deficiency on Aβ plaque burden have yielded mixed finding with studies demonstrating reduced, increased or no change in amyloid pathology. While the reasons for observed discrepancies were originally unclear it is suggested use of different animal models and time of analysis may explain contrasting observations. Wang et al. (2015) demonstrated TREM2 deficiency increased plaque burden in 8 month 5XFAD while Jay et al. (2015) demonstrated reduced plaque burden in 4 month APP/PS1 (Jay et al., 2015, Wang et al., 2015). Subsequent studies in 8 month APP/PS1 mice demonstrated worsened Aβ plaque burden demonstrating TREM2 may play divergent roles at early and late stages of disease (Jay et al., 2017). Furthermore, while *in vivo* over expression of TREM2 is associated with reduced Aβ plaque load, neuropathology and cognitive impairment in 7 month APP/PS1 mice this effect is lost in older 18 month mice (Jiang et al., 2017b, Jiang et al., 2014a). Microglia from aged mice showed diminished phagocytosis of Aβ attributed to reduced expression of Aβ-binding receptors which could not be rescued by TREM2 overexpression *in vitro* (Jiang et al., 2017b). Given that the effects of TREM2 on Aβ appear to be somewhat dependant on microglial phagocytic function such studies suggest potential therapeutic interventions targeting TREM2 should be implemented earlier in the disease process.

Although studies investigating the impact of TREM2 on Aβ burden report inconsistent results, reduced clustering of microglia around Aβ plaques is commonly observed suggesting TREM2 is required for microglia to detect and contain Aβ plaques. TREM2 is suggested to play a key role in enabling microglia to detect and surround Aβ plaques forming a barrier-like structure. Using high resolution confocal and super resolution microscopy, Yuan et al. (2016) observed TREM2-enriched microglial processes enveloping amyloid fibrils and early-stage Aβ plaques preventing outward extension. In TREM2 or DAP12 haploinsufficient mice this barrier function was impaired resulting in reduced plaque compaction associated with greater neuronal dystrophy and tau hyperphosphorylation (Yuan et al., 2016). Importantly, AD patients carrying R47H variants similarly demonstrate reduced plaque compaction associated with increased neuronal dystrophy compared to control AD patients (Yuan et al., 2016). It is therefore suggested TREM2 serves a neuroprotective function by reducing surface area of neurotoxic amyloid fibrils and exposure to surrounding neurons.

Although impact of TREM2 deficiency on tau pathology is less well studied similar discrepancies have been observed. In response to TREM2 deficiency, both increases and decreases in phosphorylated tau accumulation have been observed in dystrophic neurites surrounding Aβ plaques in AD mouse models (Jay et al., 2015, Wang et al., 2015, Wang et al., 2016). TREM2 knockdown exacerbates tau pathology in P301S mice whilst overexpression attenuates pathology suggesting TREM2 confers neuroprotection to tau-related pathology (Jiang et al., 2015, Jiang et al., 2016). Although the precise mechanisms by which TREM2 confers protection to tau require further study, protective effects are attributed to attenuation of neuroinflammation and suppression of tau kinases cyclin dependant kinase 5 (CDK5) and GSK3β. In a separate tauopathy model (PS19), Leyns et al. (2017) demonstrated TREM2 deficiency had no impact of tau accumulation but reduced neuroinflammation and neurodegeneration (Leyns et al., 2017). Similarly, Sayed et al. (2018) demonstrated TREM2 deficiency had no impact on tau pathology and protected from brain atrophy due to reduced neuroinflammation (Sayed et al., 2018). Interestingly however, TREM2 haploinsufficiency increased tau pathology and was associated with worsened

neuroinflammation and brain atrophy suggesting TREM2 deficiency or haploinsufficiency yield differential effects on microglial function and tau pathology (Sayed et al., 2018).

1.13.2 Demyelination/ remyelination

Studies investigating the role of TREM2 in the context of MS similarly demonstrate attenuated microgliosis in areas of white matter damage in TREM2-/- mice. In the cuprizone model of demyelination, Poliani et al. (2015) demonstrated TREM2 deficiency impaired clearance of myelin debris and subsequent remyelination leading to persistent demyelination (Poliani et al., 2015). Immunohistochemical analysis revealed that the extent of microgliosis was dampened and failed to resolve most likely due to accumulating myelin debris (Poliani, et al., 2015). Investigation of the microglial transcriptome revealed reduced expression of transcripts associated with microglial activation, lipid metabolism and phagocytosis (Poliani, et al., 2015). Similarly, Cantoni et al., (2015) demonstrated exacerbated white matter pathology in response to cuprizone treatment in TREM2-/- mice associated with defective microgliosis.

Investigation of white matter gene expression revealed TREM2 deficient mice failed to upregulate genes associated with lipid metabolism (Poliani et al., 2015). Interestingly, TREM2 deficiency did not impact myelin uptake by primary microglia. Instead it was suggested microglial degradation of internalised myelin was impaired as TREM2-/- microglia demonstrated accumulations of myelin debris containing phagosomes by electron microscopy (Cantoni et al., 2015). In a separate study, blocking TREM2 function in EAE similarly exacerbated CNS pathology whilst intravenous injection of TREM2 transduced BMDMs enhanced removal of degraded myelin, and ameliorated myelin and axonal pathology (Piccio et al., 2007, Takahashi et al., 2007).

1.13.3 Stroke

Several studies have also suggested TREM2 plays a key role in mediating microglial responses to cerebral ischaemia. Kawabori et al. (2015) demonstrated reduced tissue resorption and poorer functional recovery in TREM2-/- mice in response to MCAO (Kawabori, et al., 2015). Reduced microgliosis and phagocytosis of apoptotic cells were observed in areas of injury in addition to reduced microvessel density suggesting TREM2 may also play a key role in angiogenesis (Kawabori, et al., 2015). While Sieber et al. (2013) did not observe any difference in ischaemic lesion severity, microgliosis was reduced and investigation of pro-inflammatory genes demonstrated TREM2 deficiency attenuated inflammation in the sub-acute phase following MCAO associated with reduced CD3+ T cell infiltration (Sieber, et al., 2013). In contrast, Wu et al. (2017) demonstrated TREM2 gene silencing exacerbated neuroinflammation *in vitro* and *in vivo* whilst TREM2 overexpression attenuated neuroinflammation and limited neuronal apoptosis (Wu et al., 2017). More recently, Kurisu et al. (2018) demonstrated TREM2-/- mice exhibit impaired myeloid cell activation associated with greater infarct volume and reduced functional recovery (Kurisu et al., 2018). Interestingly, transplantation with WT bone marrow failed to ameliorate deficits associated with TREM2 deficiency suggesting TREM2 expression on CNS resident microglia plays a key role in mediating recovery following MCAO (Kurisu, et al., 2018).

1.13.4 Disease associated microglia

Recent single cell RNA sequencing in models of AD, ALS and aging identified a subset of microglia named disease associated microglia (DAM). DAM are characterised by downregulation of homeostatic genes including *P2ry12, Tmem119, Cx3cr1, Cst3* and upregulation of genes associated with lysosomal function, phagocytosis and lipid metabolism such as *Lpl, Apoe, Axl* and *Trem2* (fig. 1.5) (Keren-Shaul et al., 2017). DAM are observed surrounding areas of pathology but are absent in unaffected regions. Microglia demonstrate similar DAM-like gene expression profiles across models of tauopathy and demyelination (Krasemann et al., 2017, Friedman et al., 2018). Furthermore, DAM markers are also observed in post-mortem AD brain suggesting the DAM phenotype may represent a conserved

microglial signature adopted in response to certain forms of CNS damage (Keren-Shaul et al., 2017). However, further work is required to conclude if microglia exhibit a similar phenotype across other contexts of neurodegenerative disease and determine whether this subset is beneficial or detrimental.

Importantly, recent findings demonstrate TREM2 signalling is necessary for microglia to fully acquire a DAM phenotype via ApoE signalling (Krasemann et al., 2017). In the absence of TREM2, microglia do not exhibit a DAM phenotype but instead display an intermediate phenotype suggesting TREM2 plays a key role in sustaining microglial activation (Keren-Shaul et al., 2017, Krasemann et al., 2017). Although future work is crucial for elucidating the precise function of DAM in the context of neurodegeneration, amplifying DAM function via TREM2 may represent a potential therapeutic strategy for the treatment of neurodegenerative diseases.

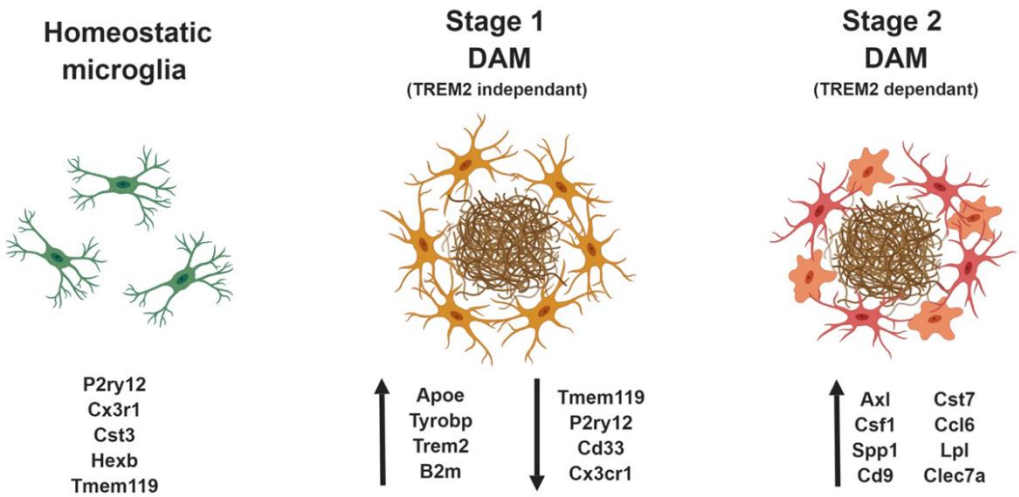

Figure 1.5: DAM induction. Microglia respond to CNS perturbation via a TREM2 independent mechanism of which the current signal is unknown, resulting in downregulation of homeostatic genes and upregulation of TREM2 adaptor/ regulator genes. A subsequent TREM2 dependant pathway ensues in which microglia upregulate several genes associated with phagocytosis, lipid metabolism and lysosomal pathways. Adapted from Keren-Shaul et al. 2017.

1.14 Summary and aims of thesis

Given that neuroinflammation and cerebrovascular dysfunction are suggested to play key roles in dementia pathogenesis it is crucial to determine how these processes converge to mediate neurodegeneration and cognitive impairment. Although neuroinflammation is implicated in VCI, the precise function of microglia and how they contribute to loss of white matter integrity and cognitive impairment remains unclear. Furthermore, it remains unknown if microglia exclusively contribute to the neuroinflammatory response or if peripherally derived leucocytes also play a role. It is therefore crucial to characterise the cellular and molecular neuroinflammatory profile and elucidate how this may contribute to disease pathogenesis.

As neuroinflammation is suggested as a key mechanism contributing to white matter damage and cognitive impairment modulation of the neuroinflammatory profile could influence disease trajectory. TREM2 regulates several microglial functions including sensing of CNS perturbation, immunomodulation as well as clearance of damage and debris across various neurodegenerative disease settings. However, it is currently unknown how TREM2 functions in the context of chronic cerebrovascular dysfunction. As treatments are currently lacking for the treatment of cSVD and other dementias, modulation of TREM2 activity offers a promising therapeutic strategy. It is therefore crucial to gain a better understanding of TREM2 function to identify potential mechanisms which could be modulated to promote pro-regenerative functions whilst limiting detrimental neuroinflammation in the context of cSVD as well as other causes of cognitive impairment and dementia.

The overall aim of this thesis was therefore to define key elements of the temporal cellular and molecular neuroinflammatory profile in an experimental model of chronic cerebral hypoperfusion. Using this model, we also aimed to investigate how TREM2 deficiency impacts neuroinflammation and white matter damage. It was hypothesised chronic cerebral hypoperfusion would impact detrimentally on myelin integrity and induce inflammation. It was further hypothesised that TREM2 deficiency would affect this response and exacerbate white matter damage.

1.15 Aims

To address the above hypothesis, the thesis investigated the following aims:

1. Develop and optimise the BCAS model of chronic cerebral hypoperfusion to precipitate robust white matter pathology.
2. To characterise the temporal cellular and molecular neuroinflammatory profile resulting from chronic cerebral hypoperfusion.
3. To determine the impact of TREM2 deficiency on white and grey matter pathology and neuroinflammatory profile in response to chronic cerebral hypoperfusion.

Chapter 2:

Methods

2.1 Mice

Male mice were used throughout (ages are provided in relevant results chapters). Wild type and TREM2-/- C57Bl/6Ntac mice were bred in house, and imported C57Bl/6J mice (Charles Rivers, UK) were housed in cages of up to five under temperature (19-24 ^{o}C) and humidity (55 % ± 10 %) controlled conditions. Mice were on a 12 h light (7:00 – 19:00) dark (19:00-7:00) cycle and given *ad libitum* access to food and water. All procedures were carried out at the University of Edinburgh under the authority of UK Home Office project and personal licenses and in accordance with the Animals (scientific procedures) Act 1986 and European Directive 2010/ 63/ EU.

2.2 Generation of TREM2 deficient mice

TREM2-/- mice (Trem2tm1(KOMP)Vlcg) were generated on a C57BL/6Ntac background and imported from the UC- Davis Knock-Out Mouse Project (KOMP) and bred in-house. Litters derived from TREM2+/- mice were utilised to generate TREM2+/+ and TREM2-/- breeding pairs to maintain genetic diversity and subsequent litters were used for experiments. Loss of TREM2 expression was achieved by introducing a velocigene ZEN-Ub1 reporter cassette into the TREM2 locus via homologous recombination creating a deletion size of 5485 base pairs in chromosome 17 between 48485765 and 4849349 replacing exons 2 and 3, as well as the majority of exon 4 (fig. 2.1).

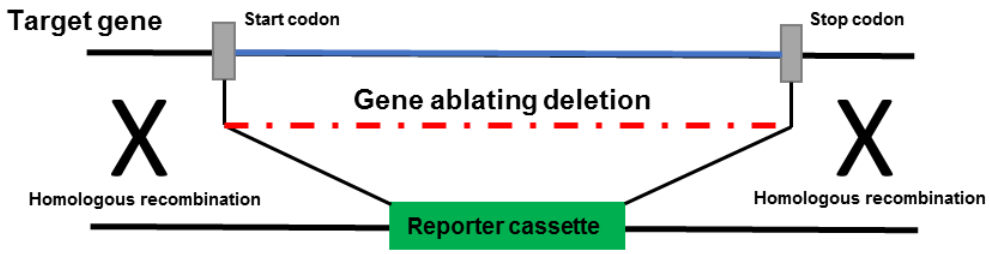

Figure 2.1: Method of gene deletion to generate TREM2-/- mice. The ZEN-Ub1 reporter cassette is inserted into the *Trem2* gene locus via homologous recombination creating a deletion size of 5485 base pairs in chromosome 17 replacing exons 2 and 3 and the majority of exon 4.

2.3 Genotyping of the TREM2 colony

Ear notches were obtained from litters derived from TREM2+/- breeding pairs to conduct genotyping and distinguish TREM2+/+, TREM2+/- and TREM2-/- mice for subsequent breeding pair generation and colony management. DNA was isolated using a DNeasy Blood and Tissue kit (Qiagen) following manufacturer's instructions. Firstly, tissues were digested in 180 µl buffer RLT and 20 µl proteinase K overnight on a shaker at 55 ^{o}C. Digested samples were then combined with 200 µl buffer AL and vortexed before adding 200 µl 100 % ethanol. Samples were vortexed again and transferred to a DNeasy Mini spin column placed in a 2 ml collection tube and centrifuged at 6000 g for 1 min at room temperature (RT). The flow through and collection tube were discarded and the spin column was placed in a new 2 ml collection tube. 500 µl buffer AW1 was added to the spin column and samples were centrifuged for 1 min at 6000 g at RT. The flow through and collection tube were again discarded and the spin column was placed in a new 2 ml collection tube and 500 µl buffer AW2 was added to the spin column and samples centrifuged at 20,000 g for 3 min at RT. The flow through and collection tube were discarded and the spin column was placed in a sterile 1.5 ml eppendorf and 200 µl buffer AE added to the spin column. Spin columns were incubated for 1 min at RT and centrifuged for 1 min at 6000 g at RT to elute DNA. The flow through was then re-added to the spin column and centrifugation repeated to maximise DNA yield. DNA samples were then stored at 4 ^{o}C prior to amplifying via polymerase chain reaction (PCR). For the PCR reaction, previously designed primers (Sigma) (table 2.1) were utilised to detect and amplify TREM2+/+, TREM2+/- and TREM2-/- DNA segments.

Per sample, 1 µl DNA was combined with 48 µl JAX megamix blue (Clent Life Science) and 0.5 µl forward and 0.5 µl reverse primer. A water only control was also included to ensure reagents were not contaminated with DNA. Samples were then briefly centrifuged and added to a T100 thermocycler (Bio Rad) to amplify DNA (table 2.2).

Primers	Sequence 5’ – 3’	Product length (bp)
TREM2+/+ forward strand	CCTTGTGTCCTTGAACCAGC	200
TREM2+/+ reverse strand	AAGGGAGGCTGGTAGAGAGA	
TREM2-/- forward strand	GCAGCCTCTGTTCCACATACACTTCA	598
TREM2-/- reverse strand	ATCTCAGACTGCATTCTCCCACTCC	

Table 2.1: Oligonucleotide sequences of primers used to identify WT, TREM2+/- and TREM2-/- mice.

Stage	Temperature (^{o}C)	Time	Cycles
Initial denaturation	95	3 min	1
Denaturation	95	30 sec	30
Annealing	60	30 sec	
Elongation	72	45 sec	1
Final extension	68	10 min	1

Table 2.2: Thermal profile for DNA amplification.

Once the PCR had finished DNA expression of TREM2 or the inserted reporter cassette in TREM2-/- mice was detected based on fragment size distinction via gel electrophoresis (fig. 2.2). A 1.5 % agarose gel was created by combining molecular grade agarose (Bioline) with 1X TBE buffer and heating in a microwave. Once the agarose had dissolved 1X DNA SYBRsafe (Cambridge Bioscience) was added to visualise DNA bands. The solution was then poured into an electrophoresis tank containing fitted combs to create sample chambers and left to set. Once set, combs were removed and the gel was submerged in 1X TBE buffer. Sample was then added to each well and a 100 bp DNA ladder (New England BioLabs) was included to determine band size. Sixty volts was applied and DNA samples were allowed to migrate across the gel for 45 minutes. Gels were then placed in a D-DiGit™ gel scanner (Li-Cor) to visualise bands and determine genotype.

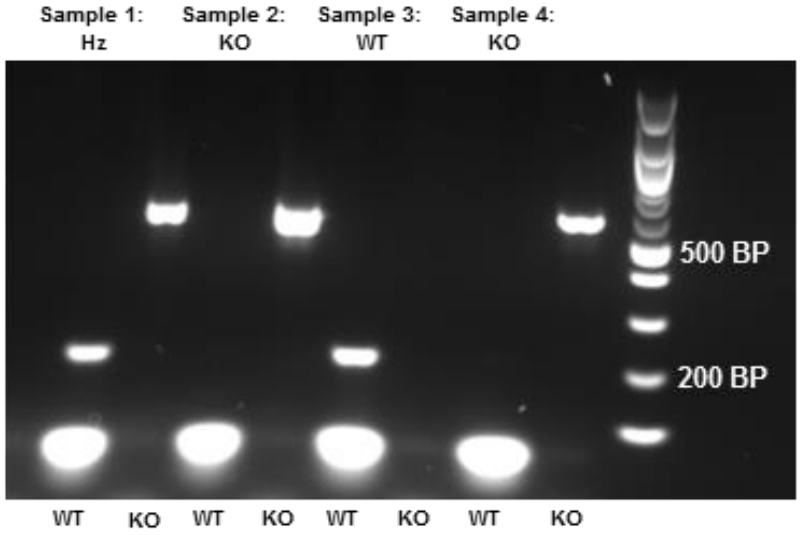

Figure 2.2: Gel electrophoresis of TREM2+/+, TREM2+/-, TREM2-/- DNA. TREM2+/+ mice are identified by a single 200 bp product in lanes detecting the *Trem2* gene only. In TREM2+/- mice, an additional 598 bp product is observed in lanes detecting the inserted reporter cassette. In TREM2-/- mice, a single 598bp band is observed only in lanes detecting the inserted reporter cassette.

2.4 Surgical Procedures

2.4.1 Bilateral common carotid artery stenosis

BCAS was conducted to induce chronic cerebral hypoperfusion in mice (fig. 2.3). Mice were anaesthetised in an induction chamber with 5 % isoflurane in O_2 (200 ml/ min) and N_2O (500 ml/ min) and then transferred to a face mask where anaesthesia was maintained at 2 % isoflurane in O_2 (200 ml/ min) and N_2O (500 ml/ min). The neck region of mice was shaved and treated with iodine, and a drape was placed over mice to maintain sterility. Temperature was maintained between 36.5 – 37.5 ^oC using a rectal probe and heat mat. A midline cervical incision was first made and each common carotid artery was dissected from overlying connective tissue. Two 4-0 suture threads were placed beneath the left common carotid artery and lifted to expose a portion of the artery inferior to the common carotid artery bifurcation. Induction of anaesthesia and exposure of carotid arteries prior to microcoil placement was conducted within 20 min. A microcoil (Sawane Spring Company, Japan) with an internal diameter of either 0.16 mm or 0.18 depending on the specific experiment was then placed on the left carotid artery by wrapping the artery around the coil. Wrapping carotid arteries around microcoils was conducted within 5 min to minimise ischaemic damage. The wound site was then sutured and treated with 4 % lidocaine (LMX4) (w/ w) and mice were recovered in a 30 ^oC chamber for 30 min. Mice were then re-anaesthetised and the same procedure was conducted on the right carotid artery. The wound site was then sutured and treated with 4 % lidocaine (LMX4) (w/ w) again.

Mice were then given 20 µl/ g saline subcutaneously and recovered in a 30 ^oC incubator for 1 h. For the first 72 h of recovery, mice were weighed twice daily and provided 20 µl/ g saline subcutaneously once daily to maintain hydration. Following this, mice were weighed twice a week and their welfare evaluated by assessing posture, motility/ exploratory behaviours in addition to ability to eat and drink. Mice demonstrating signs of overt focal brain damage immediately after surgery including circling or barrel rolling were euthanised. Mice demonstrating persistent laboured breathing and lack of movement after 72 h or weight loss greater than 30 % were also euthanised.

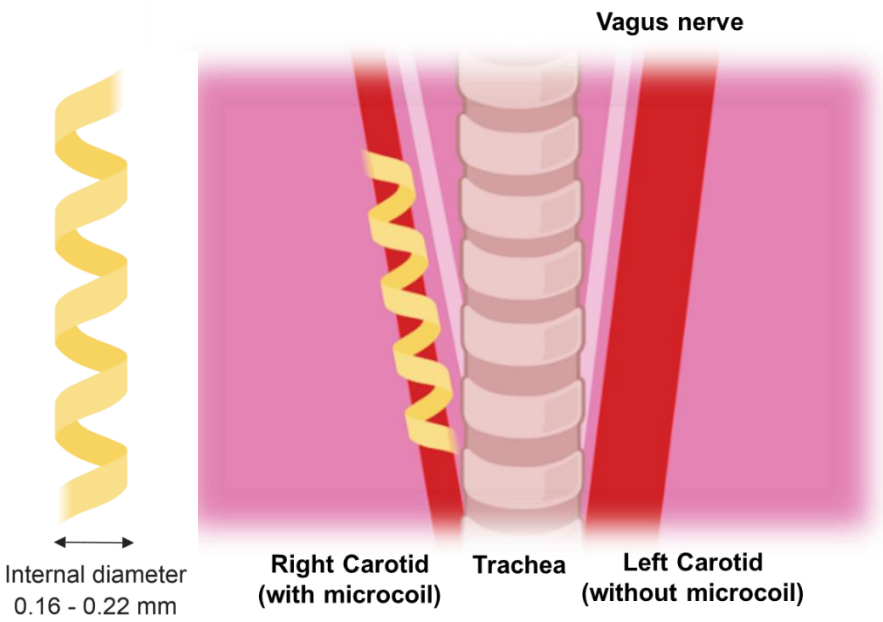

Figure 2.3: BCAS as a model of chronic cerebral hypoperfusion. Chronic cerebral hypoperfusion was achieved by placing microcoils with internal diameters ranging from 0.16 – 0.22 mm around the common carotid arteries of mice resulting in vessel narrowing and cerebral hypoperfusion.

2.4.2 Laser speckle contrast imaging

Laser speckle flowmetry was conducted to assess cerebral blood flow changes in blood vessels on the cortical surface of mice following BCAS or sham surgeries. When laser light illuminates a surface the backscattering of light creates an interference pattern known as speckle pattern. The speckle intensity will change depending on movement of the illuminated object such as red blood cells moving through a blood vessel therefore enabling quantification of blood flow. TREM2+/+ and TREM2-/- mice were anaesthetised in an induction chamber with 5 % isoflurane in O_2 (500ml/ min). Mice were then transferred to a stereotaxic frame and ventilated with a nose cone at 150 breaths per min with 3 % isoflurane in O_2 (500 ml/ min). Mice were secured in place with ear and nose bars and temperature monitored and maintained between 36.5 ^oC – 37.5 ^oC using a rectal probe and heat mat. A midline incision was first made across the scalp and skin deflected to reveal the skull. A thin film of ultra sound gel pre-warmed to 37 ^oC was applied to the skull to prevent drying. Cerebral blood flow was then recorded using a laser speckle contrast imager (Moor FLPI2 Speckle Contrast Imager, Moor Instruments, UK) for 2 min. The wound was then sutured and treated with 4 % lidocaine (LMX4) (w/ w) and mice were placed in a 30 ^oC recovery chamber for 1 h.

Speckle contrast images were then analysed using MoorFLPI-2 Review software (version 4.0). Regions of interest were placed across forebrain regions supplied by the middle cerebral artery on left and right hemispheres and mean flux was calculated over the period of a minute across each recording (fig. 2.4). Mean flux values recorded at 24 h and 28 d were then divided by baseline values obtained prior to conducting BCAS surgery and multiplied by 100 to determine the percentage of cerebral blood flow reductions from baseline.

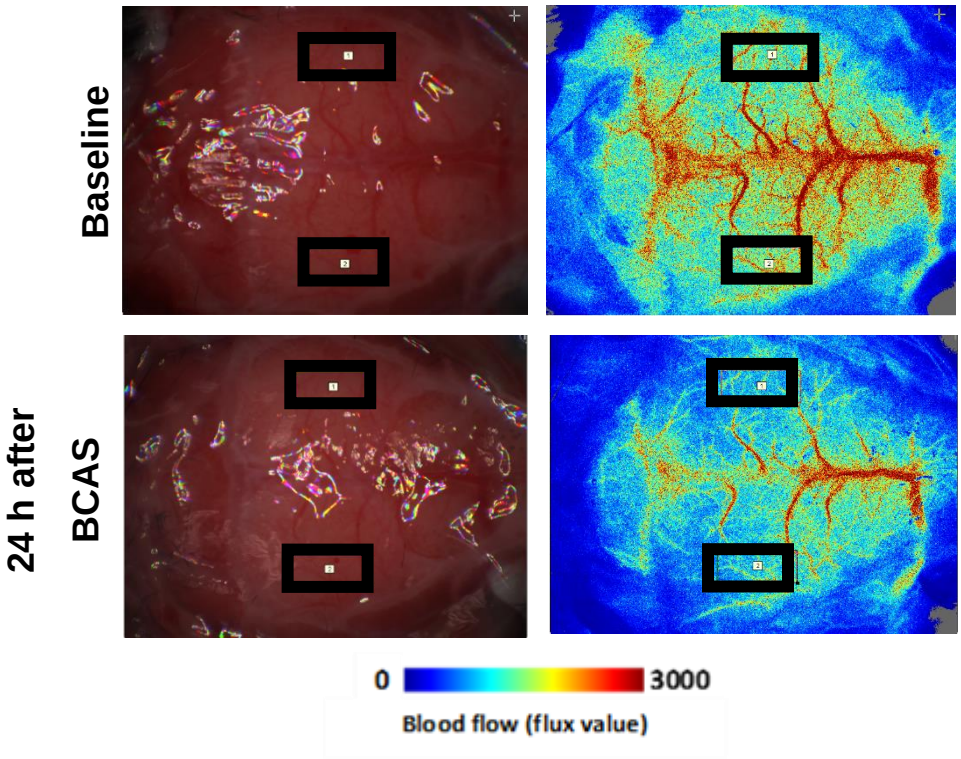

Figure 2.4: Laser speckle contrast image analysis. Bright field and speckle contrast images were used to place regions of interest on the mouse skull prior to, and after BCAS to obtain flux data on cortical perfusion in response to BCAS.

2.4.3 Transcardiac perfusion

Mice were terminally anaesthetised and saline perfused to minimise contamination of brain tissue with blood components. On the day of tissue harvest, mice were weighed and deeply anaesthetised with 5 % isoflurane in O_2 (200 ml/ min) and NO_2 (500 ml/ min) in an induction chamber. Mice were transferred to a face mask and anaesthesia maintained at 2 % isoflurane

in O_2 (200 ml/ min) and N_2O (500 ml/ min). A transverse incision was first made inferior to the sternum and connective tissue dissected to reveal the diaphragm. The diaphragm was then dissected and rib cage retracted to expose the thoracic cavity and heart. The right atrium was cut to allow outflow of blood. A 25G butterfly infusion needle was then carefully inserted into the apex of the left ventricle and animals were perfused transcardially with 20 ml saline containing 2 ml 3.8 % sodium citrate (w/ v) at a rate of 3 ml/ min. For microglial isolation experiments described in section 2.8, saline was additionally treated with 1 % diethyl pyrocarbonate (DEPC) (v/ v) (Sigma) to inhibit RNases. Once the perfusion was complete, brain tissue was extracted for downstream analyses.

2.5 Tissue processing for pathological assessment

For brain tissue used in pathological analyses, tissue was first post-fixed for 24 h in 4 % paraformaldehyde (PFA) (w/ v) (see appendix III) at 4 ^{o}C. If whole brains were used, brains were placed in a coronal matrix and separated into 4 mm rostral and 3 mm caudal portions. A MB35 premier microtome blade (ThermoScientific) was first placed at the junction between the olfactory bulb and cerebral cortex 3.58 mm anterior to bregma. A second microtome blade was then placed 0.56 mm posterior to bregma creating a rostral tissue portion and a final microtome blade was placed 3.56 mm posterior to bregma creating a caudal tissue portion. Olfactory and cerebellum tissues were discarded and rostral and caudal samples were dehydrated in a series of solvents by staff within Easter Bush Pathology (Veterinary Teaching Building) or the histology department (Shared University Research Facilities, The Queen's Medical Research Facility) over a 14 h period (table 2.3) and embedded in paraffin. A Leica RM2235 microtome was used to cut 6 µm thick coronal sections. Sections were then placed in a 40 ^{o}C water bath to remove tissue creases. Once removed, tissue sections were placed on super frost plus slides (Thermo Scientific) and dried overnight and stored at RT.

Treatment	Duration
70% ethanol	1 h
95% ethanol	1 h
Absolute ethanol	4x1 h
Xylene	3x1 h
Wax	3x 1 h 20 mins

Table 2.3: Processing schedule for paraffin embedded brain tissue.

2.6 Immunohistochemistry and histology

2.6.1 Immunohistochemistry

Sections were placed in xylene (Fisher Scientific) twice for 10 min each and submerged in decreasing concentrations of ethanol (99 %, 95 %, and 70 %) for 5 min each and rinsed in distilled H_2O (dH_2O) to rehydrate. Tissue sections requiring antigen retrieval were then placed in 0.01 M tri-sodium citrate antigen retrieval buffer (see appendix III) and heated in a Sharp 1000W R-21 ATP microwave for 10 min and cooled. All tissue sections were then treated with 0.3 % H_2O_2 (v/ v) (Sigma) in methanol (Fischer Scientific) for 10 min to block endogenous peroxidase activity. Sections were then rinsed with dH_2O and washed with 0.01 M phosphate buffered saline (PBS) (Sigma). 10 % normal serum (Vector) (v/ v) derived from the species of the secondary antibody in 0.01 M PBS containing 5 % bovine serum albumin (BSA) (Sigma) (w/ v) was used to block sections for 1 h at room temperature (RT). Sections were then treated overnight with primary antibody and 2 % normal serum in 0.01 M PBS (v/ v) or 2 % normal serum in 0.01 M PBS only to assess specificity of secondary antibodies at 4 ^{o}C (table 2.4) (fig. 2.5 – 6). The following day, sections were washed with 0.01 M PBS and treated with a biotin-conjugated IgG secondary antibody (Vector) for 1 h at RT (table 2.4). Sections were then washed with 0.01 M PBS and treated with avdidin-biotin peroxidase complex (Vector) for 30 min at RT. Following this, sections were washed with 0.01 M PBS and treated with 0.015 %

H_2O_2 + 0.5 mg/ ml DAB (Sigma) in dH_2O for 3 min. Once staining had developed, sections were washed with dH_2O. Sections were then placed in increasing concentrations of ethanol (70 %, 95 % and 99 %) for 3 min each to dehydrate and then xylene twice for 5 min. Coverslips were then applied using Pertex mounting medium (CellPath) and slides were left to dry. Representative images demonstrating IBA1, GFAP and MAG staining and secondary antibody specificity are shown in figures 2.5 – 2.6.

Antigen	Antigen retrieval	Primary antibody	Conc	Secondary antibody	Dilution
Ionised calcium binding adaptor protein 1 (IBA1)	+ (Tri-sodium citrate)	Rabbit anti-mouse IBA1 polyclonal (Wako)	200 ng/ ml	Biotinylated goat anti-rabbit secondary (Vector)	150 µg/ ml
Myelin association glycoprotein (MAG)	-	Mouse anti-mouse MAG monoclonal (Abcam)	14.3 ng/ ml	Biotinylated goat anti-mouse secondary (Vector)	150 µg/ ml
Glial fibrillary acidic protein (GFAP)	+ (Tri-sodium citrate)	Rat anti-mouse GFAP monoclonal (2.2B10) (ThermoScientific)	500 ng/ ml	Biotinylated goat anti-rat secondary (Vector)	150 µg/ ml

Table 2.4: Optimised conditions for immunostaining (IBA1, MAG & GFAP) in paraffin embedded brain tissue via immunoperoxidase-based detection.

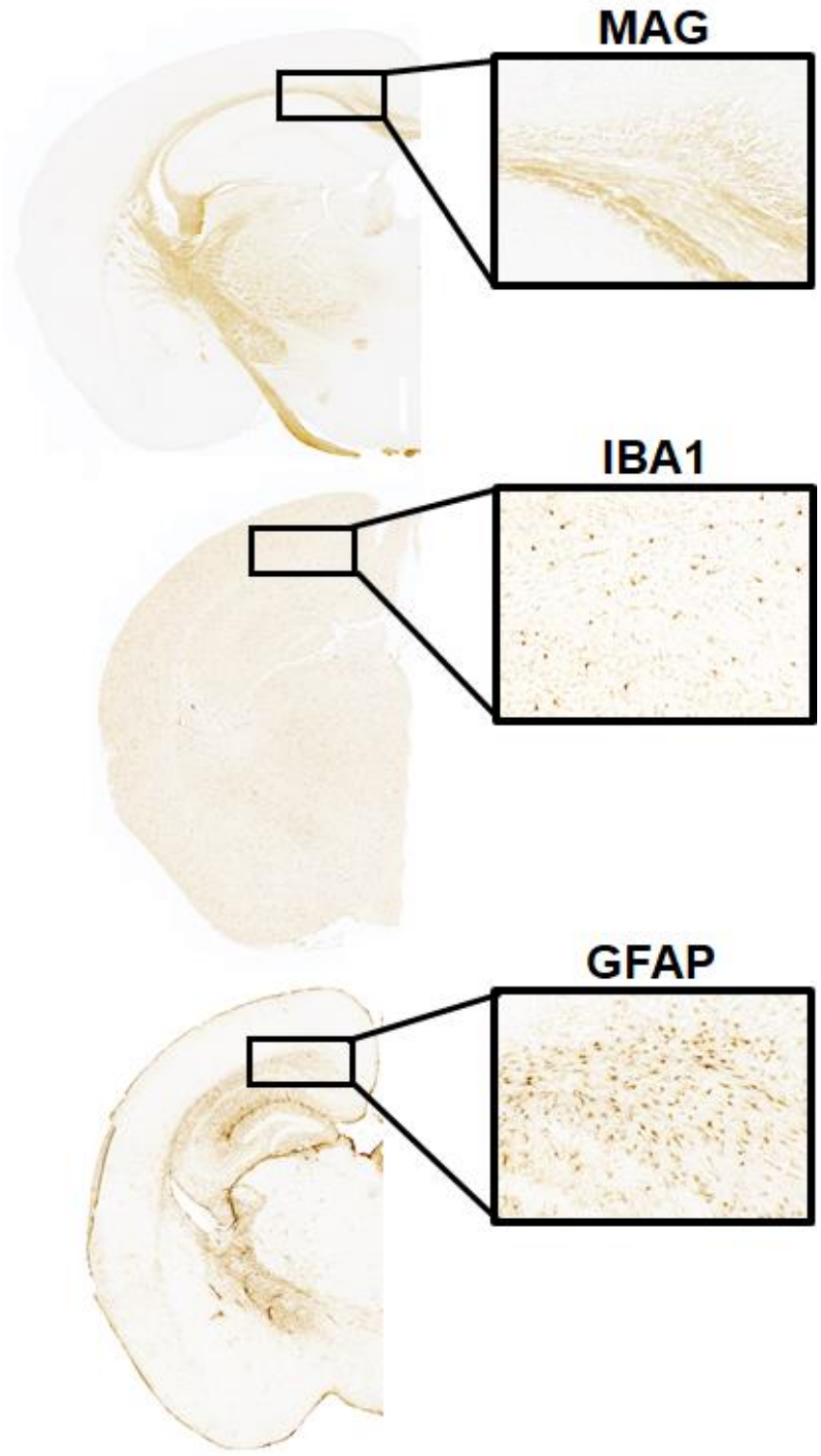

Figure 2.5 Representative low magnification images of MAG, IBA1 and GFAP immunostaining in paraffin embedded brain tissue via immunoperoxidase-based detection.

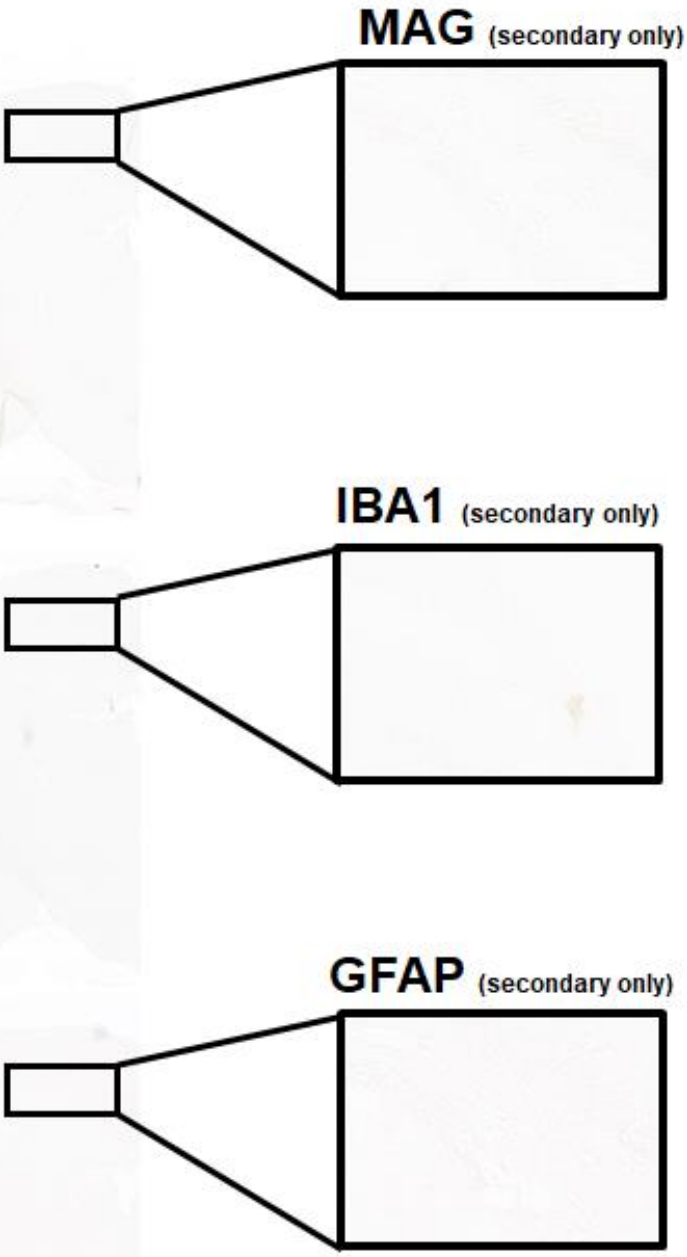

Figure 2.6: Representative low magnification images showing specificity of secondary antibodies to MAG, IBA1 and GFAP antibodies in paraffin embedded brain tissue via immunoperoxidase-based detection.

2.6.2 Myelin associated glycoprotein immunostaining quantification

Myelin associated glycoprotein (MAG) immunostaining was conducted to assess white matter integrity in response to BCAS. MAG is a glycoprotein expressed on distal portions of oligodendrocyte processes at the axon-glial interface. MAG is preferentially lost in response to ischaemic or inflammatory damage compared to other myelin components such as myelin basic protein (MBP) enabling detection of subtle white matter changes (Aboul-Enein, 2003). MAG immunostaining was analysed using a Nikon Brightfield light microscope or Zeiss Axio Imager 2 at 200 X magnification in regions of interest in one tissue section. Regions of interest were chosen and are described in respective results chapters. A semi-quantitative grading scale was implemented to quantify the extent of myelin damage in each white matter tract consisting of 0 (no white matter debris, vacuolation or disorganisation of white matter fibres), 1 (mild white matter debris, vacuolation and disorganisation of white matter fibres), 2 (moderate white matter debris, vacuolation and disorganisation of white matter fibres) and 3 (extensive white matter debris, vacuolation and disorganisation of white matter fibres) (fig. 2.7). If both hemispheres were analysed, severity scores of white matter regions from each hemisphere were summated providing a total possible score of 6. Scores from each white matter region were also summated to provide a total white matter damage score.

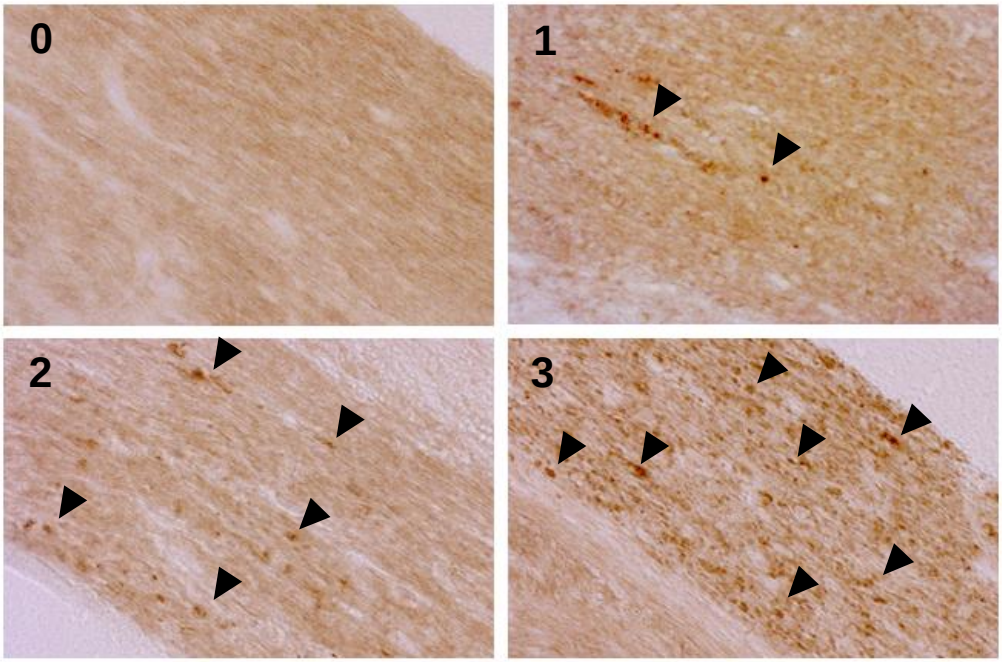

Figure 2.7: Assessment of myelin integrity using MAG immunostaining. In areas of white matter damage, myelin debris can be observed as darkened globular structures (black arrows) enabling quantification of the extent of myelin damage. A scoring method was utilised consisting of 0 (no white matter debris or disorganisation of white matter fibres), 1 (mild white matter debris and disorganisation of white matter fibres), 2 (moderate white matter debris, vacuolation and disorganisation of white matter fibres) and 3 (extensive white matter debris, vacuolation and disorganisation of white matter fibres).

2.6.3 Ionised calcium binding adaptor protein 1 and glial fibrillary acidic protein immunostaining quantification

Ionised calcium binding adaptor protein-1 (IBA1) is expressed by macrophages and microglia in the CNS and is upregulated following cell activation enabling investigation of microglial responses to CNS injury. On the other hand, GFAP is an intermediate filament protein almost exclusively expressed by astrocytes. Although astrocytes are widely distributed throughout the CNS, immunostaining primarily labels fibrous astrocytes of the white matter in the healthy brain. However, GFAP is upregulated in response to cell activation enabling assessment of reactive gliosis in response to CNS injury.

To investigate glial responses to BCAS, images of IBA1 and GFAP immunostaining were obtained from one brain section per animal on a Zeiss Axio Imager 2 or Axioscan slide scanner at 200 X magnification. IBA1+ cell bodies were quantified in each white matter region by placing 4 regions of interest measuring 0.1 – 0.2 mm^2 across each white tract per hemisphere using ImageJ software. If only one hemisphere was analysed IBA1+ cell bodies would be manually counted in four regions of interest per white matter region whilst if two hemispheres were analysed IBA1+ cell bodies would be manually counted in 8 regions of interest. Values from each region of interest were then averaged to provide the number of IBA1+ cells per 0.1 – 0.2 mm^2 in each white matter region. To quantify total IBA1+ cell number in whole brain sections, images of brain sections were first converted to 8-bit and thresholded to distinguish IBA1+ cell bodies from background on imageJ. The analyse particles plugin was then used to detect cell bodies and particle number was calculated to provide total IBA1+ cell counts in whole brain sections.

GFAP immunostaining was quantified in white matter regions by converting images to 8-bit and applying thresholding to distinguish GFAP from background staining and determining percentage area of staining in areas of interest. If two hemispheres were analysed, values obtained from white matter regions in left and right hemispheres were averaged. The same method of thresholding and quantification was also utilised to quantify total GFAP immunostaining in whole brain sections.

2.6.4 Histology

Adjacent tissue sections were stained with haematoxylin and eosin (H&E) to detect neuronal pathology. Tissue sections were first rehydrated as described in section 2.6.1 and placed in Harris' haematoxylin (TCS Biosciences Ltd) for 30 s. Tissue sections were then washed in dH20 and submerged in Scott's tap water (Leica Biosystems) for 30 s and washed in dH20 for 30 s. Sections were then placed in eosin (Leica Biosystems) for 3 min and rinsed in dH20 before placing in 70 % ethanol for 5 min, 95 % ethanol for 5 min, 99 % ethanol for 5 min and xylene twice for 5 min. Coverslips were applied using Pertex mounting medium and dried. Grey matter regions analysed included the hippocampus, cortex, thalamus, striatum and hypothalamus. Neuronal pathology was identified by condensation of nuclei, vacuolation and pallor within the parenchyma.

2.7 Flow cytometry

2.7.1 Preparation of a brain cell suspension

Flow cytometry was utilised to quantify changes in the immune cell composition of the brain following BCAS. Flow cytometry is a laser-based technique enabling multi-parameter analysis of cells. When cell suspensions are acquired by the cytometer they are aligned in sheath fluid so that cells pass laser light one cell at a time. Once the laser light contacts cells the forward and side scattering of light are detected providing information on both the size and granularity of cells, respectively. Furthermore, cell antigens can be labelled with fluorescent-conjugated antibodies which upon excitation with laser light at a particular wavelength, emit light. Fluorescence emission is then filtered and detected by sensors at a specific wavelength and converted into a digital value providing information on antigen expression.

Following transcardiac perfusion, brains were extracted and placed in a coronal matrix. The cerebellum and olfactory bulb were dissected and removed, and a portion of forebrain dissected and placed in 5 ml ice cold 1X Hank's buffered saline solution (HBSS) (without Ca^{2+} and Mg^{2+}) (Gibco, Life Technologies). Tissue was then diced finely using a scalpel and centrifuged at 400 g for 5 min at 4 ^{o}C. Supernatant was discarded and samples were incubated

in 10 ml enzyme cocktail (50 U/ ml collagenase type IV (Gibco, Life Technologies), 0.5 U/ ml dispase II (Gibco, Life Technologies), 200 U/ ml DNase I (Roche), 10µM tosyl-L-lysine chloromethyl ketone hydrochloride (TLCK) (Sigma) in 1X HBSS (containing Ca^{2+} and Mg^{2+}) (Gibco, Life Technologies) on a roller/ shaker for 1 h at 37 ^{o}C. 1 ml foetal bovine serum (FBS) (Gibco, Life Technologies) was then added to deactivate enzyme activity and digested brain tissue was transferred to a 15 ml Dounce tissue homogeniser on ice and manually homogenised using 20 passes of a loose fitting pestle. Homogenate was then transferred to a new 15 ml falcon and centrifuged at 400 g for 5 min at 4 ^{o}C with no brake. Supernatant was aspirated to waste and homogenate resuspended in 8 ml 35 % percoll (GE healthcare) in 1XHBSS (v/ v). To create this, 100 % isotonic Percoll was first made by diluting 10XHBSS (without Ca^{2+} & Mg^{2+}) (Gibco, Life Technologies) in percoll 10 fold. 100 % isotonic percoll was then diluted to 35 % with 1XHBSS (without Ca^{2+} & Mg^{2+}). Homogenate resuspended in 35 % percoll was then carefully overlaid with 5 ml 1XHBSS (without Ca^{2+} or Mg^{2+}) and samples were centrifuged at 800 g for 45 min at 4 ^{o}C with no brake for density separation of cells from myelin.

Following centrifugation, supernatant was aspirated to waste and samples were resuspended in 5 ml 1XHBSS (without Ca^{2+} or Mg^{2+}) and transferred to a new 15 ml falcon. Samples were then centrifuged at 400 g for 5 min and supernatant was aspirated to waste. Samples were then resuspended in 1 ml FACS buffer (see appendix III). 20 µl of cell suspension was combined with 20 µl trypan blue (0.4 %) (Gibco, Life Technologies) to differentiate live and dead cells and a cell count was calculated using a haemocytometer. Briefly, the number of live cells in 16 squares was counted and multiplied by two as cells were diluted 1:1 in trypan blue. Values obtained were then multiplied by 10,000 to give the total number of viable cells per ml.

2.7.2 Labelling of cell surface antigens

10 µl anti-CD16/ 32 (Clone: 93, Biolegend) was added to samples (0.5 mg / ml) to block non-specific Fc receptor binding and samples were incubated for 30 min at 4 ^{o}C on a shaker. Cells were then resuspended at a density providing 1 x 10^{6} cells/ ml in FACS buffer and seeded at a volume of 100 µl/ well in a 96-well plate (Nunc) and an additional 200 µl of FACS buffer was added to each well. Plates were centrifuged at 400 g for 3 min at 4 ^{o}C. Supernatant was

discarded thereafter and 50 µl fluorochrome-conjugated antibody was added to appropriate wells (table 2.5). Unstained and single stained samples were included as controls. Samples used to assess CNS cell composition were treated with two separate antibody cocktails to label and identify myeloid and lymphoid populations. Plates were then covered in foil and incubated for 30 min at 4 ^{o}C on a shaker. Afterwards, 200 µl FACS buffer was added to each well to wash and the centrifugation process repeated. Supernatant was discarded and cells were resuspended in 200 µl FACS buffer for acquisition. All data were acquired using a BD LSR Fortessa X20 (Becton Dickinson, Oxford, UK).

Antigen	Fluorochrome	Clone	Concentration
CD11b	APC Cy7	M1/ 70	1 µg/ ml
CD45	PE Cy7	30/ F11	1 µg/ ml
F4/ 80	Alexa flour 488	BM8	1 µg/ ml
Ly6C	Pacific blue	HK1.4	1 µg/ ml
Ly6G	APC	1A8	1 µg/ ml
CCR2	PE	475301	1 µg/ ml
CD3	PE	17A2	1 µg/ ml
B220	PE Cy7	RA3.6B2	1 µg/ ml
BrdU	FITC	-	1 µg/ ml

Table 2.5: Fluorochrome-conjugated antibodies used to investigate cell composition changes in response to chronic cerebral hypoperfusion.

2.7.3 Labelling of intracellular BrdU

Bromodeoxyuridine (BrdU) was used to investigate changes in cell proliferation in response to chronic cerebral hypoperfusion. Briefly, BrdU is a synthetic analogue of thymidine. During S phase of the cell cycle when DNA is replicating BrdU is incorporated into newly synthesised DNA substituting thymidine. Conjugated antibodies can then be used to label BrdU enabling identification of proliferating cells. The BD FITC conjugated BrdU flow kit was utilised to fix and permeabilise cells, and label BrdU following manufacturer's instructions.

Following preparation of a brain cell suspension, cells were seeded onto a separate plate at 1 x 10^5 cells per well and labelled with conjugated antibodies to cell surface antigens as described in section 2.7.2. Following this, cells were fixed and permeabilised with 100 µl BD cytofix/ cytoperm buffer and incubated at 4 ^oC on a shaker for 30 min. Cells were then washed by adding 200 µl 1X BD wash/ perm buffer and centrifuged at 400 g for 3 min at 4 ^oC. Supernatant was removed and cells were permeabilised by resuspending in 100 µl BD cytoperm permeabilisation buffer for 10 min at 4 ^oC on a shaker. The wash step was repeated again and cells were re-fixed by resuspending in 100 µl BD cytofix/ cytoperm buffer for 5 min at 4 ^oC on a shaker. The wash step was repeated and cells were treated with DNase (300 µg / ml) in PBS (with Ca^2+ and Mg^{2+}) (Gibco, life technologies) for 1 h at 37 ^oC. The wash step was repeated and cells were treated with FITC-conjugated BrdU antibody in 1X BD Wash/ Perm Buffer (1 µg/ ml) for 30 min at 4 ^oC on a shaker. The wash step was repeated and cells were resuspended in 200 µl FACS buffer prior to acquisition on a BD LSR Fortessa X20 (Becton Dickinson, Oxford, UK)

2.7.4 Data acquisition and analysis

Upon acquisition, an unstained sample was recorded and viable cells identified based on forward and side scatter properties. 2000 – 5000 cell events were recorded for unstained and single stained controls whilst 10,000 events were recorded for samples used to investigate cell composition. Once all samples had been recorded, data were saved as FCS3 files and exported for analysis. For flow cytometric quantification, data were analysed using FlowJo

version 10. Viable cells were first identified based on their forward and side scatter profile and doublets excluded (fig. 2.8). Compensation was applied to correct fluorochrome bleed through and cell populations identified based on positive and negative gating strategies using a combination of markers (table 2.6). Absolute cell counts were then calculated by the following equation:

$$\frac{(\#\ of\ cells\ in\ population\ of\ interest)}{(\#\ viable\ \ cells)}\ x\ haemocytometer\ cell\ count$$

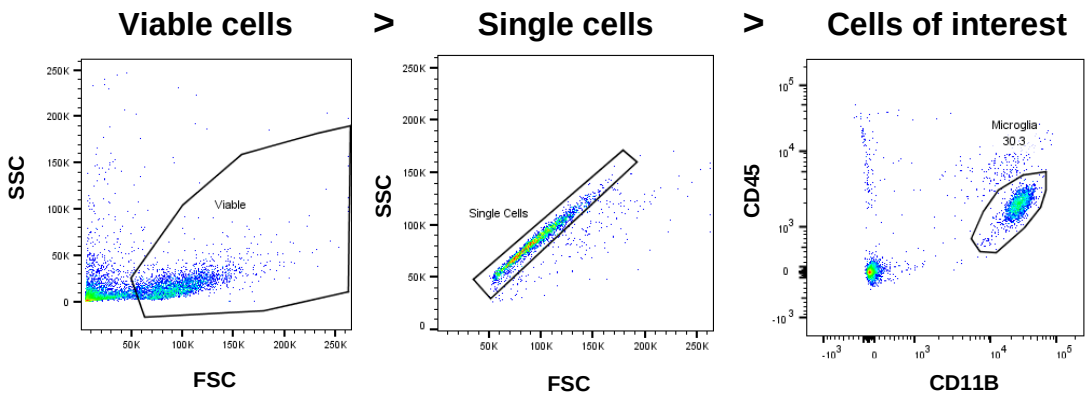

Figure 2.8: Representative dot plots showing gating strategy for identifying cells of interest. Viable cells were identified based on forward and side scatter properties. Doublets were then excluded and cell populations identified based on a combination of markers**.**

Cell type	Marker profile
Microglia	$Ly6G^{-}Ly6C^{-}CD11b^{+}CD45^{lo}$
Macrophages	$Ly6G^{-}CD11b^{+}CD45^{hi}Ly6C^{lo\text{-}hi}$
Neutrophils	$Ly6G^{+}CD11b^{+}CD45^{+}$
B cells	$CD11b^{-}B220^{+}$
T cells	$CD11b^{-}CD3^{+}$

Table 2.6: Cell surface antigen labelling profile utilised to identify cell populations in brain cell suspensions.

2.8 Fluorescence activated cell sorting of microglia

2.8.1 Tissue dissection

Following transcardiac perfusion described in section 2.4.3, brains were extracted and placed in a sagittal brain matrix and four 2 mm sagittal slices were cut and placed in ice cold 1XHBSS (without Ca^{2+} and Mg^{2+}). Each tissue slice was then placed on an ice-cold surface under a dissection microscope. Olfactory bulb and cerebellum were first removed and placed in 50 ml falcon containing ice cold 5 ml 1XHBSS to be used for downstream unstained and single-stained controls. Grey matter and white matter portions were then separated from the remaining tissue. For grey matter, a portion of cortex, hippocampus and striatum was isolated from each tissue slice and combined in a 50 ml falcon containing 5 ml ice cold 1XHBSS. For white matter, corpus callosum and portions of internal capsule were dissected and placed in a separate 50 ml falcon containing 5 ml ice cold 1XHBSS (fig. 2.9).

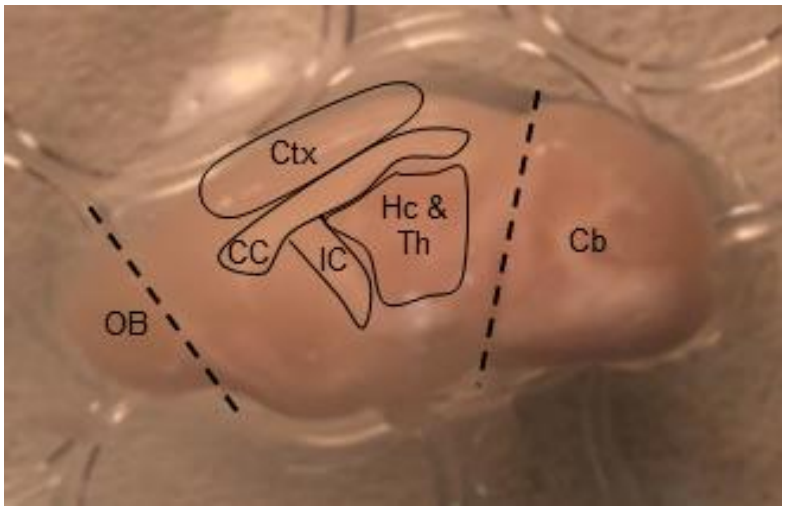

Figure 2.9: White matter and grey matter regions dissected for FACS isolation of microglia. The cerebellum (Cb) and olfactory bulb (OB) were dissected and used for unstained and single stained controls. The corpus callosum (CC) and internal capsule (IC) were dissected to isolate white matter microglia whilst the cortex (Ctx), hippocampus (Hc) and thalamus (Th) were dissected to collect grey matter microglia.

2.8.2 Preparation of brain cell suspension

Once tissue had been collected, samples were centrifuged at 400 g for 5 min at 4^{o}C and supernatant aspirated to waste. White matter samples were reconstituted in 2 ml ice cold 1XHBSS containing 12.5 mM HEPES whilst grey matter samples and samples used for unstained and single stained controls were reconstituted in 10 ml ice cold 1XHBSS, 12.5 mM HEPES. Grey matter samples and spare samples used for single and unstained controls were transferred to a 15 ml Dounce homogeniser whilst white matter samples were transferred to a 2 ml Dounce homogeniser and homogenised with 40 passes.

After tissue homogenisation, sample was transferred to a 15 ml falcon and centrifuged at 400 g for 5 min at 4^{o}C and supernatant was aspirated to waste. Samples were reconstituted in 8 ml 35 % percoll, 12.5 mM HEPES and this was then carefully overlaid with 5 ml 1XHBSS, 12.5 mM HEPES. Samples were then centrifuged at 800 g for 20 mins at 4^{o}C with no brake for density separation of myelin and from cells. Cell pellets were then resuspended in 1 ml 1XHBSS, 12.5 mM HEPES and transferred to a 5 ml polystyrene round bottomed FACS tube (Corning) and centrifuged at 400 g for 5 mins at 4 ^{o}C. Supernatant was then aspirated to waste and cells were reconstituted in 250 µl FACS buffer. 5 µl sample was then transferred to a microtube to conduct a cell count using a haemocytometer as described in section 2.7.1.

2.8.3 Labelling of cell surface antigens

Once cell counts were completed 2.5 µl anti-CD16/ 32 was added (0.5mg/ ml) to block Fc receptors for 30 min on ice. Following this, spare cells obtained from dissected cerebellum and olfactory bulb for single and unstained controls were transferred to a 96 well plate. All samples were then treated with fluorochrome-conjugated antibodies for 30 min on ice (table 2.7).

Antigen	Conjugate	Clone	Concentration
CD11b	PE	M1/ 70	1 µg/ ml
CD45	PE Cy7	30-F11	1 µg/ ml
Ly6C	APC	HK1.4	1 µg/ ml
Ly6G	Pacific blue	1A8	1 µg/ ml
F480	APC Cy7	BM8	1 µg/ ml

Table 2.7: Fluorochrome-conjugated antibodies utilised to identify cell populations in brain cell suspensions for FACS-based isolation of microglia.

Following incubation, samples were centrifuged at 400 g for 5 min at 4 ^{o}C and supernatant was aspirated to waste. Samples were then reconstituted in 250 µl FACS buffer and placed through a 40 µm filter to remove aggregated cells and large debris prior to acquisition. All samples were acquired and sorted using a BD FACSAria II (Becton Dickinson, Oxford, UK) by staff members at the Queen's Medical Research Institute Flow Cytometry and Cell Sorting Facility. Cells of interest were first identified based on forward and side scatter properties and doublets excluded. Dead cells were also excluded by gating on DAPI negative cells. 10,000 events were recorded from this population for cell composition analysis. Microglia were identified as Ly6C^{-}CD11b^{+}CD45^{lo} cells and sorted directly into 500 µl RLT cell lysis buffer (Qiagen) containing 1 % β-mercaptoethanol using a 100 µm diameter nozzle.

2.9 Microglial RNA extraction

Following cell sorting, samples were vortexed for 10 s and centrifuged for 10 min at full speed at RT to promote efficient lysis. RNA extraction was then performed using a RNeasy Plus microkit following manufacturer's instructions. First, amples were transferred to Qiashredder columns (Qiagen) and centrifuged at full speed for 2 min to homogenise. Samples were then transferred to genomic DNA (gDNA) column to remove contaminating genomic DNA and centrifuged at 8000 g for 2 min at RT. Sample was then transferred to a 15 ml falcon and 1

volume of 70 % ethanol added. Samples were inverted to mix and transferred to RNeasy MinElute spin column and centrifuged for 15 s at 8000 g at RT. Elute was removed to waste and 700 µl RW1 was added to columns. Columns were then centrifuged for 15 s at 8000 g at RT and elute was removed to waste. 500 µl RPE buffer was then added to columns before centrifugation at 8000 g for 15 s at RT. Elute was discarded and 500 µl 80 % ethanol was added to columns before centrifuging for 2 mins at 8000 g at RT. Both the collection tube and elute were discarded and the column was placed in fresh collection tube. Samples were then centrifuged at full speed for 5 min with lids left open to dry the silica membrane within the RNeasy MinElute spin column. Collection tubes and elute were discarded and again columns were placed in fresh collection tubes. Isolated RNA was then eluted by placing 14 µl nuclease-free water directly onto the silica membrane and centrifuging for 5 min at full speed at RT. This process was then repeated to increase total yield of RNA extracted. Once RNA was eluted, total yield was determined using a Nanodrop spectrophotometer and samples were stored at -80^{o}C.

2.9.1 Assessment of RNA quality

2.9.1.1 Spectrophotometer

The DS-11-FX Nanodrop spectrophotometer (DeNovix) was used to determine RNA concentration and purity of extracted RNA. RNA concentration is determined by the extent of light absorption at 260 nm. Light absorption at 230 nm and 280 nm indicates contamination of sample with protein or organic compounds from the extraction process such as guanidine or phenol, respectively. RNA purity was assessed based on 260/ 280 ratios which typically range between 2.0 -2.2.

2.9.1.2 Electrophoretic analysis

The LabChip GX24 (Perkin Elmer) was used to assess quality of extracted microglial RNA with a RNA Pico sensitivity assay following manufacture instructions (assay conducted by Pamela Brown, Biomolecular Core, Queen's Medical Research Institute). The LabChip GX24 conducts automated analysis of RNA concentration and quality using electrophoresis and

fluorescence. A RNA quality score is generated to determine the extent of degradation between 0 – 10 with 10 being intact RNA based on the calculation of several factors including 18S and 28S peak height and area, total RNA area and fast region area (region between the 18S peak and lower marker peak) (fig. 2.10).

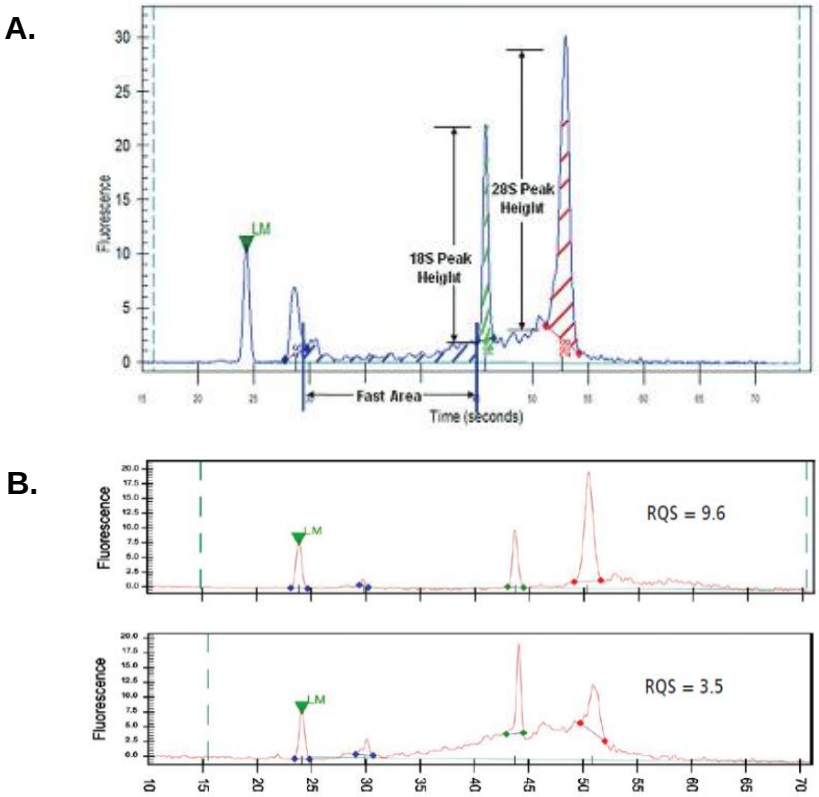

Figure 2.10: Electropherogram analysis used to determine RNA quality. (A) Representative electropherogram with parameters labelled to quantify RNA quality score. (B) Representative electropherograms showing differences between intact RNA (RQS: 9.6) and degraded RNA (RQS: 3.5). Clear 18S and 28S peaks can be observed in intact RNA samples and baseline is close to 0. However, in the degraded sample 28S peak height is reduced and smaller RNA fragments can be observed in the fast region characteristic of degraded RNA. Images obtained from PerkinElmer.

2.10 cDNA synthesis

To investigate gene expression from RNA via real time quantitative polymerase chain reaction (RT-QPCR) complementary DNA (cDNA) must first be generated by reverse transcription. Extracted RNA was first combined with 2 µl 10 mM deoxynucleotide triphosphate (dNTP) (Invitrogen) and 2 µl 0.5 µg/ µl oligo$(dT)_{15}$ (Promega) and total reaction volume was made to 14 µl with nuclease free dH20. A T100 thermal cycler was then used to heat the mixture to 65 ^{o}C for 5 min and samples were incubated on ice for 1 min. Following this samples were briefly centrifuged and combined with 0.1 M dithiothreitol (DTT) (Promega) 5x, first strand buffer, 40 U/ µl RNasin^{R} Plus Inhibitor (Promega) and 200 U/ µl Superscript^{TM} III reverse transcriptase (Invitrogen). In control samples, nuclease free water was added instead of Superscript III to test for DNA contamination. Samples were then vortexed and placed in a T100 thermal cycle and heated to 50 ^{o}C for 55 min to promote reverse transcription and then 70^{o}C for 15 min to induce enzyme inactivation. Samples were then stored at -20 ^{o}C prior to conducting RT-qPCR.

2.11 Real time quantitative polymerase chain reaction (RT-qPCR)

RT-QPCR was utilised to investigate gene expression in microglia compared to whole brain tissue. SYBR green was used as a DNA binding dye to intercalate newly formed double stranded DNA and quantify relative gene expression compared to control samples. A mastermix was first made by combining 10 ng cDNA, 1 µl ROX reference dye (diluted 1:10 from stock) (Invitrogen), 12.5 µl Platinum SYBR Green qPCR SuperMix-UDG (Invitrogen), 1.25 µl forward primer, 1.25 µl reverse primer (table 2.8) and dH_20 to a total volume of 25 µl. A stratagene Mx3005P thermocycler (Agilent) was used to conduct the RT-qPCR (table 2.9).

Primers	Sequence 5’ – 3’	Product length (bp)
Gapdh forward strand	CCTTGTGTCCTTGAACCAGC	140
Gapdh reverse strand	AAGGGAGGCTGGTAGAGAGA	
Aif1 forward strand	GCAGCCTCTGTTCCACATACACTTCA	119
Aif1 reverse strand	ATCTCAGACTGCATTCTCCCACTCC	
Tmem119 forward strand	CAGAGCTGGTTCCATAGCTCAA	102
Tmem119 reverse strand	CCGGGAGTGACACAGAGTAG	
Aldh1l1 forward strand	TGCAGAAAGTGGTGGAGGAA	126
Aldh1l1 reverse strand	CACCACGTTGGCATACTCC	
Rbfox3 forward strand	ATGGAGCGGTCGTGTATCAG	144
Rbfox3 reverse strand	AAGGATCAGCAGCGGCATAG	

Table 2.8: Oligonucleotide sequences of primers used to investigate relative gene expression in microglia compared to whole brain tissue.

Step	Temperature (ºC)	Time	Cycle
Denaturation	95ºC	10 min	1 cycle
Amplification	95ºC 60ºC 72ºC	15 sec 20 sec 1 min	40 cycles
Elongation	95ºC 55ºC 95ºC	1 min 30 sec 30 sec	1 cycle

Table 2.9: Thermal profile used to amplify cDNA for RT-qPCR analysis.

The level of gene expression was determined by the cycle threshold (Ct) value at which point fluorescence emitted from DNA-bound SYBR green increases over baseline fluorescence. Baseline fluorescence was automatically determined by stratagene Mx3005P software. Relative gene expression by isolated microglia was compared with whole brain tissue using $\Delta\Delta$Ct. Briefly, the Ct value of the used housekeeping gene, *Gapdh,* was first subtracted from Ct values of genes of interest providing the delta Ct value. The delta Ct value of control samples, in this case whole brain, were then subtracted from the delta Ct value from of genes of interest providing relative expression of genes of interest.

2.12 Statistics

Data were analysed and statistics performed on Graphpad Prism version 7.4. Distribution of data were first determined by conducting a Shapiro-Wilk test. The Mann-Whitney U test was used to investigate differences between two groups whilst the Kruskal Wallis test was used to investigate differences between three or more groups when data were not normally distributed. If data were normally distributed, differences between two groups were investigated using Student's or Welch's t test depending on data variance whilst one way analysis of variance (ANOVA with Bonferroni post hoc was used to investigate differences between 3 groups. Two way ANOVA with Bonferroni adjustment was used to assess changes in cerebral blood flow following BCAS and sham surgeries in WT and TREM2-/- mice. Additional details of statistical analyses performed can be found in results chapter methods. All data analysis was conducted with blinding to treatment and genotype. Unless stated otherwise, data are presented as mean ± standard error of the mean (SEM). For all experiments $p \leq 0.05$ was considered statistically significant.

Chapter 3:

Validation of BCAS as a suitable model to investigate neuroinflammatory responses to chronic cerebral hypoperfusion

3.1 Introduction

Chronic cerebral hypoperfusion is suggested to be a key contributor to white matter damage, age related cognitive impairment and dementia. Various animal models in which cerebral blood flow is manipulated have therefore been developed to investigate the pathological mechanisms by which cerebral hypoperfusion mediates white matter damage and cognitive decline. The BCAS model, in which microcoils are fitted on the common carotid arteries of mice to induce cerebral hypoperfusion, recapitulates various pathological features of VCI (Shibata et, al., 2004). 28 d following microcoil placement, C57BL/6J mice demonstrate diffuse white matter pathology without overt neuronal perikarya damage associated with spatial working memory impairment (Shibata et al., 2004). Furthermore, areas of white matter damage are associated with robust neuroinflammation characterised by reactive gliosis (Shibata et al., 2004, Coltman et al., 2011, McQueen et al., 2014). This model therefore provides a powerful tool to investigate the mechanisms by which neuroinflammation contributes to loss of white matter integrity and cognitive impairment.

Prior to characterising the neuroinflammatory response resulting from BCAS it was essential to validate that BCAS precipitated comparable pathology to previous studies in WT C57BL/6Ntac mice from the TREM2 colony. As it has previously been reported that use of 0.18 mm internal diameter microcoils induces reproducible myelin damage after 28 d in C57BL6/J mice, it was hypothesised that BCAS would cause loss of myelin integrity in WT C57BL/6Ntac mice. To investigate this, key markers of neuronal damage, myelin integrity and glial reactivity were utilised and pathology characterised using histology and immunohistochemistry (IHC).

3.2 Aims

1. Investigate animal recovery associated with inducing BCAS for 28 d using 0.18 mm microcoils in WT C57BL/ 6Ntac mice.

2. Determine frequency and severity of white matter and grey matter pathology, as well as glial responses resulting from BCAS after 28 d in WT C57BL/6Ntac mice.

3.3 Methods

3.3.1 Animal procedures

WT C57BL/6Ntac mice aged 2 - 3 m were utilised to investigate pathological changes resulting from BCAS. A total of 16 mice were used and randomly assigned to receive sham (n = 6) or BCAS (n = 10) surgeries. N numbers were chosen based on power analysis of data from previous BCAS studies. To achieve a significance level of $p < 0.05$, a group size of 8 was required to reach a power of 0.8. For BCAS surgeries, microcoils with 0.18 mm internal diameters were used bilaterally and sham surgeries were conducted as reported in section 2.4.1. Following surgery, mouse recovery was assessed twice daily for the first 72 h and then twice weekly thereafter.

3.3.2 Tissue harvest

28 d after surgery, mice were saline perfused and brains post-fixed in 4 % paraformaldehyde (w/ v) as described in section 2.4.3. Tissues were processed, paraffin embedded and sectioned as described in section 2.5. 6 µm tissue sections were obtained at the level of the striatum (~0.74 mm anterior to bregma) and hippocampus (~1.70 mm posterior to bregma) and histology and IHC were utilised to investigate white and grey matter pathology resulting from BCAS.

3.3.3 Histology

Neuronal pathology was assessed by H & E staining as described in section 2.6.4. Neuronal pathology was identified by condensation of nuclei, vacuolation and pallor within the parenchyma (see fig. 3.2). All staining and subsequent analysis was conducted by the author with blinding to sham and BCAS groups.

3.3.4 Immunohistochemistry

MAG and IBA1 immunostaining were conducted by the author to assess myelin integrity and microglial reactivity following BCAS, respectively, as described in sections 2.6.1 - 2.6.2. A semi-quantitative method described in section 2.6.2 was used to quantify white matter integrity in white matter tracts. As both brain hemispheres were assessed, white matter damage scores for individual white matter tracts were summated from each hemisphere providing a total possible score of 6. A 'total myelin damage' score was also calculated by summating all myelin damage scores from each animal providing a total possible score of 36.

For IBA1+ cell quantification, four regions of interest measuring 0.1 mm^2 were randomly placed across each white matter tract analysed per hemisphere (see section 3.3.5 below) using ImageJ software. IBA1+ cell bodies were then manually counted within each region of interest and values from left and right hemispheres (total of 8 regions of interest) were averaged to provide the number of IBA1+ cells per 0.1 mm^2 in each white matter tract. All immunostaining and subsequent analysis was conducted by the author with blinding to sham and BCAS groups.

3.3.5 Regions of interest

For the purpose of this study, both brain hemispheres were analysed to characterise pathology resulting from BCAS. White matter regions analysed include the corpus callosum, hippocampal fimbria, internal capsule, external capsule, optic tract and striatal bundles. Grey matter regions analysed include the cerebral cortex, hippocampus, thalamus and striatum (fig. 3.1). For IBA1 quantification, white matter regions analysed include the corpus callosum, optic tract, internal capsule, hippocampal fimbria and striatal bundles.

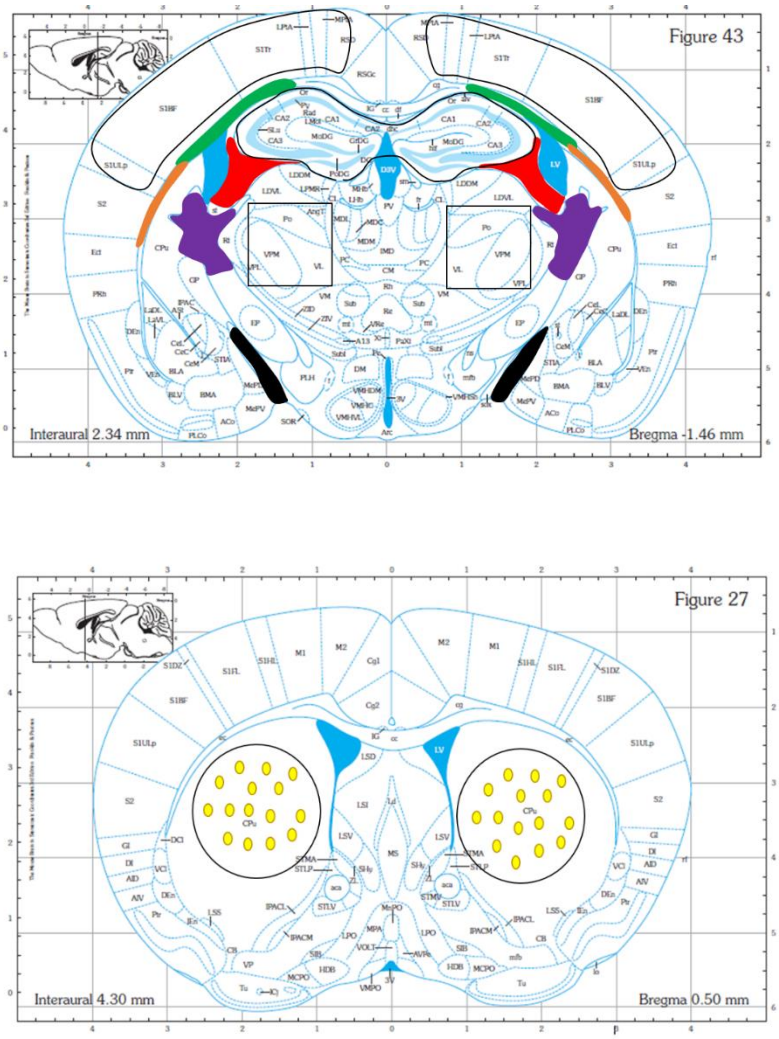

Figure 3.1: White and grey matter regions used for pathological assessment. Outlined regions demonstrate grey matter regions analysed (hippocampus, striatum, thalamus and cerebral cortex). Coloured regions demonstrate white matter tracts analysed (green: corpus callosum, orange: external capsule, red: hippocampal fimbria, purple: internal capsule, black: optic tract, yellow: striatal bundles).

3.3.6 Statistics

Fisher's exact test was used to determine if BCAS increased the probability of myelin damage occurring. Mann Whitney U test was conducted to test for differences in myelin integrity and IBA1 cell number between BCAS and sham animals. All statistical analyses were performed with Graphpad Prism software version 7.4 with statistical significance considered $p \leq 0.05$.

3.4 Results

3.4.1 Animal recovery

Following surgery, 5 of 6 sham and 6 of 8 BCAS animals were motile and responsive within 1 h of surgery and exhibited eating and drinking with normal exploratory behaviour after 24 – 48 h. Sham and BCAS mice demonstrated a maximal 5.9 % and 5.3 % loss in weight 3 d following surgery, respectively (see appendix section 8.1.1). These mice demonstrated no adverse neurological symptoms such as circling, seizures or barrel rolling and remained healthy until tissue harvest. 1 of 6 sham (16.6 % mortality) and 2 of 10 BCAS (20 % mortality) animals were culled within the first 48 h after surgery due to circling, persistent unresponsiveness and laboured breathing suggestive of overt neuronal damage or vagus nerve damage. The final cohort sizes were as follows:

Treatment group	Final cohort size (n)
Sham	5/ 6
BCAS	8/ 10

Table 3.1: Final ohort sizes 28 d after sham and BCAS surgeries.

3.4.2 Pathological assessment

3.4.2.1 H & E assessment of CNS pathology

H & E staining was conducted to assess tissue integrity and identify potential neuronal perikarya damage 28 d following BCAS or sham surgeries. No neuronal pathology was observed in any brain region examined in sham animals. 7 of 8 BCAS animals also demonstrated no evidence of neuronal pathology in any region examined. 1 of 8 BCAS animals demonstrated extensive neuronal pathology in grey matter regions including the striatum, cortex, hippocampus and thalamus characterised by the presence of shrunken, darkened nuclei and vacuolation of the neuropil (table 3.2) (fig. 3.2).

Treatment	Animals displaying neuronal pathology
Sham	0/ 5 (0 %)
BCAS	1/ 8 (12.5 %)

Table 3.2: Mice displaying neuronal pathology detected by H & E staining 28 d after sham or BCAS surgeries. One tissue section analysed per animal.

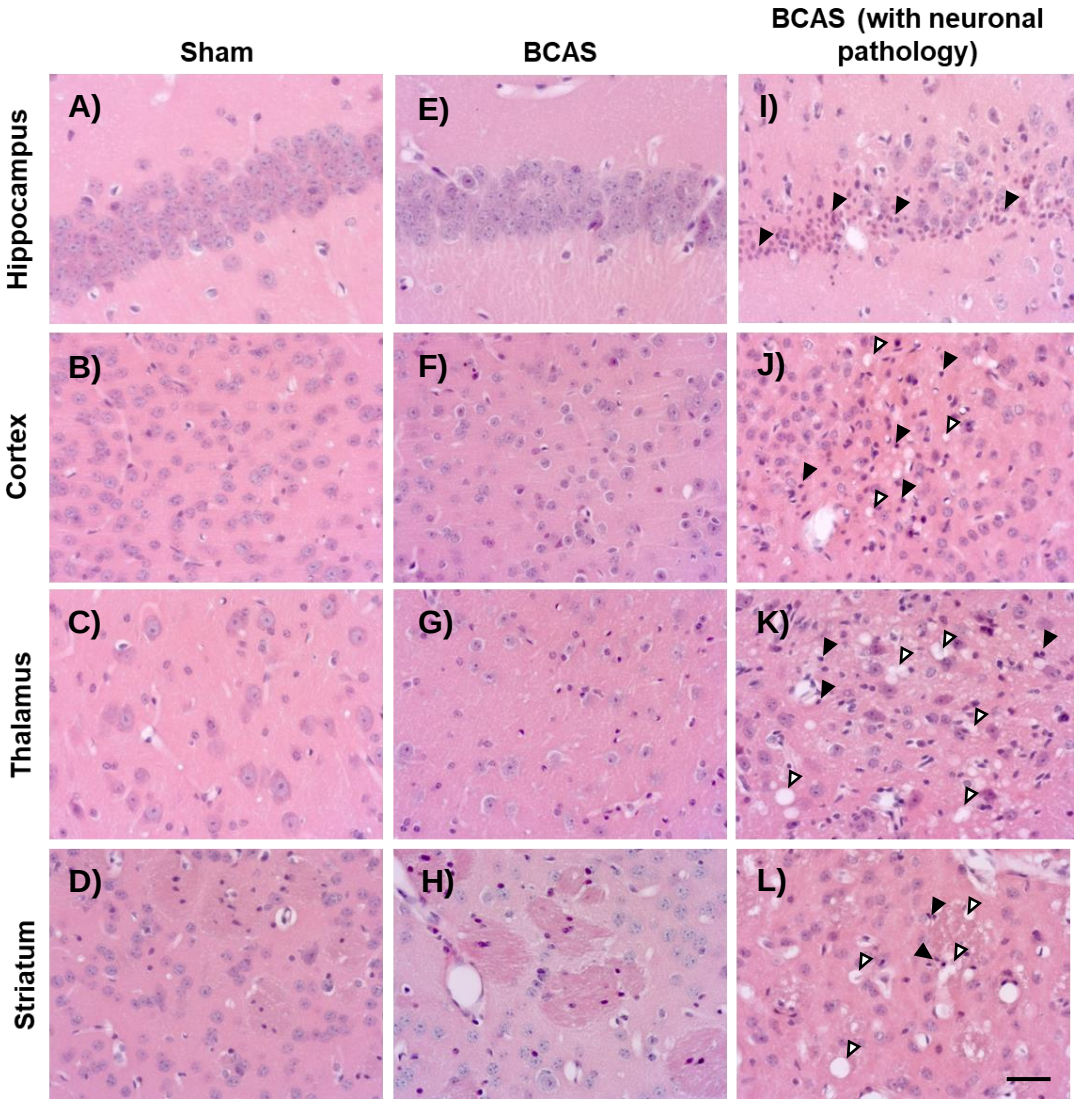

Figure 3.2: Assessment of neuronal pathology by H & E staining in sham and BCAS mice 28 d post surgery. Representative images demonstrating H & E staining of the CA1 region of the hippocampus (A, E, I), cortex (B, F, J), thalamus (C, G, K) and striatum (D, H, L) of sham animals (A-D) , BCAS mice (E-H) and a BCAS mouse demonstrating widespread neuronal pathology (I-L). Black arrows demonstrate examples of darkened, condensed nuclei. White arrows demonstrate examples of vacuolation. Scale bar: 50 µm

3.4.2.2 Assessment of myelin integrity

Myelin integrity was assessed across several white matter regions via MAG immunostaining in sham and BCAS animals 28 d post surgery and extent of myelin damage was quanitified. Loss of myelin integrity was not observed in any sham animals. In response to BCAS, 6 of 8 animals demonstrated myelin damage (fig. 3.3). Fisher's exact test demonstrated BCAS significantly increased the probability of myelin damage occurring compared to sham animals ($p \leq 0.05$) (fig. 3.3A). However, the severity and extent of myelin damage was generally subtle and anatomically confined to one or two regions rather than being diffuse as reported in previous studies (Shibata, et al. 2004., Coltman, et al., 2011).

One animal demonstrating extensive neuronal damage also demonstrated severe white matter damage with extensive myelin debris and loss of white matter fibre organisation in several white tracts analysed (data points shown in red) (fig. 3.4B). Statistical analysis of myelin damage scores in individual white matter tracts revealed no significant difference in damage between sham and BCAS animals ($p \geq 0.05$) (fig. 3.4B). However, a significant increase in total white matter damage was observed in response to BCAS compared to sham animals ($p \leq 0.05$) (fig. 3.4C).

	Mice displaying myelin damage	CC	EC	HF	IC	SB
Sham	0/ 5 (0 %)	0/ 5 (0%)	0/ 5 (0%)	0/ 5 (0%)	0/ 5 (0%)	0/ 5 (0%)
BCAS	6/ 8 (75 %)	4/ 8 (50 %)	1/ 8 (12.5 %)	2/ 8 (25 %)	3/ 8 (37.5 %)	2/ 8 (25 %)

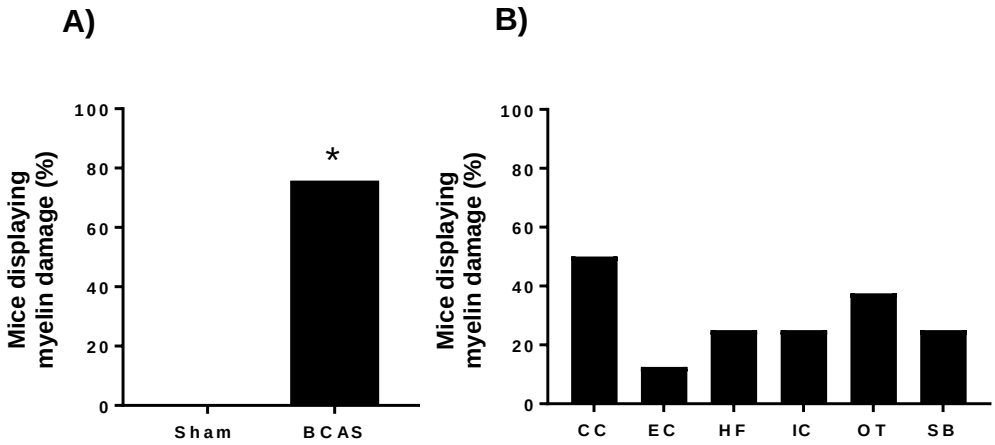

Figure 3.3: Frequency of sham and BCAS mice demonstrating myelin damage detected by MAG immunostaining 28 d post surgery. (A) Overall frequency of mice demonstrating myelin damage detected via MAG immunostaining in sham and BCAS mice. BCAS significantly increased the probability of myelin damage occurring compared to sham animals. (B) Frequency of white matter tracts demonstrating damage in response to BCAS. *P ≤ 0.05. Fisher's exact test.. One tissue section analysed per animal. N = 5 – 8 independent animals per group. CC: corpus callosum, EC: external capsule, HF: hippocampal fimbria, IC: internal capsule, SB: striatal bundles.

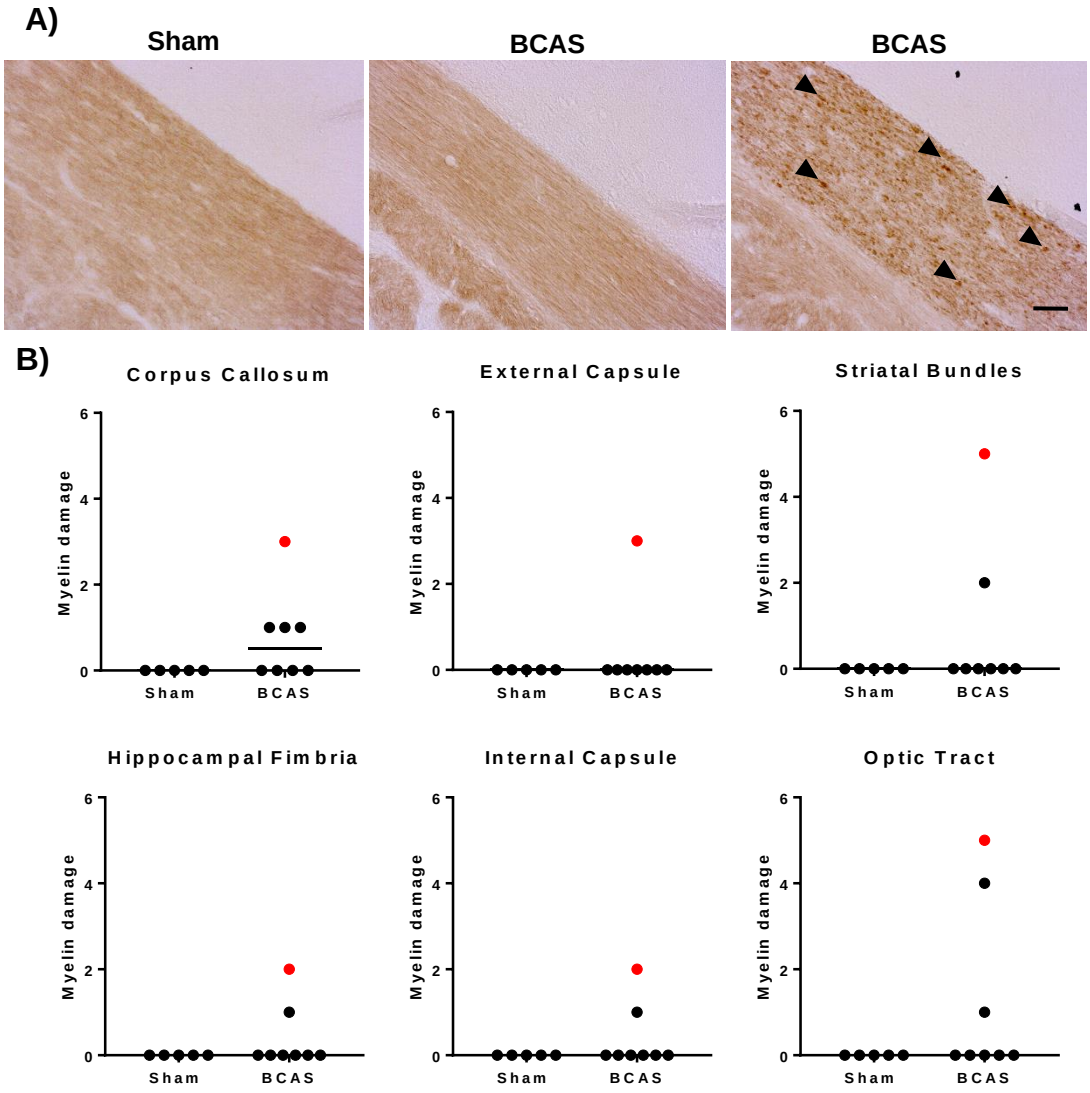

Figure 3.4: Extent of myelin damage detected by MAG immunostaining in sham and BCAS mice 28 d post surgery. (A) Representative images of MAG immunostaining of the optic tract of sham animals, BCAS animals with typical severity and distribution of white matter pathology and the BCAS animal demonstrating overt neuronal perikarya damage and widespread white matter pathology. Black arrows demonstrate examples of myelin debris. Scale bar: 50 µm. (B) Myelin damage in each white matter tract was quantified using a semi quantitive scoring method ranging from 0 (no damage) to 3 (extensive damage) via MAG immunostaining and scores from each hemisphere were summated providing a total possible score of 6 per white matter region. BCAS did not cause a significant increase in the extent of white matter damage compared to sham animals. (C) Myelin damage scores were summated from all analysed white matter tracts providing a 'total myelin damage' score per animal. BCAS significantly increased total myelin damage compared to sham animals. *P ≤ 0.05, Mann Whitney U test. Each data point represents an individual animal. One tissue section analysed per animal. Red data points represent the animal demonstrating extensive grey and white matter pathology. Bar shows median. N = 5 – 8 independent animals per group.

3.4.2.3 Assessment of microgliosis

Previous studies investigating pathological outcomes to BCAS frequently demonstrate microgliosis in regions of myelin damage. Microglial morphology was assessed by IBA1 immunostaining and number of microglia in white matter tracts were quantified in sham and BCAS animals 28 d post-surgery. No overt differences in microglial morphology were observed in grey or white matter regions in sham animals. Microglia retained a ramified morphology with small cell bodies in all regions analysed indicative of a 'non-activated' phenotype. The majority of BCAS mice similarly demonstrated no overt differences in microglial morphology (fig. 3.5A). However, 1 of 8 BCAS mice demonstrating severe white matter pathology also demonstrated extensive microgliosis in most white matter tracts analysed (data points highlighted in red) (fig. 3.5B). Quantification of IBA1 cell number revealed no significant difference in microglial number in response to BCAS in any white matter tract analysed compared to sham animals ($p \leq 0.05$) (fig. 3.5B).

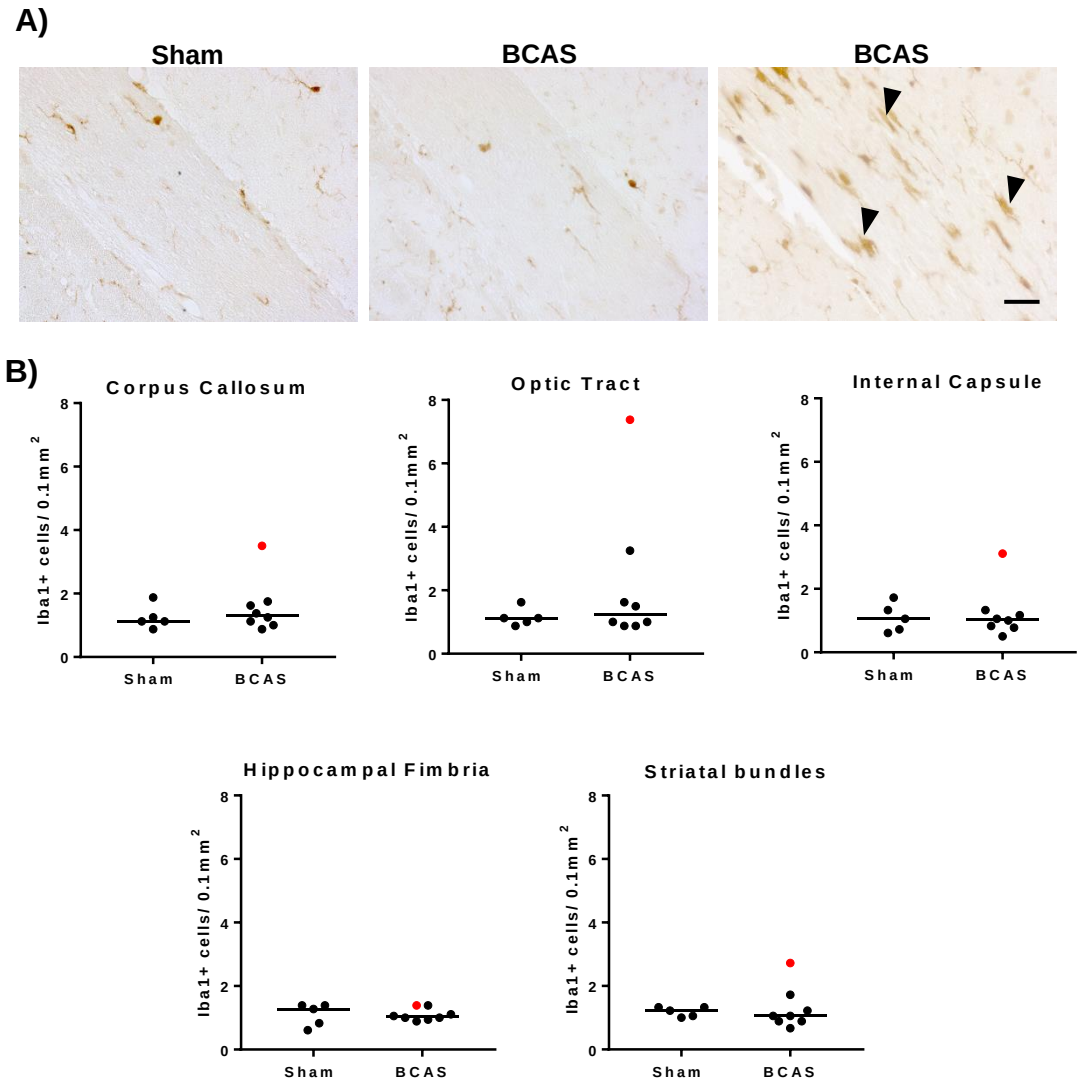

Figure 3.5: Quantification of IBA1+ cell number in sham and BCAS mice 28 d post surgery. (A) Representative images showing IBA1 immunostaining of the optic tract of sham animals, BCAS animals and the BCAS animal demonstrating extensive white and grey matter pathology. Black arrows show examples of 'reactive' microglia. Scale bar: 50 µm (B) Quantification of IBA1+ cells in individual white matter tracts demonstrated BCAS did not increase the number of IBA1+ cells in white matter tracts compared to sham animals. Each data point represents an averaged value calculated from 8 0.1mm^2 regions of interest placed across white matter tracts of an individual animal. One tissue section analysed per animal. Red data points represent the animal demonstrating extensive grey and white matter pathology. Mann Whitney U test. Bars show median. N = 5 – 8 independent animals per group.

3.5 Discussion

Previous studies utilising the BCAS model to investigate mechanisms by which chronic cerebral hypoperfusion contributes to loss of white matter integrity and cognitive decline report reproducible diffuse white matter damage and reactive gliosis associated with spatial working memory impairment after 28 d (Coltman et al., 2011). Subsequent studies investigating the longer-term impact of BCAS report additional ischaemic and haemorrhagic lesions and hippocampal atrophy associated with reference memory impairment (Holland et al., 2015). As various pathological, radiological and behavioural features have been characterised over the temporal course of BCAS, the model provides a useful platform to investigate how neuroinflammation evolves in parallel to white matter damage and cognitive impairment. The current study was therefore conducted to determine if WT C57BL/6Ntac mice demonstrate comparable neuropathology to previous studies by investigating key markers of grey and white matter integrity and glial reactivity via histology and IHC.

Overall, the results of the current study demonstrate BCAS induces subtle white matter damage in the absence of overt neuroinflammatory changes and neuronal perikarya damage 28 d post surgery in WT C57BL/6NTac mice. Neurological symptoms characteristic of overt neuronal damage were absent from the majority of mice following surgery. Of the mice which were culled prior to tissue harvest, 2 of 10 BCAS mice demonstrated circling, reduced movement and persistent laboured breathing. Post-mortem analysis revealed large blood clots covering the carotid artery surface suggesting damage to the carotid arteries. It could be postulated misplacement of microcoils during the surgical procedure caused damage to the carotid artery and induced severe reductions in cerebral blood flow leading to ischaemic damage. One sham animal also demonstrated persistent laboured breathing suggestive of vagus nerve damage. As this was the first cohort of surgeries in which animals were recovered, increased mortality associated with surgical complications was expected.

In animals which recovered until tissue harvest, analysis of H & E staining revealed that BCAS did not cause extensive neuronal damage comparable to previous studies (Shibata et al., 2004). However, BCAS induced only subtle alterations in white matter integrity as assessed by MAG immunostaining. It is unlikely that the methods utilised in this study were not of adequate sensitivity to detect alterations in white matter integrity induced by BCAS. One animal with widespread neuronal damage also demonstrated extensive myelin debris across several white matter tracts indicating that MAG immunostaining was able to detect areas of myelin damage. Previous studies have shown preferential loss of MAG compared to other myelin components in response to inflammatory or hypoxic stimuli due to its localisation on the most distal portions of oligodendrocyte processes (Aboul-Enein et al., 2003). Protein redistribution of MAG is observed from as early as 3 d after BCAS enabling its use to investigate subtle alterations in white matter integrity which may not be detected by assessing other myelin components or by using histological approaches such as luxol fast blue (Reimer et al., 2011). Furthermore, analysis of IBA1 immunostaining revealed that microglia demonstrated a 'resting' phenotype in the majority of BCAS mice across all white matter regions. In response to CNS injury including myelin damage, microglia rapidly react in an attempt to repair damage and maintain CNS homeostasis. BCAS did not cause overt changes to microglial morphology except in one animal which also demonstrated severe neuronal perikarya and white matter damage. Therefore, the absence of microgliosis further suggests that BCAS did not induce white matter injury. The infrequent and subtle white matter pathology observed in response to BCAS differs to that described in previous studies. However, potential reasons for this will be discussed in detail in chapter 4.

In the 1 BCAS animal which demonstrated extensive grey and white matter pathology, it is possible cerebral blood flow was severely reduced leading to ischaemic damage as a result of improper microcoil placement. However, a major limitation of the current study is that cerebral blood flow changes associated with placement of microcoils were not recorded. Previous studies report a 36 % reduction in cerebral blood flow 3 d after BCAS surgery using 0.18 mm internal diameter microcoils which gradually resolves to 22 % after 28 d mimicking the subtle reductions in cerebral blood flow observed in elderly individuals (McQueen et al.,

2014). We could not determine if induction of BCAS resulted in a similar degree of hypoperfusion as equipment to do so was not available. It could therefore be postulated that BCAS did not induce hypoperfusion or at least a sufficient amount to precipitate white matter damage.

An advantage of the BCAS model is that microcoils with varying internal diameters can be applied to moderate the extent of cerebral hypoperfusion and resultant white matter pathology. Previous studies have shown use of 0.18 mm internal diameter microcoils together with 0.16 mm internal diameter microcoils induces severe hypoperfusion associated with extensive white matter pathology, neuroinflammation and impaired white matter function (Miki et al., 2009, Fowler et al., 2018).

Although 0.16 mm internal diameter microcoils could be utilised to precipitate more frequent and severe white matter damage a key aim of this thesis is to investigate the impact of TREM2 deficiency on white matter integrity and glial responses to BCAS. Previous studies investigating the impact of TREM2 deficiency in models of CNS injury generally describe TREM2 exerts protective effects. Previous work in the McColl lab has demonstrated TREM2-/- mice exhibit greater infarct volumes associated with poorer functional recovery in response to MCAO (unpublished data). Kawabori et al. (2015) similarly demonstrated reduced tissue resorption and poorer functional recovery in TREM2-/- mice following MCAO (Kawabori et al., 2015). Therefore, although using smaller microcoils may precipitate more frequent and extensive white matter damage in WT mice, this may be further exacerbated in TREM2-/- mice resulting in severe pathology and increased mortality.

As white matter damage has shown to evolve with longer durations of BCAS it was considered that 28 d may be insufficient to precipitate robust white matter pathology in C57BL/ 6Ntac mice (Holland et al., 2015). Therefore, although subtle and infrequent myelin pathology was observed in response to BCAS after 28 d, it was concluded use of 0.18 mm internal diameter microcoils was worth pursuing as it was hypothesised that longer durations of recovery after BCAS induction would result in progressively more extensive white matter pathology extending to grey matter regions associated with reactive gliosis.

Chapter 4:

Investigation of the temporal neuroinflammatory response to BCAS

4.1 Introduction

Robust neuroinflammation characterised by reactive gliosis is consistently observed in areas of white matter damage in the elderly human brain and preclinical animal models of VCI (Miyanohara et al., 2018, McQueen et al., 2014, Coltman et al., 2011, Fernando et al., 2006; Simpson et al., 2007). Structural and functional white matter impairment closely correlate to microglial number and use of immunomodulatory drugs including dimethyl fumarate, cilostazol and minocycline have shown to ameliorate such changes (Manso et al., 2017, Fowler et al., 2018, Kitamura et al., 2017, Miyanohara et al., 2018).

While this suggests neuroinflammation may play a key role in influencing white matter injury and cognitive impairment there are various aspects of the neuroinflammatory response to chronic cerebral hypoperfusion which remain unclear. The precise role of microglia and whether they contribute to or protect from damage remains unclear. Furthermore, the temporal evolution of the neuroinflammatory response over longer durations has yet to be characterised. It also remains unclear if microglia exclusively contribute to the neuroinflammatory response or if peripherally-derived myeloid and lymphoid cells also infiltrate the CNS over longer durations of cerebral hypoperfusion.

Considering neuroinflammation is suggested to play a key role in mediating white matter injury and cognitive impairment it is important to develop an understanding of how the cellular and molecular neuroinflammatory response to cerebral hypoperfusion develops in parallel to white and grey matter pathology. Such information would provide insight into components of the neuroinflammatory profile which could be modulated to ameliorate white matter damage and cognitive deficits caused by cerebrovascular dysfunction.

In the previous study, characterisation of CNS pathology using IHC and histology demonstrated mild white matter pathology 28 d after BCAS. As previous studies have demonstrated white matter damage progresses with longer durations of BCAS it was hypothesised increasing the duration of BCAS from 28 d to 3 m would provoke more frequent and extensive myelin pathology in C57BL6/Ntac mice (Holland, et al., 2015).

We therefore set out to assess development of CNS pathology over extended durations of BCAS and characterise how neuroinflammation evolves in parallel. In addition to using IHC and histological approaches, flow cytometry was implemented as a sensitive measure to investigate subtle alterations in cell composition and phenotype to BCAS.

4.2 Aims

1. Define white and grey matter pathology, and microglial responses to increasing durations of BCAS in WT C57BL6Ntac mice.
2. Profile myeloid and lymphoid populations in the CNS in response to increasing durations of BCAS in WT C57BL6Ntac mice.

4.3 Methods

4.3.1 Animal procedures

Three cohorts of WT C57BL/6Ntac animals aged 8-10 w were used in this study. Animals were randomly assigned to receive sham or BCAS surgeries described in section 2.4.1 and left to recover for 1 w (cohort 1), 1 m (cohort 2) or 3 m (cohort 3). Prior to tissue harvest, all animals were injected with BrdU intraperitoneally (50 mg/ kg) for three consecutive days to label dividing cells and investigate cell proliferation resulting from increased durations of BCAS via flow cytometry. Initial numbers of sham and BCAS animals in each cohort are shown in table 4.1. N numbers were chosen based on power analysis of data from previous BCAS studies. To achieve a significance level of $p < 0.05$, a group size of 8 was required to reach a power of 0.8.

Cohort Duration of BCAS)	Sham (n)	BCAS (n)
1 (1 week)	10	12
2 (1 month)	8	10
3 (3 months)	9	8

Table 4.1 Cohort sizes prior to conducting sham and BCAS surgeries.

4.3.2 Tissue harvest

Transcardiac perfusion of mice was performed as described in section 2.4.3. Pathological assessments and flow cytometric analysis were conducted on opposing hemispheres from the same animal to characterise pathology and alterations in CNS cell composition resulting from increasing durations of BCAS. Brains were first placed in a coronal brain matrix and olfactory bulb and cerebellum removed. A microtome blade was then placed 0.80 mm posterior to bregma separating the brain into rostral and caudal portions. The right hemisphere of the caudal portion was used for flow cytometry while the left hemisphere was used for pathological

assessment. The remaining tissue from the rostral portion was separated into left and right hemispheres and right hemisphere was used for flow cytometric analysis whilst tissue from left hemisphere was taken for gene expression analysis (fig. 4.1). Tissue for gene expression analysis was snap frozen in isopentane at -65 ^{o}C and stored in Eppendorfs at -80 ^{o}C. However, this tissue was not used. Tissue used for pathological assessment was processed, embedded and sections were prepared for staining as described in section 2.5. Hind limbs were also amputated and bone marrow extracted from select animals to use as a positive control for BrdU staining.

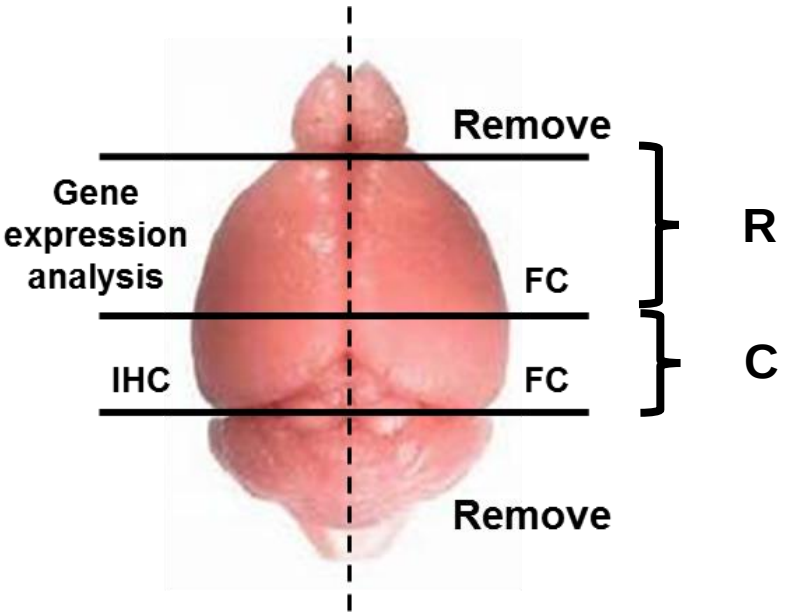

Figure 4.1: Method of tissue harvest to investigate neuroinflammatory responses to BCAS. A microtome blade was placed 0.80 mm posterior to bregma separating the brain into rostral and caudal portions. The right hemisphere of the caudal portion was used for flow cytometry while the left hemisphere was used for pathology. The remaining tissue from the rostral portion was separated into left and right hemispheres and right hemisphere was used for flow cytometric analysis whilst tissue from left hemisphere was taken for gene expression analysis C: caudal, FC: flow cytometry, IHC: immunohistochemistry, R: rostral

4.3.3 Histology

H & E staining was conducted to identify potential areas of neuronal pathology caused by increasing durations of BCAS as described in section 2.6.4. All staining and subsequent analysis was conducted by the author with blinding to sham and BCAS groups.

4.3.4 Immunohistochemistry

Myelin damage was detected by MAG immunostaining while glial reactivity was detected by IBA1 immunostaining in hemi brains on adjacent sections by the author as described in sections 2.6.1 and 2.6.2. Quantification of myelin integrity was conducted in each region of interest using a semi quantitative scoring described in section 2.6.2. A 'total myelin damage' score was also calculated by summating scores from each region of interest per animal.

For IBA1+ cell quantification, four regions of interest measuring 0.2 mm^2 were randomly placed across each white matter tract analysed (see section 4.3.5 below) using ImageJ software. IBA1+ cell bodies were then manually counted within each region of interest and averaged to provide the number of IBA1+ cells per 0.2 mm^2 in each white matter tract. All staining and subsequent analyses were conducted by the author with blinding to sham and BCAS groups.

4.3.5 Regions of interest

Grey matter regions analysed to assess neuronal pathology included the cerebral cortex, thalamus, hippocampus and striatum. White matter regions analysed to investigate the effect of increasing durations of BCAS on myelin integrity include the corpus callosum, hippocampal fimbria, internal capsule and optic tract (fig. 4.2). White matter regions analysed to quantify IBA1+ cells following BCAS include the corpus callosum, hippocampal fimbria, internal capsule and optic tract.

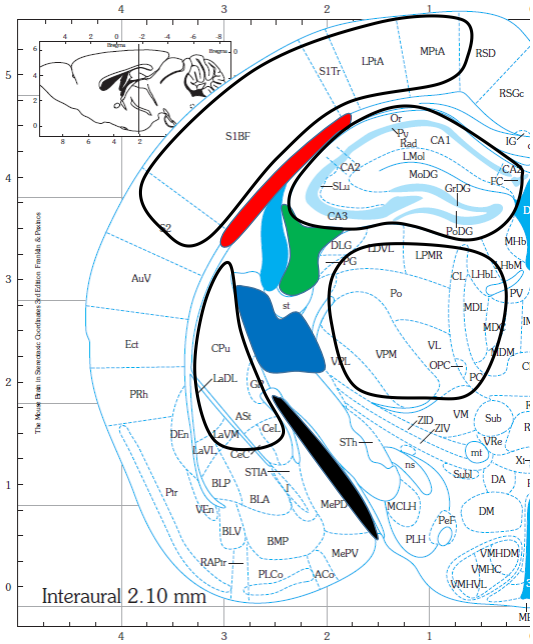

Figure 4.2: White and grey matter regions chosen for pathological assessment. Outlined regions demonstrate grey matter regions analysed (hippocampus, striatum, thalamus and cerebral cortex). Coloured regions mark white matter tracts analysed. (Red: corpus callosum, green: hippocampal fimbria, purple: internal capsule, black: optic tract).

4.3.6 Flow cytometry

Flow cytometry was utilised to investigate the impact of BCAS on CNS cellular composition and cell phenotype. After harvesting brain tissue, homogenisation and preparation of a brain cell suspension was conducted by the author as described in section 2.7. Bone marrow was also isolated and prepared from select animals as a positive control for BrdU staining. Cell populations analysed to investigate the impact of BCAS on CNS immune cell composition include microglia, macrophages, neutrophils, B cells and T cells. Marker profiles used to distinguish cell populations are described in table 4.2. Whilst labelling of cell surface antigens and data acquisition was conducted by the author, preparation of cells for intracellular BrdU labelling was conducted by Clare Latta as described in section 2.7.3.

All data was acquired using a BD LSR Fortessa X20 (Becton Dickinson, Oxford, UK). Absolute cell counts of identified myeloid and lymphoid populations were calculated as described in section 2.7.4. CD45 mean fluorescence intensity (MFI) was also calculated from identified microglia ($Ly6G^{-}Ly6C^{-}Cd11b^{+}CD45^{lo}$) to investigate the impact of BCAS on microglial phenotype. The proportion of viable $BrdU^{+}$ cells was calculated per sample to investigate the impact of BCAS on cell proliferation. Analysis and quantification of data was conducted using FlowJo version 10 by the author with blinding to sham and BCAS groups as described in section 2.7.4.

Cell type	Marker profile
Microglia	$Ly6G^{-}Ly6C^{-}CD11b^{+}CD45^{lo}$
Macrophages	$Ly6G^{-}CD11b^{+}CD45^{hi}Ly6C^{lo\text{-}hi}$
Neutrophils	$Ly6G^{+}CD11b^{+}CD45^{+}$
B cells	$CD11b^{-}B220^{+}$
T cells	$CD11b^{-}CD3^{+}$

Table 4.2: Marker profiles used to identify cell populations for flow cytometric analysis.

4.3.7 Statistics

Fisher's exact test was used to determine if BCAS increased the probability of myelin damage occurring. Mann Whitney U test was conducted to test for differences in myelin integrity between BCAS and sham treatment groups at 1 w, 1 m and 3 m. Student's unpaired t test was used to test for differences in IBA1+ cell number, CD45 MFI and cell proliferation between BCAS and sham treatment groups at 1 w, 1 m and 3m. Two way ANOVA with Bonferroni correction for *post hoc* was used to investigate the impact of BCAS on cell composition in WT and BCAS mice with time and surgery as between subject factors. All statistical analyses were performed with Graphpad Prism software version 7.4 with statistical significance considered $p \leq 0.05$.

4.4 Results

4.4.1 Animal recovery

Following surgery, no sham or BCAS mice demonstrated adverse neurological symptoms such as circling, seizures or barrel rolling indicative of overt neuronal damage. Mice were motile and responsive within 1 h of surgery. Within 24 – 48 h mice were also observed eating and drinking with normal exploratory behaviour. All animals remained healthy until tissue harvest. In cohort 1 (1 week), sham and BCAS mice demonstrated a maximal 3.1 % and 5.6 % loss in weight 3 d following surgery, respectively. In cohort 2 (1 month) sham and BCAS mice demonstrated a maximal 2.8 % and 6.4 % loss in weight 3 d following surgery, respectively. In cohort 3 (3 months), sham and BCAS mice demonstrated a maximal 5 % and 10.2 % loss in weight 3 d following surgery, respectively (see appendix sections 8.2.1 – 8.2.3). The final cohort sizes were as follows:

Cohort (Duration of BCAS)	Sham (n)	BCAS (n)
1 (1 week)	10/ 10	12/ 12
2 (1 month)	8/ 8	10/ 10
3 (3 months)	9/ 9	8/ 8

Table 4.3: Final cohort sizes following sham and BCAS surgeries (1 w, 1 m & 3 m).

4.4.2 Pathological Assessment

4.4.2.1 H & E assessment of CNS pathology

H & E staining was utilised to investigate if BCAS over various durations provoked neuronal pathology. No sham animals displayed evidence of neuronal pathology at any time point analysed. Furthermore, there was no evidence of neuronal pathology in any grey matter region analysed 1 w, 1 m and 3 m following BCAS (table 4.4, fig. 4.3).

Treatment	1 week	1 month	3 months
Sham	0/ 10 (0 %)	0/ 8 (0 %)	0/ 9 (0 %)
BCAS	0/ 12 (0 %)	0/ 10 (0 %)	0/ 8 (0 %)

Table 4.4: Mice displaying neuronal pathology identified via H & E staining following sham and BCAS surgeries (1 w, 1 m and 3 m). No animals demonstrated evidence of neuronal pathology 1 w, 1 m or 3 m following BCAS surgeries. Regions analysed include the thalamus, hippocampus, cortex and striatum. One tissue section analysed per animal.

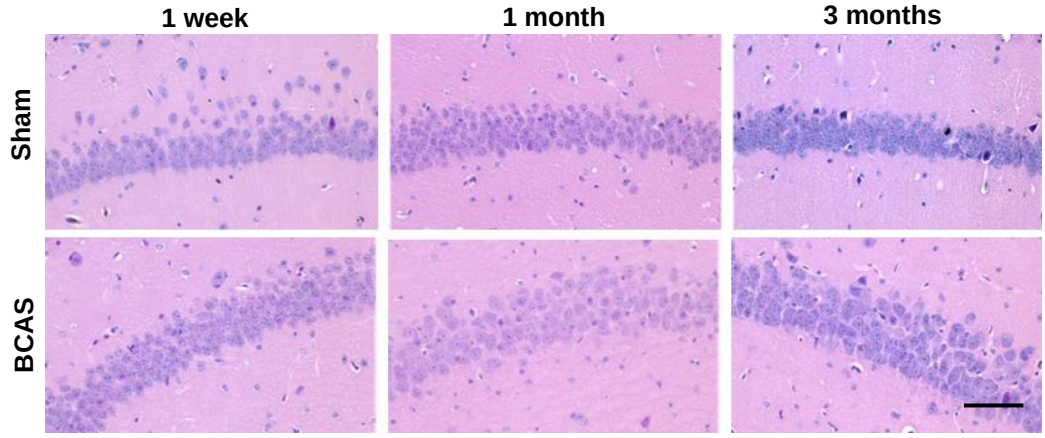

Figure 4.3: Representative images of H & E staining in the CA1 region of the hippocampus 1 w, 1 m and 3 m following sham and BCAS surgeries. Scale bar: 100 μm

4.4.2.2 Assessment of myelin integrity

MAG immunostaining was conducted to investigate the impact of increasing durations of BCAS on myelin integrity. Sham animals displayed minimal myelin damage at any time point analysed (1 w: 0 of 10, 1 m: 1 of 8, 3 m: 0 of 9). Induction of BCAS resulted in infrequent myelin damage at all time points analysed (1 w: 3 of 12, 1 m: 4 of 10, 3 m: 4 of 8) (table 4.5). Damage was subtle and anatomically confined to one or two white matter regions per animal. 1 w after BCAS, myelin damage was most frequently observed in the corpus callosum (3 of 12) followed by the optic tract (1 of 12) and internal capsule (1 of 12). No damage was observed in the hippocampal fimbria. After 1 m, damage was observed in the corpus callosum (1 of 10), optic tract (1 of 10), internal capsule (1 of 10) and hippocampal fimbria (1 of 10). After 3 m, damage was most frequently observed in the corpus callosum (3 of 8) and optic tract (2 of 8) but was absent in the internal capsule or hippocampal fimbria (fig. 4.4). Increasing BCAS duration did not increase the probability of overall myelin damage occurring ($p \geq 0.05$). No significant difference in myelin integrity was observed compared to sham animals in individual white matter tracts at any time point analysed ($p \geq 0.05$) (fig. 4.5B). Furthermore, no difference in total myelin damage was observed following BCAS compared to sham animals at any time point analysed ($p \geq 0.05$) (fig. 4.5C).

Treatment	1 week	1 month	3 months
Sham	0/ 10 (0 %)	1/ 8 (12.5 %)	0/ 9 (0 %)
BCAS	3/ 12 (25 %)	4/ 10 (40 %)	4/ 8 (50 %)

Table 4.5: Mice displaying myelin damage detected by MAG immunostaining following sham and BCAS surgeries (1 w, 1 m & 3 m). BCAS caused infrequent myelin damage at all time points analysed. Increasing duration of BCAS did not increase the probability of myelin damage occurring. Fisher's exact test. One tissue section analysed per animal.

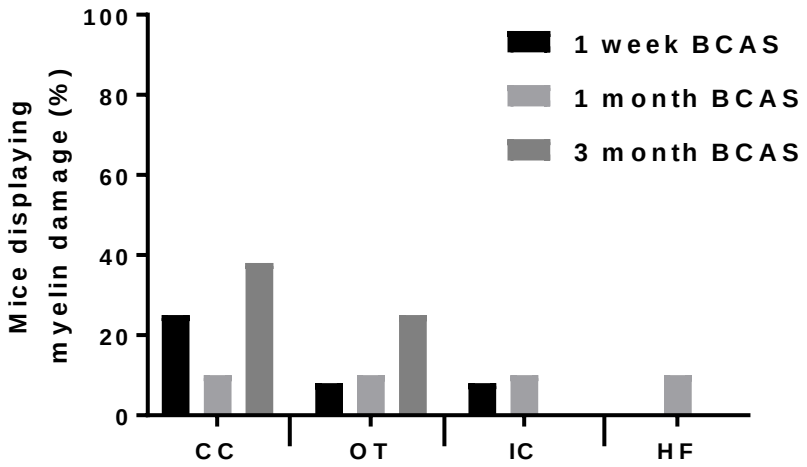

Figure 4.4: Frequency of myelin damage detected by MAG immunostaining 1 w, 1 m and 3 m following BCAS. One tissue section analysed per animal. CC: corpus callosum, HF: hippocampal fimbria, IC: internal capsule, OT: optic tract.

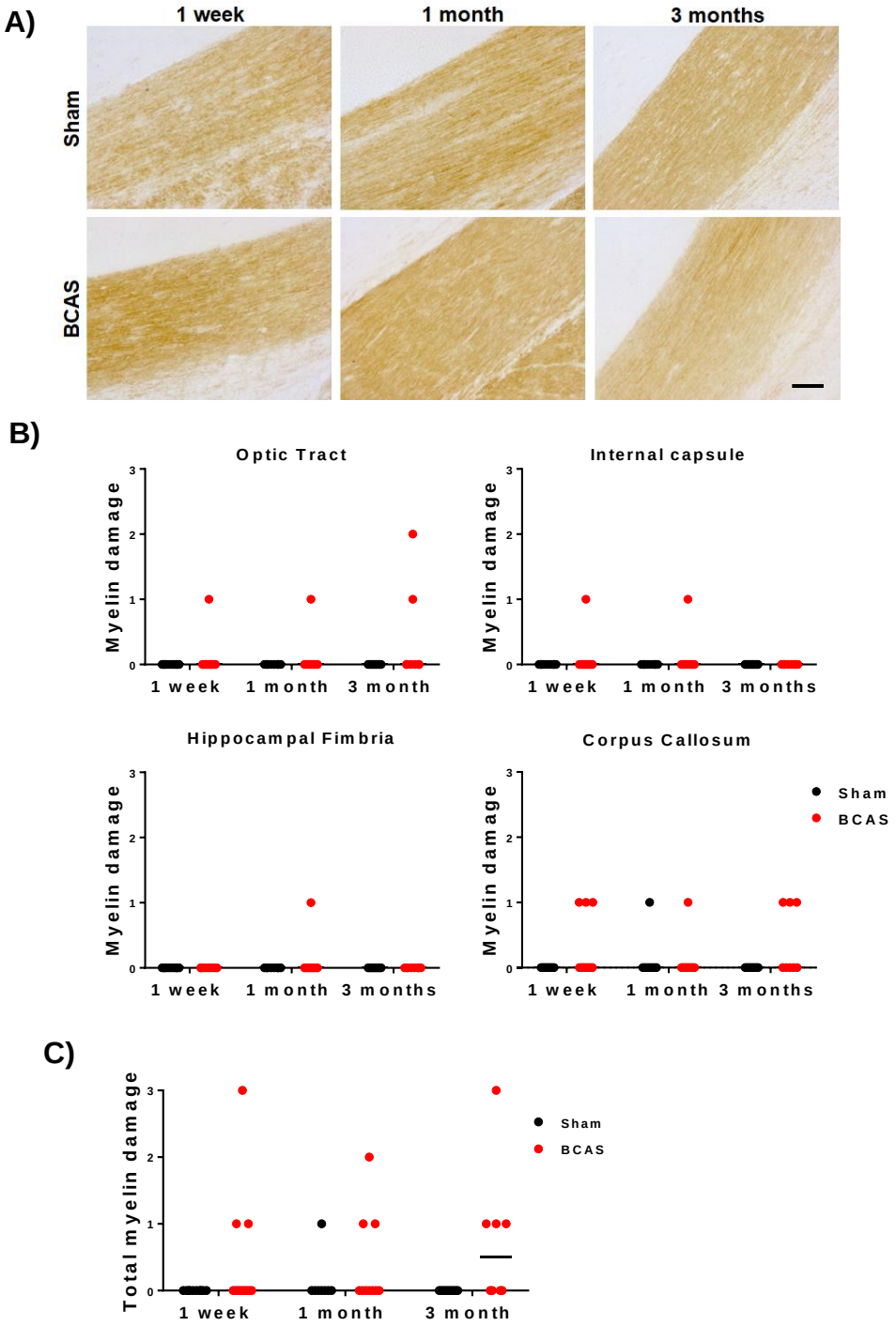

Figure 4.5: Quantification of myelin integrity detected by MAG immunostaining 1 w, 1 m and 3 m following BCAS. (A) Representative images showing MAG immunostaining of the optic tract 1 w, 1 m and 3 m after BCAS and sham surgeries. Scale bar: 50 µm (B) Myelin damage in each white matter tract was quantified by MAG immunostaining using a semi quantitive scoring method ranging from 0 (no damage) to 3 (extensive damage) providing a total possible score of 3 per white matter region. BCAS did not cause a significant increase in the extent of white matter damage compared to sham animals at any time point analysed. (C) Myelin damage scores were summated from all analysed white matter tracts providing a 'total myelin damage' score per animal. No difference in total myelin damage was observed following BCAS surgeries at any time point analysed. Mann Whitney U test. One tissue section analysed per animal. Each data point represents an independent animal. Bars show median. N = 6 – 12 independent animals per group.

4.4.2.3 Assessment of microgliosis

Microglial morphology was assessed by IBA1 immunostaining and microglial number quantified to investigate how microglial react to increasing durations of BCAS. No overt differences in microglial morphology were observed in grey or white matter regions in response to BCAS at any time points analysed. Microglia largely retained a ramified morphology with small cell bodies in all regions analysed. Only one mouse displaying moderate white matter damage in the optic tract (severity score 2) demonstrated detectable microgliosis (fig. 4.6). Quantification of IBA1+ cells in white matter tracts revealed increasing durations of BCAS had no significant effect on microglial number compared to sham mice ($p \geq 0.05$) (fig. 4.7).

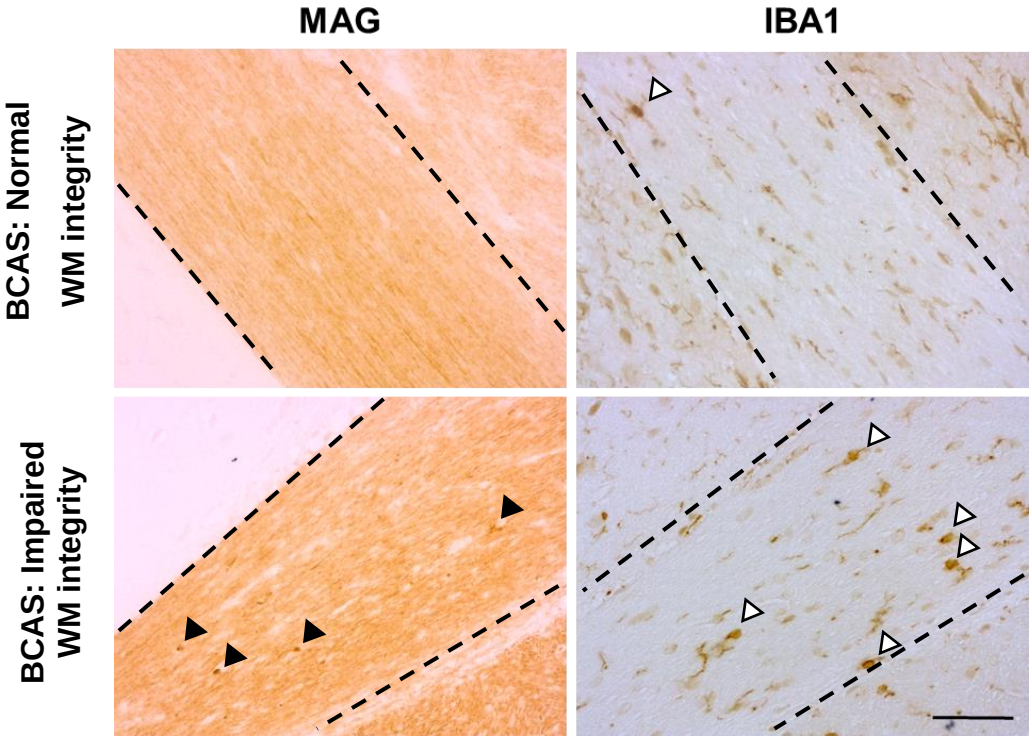

Figure 4.6: Representative images of MAG and IBA1 immunostaining showing microgliosis in areas of white matter damage. Black arrows show areas of white matter debris. White arrows show IBA1 + cell bodies. Dotted lines mark borders of optic tract Scale bar: 50 μm.

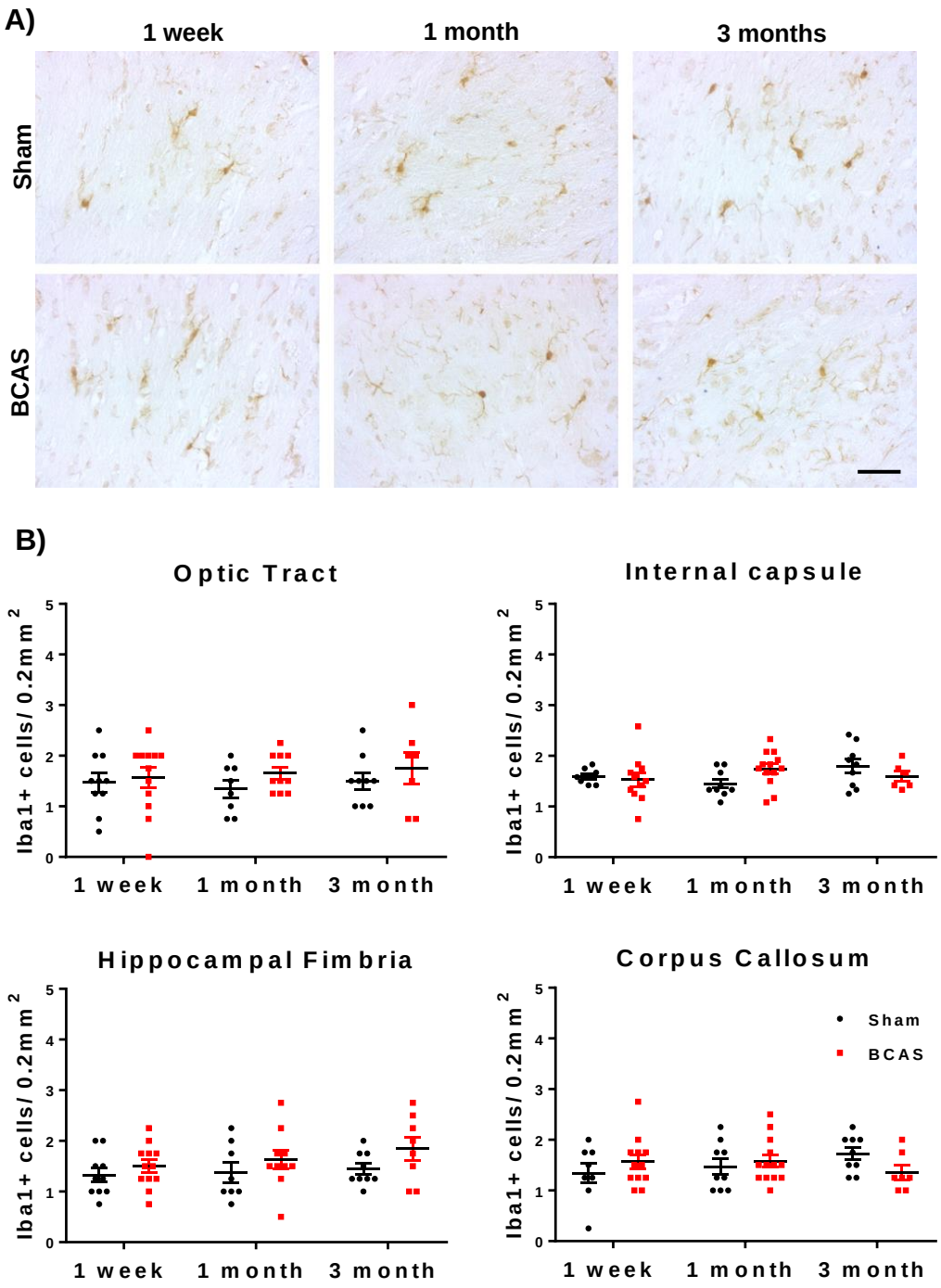

Figure 4.7: Quantification of IBA1+ cell number 1 w, 1 m and 3 m following BCAS. (A) Representative images of IBA1 immunostaining of the internal capsule 1 w, 1 m and 3 m following sham and BCAS surgeries. Scale bar: 50 μm (B) Quantification of IBA1+ cells in individual white matter tracts demonstrated IBA1+ cell number was unchanged in all white matter tract analysed following BCAS at all time point analysed. Each data point represents a value calculated and averaged from 4 regions of interest measuring 0.2 mm^2 placed across each white matter tract from an independent animal. One tissue section analysed per animal. Student's unpaired test. Bars show mean ± SEM. N = 6 - 12 independent animals per group.

4.4.3 Flow cytometric analysis

Although pathological assessment revealed BCAS did not induce detectable white or grey matter pathology at the level of the hippocampus it could be possible that pathology may have developed elsewhere in the brain outside of the regions of interest selected. Flow cytometry was conducted on opposing hemispheres to determine if increasing durations of BCAS provoked alterations in microglial phenotype or inflammatory cell composition.

Analysis of myeloid and lymphoid cell populations revealed microglia were the primary cell type constituting 75-85 % of the total cell population while all other identified myeloid and lymphoid cell populations formed < 1 % of the total cell population (fig. 4.8). BCAS animals demonstrated similar numbers of each cell type compared to sham animals at all time points analysed. Interestingly, both sham and BCAS animals showed increased numbers of T cells and microglia 3 months post surgery. Two way ANOVA demonstrated significant effects of time on microglial $F(2, 51)=25.1$, $p<0.0001$) and T cell $F(2, 51)=17.44$ $p<0.0001$) number. Post hoc analysis demonstrated microglia and T cells were significantly increased in sham and BCAS mice 3 months post-surgery compared to mice 1 week and 1 month following sham and BCAS surgeries ($p<0.0001$). However, no surgery or interaction effect was detected at any time point analysed ($p \geq 0.05$) (fig. 4.8). Furthemore, no significant time, surgery or interaction effects on cell number were detected for any other cell type at any time point analysed ($p \geq 0.05$).

As increased CD45 expression is typically associated with microglial activation, CD45 MFI was also measured. In response to BCAS, no significant difference in CD45 MFI was observed compared to sham animals at any time point analysed ($p \geq 0.05$) (fig. 4.9). Analysis of BrdU labelling demonstrated increased expression on bone marrow-derived cells suggesting that cell proliferation could be detected (fig. 4.10). However, no significant difference in the proportion of BrdU positive cells was observed with increasing durations of BCAS compared to sham animals ($p \geq 0.05$) (fig. 4.10).

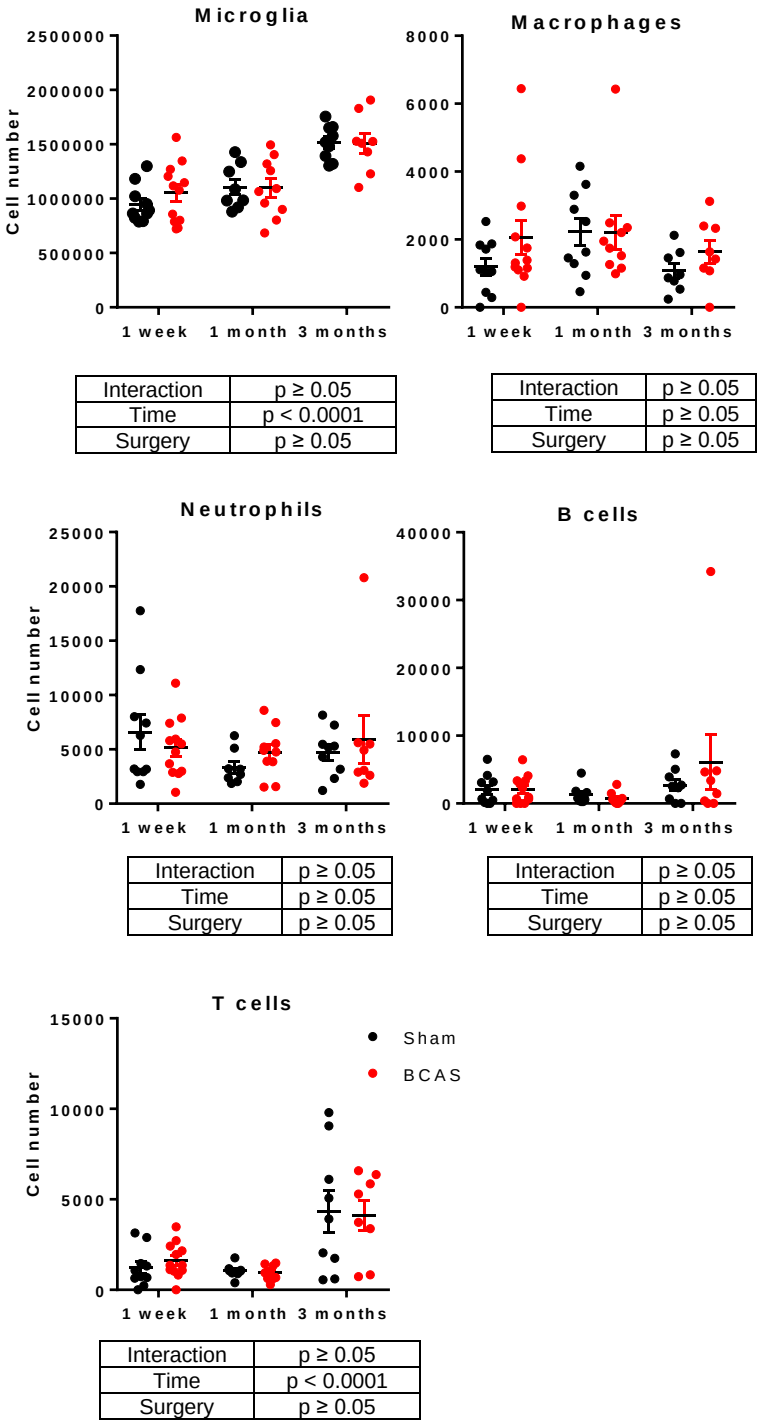

Figure 4.8: Quantification of CNS myeloid and lymphoid populations 1 w, 1 m and 3 m following BCAS. Microglia and T cells were significantly increased in mice 3 m post-BCAS and sham surgeries compared to mice 1 w and 1 m post-BCAS and sham surgeries. No effects of BCAS surgery or interaction effects were observed in any cell population at any time point analysed.Two way ANOVA with Bonferroni correction for post hoc. Each data point represents an independent animal. Data show mean ± SEM. N = 8 – 12 independent animals per group.

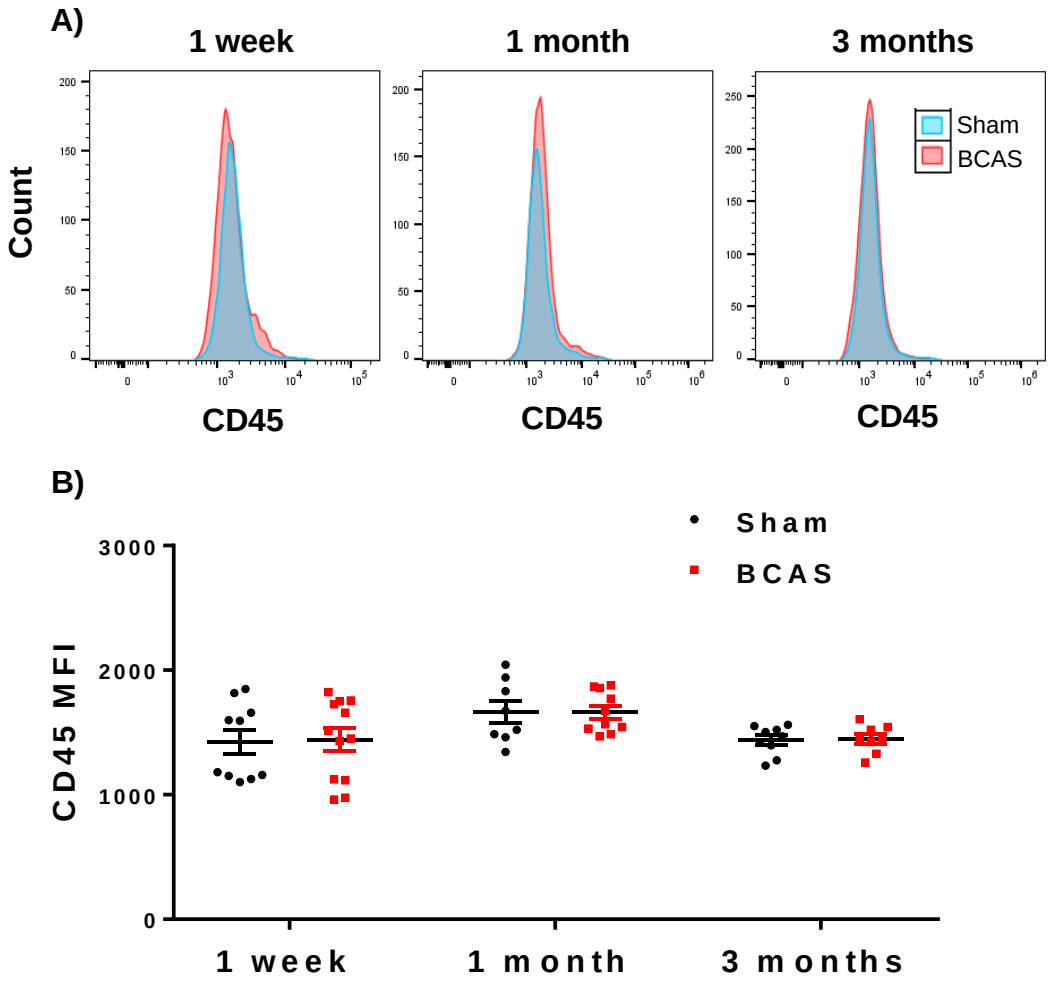

Figure 4.9: Quantification of CD45 MFI 1 w, 1 m and 3 m following BCAS. (A) Representative histogram plots of CD45 fluorescence in sham and BCAS animals at 1 w, 1 m and 3 m. (B) Quantification of MFI in 1 w, 1 m and 3 m following sham or BCAS surgeries by flow cytometry. CD45 MFI was unchanged after 1 w, 1 m or 3 m BCAS compared to sham animals. Student's unpaired t-test. Each data point represents an independent animal. Data show mean ± SEM. N = 8 – 12 independent animals per group.

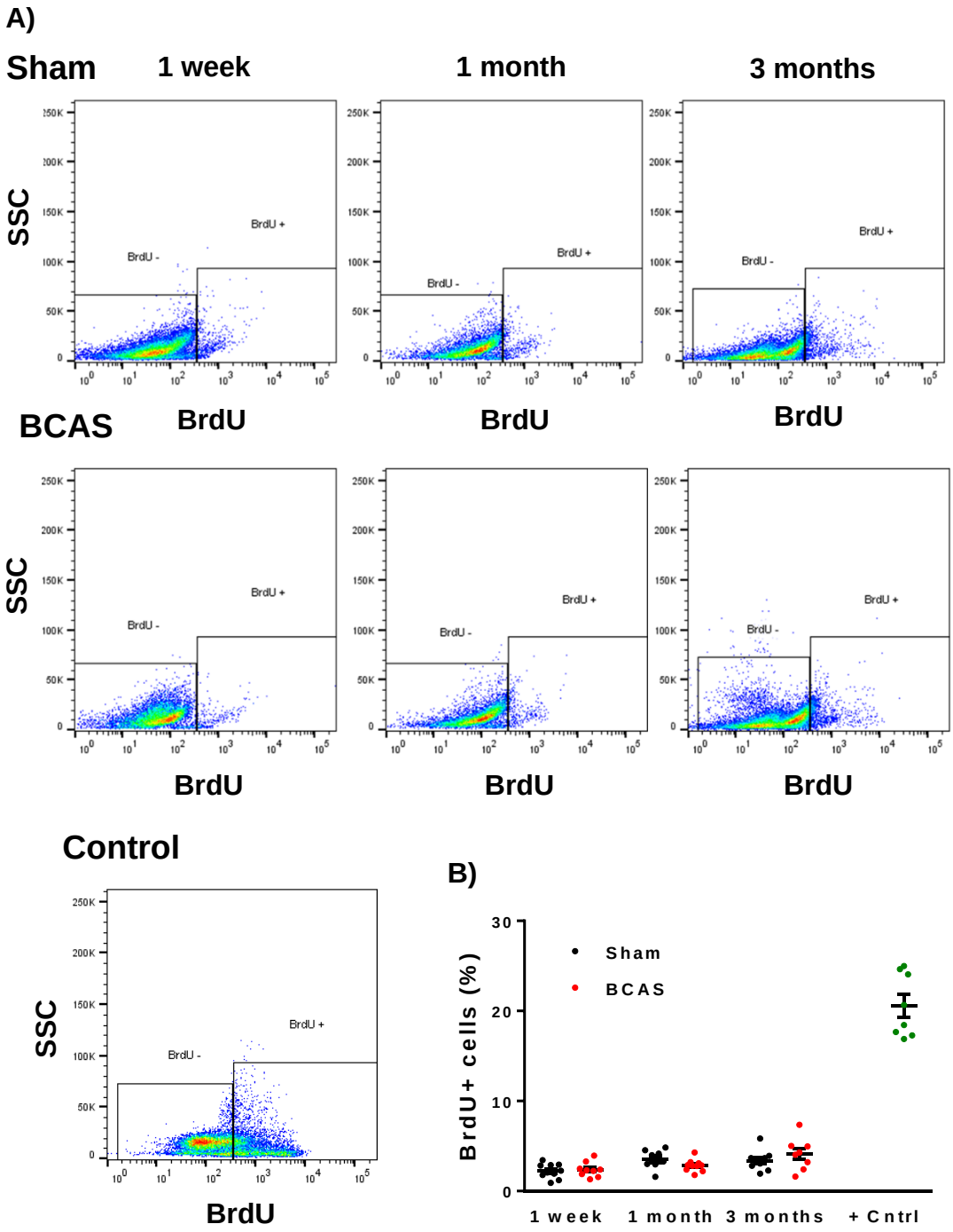

Figure 4.10: Quantification of cell proliferation 1 w, 1 m and 3 m following BCAS. (A) Representative dot plots of total BrdU positive cells 1 w, 1 m and 3 m following sham and BCAS surgeries. Bone marrow-derived cells were used as a positive control from selected animals. (B) Quantification of BrdU+ cells 1 w, 1 m and 3 m following sham and BCAS surgeries. The proportion of viable BrdU+ cells was unchanged1 w, 1 m or 3 m after BCAS compared to sham animals. Student's unpaired t-test. Each data point represents an individual animal. Data show mean ± SEM. N = 8 – 12 independent animals per group.

4.5 Discussion

From this study it can be concluded that induction of BCAS using 0.18 mm internal diameter microcoils for extended periods does not provoke grey matter pathology and only infrequent and mild alterations in myelin integrity in WT C57BL6/Ntac mice. Furthermore, no overt changes in microglial reactivity or alteration in other myeloid or lymphoid cell populations were observed.

Although a robust neuroinflammatory response is commonly observed in areas of white matter damage in preclinical models of VCI and the elderly, the precise contribution to white matter injury and cognitive impairment remains unclear. It is unknown how the neuroinflammatory response to hypoperfusion develops over time or how CNS inflammatory cell composition evolves with this. Previous studies have demonstrated microglial number closely correlates to loss of white matter structural and functional integrity (Fowle et al., 2018, Manso et al., 2018) and pharmacological or genetic modulation of the neuroinflammatory response has shown to ameliorate white matter structure and function in various models of chronic cerebral hypoperfusion (Manso et al., 2018). Although such findings suggest inhibition of microglial activation may be beneficial in the context of chronic cerebral hypoperfusion it is difficult to make firm conclusions about the precise role of microglia. Firstly, pharmacological interventions used to dampen neuroinflammation in models of VCI such as minocycline affect additional cell types including astrocytes, oligodendrocytes and neurons have also been reported (Moller et al., 2016). Studies specifically ablating microglial function in models of VCI are limited and the impact of chronic cerebral hypoperfusion on the microglial transcriptome is unknown. Therefore, the precise function of microglia in this context remains unclear.

Inflammatory mediators secreted upon microglial activation including cytokines, ROS and proteases are likely to contribute to cerebrovascular pathology and white matter damage. IL-1β and TNF-α downregulate tight junction proteins on endothelial cells increasing BBB permeability (Wu, et al., 2010, Yamagata, et al., 2004, Mark, et al., 1999, Wong, et al., 2007). Excess IL-1β may also be detrimental to myelin integrity as treatment with an IL-1R antagonist

ameliorates hypomyelination following intracerebral LPS injection in neonatal mice (PangCai and Rhodes, 2003).

Furthermore, TNF-α-treated oligodendrocytes demonstrate increased apoptosis *in vitro* and overexpression promotes a chronic demyelinating disease with early mortality in rodents (Buntinx et al., 2004, Probert et al., 1995). Microglia are also a source of MMPs including MMP2 which has shown to contribute to white matter damage and BBB disruption in response to BCAS (ihara et al., 2001, Nakaji et al., 2006). However, release of such inflammatory mediators may also serve beneficial functions. Mice lacking TNF-α or IL-1β demonstrate delayed remyelination and impaired OPC maturation in the cuprizone model of demyelination (Arnett et al., 2001, Mason et al., 2001). Furthermore, microglial phagocytosis of myelin debris is also essential for remyelination and microglia are a source of various trophic mediators including BDNF, IGF-1 and LIF (Lampron et al., 2015, Goldstein et al., 2016).

Although microglia are predominant mediators of neuroinflammation being the primary innate immune cells of the CNS, various other cell types also contribute to the neuroinflammatory response. Inhibition of astrocyte-derived NFκB ameliorated white matter damage, gliosis and memory deficits resulting from BCAS suggesting astrocytes also contribute to inflammatory-mediated damage (Saggu et al., 2016). This is further supported by a recent study in which astrocyte-specific overexpression of the transcription factor *Nrf2* reduced inflammation and improved white matter integrity and memory performance after BCAS (Sigfridsson et al., 2018).

Pericytes, endothelial cells, perivascular macrophages and meningeal macrophages have also been reported to release inflammatory mediators. However, their contribution to hypoperfusion-mediated inflammation and subsequent white matter injury remains unclear. Considering neuroinflammation is suggested to play a key role in mediating white matter injury and cognitive impairment it is crucial to gain a detailed understanding of the cellular and molecular neuroinflammatory profile and how inflammatory cells function in this context. This study therefore sought to provide insight into the key cellular players in the neuroinflammatory

response to chronic cerebral hypoperfusion and determine if microglia exclusively contribute to the neuroinflammatory response or if peripherally derived leucocytes also play a role.

In the previous study, subtle alterations in myelin integrity were observed 28 d following induction of BCAS. Separate studies demonstrate rapid loss of axon-glial integrity 3 d after BCAS and diffuse white matter damage extending over various white matter tracts after 28 d (Coltman et al., 2011, Reimer et al., 2011). Extending the duration of BCAS to 6 m further exacerbates pathology with multiple ischaemic and haemorrhagic lesions observed throughout the brain in grey and white matter regions (Holland et al., 2015). As only mild alterations in white matter integrity were observed after 28 d it was initially thought the duration of BCAS was insufficient to provoke significant white matter pathology and reactive gliosis. It was therefore hypothesised that increasing the duration of hypoperfusion further would elicit more extensive pathology.

In the current study, histological assessment of CNS tissue revealed increasing durations of BCAS did not cause overt neuronal pathology at any time point analysed comparable with previous studies (Shibata et al., 2004, Coltman et al., 2011). Although BCAS has shown to induce robust white matter changes after 28 d this study found only infrequent and negligible alterations in myelin integrity at both 28 d and 3 m with no progression of damage.

As discussed in the previous chapter, it is unlikely that the methods utilised in this study were not of adequate sensitivity to detect subtle alterations in white matter integrity induced by BCAS. Previous studies have also demonstrated rapid disruption of paranodal proteins detected via loss of Caspr and Neurofascin colocalisation and increased voltage-gated sodium channel length in response to cerebral hypoperfusion (Reimer et al., 2011, Koizumi et al., 2018). This was not conducted in this study but would have proved useful to further investigate if chronic cerebral hypoperfusion induced subtle alterations in paranodal integrity.

As loss of axon glial and nodal/ paranodal integrity develop prior to other pathological hallmarks including endothelial dysfunction, pericyte loss and BBB breakdown it is also unlikely other pathologies would be detected in the absence of reduced white matter integrity. The absence of white matter pathology is further supported by lack of microgliosis in analysed white matter tracts. Previous studies have demonstrated microglial activation in adjacent sections corresponding to areas of white matter damage (Coltman et al., 2011, Liu et al., 2015, Manso, et al., 2018). As microglial morphology and number remained largely unchanged in analysed white matter regions at all time points it is likely that BCAS failed to induce white matter injury.

Although alterations in white matter structure and glial reactivity were investigated, white matter function was not assessed. However, it is unlikely that behavioural or functional abnormalities would be detected as previous studies typically describe impaired spatial working memory and reduced white matter conduction velocity in the presence of white matter pathology (Coltman et al., 2011, Fowler et al., 2018, Manso et al., 2018). Interestingly, a recent study using a modified version of BCAS described defects in network connectivity and spatial learning in the absence of detectable white matter pathology or reactive gliosis (Boehm-Sturm et al., 2017). Although luxol-fast blue was used to examine gross myelin changes which may not reveal more subtle alterations in myelin integrity it is surprising glial reactivity was not observed. It could therefore be postulated that white matter connectivity may still have been impaired in the absence of structural abnormalities detected by IHC. However, this was beyond the scope of this study.

As pathological assessment was only conducted on a single hemisphere at the level of the hippocampus it could be suggested that pathology developed elsewhere in the brain. However, this is unlikely as flow cytometry on bulk tissue from opposing hemispheres failed to detect any BCAS-related differences in cell composition or phenotype. As flow cytometric analysis presents information on cell characteristics on a cell-by-cell basis it is unlikely the technique was not of adequate sensitivity to detect BCAS-related alterations in cell composition and phenotype.

Although bone marrow derived cells were utilised as a positive control to ensure cell proliferation could be detected via BrdU labelling, a positive control was not implemented to determine if changes in cell composition or phenotype could be detected via flow cytometry. Extracted brain tissue was treated with proteolytic enzymes prior to tissue homogenisation. Subsequent optimisation experiments for FACS-based microglial isolation described in chapter 6 demonstrated enzyme treatment alters microglial phenotype increasing microglial granularity and CD45 MFI suggestive of microglial activation. Although previous studies in the McColl lab have demonstrated detectable neuroinflammatory changes using this method in models of stroke and sterile inflammation it could be argued that more subtle alterations in cell composition or phenotype may have been masked by phenotypic alterations caused by enzyme digestion prior to data acquisition.

BCAS did not alter CNS cell composition compared to sham animals at any time point analysed. However, both sham and BCAS mice demonstrated increased numbers of microglia and T cells in the CNS 3 m post-surgery. Age-dependant changes in CNS immune composition have been reported in aged mice including T cell infiltration and increased microglial density (Poliani et al., 2015, Dulken et al., 2019). However, many of the changes have been reported in mice aged between 12- 24 months whilst mice used in this study were just 5-6 m of age at tissue harvest. Whilst increased numbers of microglia were detected via flow cytometry 3 months post sham and BCAS surgery, no such changes were observed in white matter regions analysed by IHC. It could be postulated changes in microglial density occurred in brains regions outside those analysed by IHC. In addition to this, changes in T cell composition were not validated via IHC in opposing brain hemispheres. It therefore, remains unclear precisely why increased numbers of microglia and T cells were observed 3 months following sham and BCAS surgeries.

Although studies investigating changes in CNS cell composition following cerebral hypoperfusion are limited, a recent study demonstrated lymphocyte infiltration does not occur 1 m after BCAS (Fuechtemeier et al., 2015). A separate study using IHC also demonstrated lack of neutrophil infiltration in response to BCAS (Miyanohara et al., 2018). Furthermore,

studies utilising microglial-specific markers such a TMEM119 or adoptive transfer suggest macrophage infiltration does not occur in response to BCAS implying that microglia are the predominant contributors to the neuroinflammatory response following chronic cerebral hypoperfusion (Manso et al., 2018, Miyanohara et al., 2018). On the other hand, post mortem studies have identified leucocyte infiltration in the vascular wall and perivascular spaces of cSVD patients (Wardlaw, Smith and Dichgans, 2013). As preclinical studies were conducted only 1-3 m following BCAS surgery it could be postulated that infiltration of peripheral myeloid or lymphoid cells occur at later time points when more profound vascular pathology is observed including BBB breakdown.

White matter tissue was also dissected from animals and stored to conduct gene expression analysis to characterise the temporal molecular neuroinflammatory profile resulting from BCAS. However, this was not completed as it is unlikely that any gene expression changes would be detected given the lack of pathology or glial reactivity. This is supported from gene expression analysis demonstrating no detectable changes in key inflammatory genes in isolated white matter with significant pathology and reactive gliosis following BCAS (Manso et al., 2018). Alterations in the molecular neuroinflammatory profile would likely be determined via transcriptomic analysis of isolated microglia, however, this was beyond the scope of this study.

Overall, the data from the current study demonstrates use of 0.18 mm internal diameter microcoils is insufficient to induce overt white matter pathology and neuroinflammation in WT C57BL/6Ntac mice. As previous studies have utilised similar methods and detected white matter damage and neuroinflammatory changes it is unlikely that lack of sensitivity is a primary reason. It remains unclear why use of 0.18 mm internal diameter microcoils failed to induce detectable white matter changes comparable to previous studies. As stated previously, a limitation of the current study is that changes in cerebral blood flow could not be measured as equipment to do so was unavailable. Use of a hypoxia probe similar to that used by Koizumi et al. (2018) following BCAS may have proved useful to validate if induction of BCAS caused tissue hypoxia (Koizumi, et al., 2018). Therefore, whilst previous studies have reported use of

0.18 mm internal diameter microcoils reproducibly reduces cerebral blood flow it cannot be assumed in this case. It may be that the internal diameter of microcoils were too large resulting in insufficient carotid artery stenosis. It could also be postulated that cerebral blood flow was reduced but animals were able to effectively compensate via autoregulation.

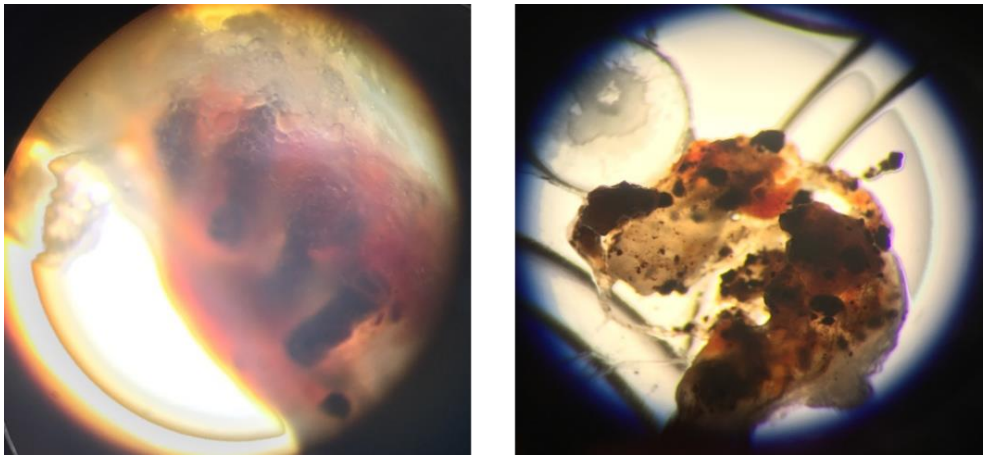

Figure 4.11: Microcoil integrity 28 d following implantation. Microcoils extracted 28 d following surgery appeared rusted and disinitergrated upon dissection. Therefore, compromised microcoil integrity may have prevented sufficient stenosis and cerebral hypoperfusion to precipitate white matter damage in the current study.

Previous studies using 0.18 mm internal diameter microcoils consistently demonstrate an acute reduction in cerebral blood flow after microcoil placement (Shibata et al. 2004, McQueen et al. 2014). Although partial recovery of cerebral blood flow occurs over time, hypoperfusion is typically maintained over extended durations. However, Füchtemieier et al. (2015) demonstrated near-complete recovery of cerebral blood flow after 28 d and negligible pathology attributed to loss of microcoil integrity (Füchtemieier, et al., 2015). Microcoils dissected from selected animals used in this study were covered in brown fibrous material and appeared rusted. Furthermore, microcoils disintegrated when attempting to remove encased carotid arteries (fig. 4.11). It could therefore be postulated that compromised microcoil integrity may have prevented sufficient stenosis and cerebral hypoperfusion to precipitate white matter damage. However, as stated before, cerebral blood flow measurements were not taken in this study so this can only be suggested.

It is unlikely that surgical error and misplacement of microcoils is a cause for lack of pathology as improper placement typically causes profound reductions in cerebral blood flow and overt cerebral ischaemia. Animals were anaesthetised with inhalational isoflurane which has previously demonstrated to elicit neuroprotection in various preclinical stroke models (Jiang et al., 2017a). Longer anaesthetic preconditioning is associated with reduced ischaemic injury and neurological deficit in response to MCAO (Gaidhani et al., 2017). As this model was novel within the lab group it took longer to dissect and isolate carotid arteries from surrounding tissue. It could therefore be postulated that longer durations of anaesthesia prior to microcoil placement may have elicited protection to BCAS.

Animals were additionally anesthetised with 70 % nN_2O. N_2O is an N-methyl-D-aspartate (NMDA) receptor antagonist suggested to exert neuroprotection. However, studies investigating the protective role of N_2O have yielded inconsistent results. For example, addition of 50 % N_2O 2 h after transient MCAO reduced infarct volume in rats (Haelewyn et al., 2008). In other studies, addition of 70 % N_2O to anesthetic had no effect on ischaemic pathology (Yokoo et al., 2004). The specific impact of N_2O on CNS pathology in response to BCAS has never been investigated. Previous studies have however implemented N_2O and identified white matter pathology 28 d after BCAS suggesting N_2O does not exert profound protection to BCAS (Miyanohara et al., 2018, Kakae et al., 2019).

Additional factors including temperature, handling, environmental enrichment, diet and microbiota can all impact outcome from cerebrovascular-mediated injury (Hase et al., 2017, Benakis et al., 2016). As procedures and recovery were carried out in a separate unit to previous studies in which animal housing, diet and maintenance differ, it could be suggested that a combination of factors impacted the extent of pathology caused by BCAS. Age has also demonstrated to contribute to the severity of CNS pathology resulting from BCAS. 21 m old mice demonstrate greater white matter pathology associated with exacerbated neuroinflammation and cognitive deficits compared to 3 m old mice following BCAS (Wolf et al., 2017). Mice used in this study were 8-10 w of age and may have had increased resilience to white matter injury resulting from BCAS. However, previous studies have utilised mice of a

similar age and detected robust white matter injury in response to BCAS making age an unlikely contributor to discrepancies observed (Khan et al., 2015).

Susceptibility to ischaemic injury is also highly dependent on mouse strain due to variation in cerebrovascular anatomy (Barone et al., 1993). C57BL/6J mice are preferentially used in preclinical models of VCI due to underdevelopment of the posterior communicating arteries within the circle of Willis (Kitagawa et al., 1998). The posterior communicating arteries enable communication between the basilar artery of the vertebral circulation and the posterior cerebral arteries which arise from the carotid circulation. Therefore, if underdeveloped, compensatory blood flow from the vertebral circulation is impaired if carotid circulation is compromised and vice versa reducing the threshold for ischaemic injury.

As WT and TREM2-/- mice were bred on a C57BL6/Ntac background it could be postulated that genetic differences could explain discrepancies in BCAS-induced pathology. Various studies have demonstrated genetic and phenotypic differences between C57BL/6 substrains in behavior, immune and metabolic responses (Fontaine and Davis, 2016, Simon et al., 2013, Bryant et al., 2008). Indeed, a recent study utilising FVB/C57BL/6JF1 demonstrated BCAS caused loss of white matter integrity limited to the optic tract which was more extensive compared to mice on a pure C57BL/6J background (Sigfridsson, et al., 2018). No overt differences in circle of Willis anatomy have been observed between C57BL/6N or C57BL/6J animals. Furthermore, laser speckle contrast imaging has demonstrated no difference in cortical blood flow between C57BL/6N and C57BL/6J substrains (ZhaoMulligan and Nowak, 2019). Whether substrain differences exist in cerebrovascular architecture supplying deeper subcortical regions remains to be established.

A prominent genetic difference identified between C57BL/6 substrains includes a deletion spanning exons 7 to 11 of the gene encoding nicotinamide nucleotide transhydrogenase (*Nnt*) in C57BL/6J mice resulting in complete loss of function (Mekada et al., 2009). *Nnt* is an enzyme found in the inner mitochondrial membrane and plays a key role in reducing NADP+ to NADPH enabling subsequent elimination of ROS generated during ATP generation. Liver mitochondria isolated from C57BL/6J mice demonstrate increased ROS release (Ronchi et

al., 2013). Furthermore, Lopert and Patel demonstrated *Nnt* deletion in brain mitochondria increased ROS production, oxidative stress and cell death (Lopert and Patel, 2014). It could therefore be suggested that mitochondrial dysfunction resulting from BCAS is further exacerbated in C57BL6/J mice compared to C57BL6/Ntac due to the absence of *Nnt* resulting in greater ROS generation and oxidative stress-induced damage.

Indeed, oxidative stress is a key mechanism contributing to matter injury resulting from chronic cerebral hypoperfusion. Surprisingly, studies investigating effect of substrain on ischaemic injury have demonstrated the opposite. Despite having similar defects in posterior communicating artery development, C57BL/6N animals have increased infarct volume in response to MCAO (Zhao et al., 2019). Furthermore, neuronal cell death and neuroinflammation is exacerbated in C57BL/6N mice following postnatal hypoxia compared to C57BL/6J mice (Wolf, et al., 2016). The reasons as to why C57BL/6N mice demonstrate more severe ischaemic pathology compared to C57BL/6J mice remain unclear. One possible explanation is reversal of *Nnt* function first described by Nickel and colleages in response to excessive metabolic demand (Nickel et al., 2015). Using a model of heart failure, it was demonstrated that *Nnt* function reverses from being anti-oxidative to pro-oxidative exacerbating oxidative stress and cell death. Such findings suggest C57BL/6Ntac mice would develop more extensive pathology compared to C57BL/6J mice in response to BCAS. It cannot be concluded if substrain was a key contributor to lack of pathology observed in this study as this has never been investigated in the BCAS model. It is likely that a combination of genetic and environmental factors contributed to increased resilience to BCAS-related damage. Although increasing the duration of hypoperfusion to 6 m may increase the extent of damage this was not considered feasible to investigate due to time constraints.

As stated previously, an advantage of the BCAS model is that microcoils with varying internal diameters can be applied to the carotid arteries to modify the extent of hypoperfusion. Initial studies revealed application of 0.16 mm internal diameter microcoils bilaterally increased mortality to 75 % and induced severe white and grey matter damage (Shibata et al., 2004). More recent studies have implemented a 0.16 mm internal diameter microcoil in combination

with a 0.18 mm internal diameter microcoil to increase perfusion deficits. These studies have demonstrated robust white matter damage and neuroinflammation just 6 days after surgery associated with reduced mortality (18 %) (Miki et al., 2008, Fowler, et al., 2018). The 30 min recovery period between placement of microcoils is suggested to allow for restoration of haemodynamics thus placement of microcoils at the same time is suggested to increase the extent of hypoperfusion and white matter damage. This was implemented however no change in extent of white matter damage or neuroinflammation was observed in a small cohort of WT or TREM2-/- mice (see appendix I).

Prior to investigating the impact of TREM2 deficiency it was crucial to optimise the BCAS model to precipitate white matter pathology and overt neuroinflammatory changes. 0.16 mm internal diameter microcoils were used together with 0.18 mm internal diameter microcoils and 0.16 mm internal diameter microcoils were also tested bilaterally. Mortality, cerebral blood flow dynamics and resultant pathology were investigated in WT and TREM2-/- mice to determine a suitable model to investigate downstream pathology and neuroinflammatory changes resulting from BCAS and determine the role of TREM2 in this context.

Chapter 5:

Investigating the impact of TREM2 deficiency on CNS pathology and glial responses to BCAS

5.1 Introduction

TREM2 is an immunoreceptor expressed by CNS resident microglia with key roles in microglial survival, proliferation, phagocytosis, metabolic adaptation and immomodulation (Jay, et al., 2017). Genetic studies demonstrating TREM2 mutations predispose to neurodegenerative conditions and dementia highlight the importance of microglial dysfunction and innate immunity in dementia pathogenesis (Guerreiro et al., 2013a, Guerreiro et al., 2013b, Jonsson et al., 2013). Since this discovery, numerous studies have been conducted to determine how TREM2 regulates microglial processes across neurodegenerative disease settings including AD, MS, stroke and prion disease (Kober and Brett, 2017).

Studies repeatedly demonstrate TREM2 deficiency dampens microglial responses to CNS injury. Although this is generally associated with exacerbated CNS pathology the impact on end stage disease can vary. Given the significance of neuroinflammation in VCI and dementia pathogenesis, it is crucial to understand how TREM2 functions in the context of chronic cerebrovascular dysfunction associated with ageing and dementia. If TREM2 exerts protective effects, investigation of mechanisms warrants further study as this may lead to the identification of novel therapeutic strategies.

In the previous study, BCAS failed to provoke detectable CNS pathology or neuroinflammatory changes in WT C57BL6/Ntac mice. Cerebral blood flow was not measured meaning it could not be concluded if cerebral hypoperfusion was achieved following BCAS surgery. It was therefore important to optimise the BCAS procedure, validate cerebral blood flow was reduced following microcoil placement, and ensure BCAS provoked sufficient CNS pathology to investigate the role of TREM2. In addition to modifying the BCAS surgery to induce more substantial hypoperfusion, laser speckle flowmetry was utilised to assess cerebral blood flow in WT and TREM2-/- mice following BCAS. In this study, it was hypothesised that use of microcoils with smaller internal diameters would evoke myelin pathology and that this would be exacerbated in TREM2-/- mice.

5.2 Aims

1. Optimise the BCAS procedure and validate induction of chronic cerebral hypoperfusion in WT and TREM2-/- mice.
2. Characterise CNS pathology and glial responses resulting from 28 d BCAS in WT and TREM2-/- mice using histology and IHC.

5.3 Methods

5.3.1 Animal procedures

WT and TREM2-/- male mice aged 7 - 9 m were assigned to receive sham or BCAS surgeries. In cohort 1, the BCAS procedure described in 2.4.1 was modified so that a smaller 0.16 mm internal diameter microcoil was fitted on the right carotid artery whilst a 0.18 mm internal diameter microcoil was placed on the left carotid artery (WT: n = 10, TREM2-/-: n = 6). In cohort 2, animals were fitted with 0.16 mm internal diameter microcoils bilaterally to induce greater perfusion deficits (WT: n = 13, TREM2-/-: n = 12). Sham surgeries were conducted as described in 2.4.1. Due to lack of breeding and limited animal numbers, a single group of WT and TREM2-/- mice were used as shams for both cohort 1 and cohort 2 (WT: n = 7, TREM2-/-: n = 6). N numbers were chosen based on power analysis of data from previous BCAS studies. With a significance level of $p < 0.05$, a group size of 8 was required to reach a power of 0.8. All BCAS and sham surgeries were conducted by the author.

Laser speckle contrast flowmetry was utilised to investigate changes in cerebral blood flow caused by placement of microcoils in WT and TREM2-/- mice. Measurements were taken as described in section 2.4.2 to obtain a baseline value prior to BCAS or sham surgeries and then again 24 h and 28 d after surgeries. Values obtained at 24 h and 28 d were divided by baseline values and multiplied by 100 to determine the percentage change in cerebral blood flow caused by BCAS or sham surgeries. All laser speckle contrast imaging and subsequent analysis was conducted by the author with blinding to treatment and genotype. After surgeries, animals were monitored twice daily for 72 h and then twice weekly. Initial cohort sizes are shown in table 5.1.

	Microcoils	WT (n)	TREM2-/- (n)
Cohort 1 (Mixed coil)	Right CA: 0.16 mm Left CA: 0.18 mm	Sham: 7 BCAS: 10	Sham: 6 BCAS: 6
Cohort 2 (2x 0.16 mm coil)	0.16 mm bilaterally	Sham: 7 BCAS: 13	Sham: 6 BCAS: 12

Table 5.1: Cohort sizes prior to conducting 28 d sham and BCAS surgeries. CA: carotid artery

5.3.2 Tissue harvest

Animals were culled 28 d after BCAS or sham surgeries and saline perfused transcardially by the author as described in section 2.4.3. Whole brains were extracted and submerged in 4 % PFA (w/ v) for 24 h. Brains were placed in a coronal brain matrix and olfactory and cerebellum were removed. A microtome blade was then placed 0.22 mm posterior to bregma separating brain tissue into rostral and caudal portions. Subsequent tissue processing and paraffin embedding was conducted by QMRI Histology Services and 6 µm tissue sections were prepared for staining by the author as described in section 2.5.

5.3.3 Histology

H & E staining was conducted as described in section 2.6.4 to assess neuronal pathology and white matter lesions resulting from BCAS. The extent of grey matter damage was quantified by summating the total number of areas displaying neuronal pathology in each animal. White matter lesions were defined as areas of white matter demonstrating extensive vacuolation. All staining and assessment was conducted by the author with blinding to treatment and genotype.

5.3.4 Immunohistochemistry

Loss of myelin integrity was detected by MAG immunostaining while glial reactivity was detected by IBA1 and GFAP immunostaining on adjacent sections as described in sections 2.6.2 – 2.6.3. Myelin damage was quantified using a semi quantitative scoring method described in section 2.6.2. As both hemispheres were used, myelin damage scores from individual white matter tracts were summated from left and right hemispheres providing a possible total score of 6. Total myelin damage scores were calculated per animal by summating scores from all white matter tracts providing a possible total score of 24.

For IBA1 quantification, four regions of interest measuring 0.2 mm^2 were randomly placed across white matter tracts in each hemisphere (see section 5.3.5 below) using ImageJ software. IBA1+ cell bodies were then manually counted within each region of interest (8 regions of interest in total) and averaged to provide the number of IBA1+ cells per 0.2 mm^2 in each white matter region. Total IBA1+ cell number was also quantified in whole brain sections using the analyse particles plugin on ImageJ as described in section 2.6.3. For quantification of GFAP, images were thresholded to detect GFAP positive staining and the % area of staining was measured in each white matter region using image J software. Total GFAP coverage across brain sections was also quantified using this method. As WT and TREM2-/- mice demonstrated differences in myelin damage, IBA1+ cell counts and GFAP % area values were divided by myelin damage scores to correct for between group differences in pathology severity.

5.3.5 Regions of interest

Both brain hemispheres were used for pathological characterisation. Grey matter regions analysed to investigate neuronal pathology caused by BCAS include the cerebral cortex, thalamus, striatum and the CA1, CA2, CA3 and dentate gyrus of the hippocampus. White matter regions analysed to determine the impact of BCAS on myelin integrity using histology and IHC include the corpus callosum, internal capsule, hippocampal fimbria and optic tract (fig. 5.1). Glial reactivity was assessed and quantified in whole brain sections and individual white matter tracts including the corpus callosum, internal capsule, hippocampal fimbria and optic tract.

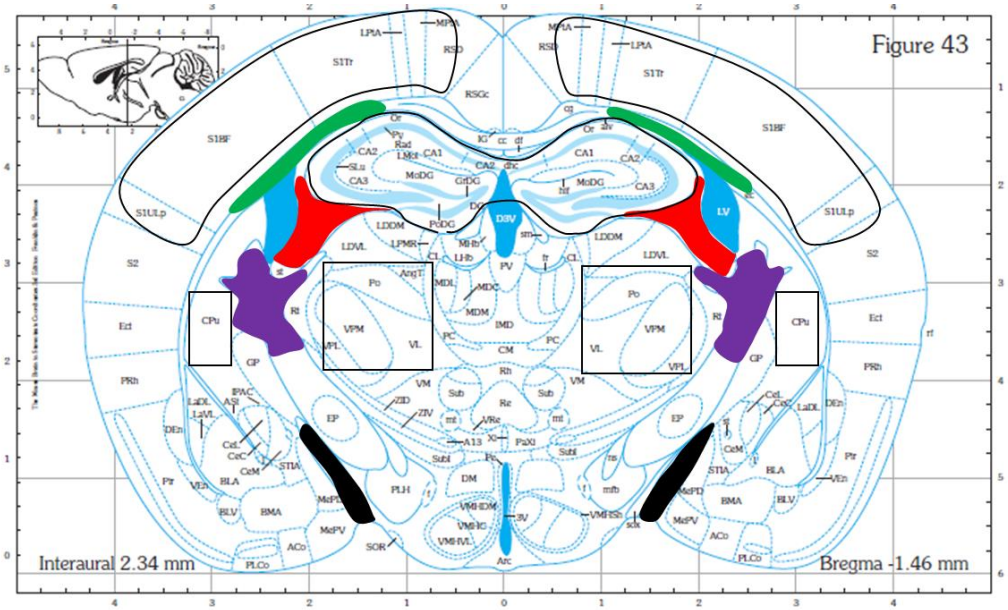

Figure 5.1: White and grey matter regions used for pathological assessment. Outlined regions demonstrate grey matter regions analysed (hippocampus, striatum, thalamus and cerebral cortex). Coloured regions demonstrate white matter tracts analysed (green: corpus callosum, red: hippocampal fimbria, purple: internal capsule, black: optic tract).

5.3.6 Statistics

Two way ANOVA with Bonferroni correction for *post hoc* was used to investigate the impact of BCAS on cerebral blood flow in WT and TREM2-/- mice with genotype and surgery as between subject factors. For pathological characterisation and investigation of glial responses, sham groups were excluded from analysis and key comparisons focused on differences between WT and TREM2-/- mice following BCAS only. Fisher's exact test was used to determine if TREM2 deficiency increased the probability of grey matter or white matter damage occurring in response to BCAS compared to WT mice. Mann Whitney U test was used to investigate the impact of TREM2 deficiency on white and grey matter pathology following BCAS. Welch's unpaired t-test was used to investigate the impact of TREM2 deficiency on IBA1+ cell number and GFAP coverage in response to BCAS. Spearman's rank correlation was used to investigate the relationship between total myelin damage and IBA1+ cell number in addition to GFAP coverage in WT and TREM2-/- mice following BCAS. SPSS version 22 (IBM Corp.) was used to conduct two way ANOVA. All other statistical analysis, were performed with Graphpad Prism software version 7.4 with statistical significance considered $p \leq 0.05$.

5.4 Results

5.4.1 Animal recovery

All animals receiving sham surgeries survived until tissue harvest and demonstrated no adverse neurological symptoms such as circling, seizures or barrel rolling indicative of overt focal brain damage. In cohort 1 (mixed coil), 0 of 10 TREM2-/- animals were culled, whilst 3 of 10 WT animals were culled within the first 48 h after BCAS surgery due to poor recovery observed by persistent circling or barrel rolling which is usually indicative of severe haemorrhage (16 % mortality). Remaining animals were motile and responsive within 1 h of surgery and were observed eating and drinking with normal exploratory behaviour within 24 - 48 h. BCAS caused a maximal 9.9 % and 8.9 % loss in weight in WT and TREM2-/- mice 3 d following surgery, respectively (see appendix section 8.2.4).

In cohort 2 (2x 0.16 mm coil), 5 of 13 WT animals and 3 of 12 TREM2-/- animals were culled within the first 48 h after BCAS surgery due to poor recovery (32 % mortality). Remaining animals were responsive within 1 – 2 h post-surgery and normal exploratory behaviour and eating and drinking were observed after 48 - 72 h. BCAS caused a maximal 9.9 % and 12.4 % loss in weight 5 d following surgery in WT and TREM2-/- mice, respectively (see appendix section 8.2.5). Final cohort sizes are shown in table 5.2.

	Microcoils	**WT (n)**	**TREM2-/- (n)**
Cohort 1 (Mixed coil)	Right CA: 0.16 mm ID Left CA: 0.18 mm ID	Sham: 7 / 7 BCAS: 7/ 10	Sham: 6/ 6 BCAS: 6 / 6
Cohort 2 (2x 0.16 mm coil)	0.16 mm ID bilaterally	Sham: 7/ 7 BCAS: 8/ 13	Sham: 6 / 6 BCAS: 9 / 12

Table 5.2: Final cohort sizes following 28 d sham and BCAS surgeries in WT and TREM2-/- mice. CA: carotid artery, ID: internal diameter.

5.4.2 Laser speckle flowmetry

Laser speckle contrast flowmetry was performed prior to surgery and 24 h and 28 d after surgery to validate BCAS induced cerebral hypoperfusion and assess whether TREM2 defiency affected cerebral blood flow. Blood flow data was calculated as percentage change from baseline flow values. In cohort 1, analysis of percentage change in blood flow from baseline revealed significant effects of time $F(2, 32)=18.485$, $p < 0.0001$) and surgery ($F(1, 16)=15.769$, $p < 0.0001$), but no effect of genotype ($p < 0.05$). No significant interaction between surgery and genotype was detected ($p < 0.05$). However, a significant interaction between time and surgery was detected $F(2, 32)=9.561$, $p < 0.001$). Post-hoc analysis demonstrated that blood flow was significantly reduced 24 h after surgery in WT mice ($p < 0.01$) and TREM2-/- mice ($p < 0.05$). However, 28 d following surgery WT and TREM2-/- mice demonstrated no significant difference in blood flow compared to shams ($p < 0.05$). (fig. 5.2).

In cohort 2, analysis of percentage change in blood flow from baseline also revealed significant effects of time $F(2, 52)=78.009$, $p < 0.0001$) and surgery ($F(1, 26)=93.136$, $p < 0.0001$). Similarly, there was no effect of genotype ($p > 0.05$) and no significant interaction between surgery and genotype ($p > 0.05$). However, a significant interaction between time and surgery was detected ($F(2, 52)=39.969$, $p < 0.0001$) and post-hoc analysis demonstrated that blood flow was significantly reduced in both WT and TREM2-/- mice compared to shams 24 h ($p<0.0001$) and 28 d ($p<0.0001$) following BCAS) (fig. 5.3).

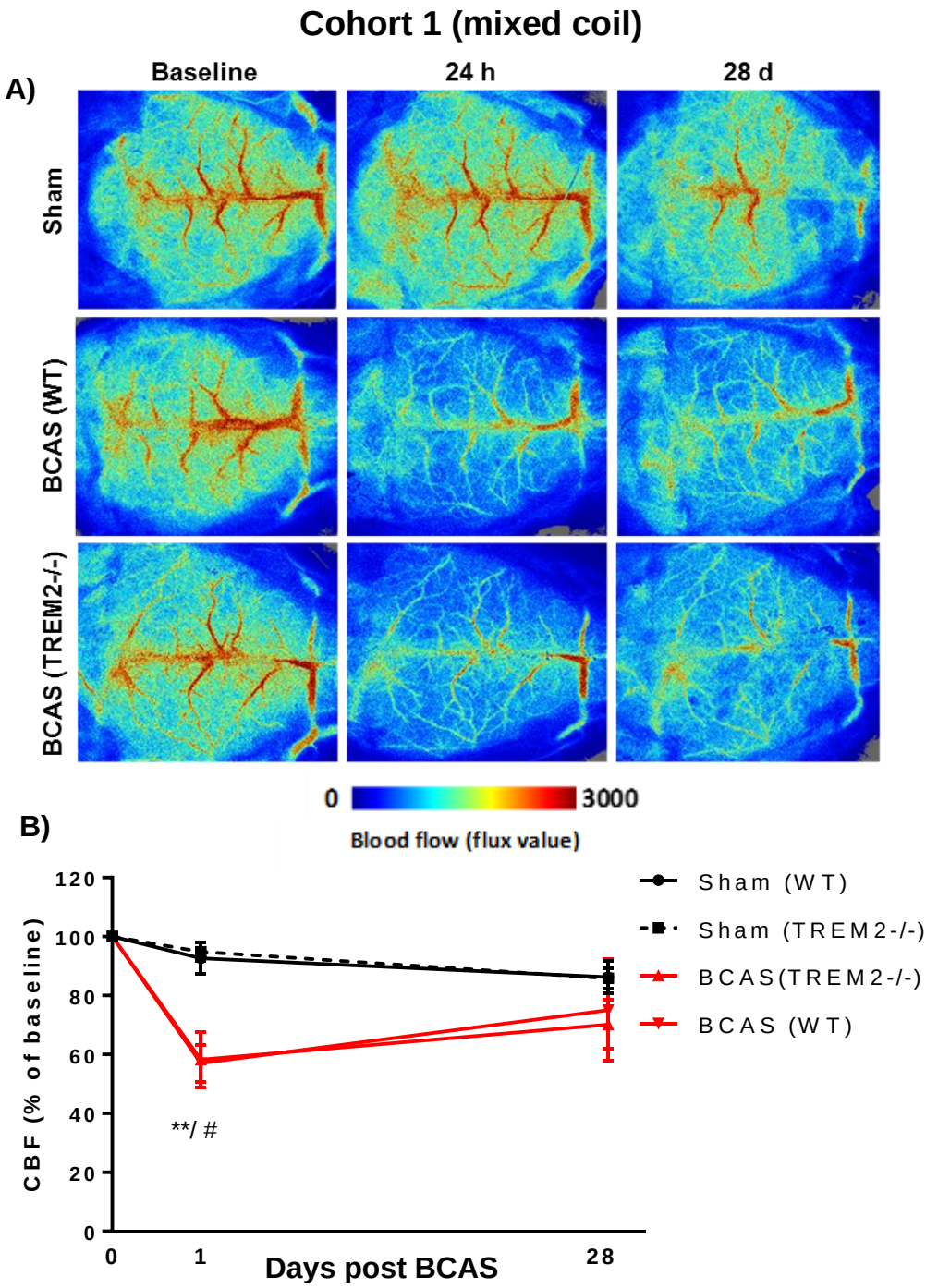

Figure 5.2: Quantification of cerebral blood flow in WT and TREM2-/- mice 28 d post sham and BCAS surgeries in cohort 1 (mixed coil). (A) Representative laser speckle images showing cortical cerebral blood flow in sham and BCAS WT and TREM2-/- mice at baseline, 24 h and 28 d after surgery. (B) Quantification of cerebral blood flow in sham and BCAS WT and TREM2-/- mice at baseline, 24 h and 28 d after surgery. 24 h following BCAS surgery, WT and TREM2-/- mice demonstrated a 35 % and 36 % reduction in cerebral blood flow compared to sham animals, respectively. After 28 d, WT and TREM2-/- mice demonstrated an 11.2 % and 15.7 % reduction in cerebral blood flow compared to sham animals. TREM2 deficiency had no impact on cerebral blood flow. **P ≤ 0.01 WT BCAS vs WT sham, # P ≤ 0.05 TREM2-/- BCAS vs TREM2-/- sham. Two way ANOVA with Bonferroni correction for post hoc. Data show mean ± SEM. N = 3 - 7 independent animals per group.

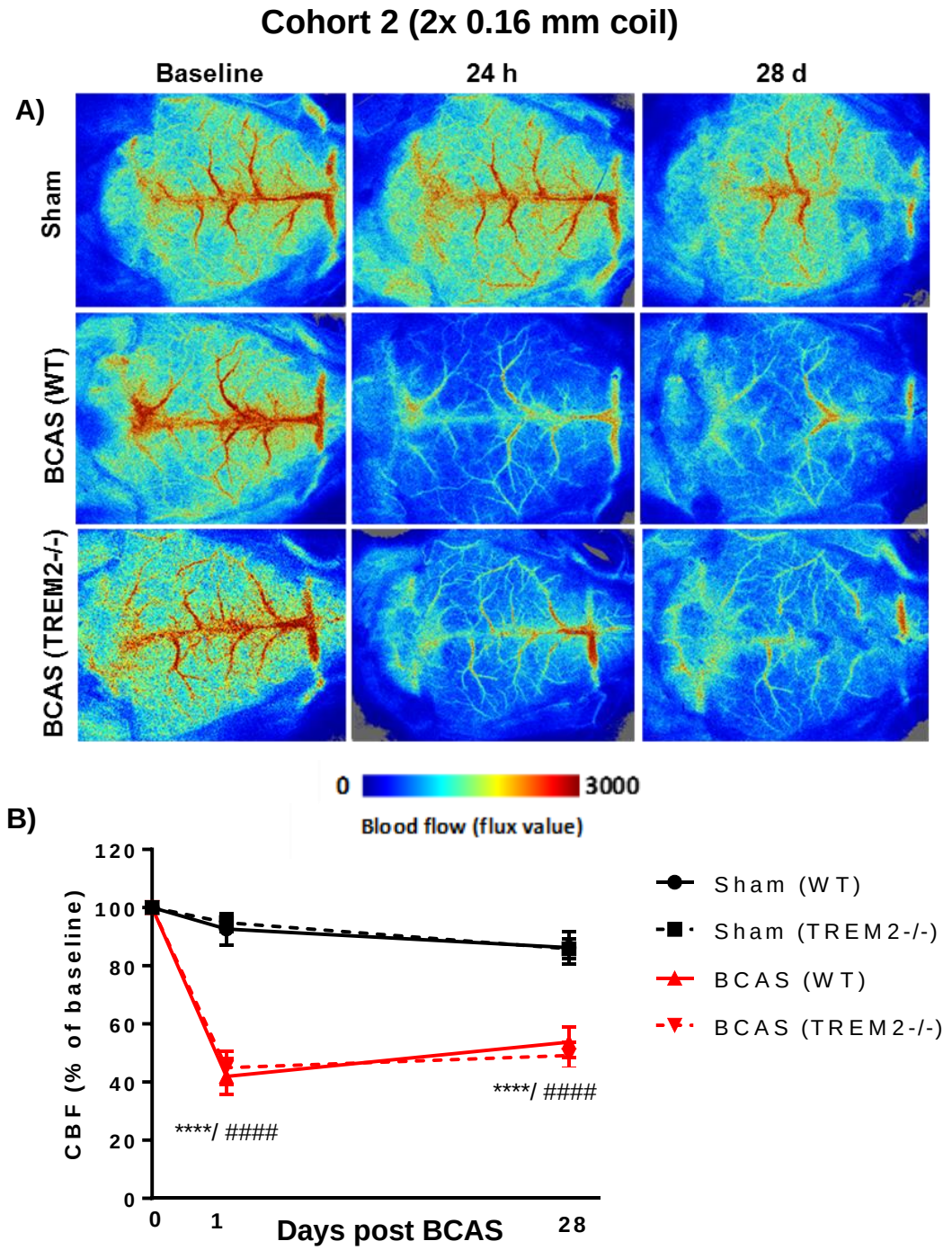

Figure 5.3: Quantification of cerebral blood flow in WT and TREM2-/- mice 28 d post sham and BCAS surgeries in cohort 2 (2x0.16 mm coils). (A) Representative laser speckle images showing cortical cerebral blood flow in sham and BCAS WT and TREM2-/- mice at baseline, 24 h and 28 d after surgery. (B) Quantification of cerebral blood flow in sham and BCAS WT and TREM2-/- mice at baseline, 24 h and 28 d after surgery. 24 h following BCAS surgery, WT and TREM2-/- mice demonstrated a 50.74 % and 49.92 % reduction in cerebral blood flow compared to sham animals, respectively. After 28 d cerebral blood flow remained reduced and WT and TREM2-/- mice demonstrated a 32.53 % and 36.75 % reduction in cerebral blood flow compared to sham animals. TREM2 deficiency had no impact on cerebral blood flow. ****P ≤ 0.0001 WT BCAS vs WT sham, ####P ≤ 0.0001 TREM2-/- BCAS vs TREM2-/- sham. Two way ANOVA with Bonferroni correction for post hoc. Data show mean ± SEM. N = 6 - 9 independent animals per group.

5.4.3 Pathological assessment

5.4.3.1 H & E assessment of CNS pathology

H & E staining was conducted on brain sections to investigate tissue integrity and characterise neuronal damage resulting from BCAS in WT and TREM2-/- mice. No sham animals displayed evidence of neuronal damage. In cohort 1 (mixed coil), neuronal pathology was confined to hippocampal regions and observed in 2 of 7 WT mice and 2 of 6 TREM2-/- mice in response to BCAS (fig. 5.4A & B). Fisher's exact test demonstrated TREM2 deficiency did not increase the probability of neuronal pathology occurring in response to BCAS ($p \geq 0.05$) (fig. 5.4A). Furthermore, TREM2 deficiency had no impact on the extent of neuronal pathology ($p \geq 0.05$) (fig. 5.5).

In cohort 2 (2x 0.16 mm coil), BCAS resulted in neuronal damage across multiple grey matter regions in 4 of 8 WT mice and 5 of 9 TREM2-/- mice (fig. 5.6A & B). Fisher's exact test demonstrated TREM2 deficiency did not increase the probability of neuronal pathology occurring in response to BCAS ($p \geq 0.05$) (fig. 5.6A). Although TREM2-/- mice demonstrated more extensive grey matter damage than WT mice this did not reach statistical significance ($p = 0.817$) (fig. 5.7).

In cohort 1 (mixed coil), assessment of H & E staining demonstrated no evidence of overt white matter lesions in response to BCAS in WT and TREM2-/- mice. In cohort 2 (2x 0.16 mm coil) however, focal necrotic lesions were observed in the internal capsule characterised by extensive vacuolisation in 5 of 9 TREM2-/- mice while no such lesions were observed in WT mice in response to BCAS (fig. 5.9A & B). Fisher's exact test demonstrated TREM2 deficiency significantly increased the probability of white matter lesions occurring in response to BCAS ($p \leq 0.05$) (fig. 5.9A).

Assessment of grey matter damage: Cohort 1 (mixed coil)

Cohort 1	Animals displaying grey matter pathology	Cerebral Cortex	CA1	CA2	CA3	DG	Striatum	Thalamus
BCAS WT	2/7 (29%)	0/7 (0%)	2/7 (29%)	1/7 (14%)	0/7 (0%)	0/7 (0%)	0/7 (0%)	0/7 (0%)
BCAS TREM2-/-	2/6 (33%)	0/6 (0%)	1/6 (17%)	0/6 (0%)	1/6 (17%)	1/6 (17%)	0/6 (0%)	0/6 (0%)

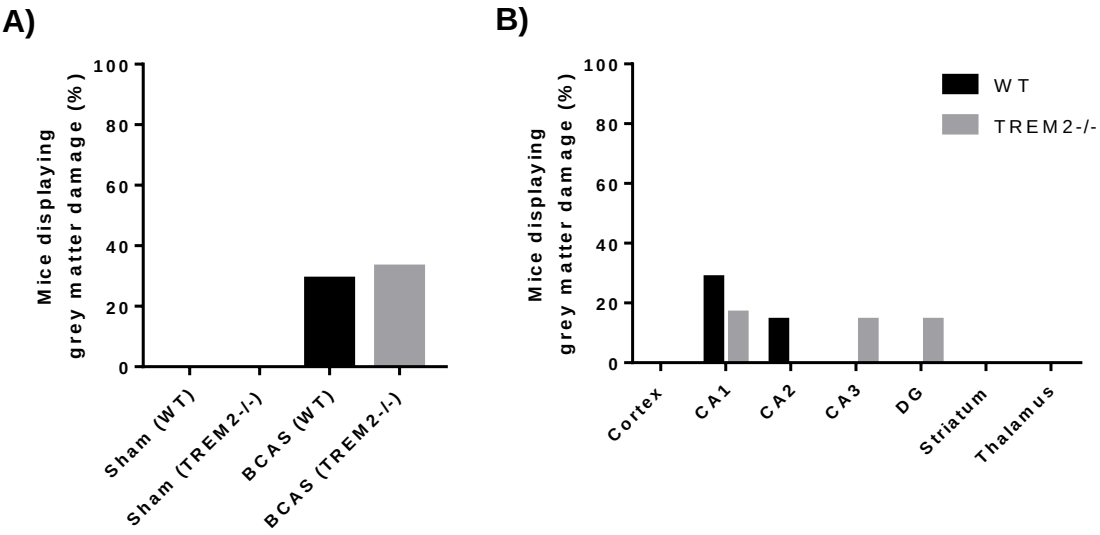

Figure 5.4: Frequency of WT and TREM2-/- mice demonstrating neuronal pathology detected by H & E staining 28 d post BCAS in cohort 1 (mixed coil). (A) Overall frequency of mice demonstrating grey matter damage detected via H & E staining in WT and TREM2-/- mice following sham and BCAS surgeries. TREM2 deficiency did not increase the probability of grey matter damage occurring 28 d following BCAS surgery. (B) Frequency of grey matter regions demonstrating damage in WT and TREM2-/- mice following BCAS. Fisher's exact test. One tissue section analysed per animal. N = 6 – 7 independent animals per group.

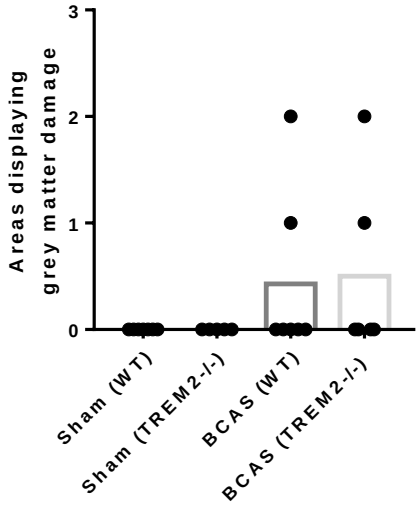

Figure 5.5: Total number of areas demonstrating neuronal pathology in WT and TREM2-/- mice 28 d post BCAS in cohort 1 (mixed coil). The total number of grey matter regions displaying damage detected by H & E were summated in WT and TREM2-/- mice. The total number of grey matter regions displaying damage were unchanged in TREM2-/- mice compared to WT mice 28 d following BCAS. Mann Whitney U test. Bars shows median. One tissue section analysed per animal. N = 6 – 7 independent animals per group.

Assessment of grey matter damage: Cohort 2 (2x 0.16 mm coil)

Cohort 2	Animals displaying grey matter damage	Cerebral Cortex	CA1	CA2	CA3	DG	Striatum	Thalamus
BCAS WT	4/8 (50%)	3/8 (38%)	3/8 (38%)	3/8 (38%)	3/8 (38%)	2/8 (25%)	2/8 (25%)	2/8 (25%)
BCAS TREM2-/-	5/9 (56%)	4/9 (44%)	5/9 (56%)	5/9 (56%)	3/9 (33%)	3/9 (33%)	1/9 (11%)	4/9 (44%)

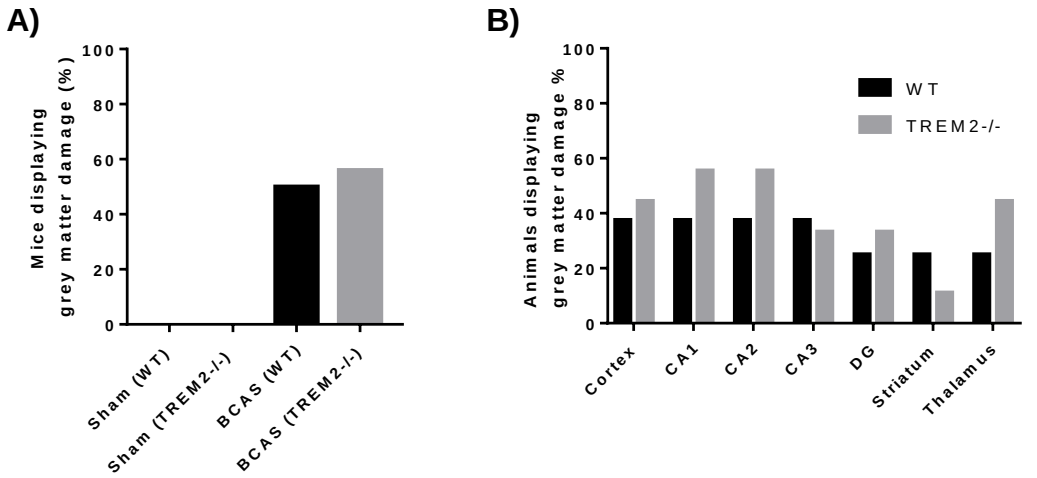

Figure 5.6: Frequency of WT and TREM2-/- demonstrating neuronal pathology detetcted by H & E staining 28 d post BCAS surgeries in cohort 2 (2x 0.16 mm coil). (A) Overall frequency of mice demonstrating grey matter damage detected by H & E staining in WT and TREM2-/- mice following sham and BCAS surgeries. TREM2 deficiency did not increase the probability of grey matter damage occurring 28 d following BCAS surgery. (B) Frequency of grey matter regions demonstrating damage in WT and TREM2-/- mice following BCAS. Fisher's exact test. One tissue section analysed per animal. N = 6 – 9 independent animals per group.

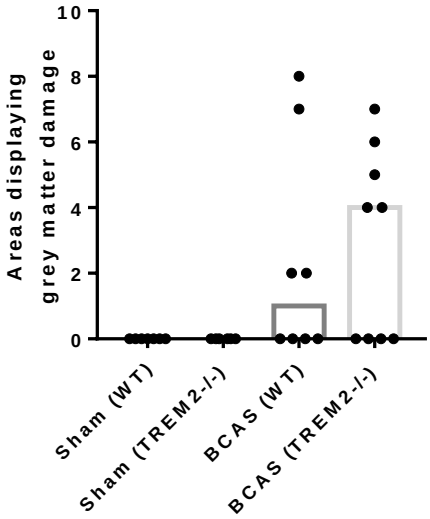

Figure 5.7: Total number of areas demonstrating neuronal pathology detected by H & E staining in WT and TREM2-/- mice 28 d post BCAS surgeries in cohort 2 (2x 0.16 mm coil). The total number of grey matter regions displaying damage were summated in WT and TREM2-/- mice. Although statistically non-significant, the total number of areas demonstrating grey matter damage was increased in TREM2-/- mice compared to WT mice 28 d following BCAS. Mann Whitney U test. Each data point represents an independent animal. Bars shows median. One tissue section analysed per animal. N = 6 – 9 independent animals per group.

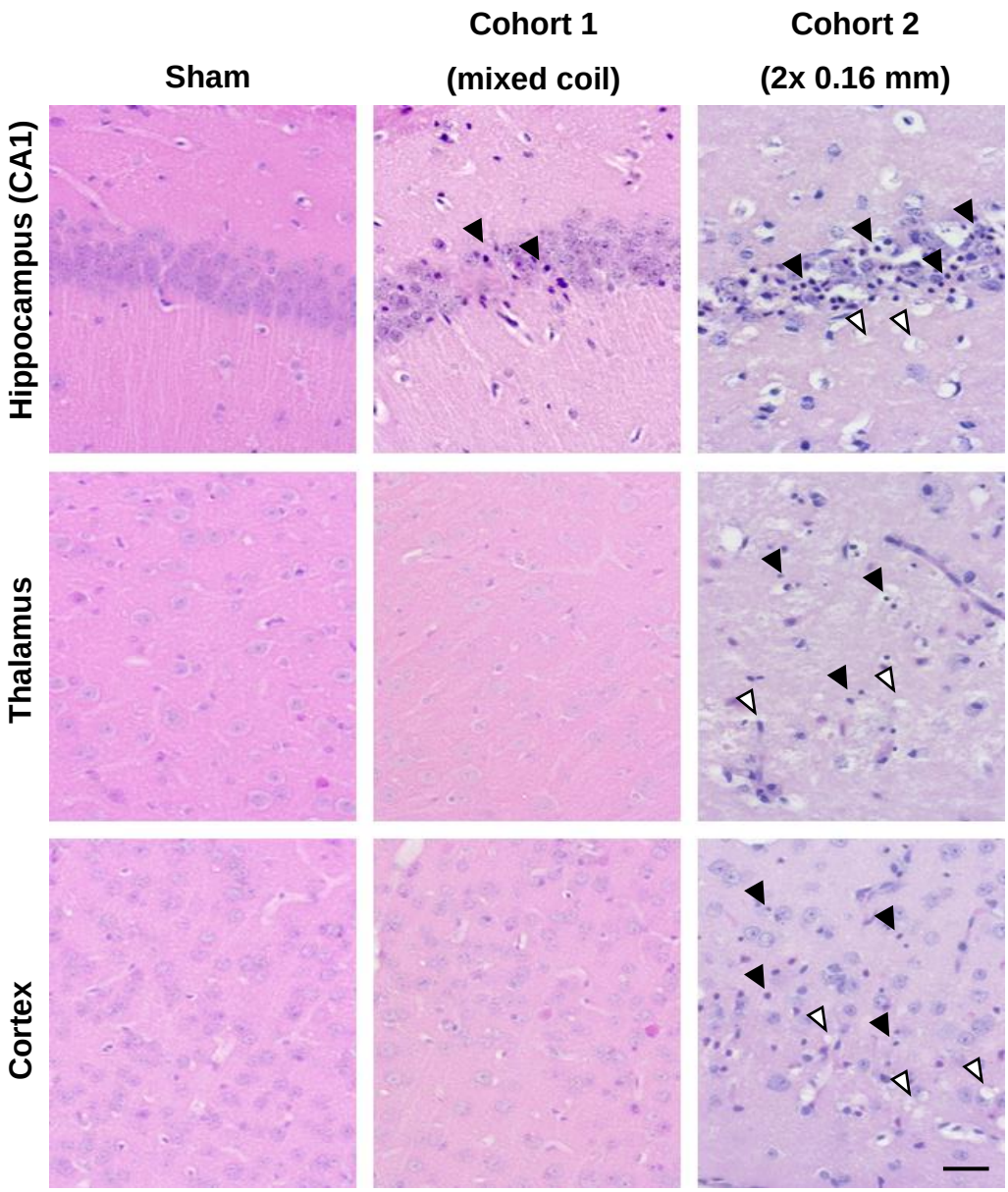

Figure 5.8: Representative images of H & E staining in grey matter regions 28 d post sham and BCAS surgeries in cohorts 1 and 2. In cohort 1 (mixed coil), neuronal pathology was limited to the hippocampus of WT and TREM2-/- mice following 28 d BCAS. In cohort 2 (2x 0.16 mm coil) however, neuronal pathology was more severe and observed across multiple grey matter regions.Black arrows demonstrate small condensed nuclei of apoptotic neurons. White arrows demonstrate vacuolation. Scale bar: 50 µm.

A)

	Cohort 1 (mixed coil) White matter lesions	Cohort 2 (2x 0.16 mm coil) White matter lesions
BCAS WT	0/7 (0%)	0/8 (0%)
BCAS TREM2-/-	0/6 (0%)	5/9 (56%)

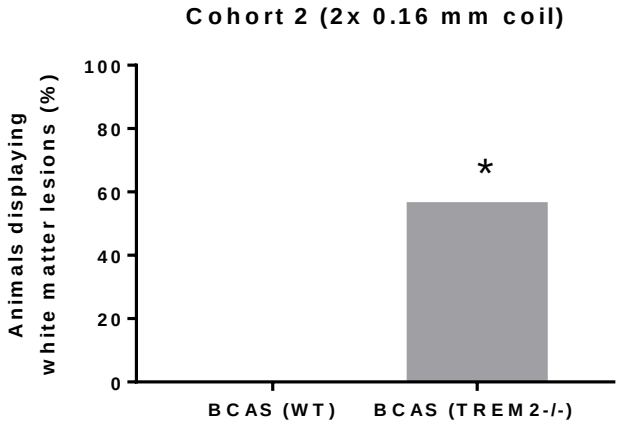

B)

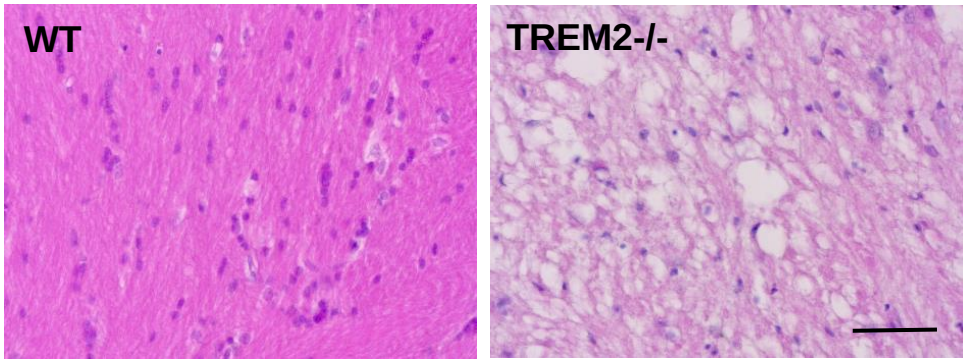

Figure 5.9: Frequency of white matter lesionsdetected by H & E staining in WT and TREM2-/- mice 28 d post BCAS surgeries. (A) Frequency of WT and TREM2-/- BCAS mice demonstrating white matter lesions in cohorts 1 and 2. The probability of developing white matter lesions was significantly increased in TREM2-/- mice compared to WT mice following BCAS. (B) Representative images of H & E staining of the internal capsule in WT and TREM2-/- BCAS animals demonstrating differences in tissue integrity in cohort 2 (2x 0.16 mm coil) Scale bar: 50 µm. *P ≤ 0.05. Fisher's exact test. One tissue section analysed per animal. N = 6 – 9 independent animals per group.

5.4.3.2 Assessment of myelin integrity

MAG immunostaining was conducted to investigate the impact of TREM2 deficiency on myelin integrity in response to BCAS. Animals receiving sham surgeries demonstrated no alterations in myelin integrity. In cohort 1 (mixed coil) BCAS precipitated small foci of myelin debris across white matter tracts in 5 of 7 WT and 5 of 6 TREM2-/- mice (fig. 5.10, fig. 5.13). Areas most frequently demonstrating damage included the optic tract (WT: 4 of 7, TREM2-/-: 3 of 6) and corpus callosum (WT: 3 of 7, TREM2-/-: 4 of 6) (fig. 5.10B). Fisher's exact test demonstrated TREM2 deficiency did not increase the probability of myelin damage occurring following BCAS ($p \geq 0.05$) (fig. 5.10A). The extent of myelin damage was mild in all white matter regions analysed and TREM2 deficiency had no impact on the severity of myelin damage ($p \geq 0.05$) (fig. 5.11A). Furthermore, TREM2 deficiency had no impact on the extent of total myelin damage ($p \geq 0.05$) (fig. 5.11B).

In cohort 2 (2x 0.16 mm coil), use of microcoils with smaller internal diameters increased the frequency and severity of myelin damage. Myelin damage was observed in all WT and TREM2-/- BCAS mice. However, severity and spatial distribution varied considerably (fig. 5.13 & fig. 5.14). Fisher's exact test demonstrated TREM2 deficiency did not increase the probability of myelin damage occurring following BCAS ($p \geq 0.05$) (fig. 5.13A). TREM2-/- animals demonstrated exacerbated myelin damage in the internal capsule ($p \leq 0.05$) whilst non-significant trends for greater damage were observed in other white matter tracts (optic tract: $p = 0.421$, hippocampal fimbria: $p = 0.3114$, corpus callosum: $p = 0.2947$) (fig. 5.15 & fig. 5.14A). Assessment of total myelin damage also revealed TREM2-/- mice had greater damage in response to BCAS however this did not reach statistical significance ($p = 0.1078$) (fig 5.14B).

Assessment of myelin integrity: Cohort 1 (mixed coil)

	Animals displaying myelin damage	CC	HF	IC	OT
BCAS (WT)	5/7 (71%)	3/7 (43%)	1/7 (14%)	2/7 (28%)	4/7 (56%)
BCAS (TREM2-/-)	5/6 (83%)	4/6 (67%)	0/6 (0%)	2/6 (33%)	3/6 (50%)

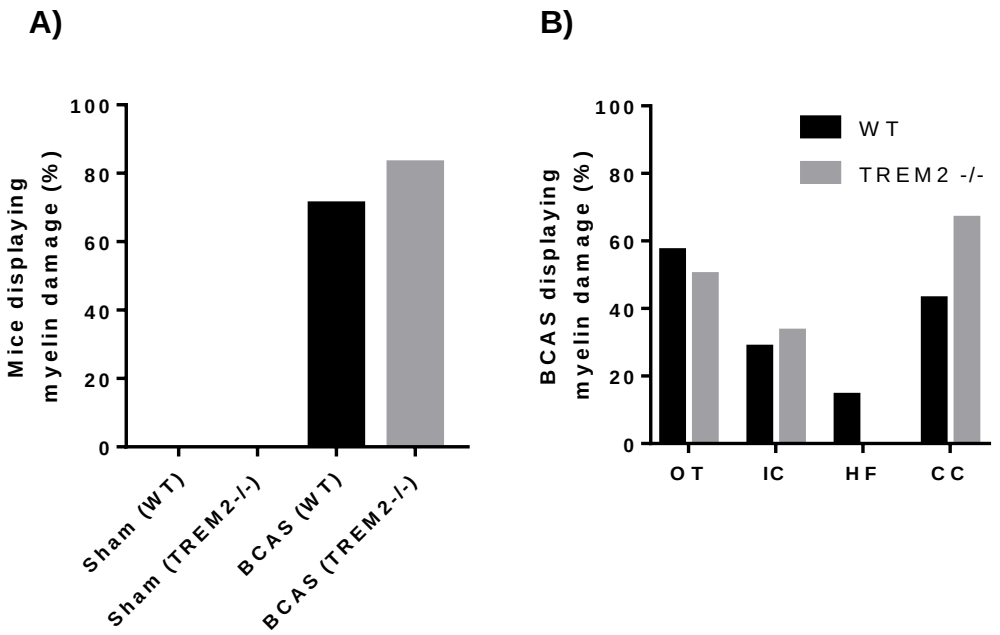

Figure 5.10: Frequency of WT and TREM2-/- mice demonstrating myelin damage detected by MAG immunostaining 28 d post sham and BCAS surgeries in cohort 1 (mixed coil). (A) Overall frequency of WT and TREM2-/- mice demonstrating myelin damage detected via MAG immunostaining 28 d following sham and BCAS surgeries. TREM2 deficiency did not increase the probability of myelin damage occurring 28 d following BCAS surgery. (B) Frequency of white matter regions demonstrating damage in WT and TREM2-/- mice following BCAS. Fisher's exact test. One tissue section analysed per animal. N = 6 – 7 independent animals per group. CC: corpus callosum HF: hippocampal fimbria, IC: internal capsule, OT: optic tract.

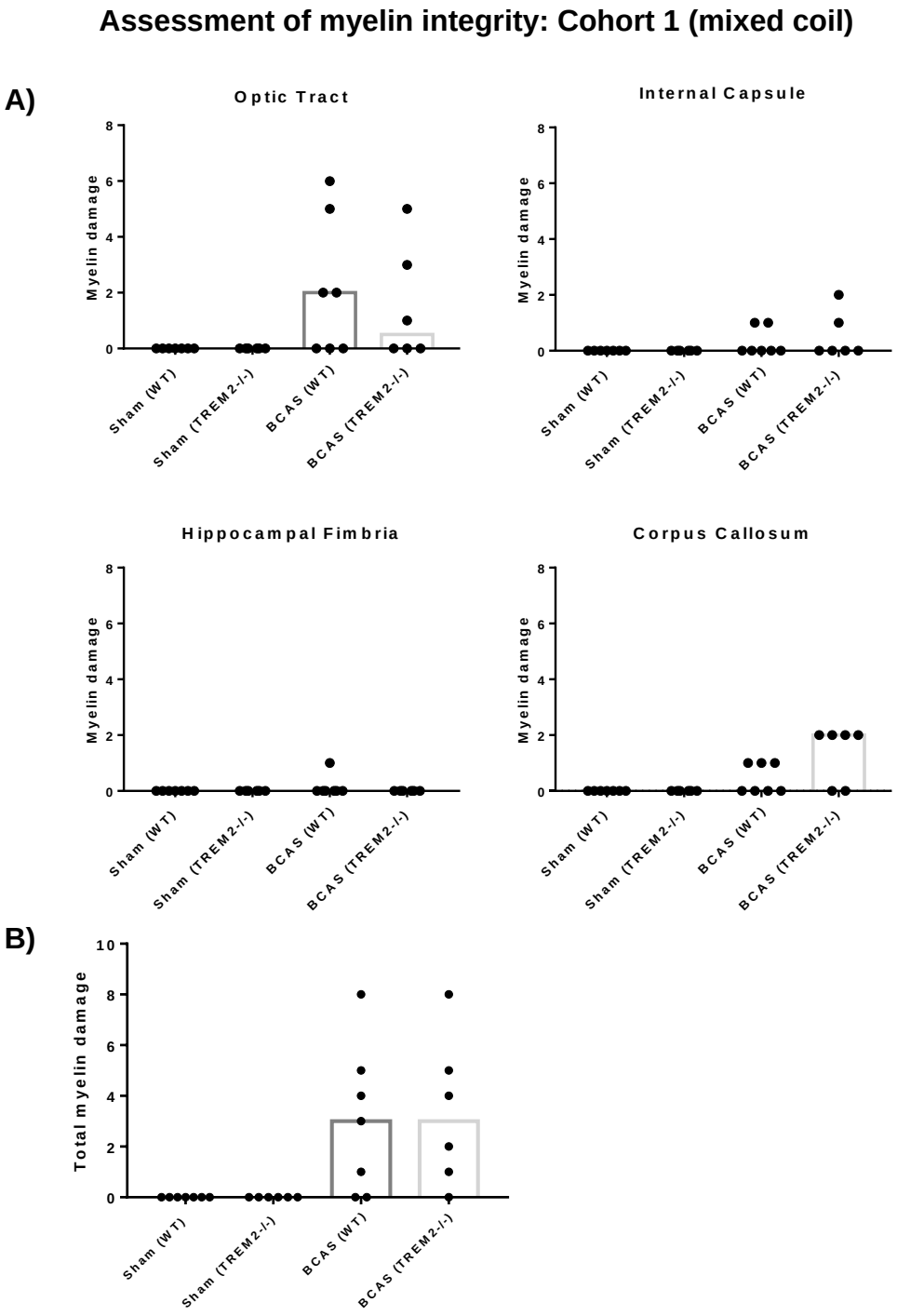

Figure 5.11: Quantification of myelin damage detected by MAG immunostaining in white matter tracts of WT and TREM2-/- mice in cohort 1 (mixed coil) 28 d post BCAS surgeries. (A) Myelin damage in each white matter tract was quantified using a semi quantitive scoring method ranging from 0 (no damage) to 3 (extensive damage) via MAG immunostaining and scores from each hemisphere were summated providing a total possible score of 6 per white matter region. TREM2 deficiency had no impact on the extent of myelin damage compared to WT mice in any white matter region analysed 28 d following BCAS. (B) Myelin damage scores were summated from all analysed white matter tracts providing a 'total myelin damage' score per animal. TREM2 deficiency had no impact on the extent of total myelin damage compared to WT animals 28 d following BCAS surgeries. Mann Whitney U test. Each data point represents an independent animal. Bars show median. One tissue section analysed per animal. N = 6 – 7 independent animals per group.

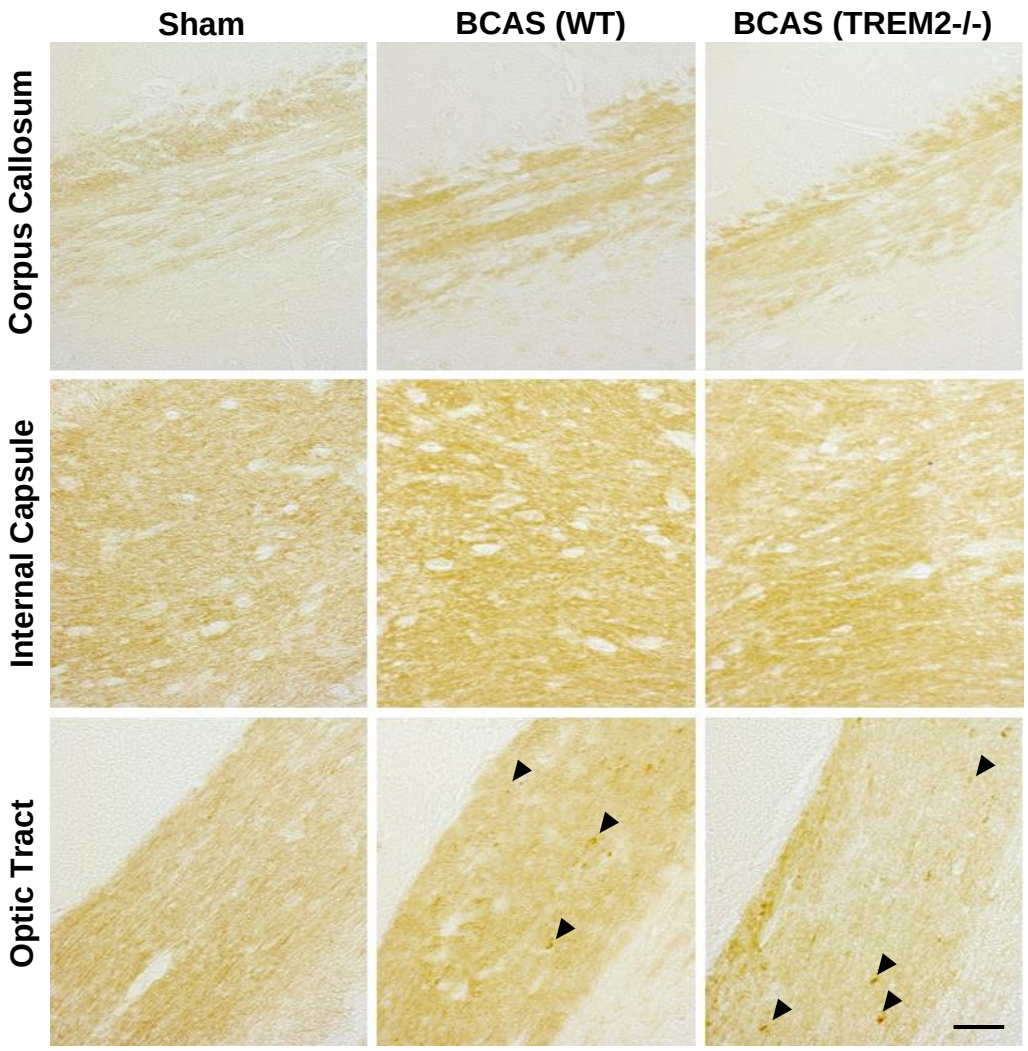

Figure 5.12: Representative images of MAG immunostaining in white matter regions of WT and TREM2-/- mice in cohort 1 (mixed coil) 28 d post sham and BCAS surgeries. White matter regions including the corpus callosum, internal capsule and hippocampal fimbria (not shown) demonstrated negligible alterations in myelin integrity in response to BCAS in WT and TREM2-/- BCAS mice. Although the optic tract showed greatest damage (black arrows show areas of myelin debris) in response to BCAS the extent of damage was mild and no difference in pathology severity was observed between WT and TREM2-/- mice. Scale bar: 50 µm.

Assessment of myelin integrity: Cohort 2 (2x 0.16 mm coil)

Cohort 2	Animals displaying myelin damage	CC	HF	IC	OT
BCAS (WT)	8/8 (100%)	6/8 (100%)	6/8 (75%)	4/8 (50%)	8/8 (100%)
BCAS (TREM2-/-)	9/9 (100%)	8/9 (89%)	8/9 (89%)	8/9 (89%)	9/9 (100%)

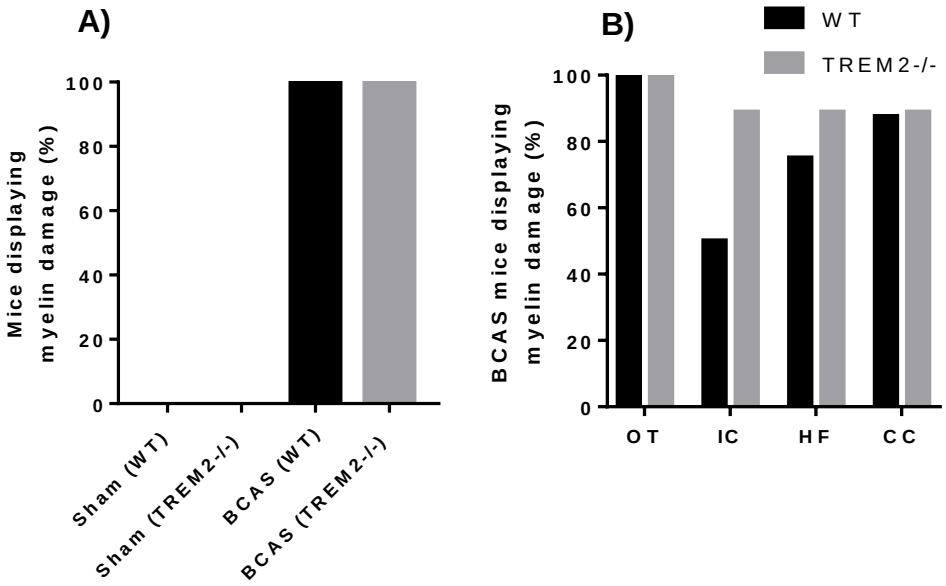

Figure 5.13: Frequency of WT and TREM2-/- mice demonstrating myelin damage detected by MAG immunostaining 28 d post sham and BCAS surgeries in cohort 2 (2x 0.16 mm coil). (A) Overall frequency of WT and TREM2-/- mice demonstrating myelin damage detected via MAG immunostaining 28 d following sham and BCAS surgeries. TREM2 deficiency did not increase the probability of myelin damage occurring 28 d following BCAS surgery. (B) Frequency of white matter regions demonstrating damage in WT and TREM2-/- mice following BCAS. Fisher's exact test. One tissue section analysed per animal. N = 6 – 9 independent animals per group. CC: corpus callosum HF: hippocampal fimbria, IC: internal capsule, OT: optic tract.

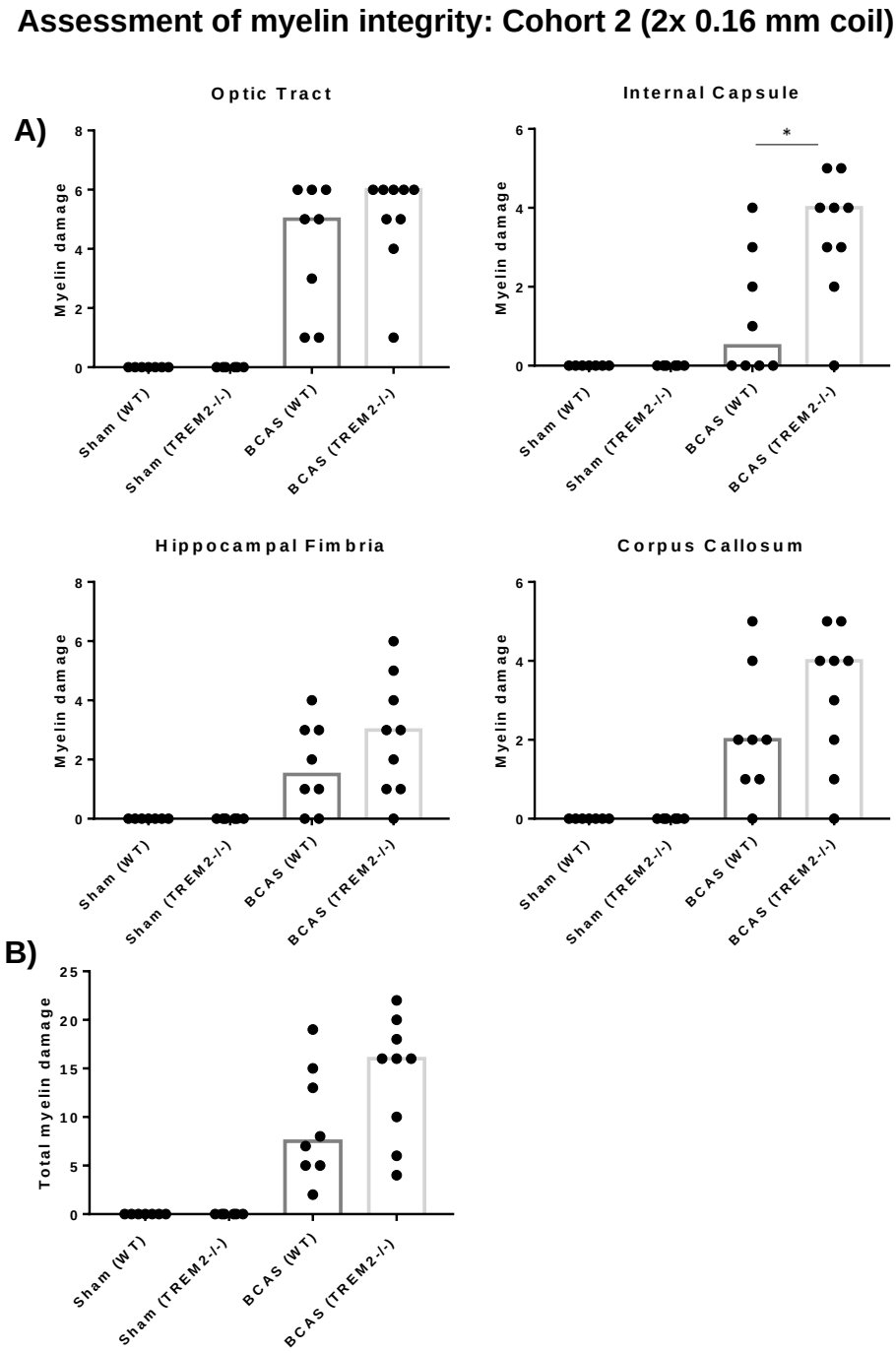

Figure 5.14: Quantification of myelin damage detected by MAG immunostaining in white matter tracts of WT and TREM2-/- mice 28 d post BCAS in cohort 2 (2x 0.16 mm coil). (A) Myelin damage in each white matter tract was quantified using a semi quantitive scoring method ranging from 0 (no damage) to 3 (extensive damage) via MAG immunostaining and scores from each hemisphere were summated providing a total possible score of 6 per white matter region. TREM2 deficiency had no impact on myelin damage in the CC, OT and HF compared to WT mice 28 d following BCAS. However, a significant increase in myelin damage was observed in the IC of TREM2-/- mice compared to WT mice 28 d following BCAS surgery. (B) Myelin damage scores were summated from all analysed white matter tracts providing a 'total myelin damage' score per animal. TREM2-/- mice demonstrated a non-significant increase in myelin damage compared to WT mice following 28 d BCAS. *P ≤ 0.05. Mann Whitney U test. Each data point represents an independent animal. Bars show median. One tissue section analysed per animal. N = 6 – 9 independent animals per group. CC: corpus callosum HF: hippocampal fimbria, IC: internal capsule, OT: optic tract.

Assessment of myelin integrity: Cohort 2 (2x 0.16 mm coil)

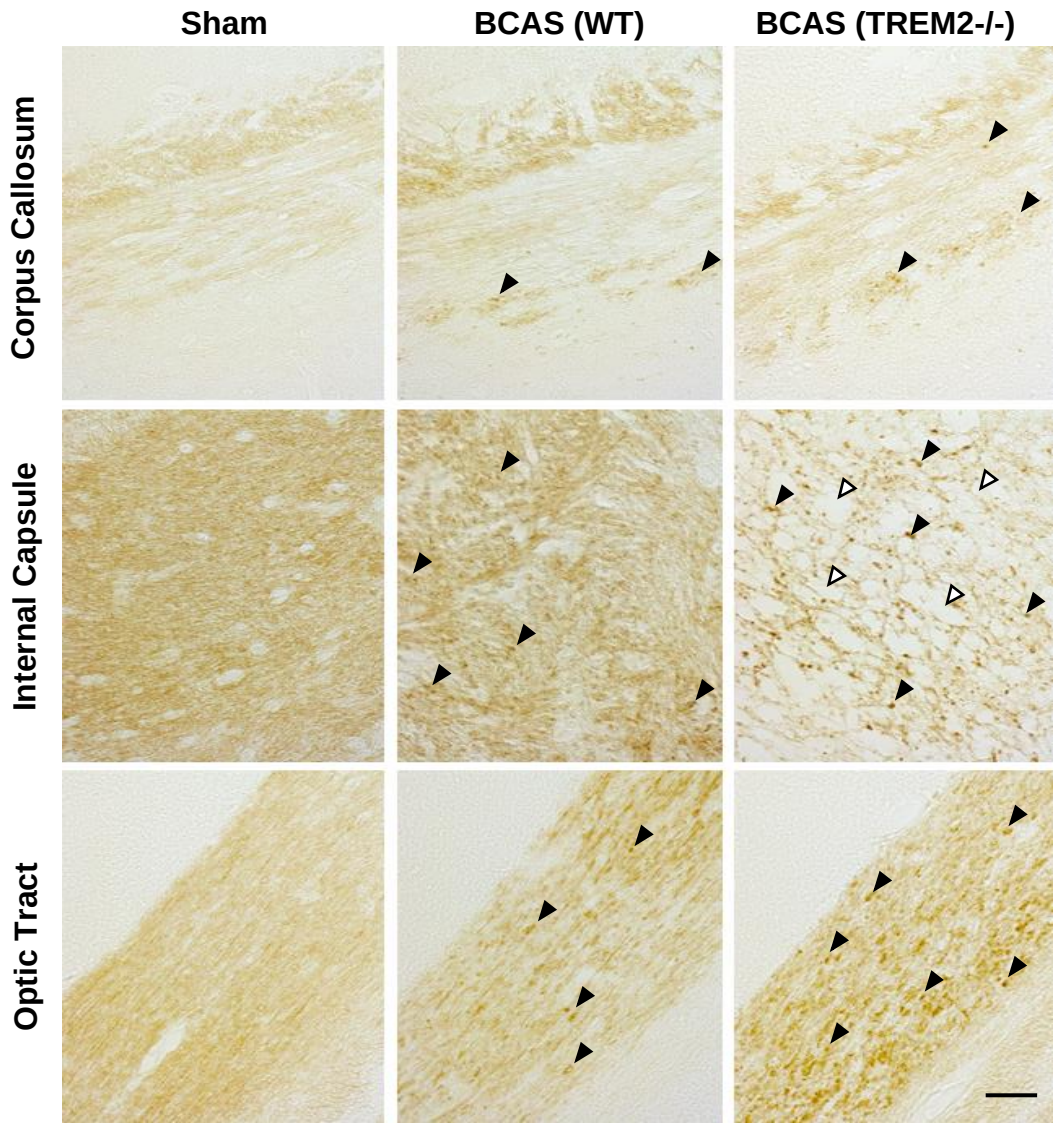

Figure 5.15: Representative images of MAG immunostaining in white matter tracts of WT and TREM2-/- mice 28 d post BCAS and sham surgeries in cohort 2 (2x 0.16 mm coil). White matter regions including the corpus callosum, internal capsule and optic tract demonstrated diffuse myelin damage in WT mice following BCAS whilst this was further exacerbated in the internal capsule in TREM2-/- mice. Black arrows demonstrate examples of myelin debris. White arrows demonstrate examples of vacuolation. CC: corpus callosum, HF: hippocampal fimbria, IC: internal capsule, OT: optic tract. Scale bar: 50 µm.

5.4.3.3 Assessment of microgliosis

Investigation of glial responses was restricted to cohort 2 (2x 0.16 mm coil) only as animals demonstrated robust white matter pathology following BCAS. IBA1 immunostaining was assessed and IBA1+ cell bodies quantified in white matter tracts and whole brain sections to characterise the impact of TREM2 deficiency on IBA1 cell responses to BCAS. Assessment of IBA1 immunostaining demonstrated accumulation of cells with an amoeboid morphology and shortened thickened processes in regions of robust pathology characteristic of cell activation. Morphologically, TREM2-/- IBA1+ cells appeared less hypertrophied compared to WT microglia in areas of pathology and were reduced in density (fig. 5.18).

In response to BCAS, TREM2-/- mice demonstrated significantly less IBA1+ cells in the optic tract compared to WT animals ($p \leq 0.05$) whilst no differences were observed in other analysed white matter tracts ($p \geq 0.05$) (fig. 5.16). Furthermore, TREM2-/- mice demonstrated no difference in total IBA1+ cell number across whole brain sections compared to WT mice following BCAS (fig. 5.17). As the extent of myelin damage varied between WT and TREM2-/- mice, IBA1+ cell counts calculated from whole brain sections were plotted against myelin damage scores to assess how TREM2 impacted microglial number for a given severity of white matter damage. Plotting total IBA1+ cell numbers calculated from whole brain sections against total myelin damage scores revealed IBA1+ cell number positively correlated with white matter damage in WT mice ($p \leq 0.001$, R^2:0.89) whilst this relationship was tempered in TREM2-/- animals ($p \leq 0.05$, R^2:0.46) (fig. 5.19).

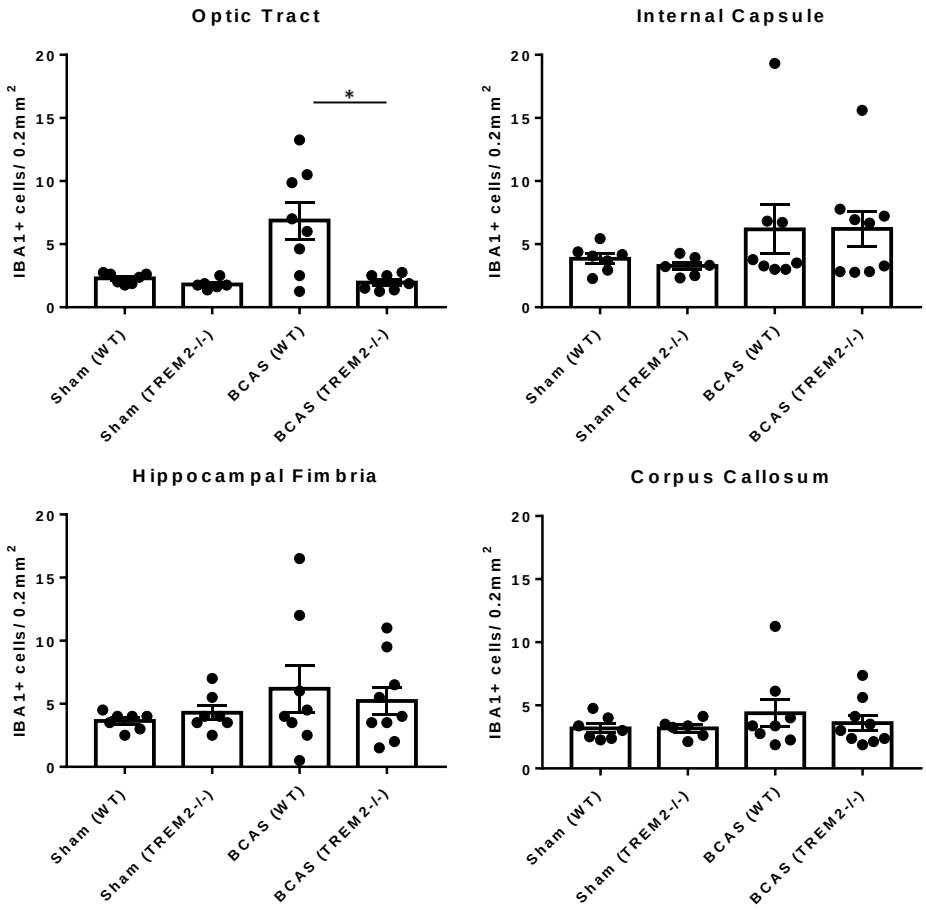

Figure 5.16: Quantification of IBA1+ cell number in white matter tracts of WT and TREM2-/- mice 28 d post BCAS. TREM2-/- mice had significantly less IBA1+ cells in the OT compared to WT mice 28 d following BCAS whilst IBA1+ cell number was unchanged in other white matter regions. *P ≤ 0.05. Welch's unpaired t test. Each data points represents a value averaged from 8 regions of interest measuring 0.2mm^2 placed across each white matter tract in left and right brain hemispheres. One tissue section was analysed per animal. Data show mean ± SEM. N = 6 – 9 independent animals per group.

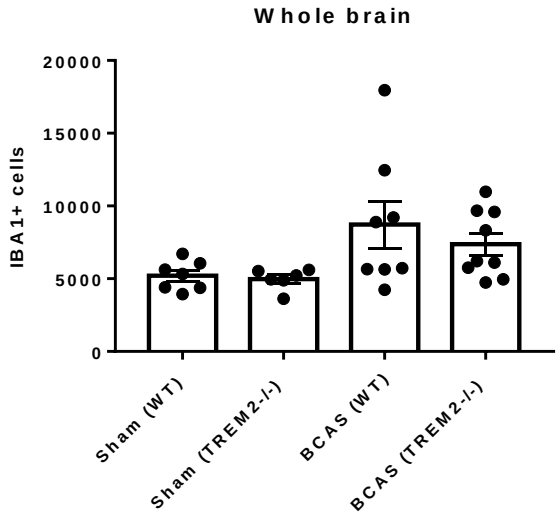

Figure 5.17: Quantification of total IBA1+ cell number in whole brain sections of WT and TREM2-/- mice 28 d post BCAS. IBA1 cell number was unchanged in TREM2-/- mice compared to WT mice in whole brain sections following 28 d BCAS. Welch's unpaired t test. Each data point represents values obtained from one tissue section per animal. Data show mean ± SEM. N = 6 – 9 independent animals per group.

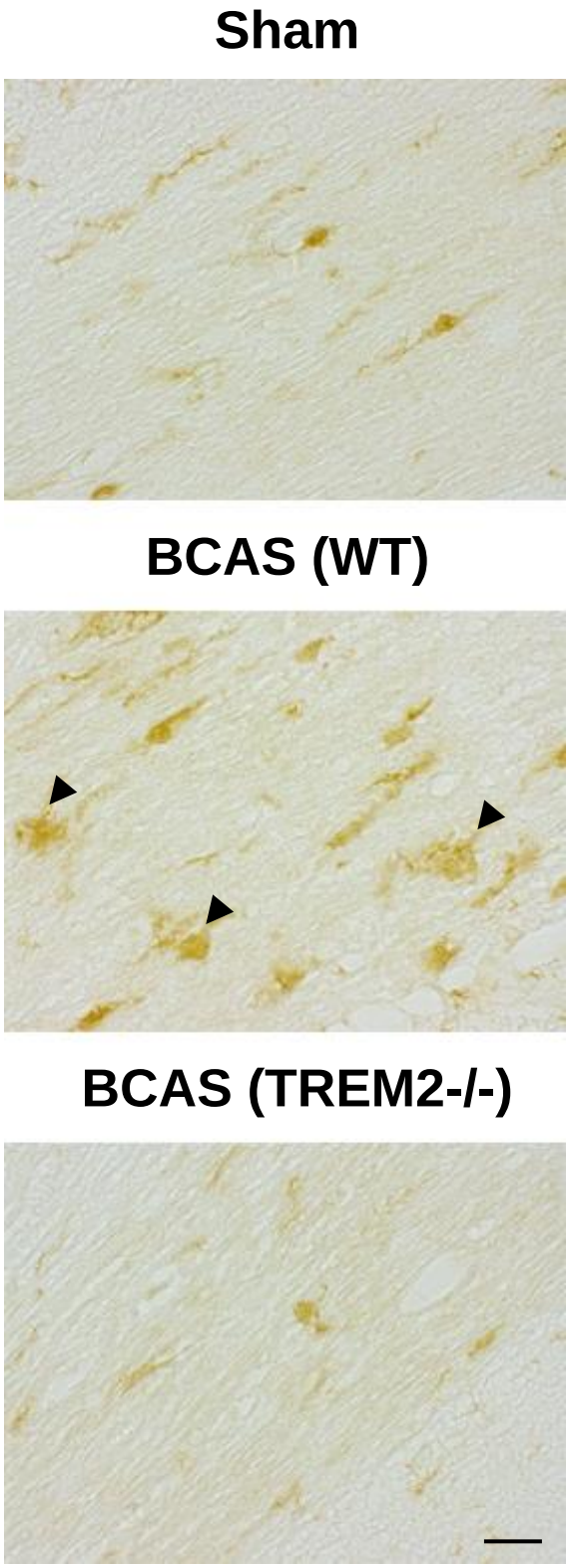

Figure 5.18: Representative images of IBA1 immunostaining in the optic tract of WT and TREM2-/- mice 28 d post BCAS. 28 d following BCAS surgeries, WT mice demonstrated accumulation of IBA1+ cells with an amoeboid morphology and shortened thickened processes in regions of robust pathology characteristic of cell activation (black arrows). However, TREM2-/- IBA1+ cells appeared less hypertrophied compared to WT microglia in areas of pathology and were reduced in density. Scale bar: 25 µm.

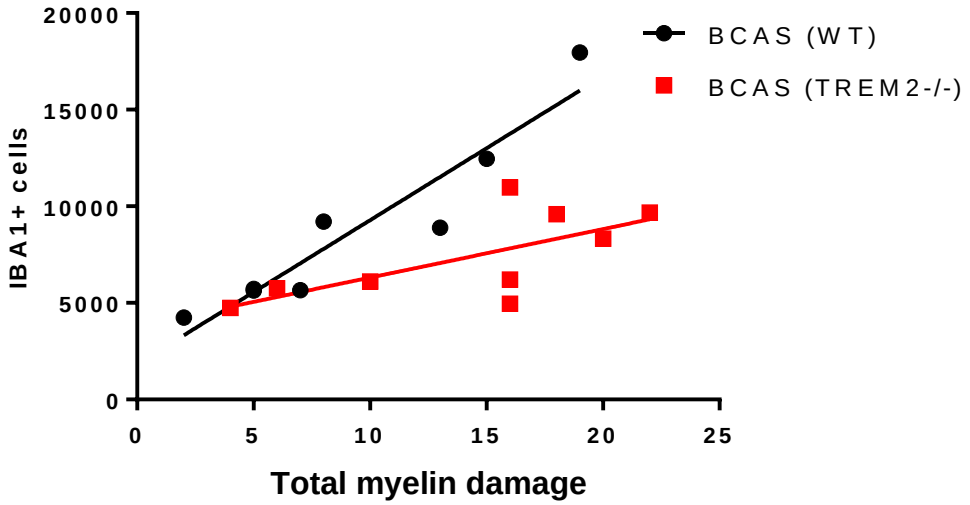

	P	R^2
BCAS (WT)	*** (0.0004)	0.89
BCAS (TREM2-/-)	* (0.0453)	0.46

Figure 5.19: The relationship between total IBA1+ cell number and overall myelin damage 28 d post BCAS in WT and TREM2-/- mice. Plotting total IBA1+ cell numbers calculated from whole brain sections against total myelin damage scores demonstrated IBA1+ cell number positively correlated with myelin damage in WT mice 28 d following BCAS whilst this relationship was tempered in TREM2-/- animals. *P ≤ 0.05, ***P ≤ 0.001. Spearman's rank correlation. Each data point represents values obtained from one tissue section per animal. N = 8 – 9 independent animals per group.

5.4.3.4 Assessment of astrocyte reactivity

GFAP immunostaining was also conducted to investigate whether TREM2 deficiency impacted astrocyte reactivity following BCAS. Assessment of GFAP immunostaining demonstrated hypertrophied astrocytes in areas of myelin damage characteristic of reactive gliosis (fig. 5.22). TREM2 deficiency did not affect GFAP coverage in white matter tracts ($p \geq 0.05$) (fig. 5.20) or whole brain sections ($p \geq 0.05$) (fig. 5.21) following BCAS. Plotting total GFAP coverage across whole brain sections against total white matter damage scores revealed GFAP coverage positively correlated to total white matter damage ($p \leq 0.05$, R^2: 0.85) in WT mice whilst this was only slightly reduced in TREM2-/- mice ($p \leq 0.05$, R^2: 0.71) (fig. 5.23).

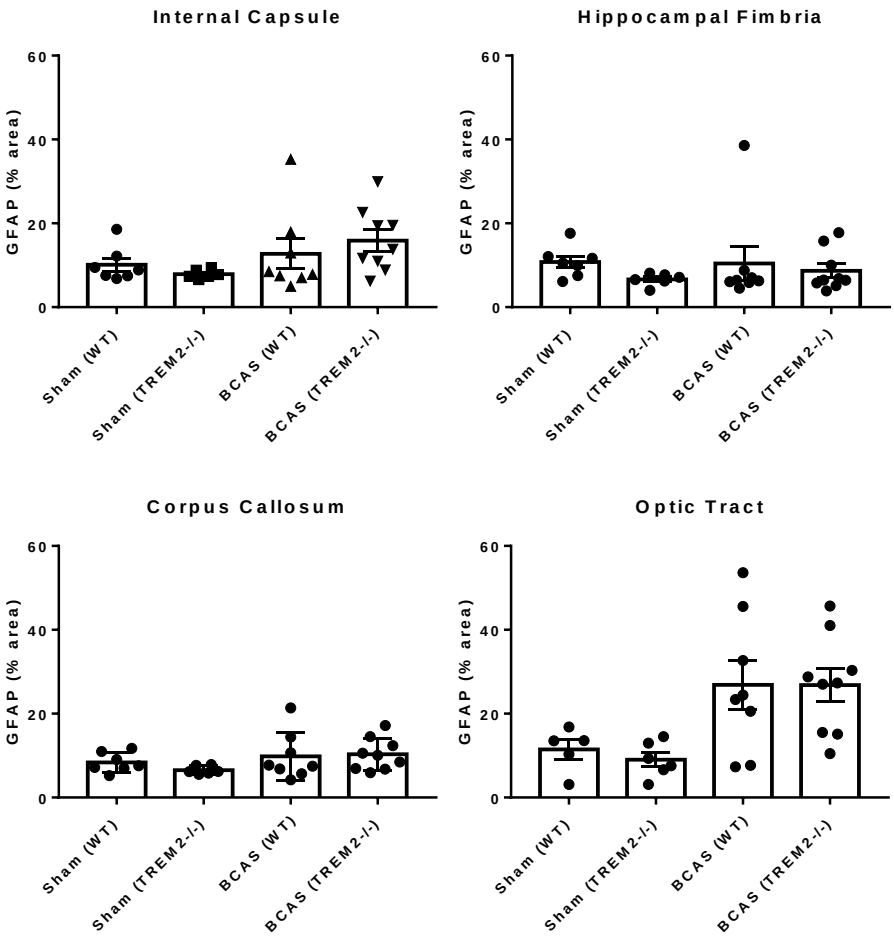

Figure 5.20: Quantification of GFAP in white matter tracts of WT and TREM2-/- mice 28 d post BCAS. GFAP % area was unchanged in TREM2-/- mice compared to WT mice in all white matter regions analysed 28 d following BCAS. *P ≤ 0.05. Welch's unpaired t test. Each data points represents a value averaged from left and right brain hemispheres from one tissue section per animal. Data show mean ± SEM. N = 6 – 9 independent animals per group.

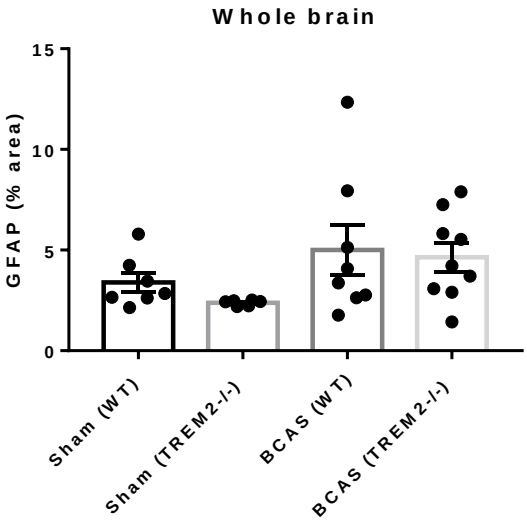

Figure 5.21: Quantification of GFAP in whole brain sections of WT and TREM2-/- mice 28 d post BCAS. GFAP % area was unchanged in TREM2-/- mice compared to WT mice in whole brain sections 28 d following BCAS. Welch's unpaired t test. Each data point represents a value obtained from one tissue section per animal. Data show mean ± SEM. N = 6 – 9 independent animals per group.

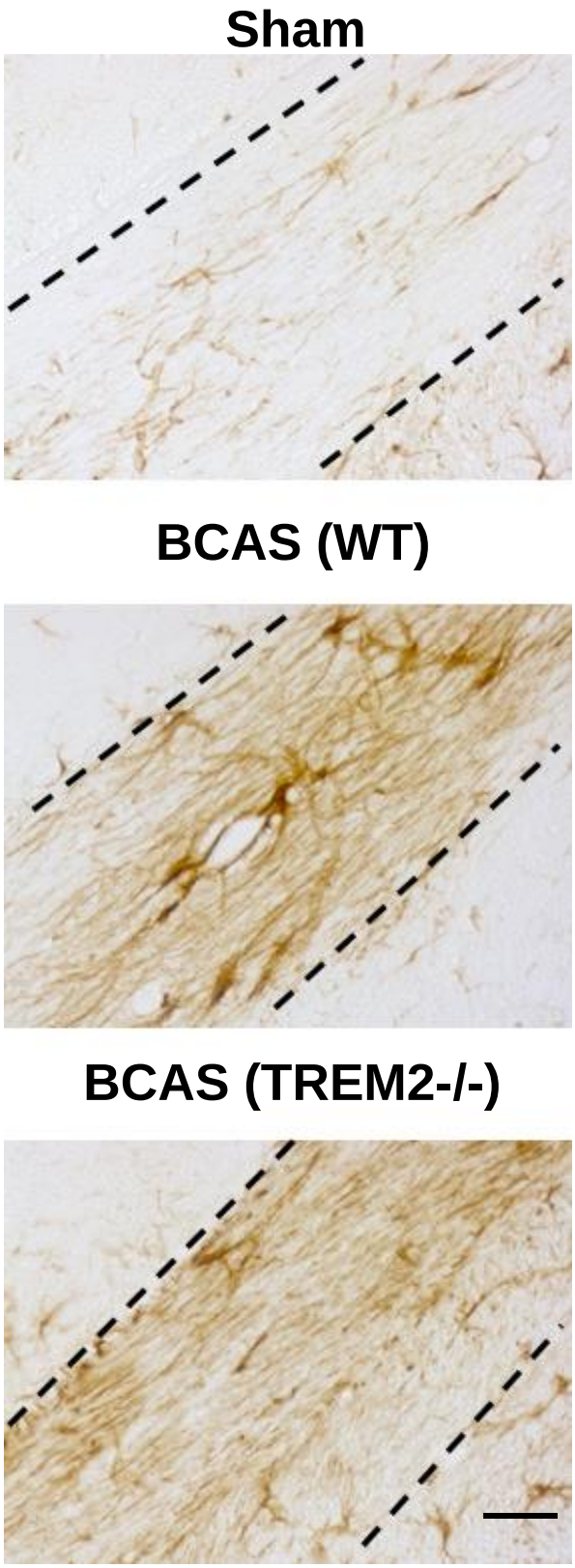

Figure 5.22: Representative images of GFAP immunostaining in the optic tract of WT and TREM2-/- mice. 28 d following BCAS surgeries, WT animals demonstrated hypertrophied astrocytes in areas of myelin damage characteristic of reactive gliosis. TREM2-/- mice demonstrated similar changes in response to BCAS. Dotted lines mark optic tract border. Scale bar: 50 µm

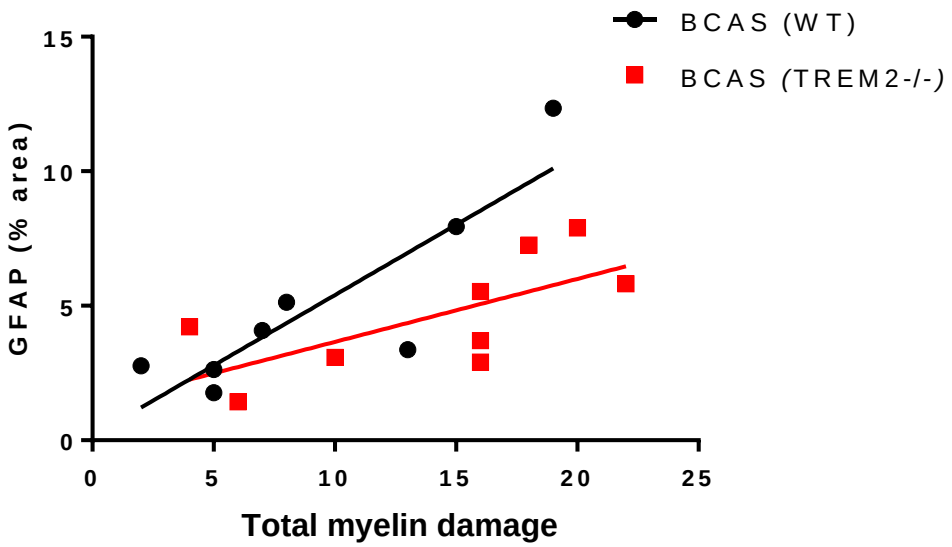

	P	R^2
BCAS (WT)	* (0.0114)	0.85
BCAS (TREM2-/-)	* (0.0380)	0.71

Figure 5.23: The relationship between total GFAP coverage and overall myelin damage in WT and TREM2-/- mice 28 d post BCAS. Plotting GFAP % area calculated from whole brain sections against total myelin damage scores demonstrated GFAP % area positively correlated with myelin damage in WT mice whilst this relationship was party tempered in TREM2-/- mice. *P ≤ 0.05. Spearman's rank correlation. Each data point represents values obtained from one tissue section per animal. N = 8 – 9 independent animals per group.

5.5 Discussion

In the previous study, induction of BCAS using 0.18 mm internal diameter microcoils failed to induce white matter pathology or neuroinflammatory changes in C57BL/6Ntac mice. Although the precise reasons for this remain unclear, it is likely a combination of genetic factors due to mouse substrain and environmental factors (e.g. housing facility, temperature, pathogen status) contributed to the phenotype observed. Cerebral blood flow was not measured therefore it cannot be concluded if application of microcoils induced chronic cerebral hypoperfusion. It was therefore crucial to optimise the BCAS model using microcoils with smaller internal diameters to precipitate robust white matter pathology in WT and TREM2-/- mice while using laser speckle flowmetry to validate perfusion status. Although cohort 1 (mixed coil) demonstrated mild and infrequent myelin pathology, cohort 2 (2x 0.16 mm coil) demonstrated diffuse myelin damage. In the absence of TREM2 expression, IBA1+ cell number was reduced in areas of myelin damage. Furthermore, several TREM2-/- mice exhibited infarcts in the internal capsule which were absent in WT mice suggesting TREM2 exerts protective effects following BCAS.

Previous reports have demonstrated both BCAS techniques induce robust white matter pathology (Shibata, et al., 2004, Miki, et al., 2009, Fowler, et al., 2018). In the current study, use of the mixed coil approach had a mortality rate of 16 % comparable with previous studies (Miki, et al., 2009, Fowler, et al., 2018). Although this was increased to 32 % in cohort 2 (2x 0.16 mm coil), this was substantially less than that reported by Shibata et al. (2004) (75 %) (Shibata, et al., 2004). It is likely a combination of genetic factors due to mouse substrain and environmental factors including housing facility, temperature and pathogen status contributed to reduced mortality. Boehm-Sturm et al. (2017) also reported reduced mortality using 0.16 mm internal diameter microcoils (Boehm-Sturm, et al., 2017). However, this is likely due to the fact this group extended the period between microcoil placement from 30 min to 24 h during which compensatory mechanisms such as autoregulation and adaptive hypoxic responses may have conferred protection to chronic cerebral hypoperfusion.

Assessment of cerebral blood flow by laser speckle flowmetry confirmed both BCAS techniques induced acute reductions in cerebral blood flow in WT and TREM2-/- mice. In cohort 1 (mixed coil), induction of BCAS caused an initial ~35 % reduction in cerebral blood flow in both WT and TREM2-/- animals compared to shams. Although previous studies report clear hemispheric differences in cerebral blood flow following microcoil placement this was not observed in the current study. Furthermore, previous reports demonstrate more substantial reductions in cerebral blood flow following microcoil placement (Miki, et al., 2009, Fowler, et al., 2018). Strain difference is an unlikely contributor as C57BL/6J and C57BL/6N mice do not demonstrate overt differences in circle of Willis anatomy (Zhao, et al., 2019). The BCAS procedure was conducted in a similar manner and factors known to influence cerebrovascular responses such as temperature as well as depth and duration of anaesthesia were controlled to minimise impact on cerebral blood flow. It therefore remains unclear why animals did not demonstrate clear hemispheric differences in cerebral blood flow.

Furthermore, the data suggests recovery of cerebral blood flow 28 d after BCAS in cohort 1 (mixed coil) close to sham levels and may explain why WT and TREM2-/- mice demonstrated mild and infrequent white matter pathology. However, it must be noted that a large number of WT of TREM2-/- mice had to be excluded from the 28 d BCAS group as the laser speckle equipment was serviced mid-study. Following servicing, all recorded blood flow flux values demonstrated an upward shift (fig. 5.24). Therefore, all BCAS animals with 24 h data recorded prior to servicing with 28 d data acquired afterwards were excluded as these data could not be used. WT and TREM2-/- 28 d BCAS groups therefore have low n numbers within this cohort (n = 3) which may not accurately represent cerebral blood flow dynamics in WT and TREM2-/- mice following BCAS.

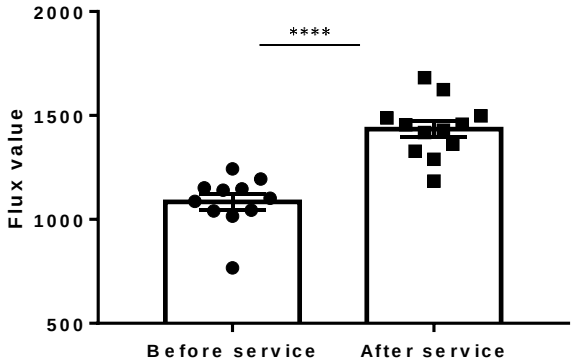

Figure 5.24: Baseline laser speckle flowmetry flux values prior to, and after servicing. Following servicing, all recorded blood flow flux values demonstrated an upward shift. ****P ≤ 0.0001. Student's unpaired t test. Each data point represents an individual animal. Data show mean ± SEM. N = 11 independent animals per group.

Using 0.16 mm internal diameter microcoils bilaterally induced a greater degree of hypoperfusion with both WT and TREM2-/- animals demonstrating a 50-60 % reduction in cerebral blood flow 24 h following BCAS comparable with previous studies (Shibata, et al., 2004, Boehm-Sturm, et al., 2017). Furthermore, cerebral blood flow remained reduced after 28 d with no differences observed between WT and TREM2-/- mice. As WT and TREM2-/- mice demonstrated similar cerebral blood flow profiles it is unlikely TREM2 deficiency affects cerebrovascular architecture or cerebral blood flow regulation. Kawabori, et al. similarly demonstrated TREM2 deficiency did not impact on cerebral blood flow in response to MCAO (Kawabori, at al., 2015). Furthermore, carbon black perfusion of the non-diseased brain demonstrated no overt differences in cerebrovascular architecture between WT and TREM2-/- mice (Kawabori, at al., 2015).

As laser speckle flowmetry only enables quantification of cortical blood flow, it is unclear how blood flow may differ in deeper subcortical regions. Use of arterial spin labelling has demonstrated cerebral blood flow is further reduced in subcortical regions following BCAS (Hattori et al., 2016b, Morimoto et al., 2018). How TREM2 deficiency impacts cerebrovascular integrity in deeper subcortical regions remains unclear. Microglia and macrophages have been suggested to play key roles in angiogenesis and arteriogenesis during development and in response to injury (Fantin et al., 2010, Liu et al., 2016). However, the role of TREM2 in this context remains unclear. Reduced microvessel density has been demonstrated at the infarct border in TREM2-/- mice following MCAO suggestive of impaired angiogenesis (Kawabori, et

al., 2015). Furthermore, recent whole genome sequencing of CNS tissue identified region and time-dependant changes in endothelial gene networks in the absence of TREM2 expression suggesting cerebrovascular function may be altered in TREM2-/- mice (Carbajosa et al., 2018). Neuroimaging studies have demonstrated Nasu Hakola disease patients exhibit reduced cerebral perfusion and glucose metabolism (Ueki et al., 2000, Montalbetti et al., 2005). Similar findings have also been observed in TREM2 p.T66M knock in mice suggesting TREM2 may play key roles in regulation of cerebrovascular integrity and brain glucose metabolism (Kleinberger et al., 2017).

Perivascular macrophages (PVM) also express TREM2 (Chertoff et al., 2013). In addition to clearance of waste products from the brain parenchyma, PVMs are also suggested to regulate peripheral cell recruitment, cerebrovasculature remodelling and regulation of cerebral blood flow (Faraco et al., 2017). Given the multifaceted roles of TREM2 in microglial and macrophage responses, it could be argued TREM2-/- PVMs may also impact cerebrovascular integrity and neuroinflammation. In future studies it will be interesting to decipher how TREM2 regulates perivascular macrophage function. Given that microglia and macrophages interact with endothelial cells with key roles in cerebrovascular maintenance it will also be important to characterise the impact of TREM2 deficiency on endothelial function and microvessel architecture in response to BCAS as this may have contributed to exacerbated damage.

Investigation of white and grey matter pathology in cohort 1 (mixed coil) revealed BCAS induced much milder and infrequent pathology compared to previous studies (Miki, et al., 2009, Fowler, et al., 2017). Observed discrepancies are likely due to a variety of genetic differences between mouse substrains as well as environmental features impacting on BCAS-induced white matter damage as discussed in chapter 4. This version of the BCAS model was therefore unfavourable due to the infrequent and mild nature of observed pathology. In cohort 2 (2x 0.16 mm coil), 0.16 mm internal diameter microcoils induced more frequent and extensive neuropathology. However, a limitation of this model is the variability of observed pathology. While ~50 % of WT and TREM2-/- BCAS animals demonstrated damage limited to white matter regions with no grey matter involvement, the remaining 50 % demonstrated

additional grey matter pathology of varying severities. Furthermore, although 0.16 mm internal diameter microcoils were used bilaterally, clear hemispheric differences in the degree of damage were observed between animals.

The spectrum of pathology observed is likely due to variation in cerebrovascular anatomy. Absence of both posterior communicating arteries is observed in 30 % of C57BL6/J mice whilst at least one posterior communicating artery is present in 60 % (McColl et al., 2004). Similar variation has also been observed in C57BL/6N mice (Zhao et al., 2019). Therefore, the extent of compensatory blood flow via the vertebral circulation will vary from mouse to mouse resulting in varying degrees of hypoperfusion and inconsistent pathology in regions dependent on posterior supply. Furthermore, microcoil internal diameter can vary by 0.1 mm impacting the degree of hypoperfusion induced by BCAS. Assessment of cerebral blood flow demonstrated variation in the degree of hypoperfusion 24 h after BCAS with reductions in cortical blood flow varying from 30 % to 84 % in WT and TREM2-/- animals.

4 of 5 animals displaying extensive grey matter damage demonstrated cerebral blood flow reductions of 65 - 85 % 24 h after BCAS surgery. It could therefore be postulated that observed pathology may be due to acute ischaemic insult rather than longer durations of cerebral hypoperfusion. To distinguish damage caused by acute or sustained reductions in cerebral blood flow it will be important to characterise the temporal evolution of CNS pathology. If acute hypoperfusion following microcoil placement is a key cause of observed pathology the GCAS or ACAS models could be implemented to circumvent this. However, as substantial hypoperfusion was required to precipitate myelin damage it is unclear if either of these models would be suitable.

Due to the extent of variation it may be necessary to apply criteria in future studies to exclude animals demonstrating extremely mild or severe hypoperfusion to ensure observed pathology is more consistent. As this was a characterisation study, exclusion criteria were not applied and all animals were included in analyses of cerebral blood flow and CNS pathology. Given the variation observed, an additional limitation of the current study is the low sample size. Larger sample sizes of 12-14 mice per group were intended to improve statistical, however,

this was not possible due to breeding issues and may explain why many of the data demonstrate non-significant trends.

Although an increase in total grey matter damage was observed in TREM2-/- animals in cohort 2 (2x 0.16mm) this did not reach statistical significance. The impact of TREM2 deficiency on neuronal pathology remains unclear as the approach used for quantification lacked sensitivity. Although multiple regions may demonstrate neuronal pathology, the method of quantification does not reveal the degree by which they are affected. A more appropriate method would be to conduct NeuN immunostaining and quantify the degree of neuronal loss to provide an accurate measure of neuronal pathology. However, this was not completed due to time constraints and will be conducted in future.

Assessment of MAG immunostaining demonstrated the optic tract was susceptible to hypoperfusion-mediated damage in WT and TREM2-/- mice. Similar findings were also reported by Sigfridsson et al. (2018) in FVB/C57Bl/6J F1 animals 28 d after BCAS (Sigfridsson, et al., 2018). Previous studies in rats have also reported susceptibility of the optic tract in response to chronic cerebral hypoperfusion (Wakita et al., 2002). This is likely due to the fact that the optic tract is supplied by the ophthalmic artery which branches from the internal carotid via the pterygopalatine and palatine artery. Therefore, application of microcoils may evoke greater hypoperfusion in regions such as the optic tract compared to other white matter regions. Given that the optic tract showed greatest susceptibility to hypoperfusion-mediated damage it will be important to assess visual function in future as behavioural studies utilise visualise cues.

TREM2 deficiency exacerbated white matter damage in the internal capsule and trends for increased damage where observed in other white matter tracts. Compiling scores similarly demonstrated a trend towards increased total white matter damage in TREM2-/- mice. As TREM2 deficiency predominantly exacerbated damage in the internal capsule it could be suggested that TREM2 function may be region dependant. It is well known microglia demonstrate regional heterogeneity in the adult CNS (Grabert et al., 2016). White matter microglia demonstrate more pronounced morphological changes and upregulation of genes

associated with phagocytosis and activation with aging compared to grey matter microglia (Hart et al., 2012, Raj et al., 2017). Furthermore, patients with microgliopathies demonstrate extensive demyelination suggesting white matter microglia may differ phenotypically from grey matter microglia. It could be postulated the internal capsule is more dependent on TREM2 function for maintenance of homeostasis resulting in exacerbated damage in its absence. However, it remains unknown whether microglia exhibit distinct phenotypic profiles within white matter regions or how TREM2 regulates this.

Investigation of IBA1+ immunostaining revealed increased IBA1+ cell number in the optic tract in response to BCAS. Despite other regions demonstrating white matter damage, only negligible changes in IBA1+ cell number were observed. Given that the extent and spatial distribution of damage varied in the corpus callosum, internal capsule and hippocampal fimbria this could explain why these areas were not associated with a robust microglial response. Interestingly, TREM2 deficiency blunted increases in IBA1+ cell number following BCAS suggesting microglial responses to BCAS are TREM2 dependant. TREM2 deficiency has been suggested to attenuate various microglial functions including survival, proliferation, migration and phagocytic capacity. Recent studies implementing single cell sequencing have demonstrated TREM2 plays a key role in reprogramming microglia to respond to CNS perturbation through upregulation of genes associated with phagocytic and lysosomal pathways as well as lipid metabolism (Keren Shaul, et al., 2017). Although the impact of TREM2 deficiency in the context of chronic cerebrovascular insufficiency has never been investigated, studies have investigated the role of TREM2 in preclinical models of stroke and demyelination.

TREM2-/- animals demonstrate worsened ischaemic damage and functional recovery in response to MCAO associated with reduced microgliosis (Kawabori, et al., 2015). A separate study similarly demonstrated increased infarct volume and neuronal apoptosis in response to MCAO following TREM2 gene silencing using small interfering RNA (Wu, et al., 2017). In the cuprizone model of oligodendrocyte degeneration and demyelination, TREM2-/- animals demonstrate worsened axonal pathology and reduced clearance of degraded myelin.

Furthermore, investigation of IBA1 immunostaining revealed reduced microglial coverage in areas of white matter pathology. Poliani et al. (2015) also observed reduced microgliosis in TREM2-/- animals accompanied by reduced myelin debris clearance and progressive loss of oligodendrocytes in response to cuprizone treatment (Poliani, et al., 2015).

The findings of the current study are in line with previous reports describing reduced microgliosis in response to CNS injury in TREM2-/- mice. TREM2-/- microglia demonstrate decreased viability and reduced proliferation via defective Wnt/ β catenin signalling (Zheng et al., 2017). It could therefore be postulated that microglia were more vulnerable to cell death or failed to proliferate in response to BCAS resulting in less IBA1+ cells in areas of myelin pathology. It remains unclear however if the dampened microglial response to BCAS was predominantly due to increased cell death or reduced proliferation.

As white matter damage was exacerbated in TREM2-/- mice this suggests TREM2 expression may protect white matter integrity in response to BCAS. Due to time constraints the results presented in this study show gross features of CNS pathology and glial responses associated with BCAS in WT and TREM2-/- mice Therefore, the precise mechanisms by which TREM2 deficiency exacerbates white matter damage resulting from BCAS remain unclear.

TREM2 deficiency may have exacerbated white matter damage by impairing microglial-mediated clearance of myelin debris in the local microenvironment. TREM2 binds to various myelin components including phosphatidylethanolamine, sphingomyelin and phosphatidylserine and regulates expression of phagocytic receptors important for myelin debris clearance (Poliani et al. 2015, Cannon et al. 2012, Cantoni et al., 2015, Wang et al., 2015). Microglial and macrophage-mediated removal of myelin debris is critical for effective remyelination to occur. Myelin debris prevents OPC differentiation into mature oligodendrocytes (Kotter et al., 2006). Furthermore, myelin components including Nogo-A, Semaphorin 4D, oliogodendrocyte myelin protein and MAG inhibit axonal growth (Huebner and Strittmatter, 2009).

In the current study it could therefore be suggested that in the absence of TREM2, microglial detection of white matter injury and subsequent activation was impaired, reducing microglial phagocytic capability leading to increased myelin debris accumulation. Accumulating myelin debris may have impaired OPC maintenance and maturation preventing remyelination, exacerbating white matter injury in response to BCAS.

It could also be suggested that microglial degradation of myelin was impaired. Safaiyan et al. (2016) recently demonstrated microglial mediated uptake of myelin results in the accumulation of intracellular undegradable deposits which contributes to microglial senescence and immune dysfunction in the aging brain (Safaiyan et al., 2016). In response to BCAS, efficient degradation of internalised myelin may require TREM2 function as recent studies demonstrated TREM2-mediated microglial activation is associated with upregulation of various lysosomal genes (Forabosco et al., 2013, Keren-Shaul et al., 2017). Therefore, in the absence of TREM2 expression, impaired clearance mechanisms may have caused an accumulation of internalised myelin leading to microglial dysfunction and exacerbated pathology.

Factors secreted by microglia also regulate various cell types within the gliovascular unit. *In vitro* studies have demonstrated treatment of OPCs with conditioned microglial media promotes survival and maturation into myelinating oligodendrocytes (Zhang et al., 2006, Miron et al., 2013). Analysis of conditioned media reveals expression of various factors important for OPC survival and differentiation including vascular endothelial growth factor (VEGF), IGF-1 and platelet derived growth factor AA (PDGF-AA) (Pang et al., 2013). In the cuprizone model of demyelination, microglia isolated from regions of remyelinating white matter demonstrate upregulation of genes associated with OPC proliferation and differentiation including TNFα, IGF-1 and fibroblast growth factor 2 (FGF-2) (Voss et al., 2012). Furthermore, microglial activation in response to focal demyelination enhances OPC generation from neural stem cells in the subventricular zone suggesting microglia play key roles in OPC maturation in response to injury (Naruse et al. 2018). In addition, microglia also play a key role in early postnatal and adult OPC maintenance in the non-disease brain (Hagemeyer et al., 2017).

Increased numbers of OPCs and mature oligodendrocytes have been reported 28 d after BCAS demonstrating the regenerative capacity of white matter in response to chronic cerebral hypoperfusion (McQueen et al., 2015, Yu et al., 2018). Although it remains unclear, this process may in part be regulated by TREM2. TREM2-/- microglia demonstrate reduced expression of mediators implicated in OPC differentiation including IGF-1 in the cuprizone model of demyelination (Poliani et al., 2015). Therefore, it could be suggested that reduced secretion of factors necessary for survival and differentiation of OPCs into myelin forming oligodendrocytes impaired the regenerative capacity of white matter resulting in exacerbated pathology following BCAS

As stated earlier, alterations in endothelial gene networks have been reported in TREM2-/- mice suggesting TREM2 regulated microglial responses may be crucial for endothelial function and cerebrovascular integrity. Microglia secrete various factors known to impact endothelial function including MMPs, ROS and cytokines such as IL-1β and TNF-α. In response to BCAS, ICAM1 expression closely correlates to the degree of microgliosis suggesting microglia contribute to endothelial activation in the context of chronic cerebral hypoperfusion (Kitamura et al., 2017). It could therefore be postulated microglial responses to BCAS may impact endothelial function and BBB integrity in TREM2-/- animals. However, the impact of TREM2 deficiency on endothelial cell function remains unknown.

In addition to IBA1+ cell number, GFAP coverage was also assessed to determine if TREM2 regulated astrocyte responses. In the current study, TREM2 deficiency did not impact white matter GFAP coverage. Kawabori et al. (2015) similarly reported no difference in GFAP coverage in TREM2-/- animals in a preclinical model of stroke (Kawabori, et al., 2015). However, TREM2-/- APPPS1 mice demonstrate reduced GFAP expression and astrocyte coverage (Jay et al., 2015). Similar findings were also observed in a model of tauopathy (Leyns et al., 2017). It could be postulated that the impact of TREM2 on astrocyte responses may be disease dependent. While astrocyte responses to misfolded protein may depend on microglial TREM2 expression, TREM2-independent astrocyte responses may be initiated following hypoxic insult.

It could also be suggested the impact of TREM2 deficiency on astrocyte responses is region specific. Although TREM2 deficiency did not impact white matter GFAP coverage, a non-significant decrease in GFAP coverage was observed across whole brain sections in TREM2-/- mice suggesting TREM2 deficiency may have impacted GFAP coverage elsewhere in the brain. Previous work in the McColl lab has demonstrated reduced GFAP coverage in CA1 regions of the hippocampus in the non-diseased brain and reduced hippocampal GFAP expression in response to MCAO in TREM2-/- mice. In future studies it will therefore be important to further characterise the impact of TREM2 deficiency on GFAP coverage in other brain regions outside the white matter. As release of microglial derived factors are suggested to regulate astrocyte function in neurodegenerative disease it will be interesting to decipher how TREM2 may affect this (Liddelow et al., 2017).

Overall, the data in the current study suggests TREM2 is necessary for microglial responses to BCAS and promotes white matter integrity. Due to time constraints, the current study characterised only basic features of pathology resulting from BCAS. In future studies it will be important to characterise additional features of white matter pathology including axonal health and investigate vascular pathologies such as endothelial dysfunction and BBB breakdown. Furthermore, the distribution of pathology throughout the brain and the impact of TREM2 deficiency remains unclear as pathological assessment was only conducted at the level of the hippocampus. In addition, although 50 % of animals demonstrated additional grey matter pathology investigation of glial responses was limited to the white matter. Therefore, further characterisation of the BCAS model is necessary to gain understanding on the distribution of CNS pathology and the impact of TREM2 deficiency.

Although TREM2 deficiency impaired microglial responses to BCAS and exacerbated white matter damage the precise mechanisms remain unclear. It is therefore crucial to gain a deeper understanding of how microglia respond to BCAS and the impact of TREM2 deficiency using whole genome expression profiling. Given that TREM2 deficiency exacerbated white matter damage investigation of the microglial transcriptome may identify novel TREM2 regulated pathways which could be manipulated to promote neuroprotection in response to BCAS.

Chapter 6:

Investigating the impact of TREM2 deficiency on microglial phenotype and CNS immune cell composition in response to BCAS

6.1 Introduction

In the previous study, induction of BCAS using 0.16 mm internal diameter microcoils caused an acute and sustained reduction in cerebral blood flow in WT and TREM2-/- mice. Pathological assessment after 28 d revealed diffuse myelin damage and 50 % of animals demonstrated additional neuronal pathology covering several grey matter regions. In the absence of TREM2 expression, the extent of microgliosis in areas of myelin damage was reduced suggesting TREM2 plays a key role in mediating microglial/ macrophage responses to BCAS. Furthermore, TREM2 deficiency exacerbated myelin damage suggesting TREM2 mediates protective responses to BCAS.

Precisely how TREM2 regulates microglial responses to BCAS remains unclear. Transcriptomic studies investigating microglial phenotype in neurodegenerative diseases have identified microglia with a conserved phenotype named disease associated microglia (DAM). Interestingly, recent single cell sequencing suggests TREM2 is required for microglia to adopt a DAM phenotype associated with attenuation of neurodegeneration (Keren-Shaul et al., 2017). However, it remains unknown if microglia adopt a similar phenotype in the context of chronic cerebrovascular-mediated degeneration. As TREM2 may confer protection to BCAS, further understanding of TREM2 regulated processes may lead to the identification of novel pathways which could be modulated to promote resilience and reduce disease burden.

In the current study we therefore sought to develop and optimise a method of fluorescence activated cell sorting (FACS) to extract WT and TREM2-/- microglia from discrete areas of brain tissue and investigate the impact of BCAS on the microglial transcriptome. Tissue was dissected from white and grey matter enriched regions and microglia were extracted. Additional markers of myeloid and lymphoid cell populations were incorporated and flow cytometric analysis was conducted in parallel to characterise the impact of TREM2 deficiency on microglial phenotype and CNS cell composition in response to BCAS.

6.2 Aims

1. Develop and optimise a FACS-based method of microglial extraction to investigate BCAS-induced alterations to the microglial transcriptome in WT and TREM2-/- mice.

2. Investigate alterations in microglial phenotype as well as CNS myeloid and lymphoid cell composition in response to BCAS in WT and TREM2-/- mice.

6.3 Methods

6.3.1 Animal procedures

Male C57BL/6J mice (2 - 3 m) were purchased from Charles River and used to validate a FACS-based method for isolation of microglia from whole brain. Male WT and TREM2-/- mice (8 - 9 m) were used to investigate the impact of TREM2 deficiency on microglial phenotype and CNS cell composition following BCAS. N numbers were chosen based on power analysis of data from previous BCAS studies. To achieve a significance level of $p < 0.05$, a group size of 8 was required to reach a power of 0.8. Animals were randomised to receive BCAS (0.16 mm internal diameter microcoils bilaterally) or sham surgeries described in section 2.4.1. Due to lack of breeding and limited animal numbers a TREM2-/- sham group was not included.

Laser speckle contrast imaging described in section 2.4.2 was conducted to validate BCAS induced chronic cerebral hypoperfusion in WT and TREM2-/- mice. Measurements were taken prior to conducting BCAS and sham surgeries to obtain a baseline value and then again 24 h and 28 d after surgeries. Laser speckle contrast imaging and subsequent analysis was conducted by the author with blinding to treatment and genotype. After surgeries, animals were monitored, and weight loss recorded twice daily for 72 h and then twice weekly. Initial cohort sizes are shown in table 6.1.

	Sham (n)	BCAS (n)
WT	7	11
TREM2-/-	-	8

Table 6.1: Cohort sizes prior to conducting BCAS and sham surgeries.

6.3.2 Tissue harvest

Animals were transcardially perfused with saline 28 d after BCAS or sham surgeries as described in section 2.4.3 by Clare Latta. Subsequent dissection of white and grey matter regions for FACS isolation of microglia described in section 2.8.1 was conducted by the author.

6.3.3 FACS isolation of microglia and flow cytometric analyses

FACS isolation of microglia and flow cytometric analyses were utilised to investigate the impact of TREM2 deficiency on CNS cellular composition and microglial phenotype in response to BCAS. Preparation of a brain cell suspension and antigen labelling of antigens was conducted by the author as described in sections 2.8.2 and 2.8.3.

Upon acquisition, DAPI- viable cells were first identified and doublets excluded. Microglia were identified as $Ly6C^{-}CD11b^{+}CD45^{lo}$ cells and sorted directly into RLT lysis buffer. Myeloid and lymphoid populations analysed included microglia, macrophages, neutrophils and lymphocytes. Marker profiles in table 6.2 were utilised to distinguish different cell populations. Microglial CD45, CD11b and F4/ 80 MFI were also quantified to investigate the impact of TREM2 deficiency on microglial phenotype in response to BCAS. All analysis and quantification of data were conducted by the author with blinding to genotype and treatment.

Cell Type	Marker Profile
Microglia	$Ly6G^{-}Ly6C^{-}CD11b^{+}CD45^{lo}$
Macrophages	$Ly6G^{-}Ly6C^{lo-hi}CD11b^{+}CD45^{hi}$
Neutrophils	$CD11b^{+}Ly6G^{+}$
Lymphocytes	$CD11b^{-}CD45^{+}$

Table 6.2: Cell surface marker profiles used to distinguish cell populations for flow cytometric analysis.

6.3.4 RNA extraction

Extraction of microglial RNA was conducted by the author using a Qiagen RNeasy microplus kit following manufacturer's instructions as described in section 2.9. RNA yield and purity was assessed using a nanodrop spectrophotometer. Samples were then stored at -80^{o}C.

6.3.5 Statistics

Student's or Welch's unpaired t test was used to test for differences between two groups in FACS optimisation experiments. Two way ANOVA with Bonferroni correction for *post hoc* was used to investigate the impact of BCAS on cerebral blood flow in WT and TREM2-/- mice with genotype and surgery as between subject factors. One way ANOVA with Bonferroni correction for *post hoc* was used to investigate differences in microglial CD45, CD11b and F4/ 80 MFI and CNS cell composition following BCAS in WT and TREM2-/- mice. All statistical analyses were performed with Graphpad Prism software version 7.4 with statistical significance considered $p \leq 0.05$.

6.4 Results

6.4.1 Validation of microglial enrichment

To determine the efficiency of the FACS extraction method, the proportion of viable microglia were compared prior to and after sorting. Prior to sorting, Ly6C^{-}CD11B^{+}CD45^{lo} microglia were identified as ~30 % of the viable brain suspension. Post sort, microglia were enriched constituting almost all viable cells indicating specific and efficient extraction of microglia via FACS (fig. 6.1). To further validate purity of isolated microglia, RNA was extracted and expression of microglial, neuronal and astrocyte genes was compared with whole brain tissue. Microglial genes *Iba1* and *Tmem119* were highly enriched in isolated microglia compared to whole brain tissue whilst expression of neuronal (*Rbfox3*) and astrocyte (*Aldh1l1*) genes were negligable suggesting the FACS procedure results in a highly enriched population of microglia (fig. 6.2).

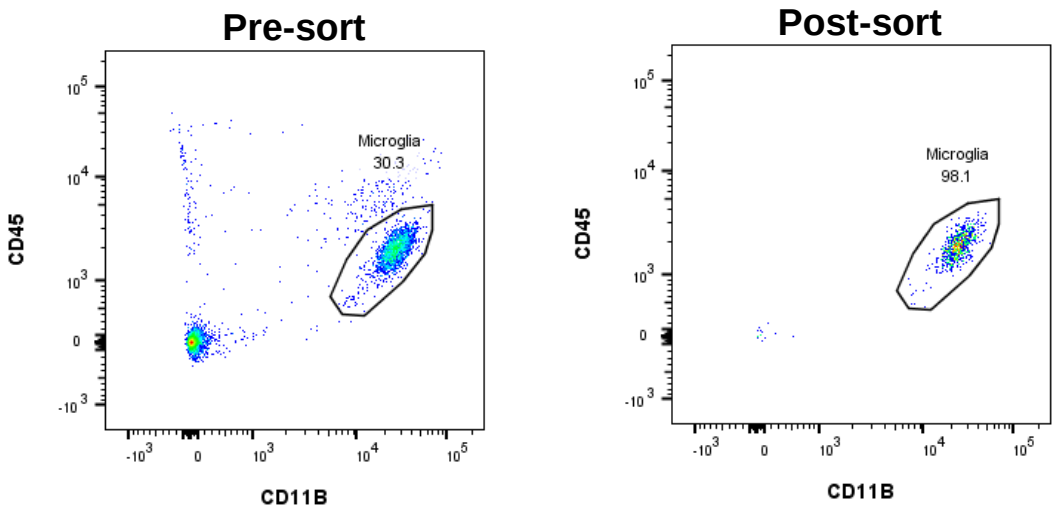

	Proportion of viable microglia
Pre-sort	30%
Post -sort	98%

Figure 6.1: Proportion of viable Ly6C^{-}CD11b^{+}CD45^{lo} microglia prior to, and after FACS sorting. The microglial population was highly enriched following FACS constituting 98% of the total cell population.

A.

	Iba1	*Tmem119*	*Rbfox3*	*Aldh1l1*	*Gapdh*
Whole brain	28.70 ± 0.35	28.73 ± 0.25	23.24 ± 0.29	25.57 ± 0.19	15.63 ± 0.16
Isolated microglia	24.92 ± 0.42	23.30 ± 0.22	32.31 ± 1.4	34.55 ± 1.60	15.82 ± 0.12

B.

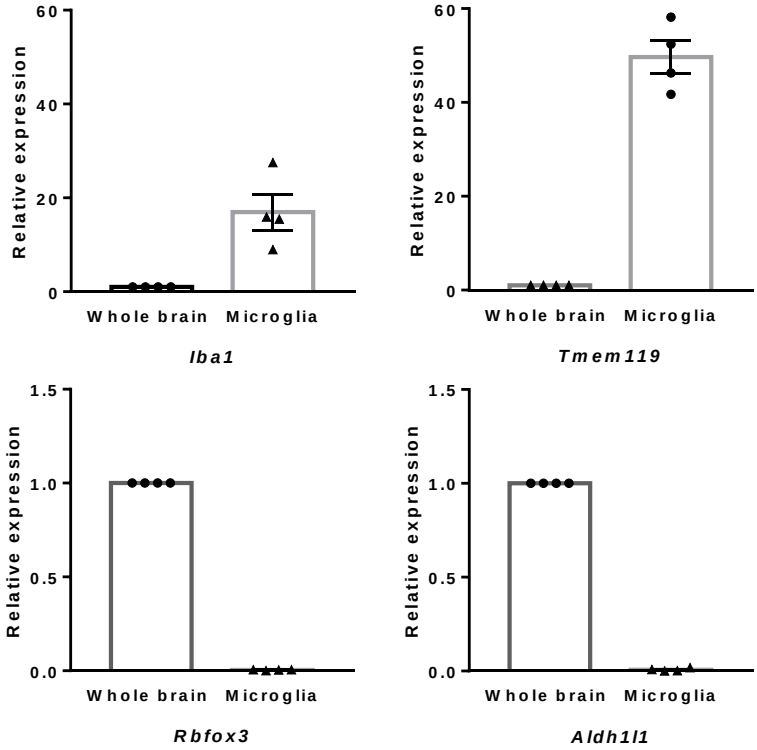

Figure 6.2: Comparison of signature gene expression in sorted microglia compared to whole brain. (A) Ct values for microglial genes (*Iba1, Tmem119*) and astrocyte (*Aldh1l1*) and neuronal genes (*Rbfox3*) in FACS isolated microglia and whole brain tissue. (B) Relative expression of microglial genes (*Iba1, Tmem119*) and astrocyte (*Aldh1l1*) and neuronal genes (*Rbfox3*) in FACS isolated microglia compared to whole brain tissue. Relative to whole brain tissue, microglial transcripts were highly enriched in FACS isolated microglia whilst expression of astrocyte and neuronal transcripts was negligible. *Gapdh* was used as a house keeper gene. Data show mean ± SEM. Each data point represents an independent microglial extraction from one brain hemisphere. N = 4 independent microglial isolation experiments per group.

6.4.2 Optimisation of fluorescence activated cell sorting of microglia

6.4.2.1 Optimising microglial yield

The methodology used to obtain a homogenous brain cell suspension for flow cytometric acquisition was further optimised for FACS-based microglial isolation to reduce cell death and maximise yield. Firstly, Pasteur pipettes were used instead of Gilson pipettes to limit cell death caused by shear stress when pipetting. The buffering agent HEPES (25mM, Fisher) was also added to all buffers to help maintain physiological pH throughout the isolation procedure.

Many microglial extraction procedures also include an enzyme digestion step to promote cell dissociation from surrounding extracellular matrix prior to tissue homogenisation. However, a limitation of this method is that enzyme treatment is suggested to alter the microglial transcriptome (Kang et al., 2018). To determine the impact of enzyme treatment on microglial phenotype, microglial cell properties were characterised by flow cytometric analysis in samples treated with or without enzymes prior to tissue homogenisation. Investigation of microglial forward and side scatter properties demonstrated enzyme treatment significantly increased microglial forward scatter (size) and side scatter (granularity) values ($p \leq 0.001$) (fig. 6.3A & B). Furthermore, microglia demonstrated increased CD45 MFI ($p \leq 0.05$) suggesting enzyme treatment alters microglial activation status (fig. 6.3C).

Flow cytometric analysis revealed enzyme treatment also reduced cell viability ($p \leq 0.05$) (fig 6.4B) and although statistically non-significant, reduced the yield of isolated microglia (fig. 6.4C) ($p \geq 0.05$). Enzyme treatment of brain tissue prior to tissue homogenisation was therefore removed from the isolation protocol to reduce microglia phenotypic alterations and increase microglial yield.

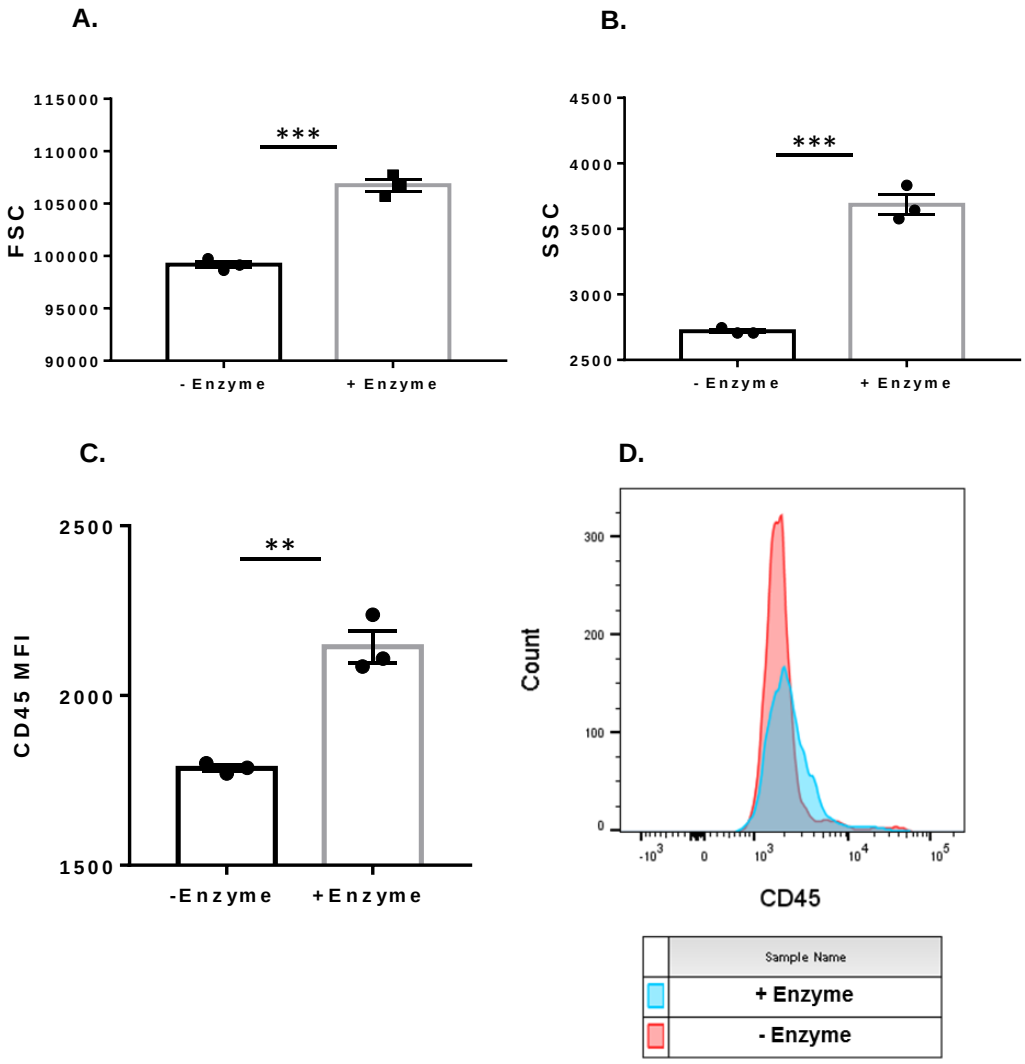

Figure 6.3: Flow cytometric analysis of microglial properties in brain samples treated with or without enzymes prior to tissue homogenisation. (A) (B) Forward and side scatter properties of microglia treated with or without enzyme digestion prior to tissue homogenisation. Enzyme treatment significantly increased microglial forward scatter and side scatter values. (C) (D) Quantification and representative histogram plots of CD45 MFI in samples treated with and without enzyme digestion. CD45 MFI was significantly increased in samples treated with enzyme. **P ≤ 0.01, ***P ≤ 0.001; Student's unpaired t test. Each data point represents an independent microglial isolation from one brain hemisphere. Data show mean ± SEM. N = 3 independent microglial isolation experiments per group.

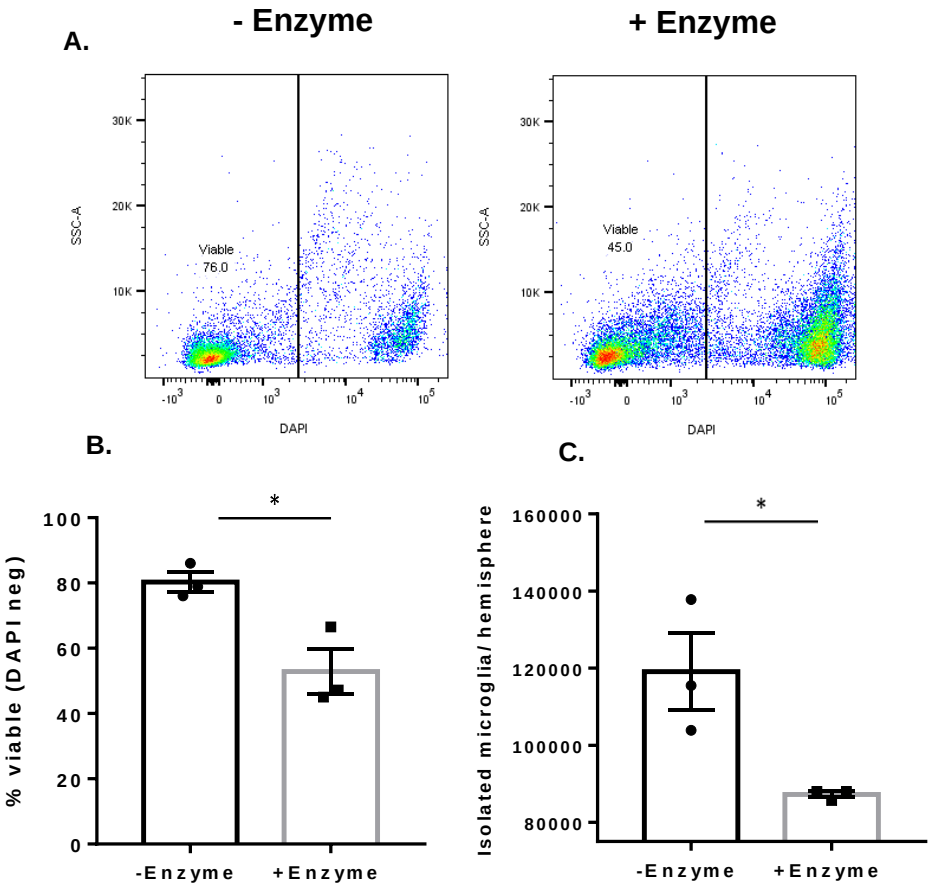

Figure 6.4: Microglial yield following FACS isolation with or without enzyme treatment. (A) Representative flow cytometry dot plots of viable cells in brain cell suspensions treated with or without enzymes prior to FACS. (B) Flow cytometric analysis of viable (DAPI negative) cells within brain cell suspensions treated with or without enzymes. Enzyme treatment significantly reduced the proportion of viable cells retrieved from brain tissue for FACS-based isolation. (C) Comparison of microglial yield in brain cell suspensions treated with or without enzymes. Enzyme treatment significantly reduced the yield of microglia obtained via FACS. *P ≤ 0.05; (B) Student's unpaired t test (C) Welch's unpaired t test. Each data point represents an independent microglial isolation from one brain hemisphere. Data show mean ± SEM. N = 3 independent microglial isolation experiments per group.

Prior to separating cells from myelin using a Percoll gradient, homogenisation of tissue is required to provide an even brain cell suspension. Previous studies in the McColl lab have demonstrated liquid-based homogenisation via 20 passes with a Dounce homogeniser is sufficient to provide a homogenous suspension from brain tissue following enzyme digestion (Grabert and McColl, 2018). As enzyme digestion was omitted it was predicted increasing the number of Dounce passes may further increase microglial yield. Investigation of microglial yield after homogenising brain tissue with 20 or 40 Dounce passes demonstrated microglial yield was enhanced when the number of Dounce passes was increased to 40 ($p \leq 0.05$) (fig. 6.5). The number of Dounce passes was therefore increased to 40 to maximise yield of extracted microglia.

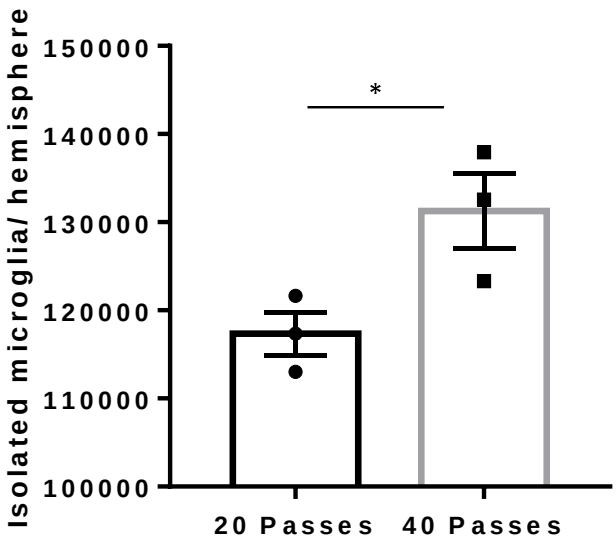

Figure 6.5: Quantification of microglial yield following liquid-based homogenisation of brain tissue using 20 and 40 passes of a Dounce homogeniser. Microglial yield was significantly increased when the number of Dounce passes was increased to 40 from 20 when homogenising brain tissue. *P ≤ 0.05; Student's unpaired t test. Each data point represents an independent microglial isolation from one brain hemisphere. Data show mean ± SEM. N = 3 independent microglial isolation experiments per group.

6.4.2.2 Optimisation of microglial RNA extraction

Prior to RNA extraction efficient cell lysis is required. Isolated cells can be sorted into media and lysed after centrifugation or sorted directly into cell lysis buffer. An advantage of the latter method is that potential gene expression changes from sorting into media are minimised. Furthermore, subsequent cell death from sorting and centrifugation are avoided therefore maximising yield. However, it must be noted that cells are sorted in 5 nl sheath fluid. Therefore, if sorting high numbers of cells, dilution of cell lysis buffer by sheath fluid may impact lysis efficiency and RNA yield.

To determine an optimal method of cell lysis prior to RNA extraction, total yield and quality of microglial RNA was quantified from microglia isolated into microglial media (see appendix III) and compared with microglia isolated directly into Qiagen RLT lysis buffer containing 10 % β-mercaptoethanol. Although statistically non-significant, RNA yield was increased when microglia were sorted directly into lysis buffer (fig. 6.6A). Furthermore, both methods of cell lysis yielded high quality RNA (fig. 6.6B). Therefore, microglia were sorted directly in cell lysis buffer in subsequent experiments to minimise potential alterations in microglial phenotype caused by sorting into media.

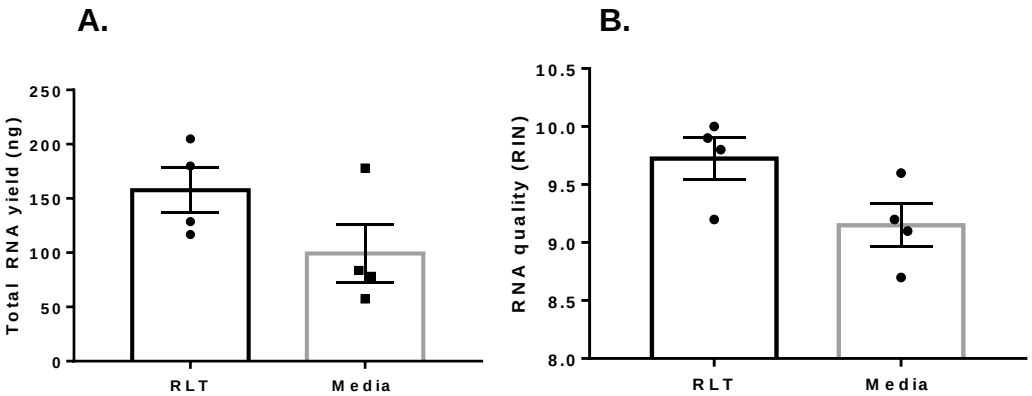

Figure 6.6: RNA yield and quality using different cell lysis methods following FACS sorting. (A) Total RNA yield was increased if microglia were sorted directly in RLT lysis buffer compared to media prior to RNA extraction. (B) RNA quality was higher if microglia were sorted directly into RLT lysis buffer compared to media prior to RNA extraction. Each data point represents an independent microglial isolation from one brain hemisphere. Data show mean ± SEM. N = 4 independent microglial isolation experiments.

6.4.3 Investigating the impact of TREM2 deficiency on microglial phenotype and cell composition in response to BCAS

6.4.3.1 Animal recovery

No animals receiving sham surgeries demonstrated adverse effects from surgery and survived until tissue harvest. 4 out of 19 BCAS mice were culled (21 % mortality) due to poor recovery characterised by circling or barrel rolling within the first 48 hours after surgery. Of these all were WT animals. Furthermore, 1 TREM2-/- mouse was excluded from analysis due to experimental error during preparation of the brain cell suspension. BCAS caused an average maximal 12.4 % loss of weight 8 d following surgery whilst TREM2-/- mice demonstrated an average maximal 12.8 % loss of weight 22 d following surgery (see appendix section 8.3.1). Final cohort sizes were as follows:

	Sham (n)	BCAS (n)
WT	7	7/ 11
TREM2-/-	-	7/ 8

Table 6.3: Final cohort sizes 28 d following BCAS and sham surgeries.

6.4.3.2 Laser speckle flowmetry

Laser speckle contrast flowmetry was performed prior to surgery and 24 h and 28 d after surgery to validate that BCAS induced cerebral hypoperfusion and determine whether TREM2 deficiency affected cerebral blood flow. Blood flow data was calculated as % change from baseline flow values. Analysis of percentage change in blood flow from baseline revealed significant effects of time $F(2, 36)=62.400$, $p < 0.0001$) and surgery ($F(1, 18)=73.638$, $p < 0.0001$). However, there was no effect of genotype ($F(1, 18)=0.083$, $p > 0.05$) (fig. 6.7). A significant interaction between time and surgery was detected ($F(2, 36)=30.252$, $p < 0.0001$) and post-hoc analysis demonstrated that blood flow was significantly reduced in WT mice compared to shams 24 h ($p<0.0001$) and 28 d ($p<0.0001$) following BCAS (fig. 6.7).

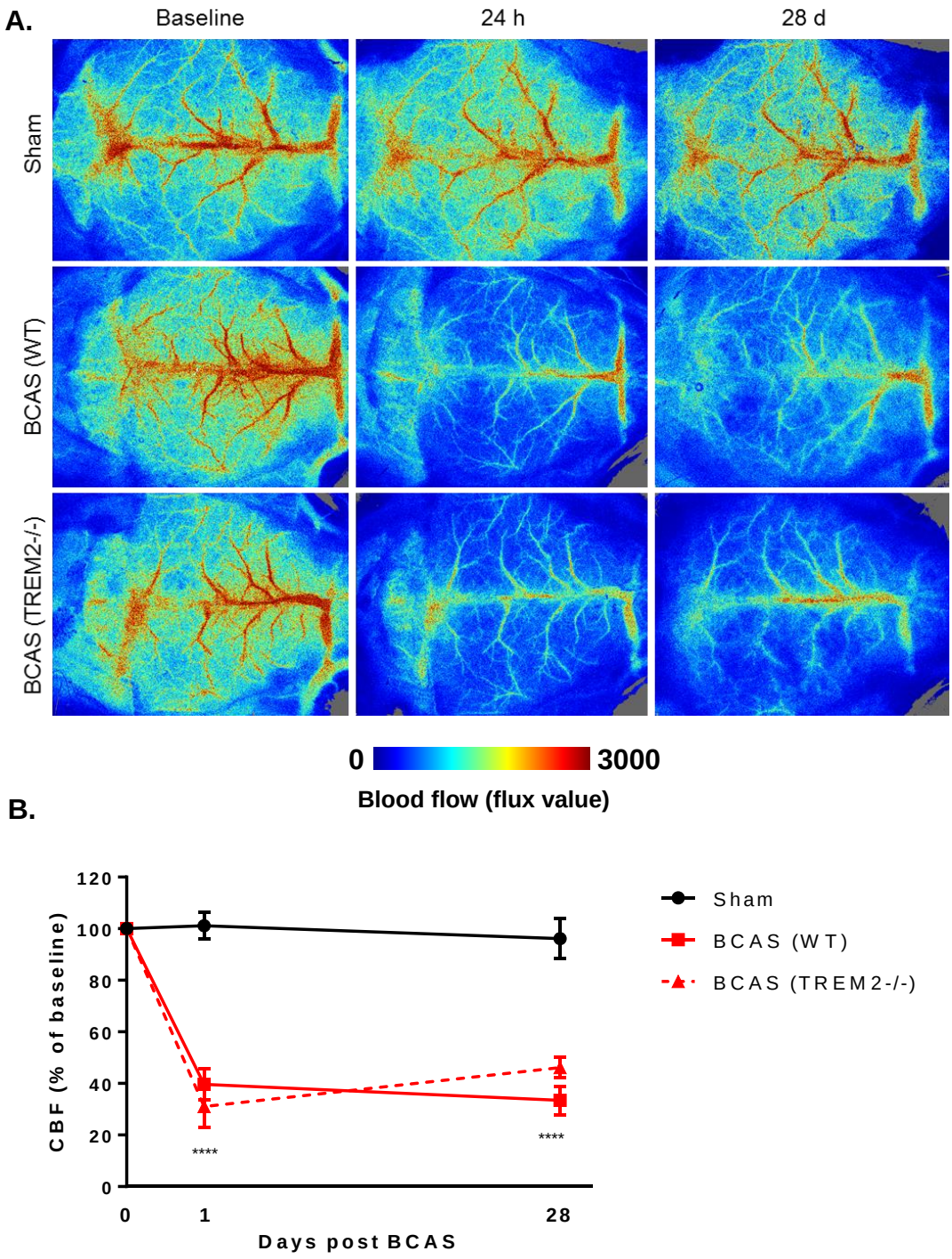

Figure 6.7: Quantification of cerebral blood flow in WT and TREM2-/- mice 28 d post sham and BCAS surgeries. (A) Representative laser speckle images showing cortical cerebral blood flow in sham and BCAS WT and TREM2-/- mice at baseline, 24 h and 28 d after surgery. (B) Quantification of cerebral blood flow in sham and BCAS WT and TREM2-/- mice at baseline, 24 h and 28 d after surgery. 24 h following BCAS surgery, WT and TREM2-/- mice demonstrated a 61.52 % and 70.11 % reduction in cerebral blood flow compared to sham animals, respectively. After 28 d cerebral blood flow remained reduced and WT and TREM2-/- mice demonstrated a 62.69 % and 50.11 % reduction in cerebral blood flow compared to sham animals. TREM2 deficiency had no impact on cerebral blood flow. ****P ≤ 0.0001 WT BCAS vs WT sham; Two way ANOVA with Bonferroni correction for post hoc. Data show mean ± SEM. N = 7 independent animals per group.

6.4.3.3 The impact of TREM2 deficiency on microglial phenotype in response to BCAS

Microglial CD45, CD11b and F4/ 80 MFIs were assessed to investigate the impact of TREM2 deficiency on microglial phenotype in white and grey matter enriched tissue following BCAS. One way ANOVA demonstrated a significant effect of surgery on CD45 MFI ($F(2, 18)=4.774$, $p \leq 0.01$) in grey matter enriched tissue. Post hoc analysis demonstrated BCAS caused a significant increase in CD45 MFI ($p \leq 0.05$) in WT mice compared to sham mice. Furthermore, this response was significantly reduced in TREM2-/- mice compared to WT mice following BCAS ($p \leq 0.05$). Although an overall effect of surgery on CD11b and F4/ 80 MFI was not detected ($p \geq 0.05$), post hoc analysis demonstrated BCAS caused a significant increase in CD11b MFI ($p \leq 0.05$) and a significant decrease in F4/ 80 MFI ($p \leq 0.05$) in WT mice compared to sham animals. Although this response was partly attenuated in TREM2-/- mice this did not reach statistical significance (F4/ 80: $p = 0.120$, CD11b: $p = 0.248$) (fig. 6.8).

Within white matter-enriched tissue, a significant effect of surgery on microglial CD11b ($F(2, 18)=4.196$, $p \leq 0.05$), CD45 ($F(2, 18)=4.774$, $p \leq 0.05$) and F4/ 80 ($F(2, 18)=5.6$, $p \leq 0.05$) MFI was detected. Post hoc analysis demonstrated that BCAS significantly increased CD11b ($p \leq 0.05$) and CD45 ($p \leq 0.05$) MFI and decreased F4/ 80 MFI ($p \leq 0.01$) in WT mice compared to sham mice. Although this response was blunted in TREM2-/- mice following BCAS this did not reach statistical significance (CD45: $p = 0.077$, F4/ 80: 0.092, CD11b: 0.161) (fig. 6.8).

A.

Marker MFI	Sham	BCAS (WT)	BCAS (TREM2-/-)
CD45 WM	1779	2578	1956
CD45 GM	1793	2272	1755
CD11b WM	19961	24737	22069
CD11b GM	19352	22187	20987
F4/80 WM	891	612	781
F4/ 80 GM	881	691	845

B.

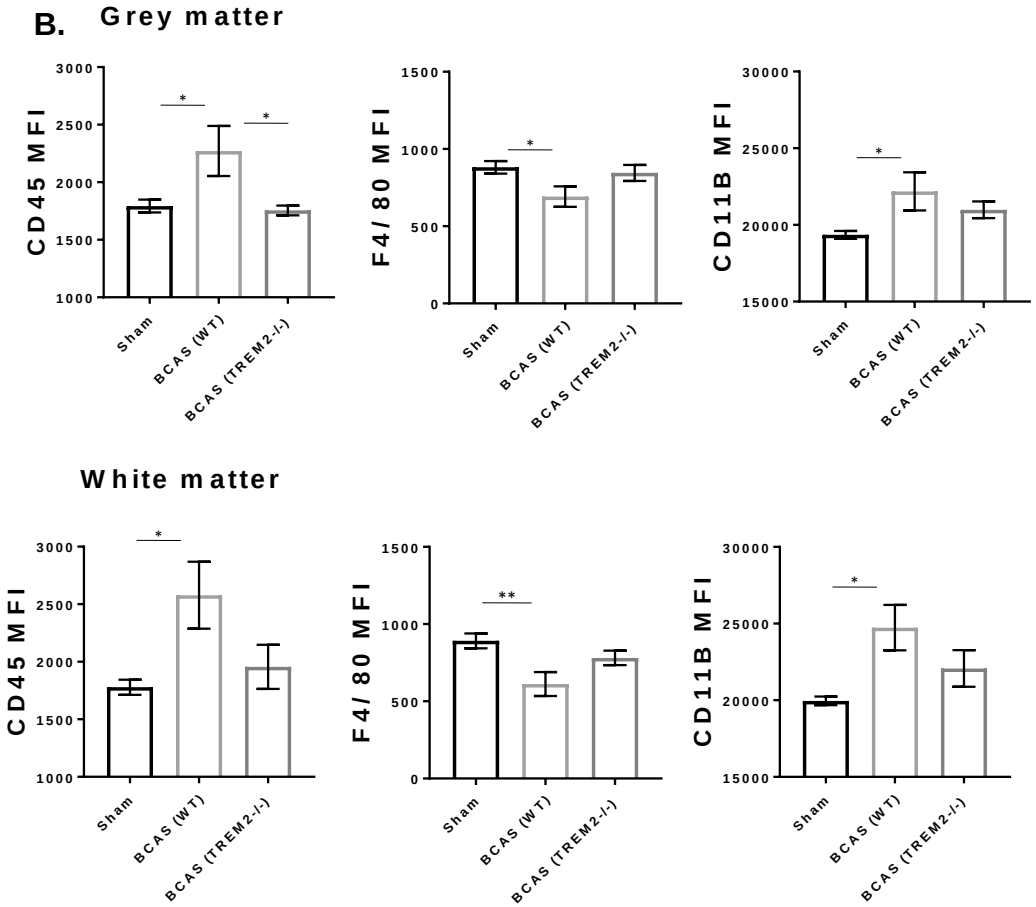

Figure 6.8: Quantification of WT and TREM2-/- microglial CD45, CD11b and F4/ 80 MFI intensities 28 d post BCAS and sham surgeries. (A) Microglial CD45, CD11b and F480 MFI values in grey and white matter regions in WT and TREM2-/- mice following sham and BCAS surgeries. (B) In grey matter enriched tissue, WT animals demonstrated a significant increase in CD45 MFI 28 d following BCAS whilst this response was significantly attenuated in TREM2-/- mice. WT animals also demonstrated a significant increase in CD11b MFI and a significant decrease in F4/ 80 MFI 28 d following BCAS. Although this response was attenuated in TREM2-/- mice, this did not reach statistical significance. Within white matter-enriched tissue, CD11b and CD45 MFI were significantly increased whilst F4/ 80 MFI was significantly decreased in WT mice 28 d post BCAS. Although this response was attenuated in TREM2-/- mice this did not reach statistical significance. *P ≤ 0.05, **P ≤ 0.01; One way ANOVA with Bonferroni post hoc. Data show mean ± SEM. N = 7 independent animals per group.

6.4.3.4 The impact of TREM2 deficiency on CNS cell composition in response to BCAS

Myeloid and lymphoid cell surface markers were used to assess the impact of TREM2 deficiency on CNS immune cell composition in grey and white matter-enriched tissue following BCAS. One way ANOVA demonstrated no significant effect of surgery on microglia, neutrophil or lymphocyte cell counts in grey matter enriched tissue ($p \geq 0.05$). However, each cell type showed a non significant increase following BCAS in WT mice (microglia: $p = 0.473$, neutrophil: $p = 0.386$, lymphocyte: $p = 0.087$) compared to sham animals. Furthermore, although non-significant this response was partly reduced in TREM2-/- mice (microglia: $p = 0.179$, neutrophil: $p = 124$, lymphocyte: $p = 0.119$) following BCAS (fig. 6.9). On the other hand, significant effects of surgery on macrophage cell counts ($F(2, 18)=5.796$, $p \leq 0.05$) were detected. Post hoc analysis demonstrated that, in comparison to sham mice, BCAS caused a significant increase in macrophages in WT mice. Furthermore, this response was significantly reduced in TREM2-/- mice following BCAS ($p \leq 0.05$).

In white matter enriched tissue, main surgery effects were not detected for microglial or neutrophil cell counts. However, WT animals demonstrated a non significant increase in each cell type following BCAS compared to sham animals (microglia: $p = 0.080$, neutrophils: $p = 0.252$). However, significant effects of surgery on macrophage ($F(2, 18)=7.301$, $p \leq 0.01$) and lymphocyte cell counts ($F(2, 18)=7.371$, $p \leq 0.01$) were detected. Post hoc analysis demonstrated that, in comparison to sham mice, BCAS caused a significant increase in macrophages ($p \leq 0.01$) and lymphocytes ($p \leq 0.01$) in WT mice. However, TREM2-/- mice demonstrated no significant difference in cell number compared to WT mice following BCAS ($p \geq 0.05$) (fig. 6.9).

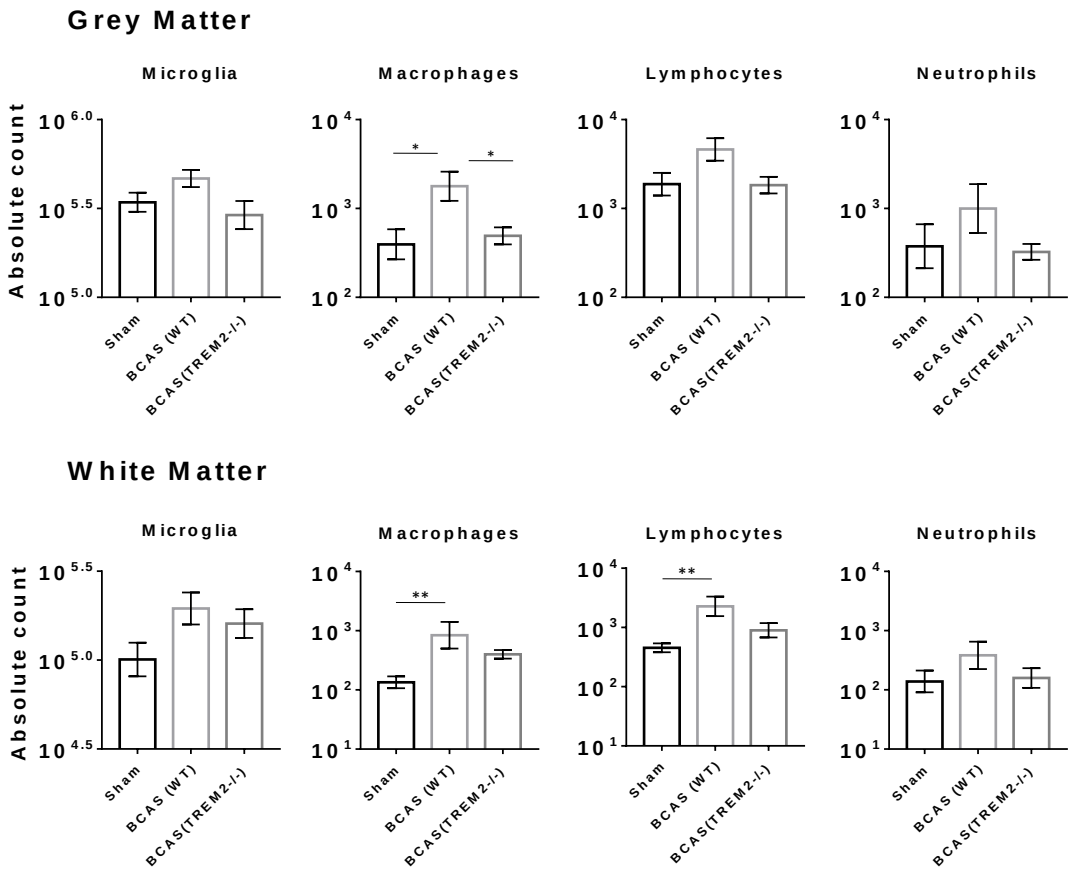

Figure 6.9: Quantification of CNS myeloid and lymphoid populations in WT and TREM2-/- mice 28 d post BCAS and sham surgeries. In grey matter enriched tissue, WT mice demonstrated a significant increase in macrophages 28 d post BCAS and this response was significantly attenuated in TREM2-/- mice. A non-significant increase in microglia, lymphocytes and neutrophils was also observed in WT mice. Although non-significant, this response was partly reduced in TREM2-/- mice. In white matter enriched tissue, macrophages and lymphocytes were significantly increased whilst a non-significant increase in microglia and neutrophils was observed 28 d post BCAS. TREM2-/- mice demonstrated no difference in cell number compared to WT mice 28 d post BCAS. *P ≤ 0.05, **P ≤ 0.001. One way ANOVA with Bonferroni post hoc. Data show mean ± SEM. N = 7 independent animals per group**.**

6.5 Discussion

In conclusion, the results presented in this study demonstrate a FACS-based method to extract microglia from whole brain was optimised enabling parallel flow cytometric analysis of cell phenotype and CNS cell composition. Investigation of microglial phenotype and CNS cell composition revealed TREM2 deficiency blunted microglial activation and peripheral leucocyte recruitment. Although microglia were isolated from grey and white matter regions and RNA extracted, whole genome expression profiling of WT and TREM2-/- microglia was not completed due to time constraints. However, information on microglial RNA yield and quality can be found in appendix II. Future studies will utilise RNA sequencing to investigate the impact of chronic cerebral hypoperfusion on the microglial transcriptome and role of TREM2 in this context. Such studies will reveal important functions of microglia and distinguish if microglia and TREM2 function differs spatially between white and grey matter regions.

The isolation procedure implemented in the current study was based on a method developed by Grabert et al. (2016) which utilised magnetic bead isolation to extract CD11b+ cells from whole brain (Grabert, et al., 2016). Although this was demonstrated as an efficient method to extract highly enriched populations of microglia, it cannot distinguish resident microglia from infiltrating CD11b expressing cells. Therefore, while this may be sufficient for isolation of microglia in the non-diseased brain, this method may not be suitable for isolation of microglia under inflammatory conditions. An advantage of FACS-based extraction is that additional antibodies and gating strategies defining cell populations based on combinatorial marker expression can be used for precise detection and isolation of cell populations and parallel flow cytometric analysis of cell phenotype and composition.

In the current study, microglia were identified and distinguished from other macrophage populations based on CD45 expression. Steady state microglia were identified as $Ly6G^{-}Ly6C^{-}CD11b^{+}CD45^{lo}$ whilst macrophages were identified as $Ly6G^{-}Ly6C^{+}CD11b^{+}CD45^{hi}$. Under inflammatory conditions it becomes increasingly difficult to distinguish microglia from macrophages as microglia upregulate CD45 expression. Although microglia upregulated CD45 expression in response to BCAS, macrophages could still be discriminated as they

demonstrated 10-fold higher CD45 expression compared to microglia. Ideally additional microglial specific markers would have been used to further validate sorted cells were indeed microglia. TMEM119 was recently described as a microglial-specific marker enabling discrimination between microglia and macrophages under steady state and inflammatory conditions (Bennett et al., 2016). An anti-TMEM119 antibody was implemented to attempt to identify microglia in initial optimisation experiments however this could not be detected via flow cytometry and its use was discontinued.

Although FACS-based extraction enables more precise isolation of microglia, various steps of the procedure including tissue homogenisation and antibody binding may alter the microglial transcriptome. Indeed, comparison of cell isolation strategies has demonstrated FACS-based isolation of microglia introduces artefact gene expression changes (Haimon et al., 2018). In future studies, the recently developed 'RiboTag approach' could be utilised to isolate microglial translatomes via immunoprecipitation of epitope-tagged ribosomes to avoid potential artefact introduced by cell isolation (Haimon, et al., 2018). To reduce potential transcriptome changes in current study, all samples were kept at 4 ^{o}C throughout the isolation procedure. Furthermore, enzyme treatment of brain tissue prior to tissue homogenisation was omitted.

Although changes in microglial gene expression were not assessed to determine whether enzyme treatment of brain tissue altered the microglial transcriptome, this is likely to have occurred as flow cytometric analysis revealed enzyme treatment increased microglia size, granularity and CD45 protein expression. It could be postulated enzyme treatment may have activated microglia via protease activating receptors. Furthermore, debris generated following enzyme digestion and tissue homogenisation may have contributed to microglial activation. While previous studies suggest enzyme treatment improves microglial yield due to improved dissociation from extracellular matrix the current study demonstrated the opposite (Grabert & McColl, 2018). Although the precise reasons for this remain unclear, the extent of debris in brain cell suspensions following enzyme treatment may have impacted on microglial viability.

Flow cytometric and RT-QPCR analysis of isolated cells demonstrated the FACS extraction protocol provided a highly enriched population of microglia with minimal contamination of other CNS cell types. Furthermore, investigation of RNA integrity revealed the RNA extraction protocol yielded high quality RNA sufficient for bulk RNA sequencing to investigate the impact of TREM2 deficiency on the microglial transcriptome in response to BCAS. However, as stated earlier, transcriptome profiling could not be completed due to time constraints. Therefore, the current study focused on flow cytometric analysis of microglial phenotype and CNS cell composition in WT and TREM2-/- mice following BCAS.

An unavoidable limitation of the current study due to sample processing requirements is that pathological assessment was not conducted in parallel. Therefore, the extent and distribution of pathology in WT and TREM2-/- mice is unknown. This would have proved useful to assess whether observed pathology was comparable to the previous study and determine whether changes in microglial phenotype and CNS cell composition were dependant on pathology severity. Given the variability of the data it is likely the extent of pathology varied between animals comparable to the previous study. Furthermore, it is likely BCAS induced both grey and white matter pathology as changes in microglial phenotype and CNS composition were observed in both regions.

In the previous study, it was demonstrated that use of 0.16 mm internal diameter microcoils induced acute and sustained reductions in cerebral blood flow in WT and TREM2-/- animals. While WT and TREM2-/- demonstrated a 50 - 60 % reduction in cerebral blood flow, this was enhanced to 60 – 70 % in the current study. It is unclear why animals demonstrated greater cerebrovascular insufficiency as methodology remained consistent between studies. Investigation of microglial phenotype by flow cytometric analysis revealed upregulation of microglial CD11b and CD45 expression and downregulation of F4/ 80 in white and grey matter regions in response to BCAS. Interestingly, such changes were more prominent in white matter enriched samples. Pathological assessment in the previous study demonstrated white matter regions were predominantly affected in response to BCAS. Although the extent of pathology is unknown in the current study, such changes could reflect increased microgliosis

in white matter regions. Although non-significant, alterations in CD11b, CD45 and F4/80 expression were blunted in TREM2-/- mice suggesting microgliosis was impaired. Similar TREM2-dependant effects have also been demonstrated by flow cytometry in the 5XFAD model of AD (Wang, et al., 2015).

Recent single cell sequencing studies suggest TREM2 signalling is required for microglia to adopt a DAM phenotype associated with attenuation of neurodegeneration. Microglia with a DAM phenotype demonstrate downregulation of homeostatic genes including *p2ry12*, *Cx3cr1*, *Cd33* and *Tmem119* and upregulation of genes associated with phagocytic and lysosomal processes as well as lipid metabolism such as *Axl, Lpl* and *Cst7* (Keren-Shaul, et al., 2017). While initial DAM activation is initiated by a TREM2 independent mechanism, TREM2 signalling is required for further activation and up regulation of genes associated with phagocytosis, lysosomal processes and lipid metabolism. Although these microglia were originally identified in models of AD, a similar phenotype has also been observed in models of MS, ALS and aging suggesting the DAM phenotype is conserved across various neurodegenerative conditions (Deczkowska et al., 2018).

Whether microglia exhibit a similar phenotype in the context of cerebrovascular-mediated neurodegeneration remains unknown. As alterations in microglial cell surface markers were blunted in the absence of TREM2 expression it could be suggested microglia were unable to adopt a DAM phenotype and instead acquired an intermediate activation state. Given that microglial phenotype is strongly influenced by microenvironment it could be argued microglia exhibit a distinct phenotype to those previously reported in other models of neurodegenerative disease. Further understanding of the impact of TREM2 deficiency on the microglial transcriptome in the current model by RNA sequencing may identify phenotypic changes specific to BCAS in addition to those commonly observed across multiple neurodegenerative disease settings which play a key role in mediating CNS pathology.

In addition to investigating the impact of TREM2 on microglial phenotype additional markers of myeloid and lymphoid populations were implemented to characterise the impact of TREM2 deficiency on CNS cell composition in response to BCAS. In addition to increased numbers of microglia, infiltration of leukocytes was also observed suggesting resident microglia and macrophages do not exclusively contribute to the neuroinflammatory response to BCAS. Given that peripheral cell infiltration was observed it will be important to further profile infiltrating myeloid and lymphoid subsets and characterise the temporal evolution to understand how this is influenced by increasing durations of BCAS. Tissue obtained in the previous study could be utilised to validate findings from the current study and investigate the spatial distribution of cell subsets. Such studies will be useful for determining how cell composition relates to pathology severity in response to BCAS.

Although vascular pathology was not characterised in the current study, it could be suggested leukocyte infiltration occurred as a result of endothelial dysfunction and BBB breakdown. Increased expression of endothelial adhesion molecules is observed in response to chronic cerebral hypoperfusion promoting leukocyte attachment and migration across the BBB (Huang, et al., 2010, Kitamura, et al., 2017). Recent *in vivo* two photon imaging also demonstrated leukocyte attachment and rolling in response to BCAS (Yata et al., 2014).

Interestingly, previous studies demonstrate no evidence of myeloid and lymphoid cell infiltration in response to BCAS (Manso, et al., 2018, Fuchtemeier, et al., 2015). Manso, et al. utilised TMEM119 to co-label IBA1 cells to distinguish microglia from infiltrating macrophages and demonstrated microglia exclusively contribute to the IBA1+ cell population (Manso, et al. 2018). As immunohistochemistry was implemented to investigate cell composition in the corpus callosum it could be postulated that leukocyte infiltration occurred elsewhere in the brain. Furthermore, cell labelling was limited to IBA1 and TMEM119 therefore it is unclear if infiltration of other cell types occurred.

While lymphocyte infiltration was observed in the current study, Fuchtemeier, et al. (2015) demonstrated absence of lymphocyte subsets in the CNS in response to BCAS. As Fuchtemeier et al. (2015) utilised 0.18 mm internal diameter microcoils to induce chronic

cerebral hypoperfusion it could be postulated resultant pathology was much less severe. Although DTI demonstrated BCAS induced white matter degeneration after 6 w, IHC was not implemented to characterise CNS pathology. In the previous study, use of 0.16 mm internal diameter microcoils resulted in extensive white matter pathology with 50 % of animals demonstrated additional grey matter pathology after 28 d. Although pathological assessment was not conducted in the current study it could be postulated that the extent of hypoperfusion induced more severe pathology evoking leukocyte recruitment from the periphery.

In the absence of TREM2 expression only negligible alterations in cell number were observed in white matter enriched samples in response to BCAS. In the previous study, initial assessment of IBA1+ cell number via IHC demonstrated no difference in IBA1+ cell number in WT and TREM2-/- mice except in the optic tract where consistent white matter damage was observed. As the extent of white matter damage differed between WT and TREM2-/- mice, subsequent correction for between group differences revealed reduced IBA1+ cell number across multiple white matter tracts in TREM2-/- mice.

Differences in microglial phenotype or cell number could not be corrected to account for potential differences in CNS pathology between WT or TREM2-/- BCAS animals in this study. This may therefore therefore explain why only modest differences were observed in TREM2 deficient animals in response to BCAS. As leukocyte recruitment was observed in response to BCAS it will be crucial to determine how these cells contribute to disease pathogenesis. As TREM2 deficiency was associated with exacerbated white matter damage and reduced leukocyte infiltration it could be hypothesised that infiltrating leukocytes play a beneficial role in response to BCAS.

Reduced peripheral infiltration may occur as TREM2 deficient animals demonstrate blunted neuroinflammatory responses in the diseased brain (Sieber, et al., 2013, Poliani, et al., 2015, Jay, et al., 2015, Leyns, et al., 2017). Microglial activation and subsequent secretion of inflammatory mediators influences expression of endothelial adhesion molecules as well as endothelial permeability and BBB integrity, all of which promote leukocyte attachments and migration across the BBB. Therefore, TREM2 deficiency may impact on endothelial function

reducing peripheral immune cell infiltration into the CNS. Furthermore, reduced chemokine expression may directly impact on leukocyte migration within the CNS.

It could also be postulated TREM2 deficiency directly impacts myeloid cells in the periphery reducing infiltration into the CNS. It remains unclear if TREM2 differentially regulates myeloid cell subsets in the context of neurodegeneration. Given that CNS-resident microglia and blood-derived macrophages are capable of immunomodulation and phagocytosis, distinguishing how TREM2 regulates different myeloid subsets will provide greater understanding of the role of TREM2 in neurodegenerative disease. In future studies, bone marrow chimerism experiments could be conducted in WT and TREM2-/- animals to elucidate whether TREM2-mediated effects in the CNS are primarily due to resident microglia and macrophages or blood-derived myeloid cells. In the context of stroke, TREM2-mediated post-stroke recovery is predominantly due to CNS resident microglia as opposed to peripheral derived macrophages (Kurisu et al., 2018). However, it remains unclear how TREM2-regulated processes impact different myeloid populations in the context of chronic vascular degenerative disease.

Overall, the data presented in this study further demonstrate TREM2 plays a key role in mediating microglial responses to BCAS. Flow cytometric analysis revealed increased microgliosis as well as leukocyte recruitment occurs in response to BCAS suggesting CNS resident microglia and macrophages do not exclusively contribute to the neuroinflammatory response. However, it remains unclear if TREM2 regulates peripheral cell infiltration as flow cytometric analysis revealed only modest reductions in infiltration in TREM2-/- mice. As alterations in microglial cell surface protein expression were blunted this suggests TREM2 is required for microglial activation in response to BCAS. However, future work is required to obtain a broader, more detailed understanding of how TREM2 deficiency impacts microglial phenotype in response to BCAS.

Chapter 7:

General discussion and conclusions

7.1 Summary of findings

It was first hypothesised that chronic cerebral hypoperfusion would impact detrimentally on myelin integrity and induce inflammation. This was supported by data presented in chapter 5 demonstrating induction of BCAS for 28 d caused loss of axon glial integrity across several white matter regions measured via MAG immunostaining (fig. 5.13 - 15). Quantification of microglial number by IBA1 immunostaining in chapter 5 demonstrated areas of white matter damage were associated with increased microglia suggesting that chronic cerebral hypoperfusion induced inflammation (fig. 5.16). This is further supported by flow cytometric data in chapter 6 showing increased numbers of microglia and peripheral leukocytes as well as upregulation of markers associated with microglial reactivity following chronic cerebral hypoperfusion (fig. 6.8 - 9). It was further hypothesised that TREM2 deficiency would affect this response and exacerbate white matter damage. Data presented in chapter 5 illustrates white matter damage was exacerbated in TREM2 deficient mice (fig 5.14) and areas of white matter damage were associated with reduced numbers of microglia compared to WT mice (fig. 5.16 - 19). Flow cytometric data in chapter 6 similarly demonstrated TREM2 deficient mice had reduced numbers of microglia and infiltrating leukocytes compared to WT mice following BCAS (fig. 6.9). In conclusion, the results presented in this thesis demonstrate optimisation of the BCAS model tailored to investigate the impact of TREM2 deficiency on CNS pathology and neuroinflammatory responses resulting from chronic cerebral hypoperfusion. In addition to demonstrating TREM2 plays an important role in regulating microglial responses to BCAS, the findings presented in this thesis suggest TREM2 confers protection against loss of myelin integrity following chronic cerebral hypoperfusion.

7.2 BCAS as a suitable model of chronic cerebral hypoperfusion

The BCAS model was utilised to mimic cerebral hypoperfusion observed in the elderly to obtain mechanistic insight into the contribution of TREM2 and neuroinflammation to white matter damage. Although previous studies have demonstrated use of 0.18 mm microcoils induces mild hypoperfusion leading to diffuse myelin damage after 28 d in C57BL/6J mice, this could not be replicated in C57BL/6Ntac mice most likely due to a combination of genetic

and environmental factors. Microcoils with smaller internal diameters were therefore implemented in chapters 5 and 6 resulting in severe hypoperfusion (~50-60 % reduction in cerebral blood flow at 24 h and 28 d). Although this modification precipitated robust white matter pathology, select animals also demonstrated stroke-like grey matter pathology.

Given that the elderly demonstrate much milder and gradual reductions in cerebral blood flow (~ 5% per decade during adult life) this questions whether the modified model accurately simulates hypoperfusion associated with cSVD (Marchal et al., 1992, Leenders, et al., 1990, Bentourkia, et al., 2000). Although it would be preferential to induce more gradual and milder hypoperfusion, this was not possible given that mild and moderate hypoperfusion evoked negligible and infrequent myelin damage as demonstrated in chapters 3-5. The GCAS or ACAS models described in section 1.4.2 could be implemented to avoid acute reductions in cerebral blood flow. However, given that substantial cerebral hypoperfusion was required to elicit robust neuropathology it is uncertain whether either of these models would be suitable.

Although the extent of hypoperfusion induced by BCAS may not model age-related cerebral hypoperfusion accurately, pathological assessment demonstrated BCAS precipitated cSVD-like pathology including diffuse myelin damage and focal white matter infarcts. Areas of myelin damage were also associated with neuroinflammation and manipulation of microglial function exacerbated myelin damage suggesting microglial dysfunction contributes to white matter damage. Therefore, the model still provides a useful platform to interrogate mechanisms by which cerebral hypoperfusion contributes to white matter damage warranting its future use.

In future, it will be important to decipher whether loss of myelin integrity is also associated with cognitive deficits comparable to VCI patients. Given that previous preclinical studies have demonstrated mild white matter damage is sufficient to elicit spatial working memory defects it is likely animals in chapters 5 and 6 also demonstrated this as diffuse myelin damage was observed across multiple white matter tracts (Coltman et al., 2011). As several mice also demonstrated hippocampal degeneration it could be postulated mice also exhibited reference memory impairment. In future it will therefore be important to conduct behavioural assessments (e.g. barnes and radial arm maze) to characterise cognitive deficits caused by

BCAS. Furthermore, electrophysiology could be utilised to assess conduction velocity of white matter and assess whether structural impairments are also associated with functional impairment.

7.3 Use of velocigene TREM2-/- C57BL6/Ntac mice

TREM2-/- C57BL/6Ntac mice were generated by introducing a floxed velocigene ZEN-Ub1 reporter cassette into the TREM2 locus preventing gene transcription and protein expression providing a useful tool to investigate the impact of TREM2 deficiency in health and disease. However, recent transcriptomic analysis of TREM2-/- microglia from this TREM2-/- line revealed reporter cassette insertion causes artificial upregulation of *Treml1* (Kang, et al. 2018). Therefore, caution must be taken when interpreting the impact of TREM2 deficiency as the consequences of *Treml1* upregulation on microglial function remain unknown. To circumvent this, Kang, et al. demonstrated removal of the floxed reporter cassette by rederivation abrogated artificial *Treml1* upregulation (Kang, et al. 2018). While future experiments expanding on work described in this thesis will continue to use TREM2-/- mice containing the inserted reporter cassette to ensure consistency, rederived TREM2-/- mice lacking the reporter cassette will be utilised for new studies investigating the impact of TREM2 deficiency.

7.4 TREM2 and neuroinflammation in VCI

Whilst neuroinflammation was initially believed to be a consequence of neurodegeneration, recent genetic studies identifying mutations in microglial-enriched genes predisposing to neurodegenerative disease demonstrate microglial dysfunction actively contributes to disease pathogenesis. However, precise understanding of microglial function within these disease contexts remains unclear due to the fact that both beneficial and detrimental functions have been reported. Studies investigating disease burden after microglial ablation report contradictory findings across different disease models. Elimination of microglia is associated with reduced neuronal loss and memory impairment in 5xFAD mice (Spangenberg et al., 2016). Similarly, transient microglial depletion and repopulation rescues behavioural deficits following inducible neuronal loss (Rice et al., 2017). On the other hand, elimination of microglia

is associated with increased infarction and cognitive deficits in models of ischaemic injury (Jin et al., 2017, Szalay et al., 2016).

In the context of VCI, preclinical studies utilising immunomodulatory drugs suggest suppressing microglial activation is beneficial for white matter structure and function (Manso et al., 2018). However, it cannot be definitively concluded that observed effects are due to inhibition of microglial activation as off target effects have been described on other cell types within the CNS including astrocytes, oligodendrocytes and neurons (Moller et al., 2016). More recently, elimination of microglia using a CSF1R inhibitor prior to BCAS was shown to reduce subsequent white matter injury and cognitive impairment suggesting microglia impact detrimentally on myelin integrity and cognition (Kakae et al., 2019).

Whilst neuroinflammation is likely to contribute to aspects of VCI, treating gross inhibition of neuroinflammation as a therapeutic strategy may be too simplistic as not all neuroinflammation is damaging. Studies manipulating TREM2 function consistently demonstrate TREM2 deficiency impairs the ability of microglia to detect and respond to CNS injury. In addition to reducing microglia clustering in areas of damage, TREM2 deficient microglia downregulate expression of genes associated with activation and demonstrate a more homeostatic-like profile. Interestingly, this is generally associated with worsened disease burden across disease models. In models of demyelination, TREM2 deficiency reduces microglial activation resulting in accumulation of myelin debris and worsened axonal pathology suggesting TREM2-mediated responses are necessary for maintenance of myelin integrity and remyelination (Cantoni et al., 2015, Poliani et al., 2015).

Although the role of TREM2 in cerebrovascular-mediated white matter injury remains understudied, the findings of this thesis provide novel insight into the impact of TREM2 deficiency on myelin integrity and neuroinflammatory responses to cerebrovascular dysfunction. The results from chapter 5 and 6 demonstrate TREM2 deficiency blunted neuroinflammation and exacerbated myelin damage following BCAS. Therefore, although inhibition of microglial activation is suggested as a potential therapeutic strategy for VCI and

other dementia causing diseases, the findings presenting here suggest reducing microglial activation may in fact be detrimental.

Although microglia secrete various inflammatory mediators which may contribute to loss of white matter integrity, microglia are also a source of trophic mediators and aid in the repair and resolution of injury. As discussed in chapter 5, clearance of myelin debris via phagocytosis is required for efficient remyelination (Lampron et al., 2015). Furthermore, microglia are a source of various trophic mediators required for OPC proliferation and maturation (Lloyd & Miron, 2019). Therefore, rather than complete inhibition, fine tuning of neuroinflammatory responses to promote regenerative processes whilst limiting damaging inflammation may provide a promising therapeutic strategy to enhance myelin integrity and reduce cognitive impairment and dementia.

It is therefore crucial to gain a better understanding of microglial function and identify pro-resolving and disease-associated phenotypes. Given that manipulation of TREM2 signalling further compromised myelin integrity following cerebral hypoperfusion it will be important to understand what downstream pathways are affected by TREM2 deficiency as exploitation of such pathways may confer resilience to myelin damage and cognitive impairment. As TREM2 signalling modulates key genes involved in phagocytosis, lysosomal function and lipid metabolism, it could be postulated targeting microglial clearance and degradation of damaged myelin may ameliorate disease burden.

Additional studies genetically manipulating microglial function will be crucial to establish the precise contribution of these processes to disease pathogenesis. Although drugs selectively targeting microglia are lacking, TREM2 could be considered as a potential target given that expression is limited to microglia and macrophages in the CNS. However, the precise function of TREM2 still remains unclear, particularly as mixed effects have been observed across disease models. In addition to elucidating common functions across neurodegenerative diseases, it will be important to determine how TREM2 function evolves with disease progression. Whilst preclinical studies have demonstrated TREM2 function depends on disease progression in models of amyloidopathy, it remains unknown whether this is also

observed in other contexts of neurodegeneration (Jay et al. 2017). Furthermore, it remains unclear whether TREM2 functions reported in rodents are similarly observed in humans. Thus, although stimulation of TREM2 signalling may elicit protection to chronic cerebrovascular dysfunction, further understanding of TREM2 function is required. Despite this, the results presented in chapters 5 and 6 demonstrate immune dysfunction contributes to loss of myelin integrity following chronic cerebral hypoperfusion. Therefore, future work should continue to characterise the temporal cellular and molecular neuroinflammatory profile resulting from chronic cerebrovascular dysfunction and elucidate the contribution of microglia to disease pathogenesis.

7.5 Future work

Future studies will continue to characterise the impact of TREM2 deficiency on microglial responses and disease burden following BCAS. Although TREM2 deficiency exacerbated myelin damage in the internal capsule, the impact of TREM2 deficiency on white matter function or behaviour remains unclear. As discussed in section 7.2, the barnes or radial arm maze could be utilised to characterise defects in working and reference memory caused by loss of white matter integrity or electrophysiology could be used to assess white matter conduction velocity. If TREM2 deficiency is also associated worsened memory function, it may be possible promoting aspect of TREM2 signalling will counteract this and ameliorate myelin damage and cognitive decline.

Although TREM2 appears to be important for maintenance of white matter integrity the precise mechanisms remain unclear. Future transcriptomic analysis of microglia isolated from discrete brain regions following BCAS will provide insight into the impact of cerebral hypoperfusion on the microglial transcriptome. In addition to this, TREM2 dependant alterations in microglial phenotype will provide insight into how microglial perturbation contributes to disease burden following BCAS.

Whilst bulk RNA sequencing of microglia is useful for understanding how microglial phenotype is altered by disease, it cannot discriminate between functionally distinct subtypes within the same tissue. Microglia are highly complex and demonstrate functional plasticity to various factors including type, duration, location and severity of stimulus. The recent development of single cell sequencing illustrates the heterogeneity of microglia and enables more precise investigation of microglial function in health and disease. Identification of microglia exhibiting a DAM-like phenotype surrounding areas of CNS injury across models of neurodegenerative disease suggest microglia adopt a conserved phenotype to CNS injury (Krasemann, et al., 2017, Keren-Shaul, et al., 2017, Hammond, et al., 2019). Although this phenotype is associated with neuroprotection in models of proteopathy, it remains unknown if similar subsets are observed in response to vascular insult.

As VCI is characterised by a spectrum of pathologies in both the white and grey matter it is likely distinct microglial populations are associated with different vascular lesions (e.g. ischaemic and haemorrhagic). Future studies implementing single cell sequencing will be important for characterising microglial diversity in preclinical models of VCI. Such studies would establish whether microglia adopt DAM-like or functionally distinct phenotypes to those described in other models of neurodegenerative disease. To validate findings in mice, it will be crucial to assess microglial phenotype in VCI patients. *Ex vivo* magnetic resonance imaging (MRI) could be conducted on post-mortem tissue to identify vascular lesions and subsequent immunohistochemistry would reveal neuroinflammatory changes associated with imaged lesions. Furthermore, single nuclear sequencing of tissue containing vascular lesions identified via *ex vivo* MRI could be implemented to assess microglial phenotypic alterations associated with vascular pathology and determine whether microglia exhibit similar changes to those observed in preclinical models. This could also be complemented with RNAscope in situ hybridisation to investigate the spatial distribution of microglial subtypes within pathological lesions.

Given that TREM2 is suggested to be necessary for microglia to adopt a DAM-like phenotype it will be important to assess how TREM2 deficiency impacts the composition and spatial distribution of microglial subsets in response to BCAS and how this relates to function. It could be postulated that TREM2-deficient microglia initiate an abnormal response to hypoperfusion and contribute to myelin damage directly or that impaired responses to secondary events such as myelin debris and BBB dysfunction leads to accumulation of noxious stimuli and exacerbation of white matter damage following BCAS. As sequencing data provides a static picture of cell phenotype at a given point in time, it will be important to understand how microglial heterogeneity evolves over disease progression. Accumulation of data sets investigating the temporal response of WT and TREM2-/- microglia would identify microglial subpopulations associated with disease and establish how these populations develop with disease progression.

As numerous stimuli are likely to influence microglial function following BCAS it will be important to decipher how microglia respond to such stimuli. Since completion of the work presented in this thesis, *in vitro* platforms are being developed by the McColl lab to characterise WT and TREM2-/- microglial responses to relevant stimuli such as hypoxia, inflammation and myelin debris. In addition to this, it will also be crucial to understand the impact of TREM2 deficiency on other cell types within the neurogliovascular unit given that multiple cell types contribute to VCI and dementia pathogenesis.

As a FACS based method was optimised for isolation of microglia this could be further developed to enable dual isolation of additional cell types such as endothelial cells following BCAS. Subsequent gene expression profiling would provide a powerful tool to investigate how microglial and vascular cell transcriptomes are affected by BCAS and TREM2 deficiency and identify mechanisms by which TREM2 may increase susceptibility to CNS injury. As TREM2 is highly enriched on microglia within the CNS, TREM2 dependant alterations in endothelial cell phenotype would suggest microglial perturbation also impacts endothelial function. To complement *in vivo* findings, use of mixed glial monolayer or transwell cultures in conditions simulating chronic cerebrovascular dysfunction (e.g. hypoxia) in combination with gene or

protein analyses would provide mechanistic insight into bidirectional signalling between microglia and other cell types. In addition to providing insight into environmental cues which drive cell phenotypes associated with disease, the above would elucidate how microglial dysfunction impacts on other cells within the neurogliovascular unit.

7.6 Conclusion

In summary, the results presented in this thesis demonstrate TREM2 deficiency exacerbates loss of myelin integrity following BCAS lending support to the role of microglial dysfunction in cerebrovascular-mediated white matter injury. Given that white matter degeneration is a key contributor to age-related cognitive decline and dementia, development of microglial- specific drugs that exploit regenerative functions offers a potential strategy to limit white matter degeneration and cognitive impairment. Prior to this, further work is required to understand microglial phenotypes in VCI and other dementia causing diseases and how this relates to function. Use of transcriptomic approaches such as single cell sequencing will prove valuable for identifying microglial subsets associated with disease in rodents and human patients and elucidate common mechanisms across disease contexts which could be modulated to promote resilience to neurodegenerative processes and cognitive impairment.

Chapter 8:

Appendix

Appendix I: Chapter 3

8.1.1 Weight changes in WT mice 28 d following sham and BCAS surgeries.

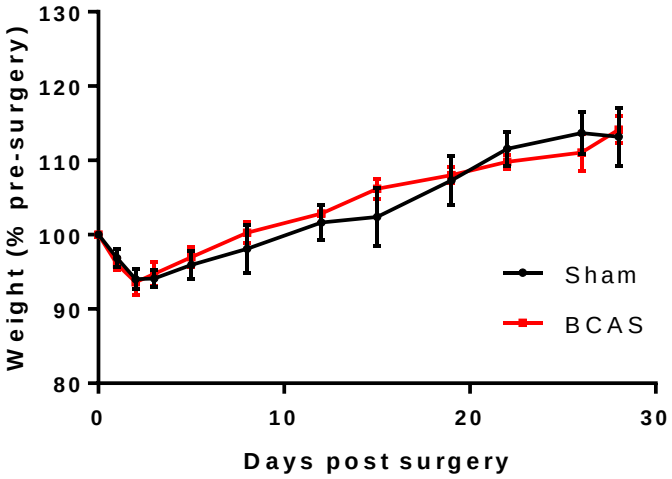

Figure S8.1: Weight change (% of pre-surgery weight) 28 d following sham and BCAS surgeries. Sham and BCAS mice demonstrated a maximal 5.9 % and 5.3 % loss in weight 3 d following surgery, respectively. Data show mean ± SEM. N = 5 – 7 independent animals per group.

Appendix II: Chapter 4Weight changes in WT mice following sham and BCAS surgeries (1 w, 1 m and 3 m).

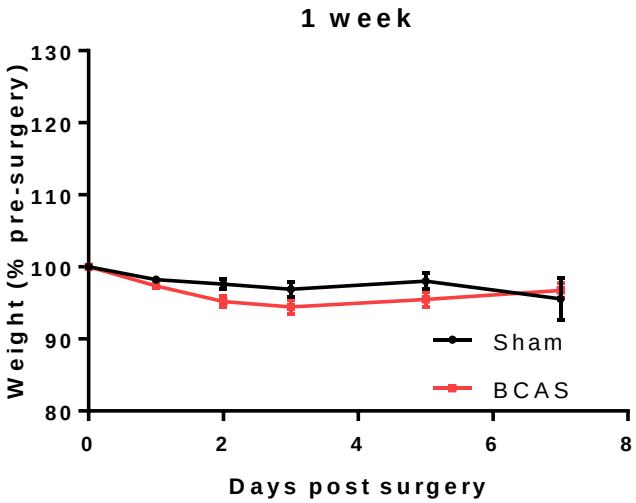

Figure S8.2: Weight change (% of pre-surgery weight) following sham and BCAS surgeries (1 week). Sham and BCAS mice demonstrated a maximal 3.1 % and 5.6 % loss in weight 3 d following surgery, respectively. Data show mean ± SEM. N = 10 - 12 independent animals per group.

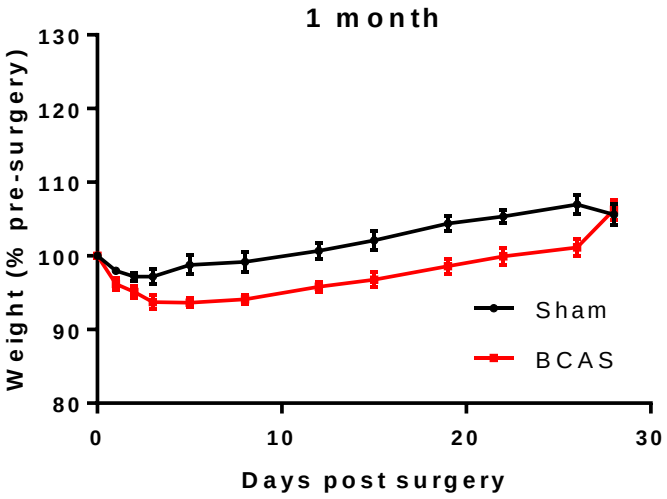

Figure S8.3: Weight change (% of pre-surgery weight) following sham and BCAS surgeries (1 month). Sham and BCAS mice demonstrated a maximal 2.8 % and 6.4 % loss in weight 3 d following surgery, respectively. Data show mean ± SEM. N = 8 – 10 independent animals per group.

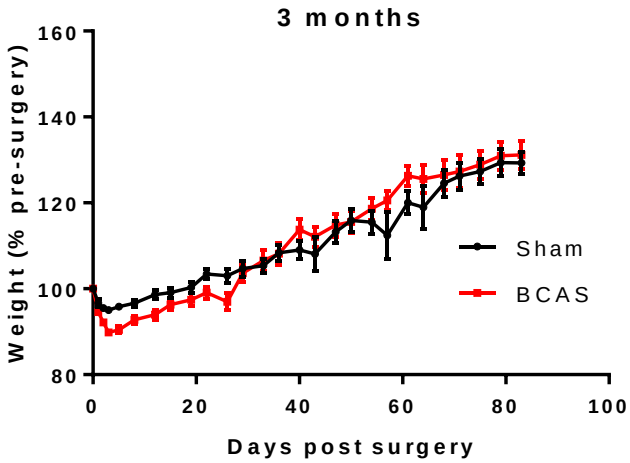

Figure S8.4: Weight change (% of pre-surgery weight) following sham and BCAS surgeries (3 months). Sham and BCAS mice demonstrated a maximal 5 % and 10.2 % loss in weight 3 d following surgery, respectively. Data show meanSEM. n = 10 - 12 independent animals per group.

8.2.2 Pathological assessment of WT and TREM2-/- mice 28 d after modified BCAS surgery (removal of 30 min recovery period between microcoil placement)

	Animals displaying grey matter damage	Cerebral Cortex	CA1	CA2	CA3	DG	Striatum	Thalamus
BCAS (WT)	0/3 (0%)	0/3 (0%)	0/3 (0%)	0/3 (0%)	0/3 (0%)	0/3 (0%)	0/3 (0%)	0/3 (0%)
BCAS (TREM2-/-)	0/3 (0%)	0/3 (0%)	0/3 (0%)	0/3 (0%)	0/3 (0%)	0/3 (0%)	0/3 (0%)	0/3 (0%)

Table S8.1: WT and TREM2-/- mice demonstrating neuronal pathology detected by H & E staining 28 d following modified BCAS surgeries. No animals demonstrated neuronal pathology 28 d following modified BCAS surgeries.

	Animals displaying myelin damage	CC	IC	OT	HF
BCAS (WT)	0/3 (0%)	0/3 (0%)	0/3 (0%)	0/3 (0%)	0/3 (0%)
BCAS (TREM2-/-)	0/3 (0%)	0/3 (0%)	0/3 (0%)	0/3 (0%)	0/3 (0%)

Table S8.2: WT and TREM2-/- mice demonstrating myelin damage detected by MAG immunostaining 28 d following modified BCAS surgeries. No animals demonstrated myelin pathology 28 d following modified BCAS surgeries.

8.2.3 Assessment of microgliosis

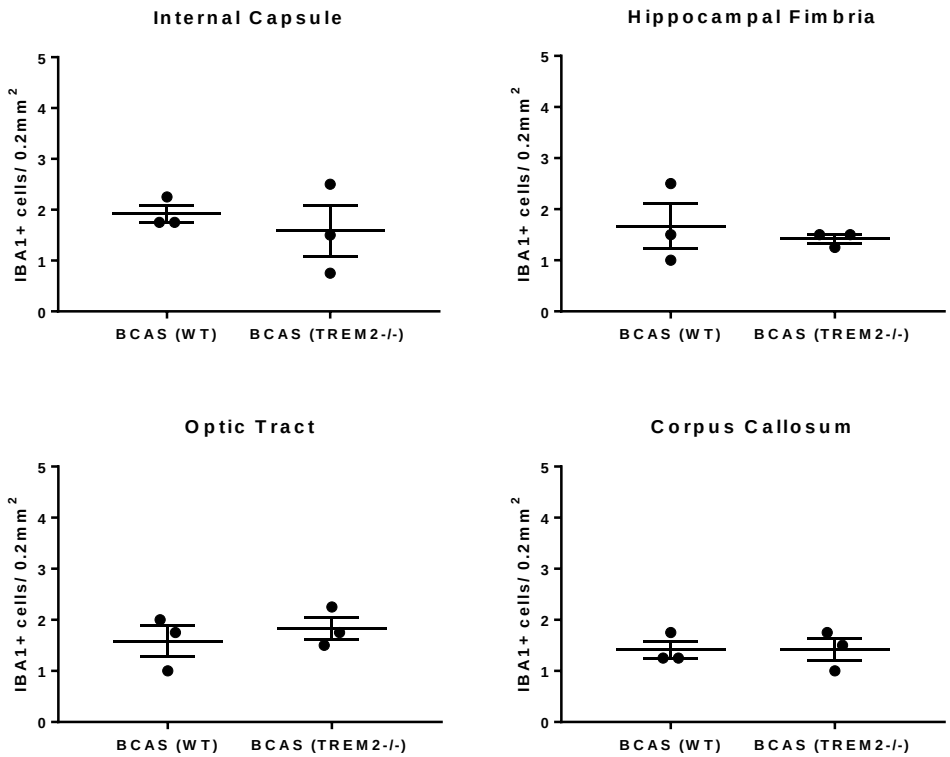

Figure S8.5: Quantification of IBA1+ cells in white matter tracts of WT and TREM2-/- mice 28 d following BCAS surgeries. BCAS did not increase the number of IBA1+ cells in white matter tracts compared to sham animals. Student's unpaired t test. Data show mean ± SEM. N = 3 independent animals per group.

8.3 Apendix III: Chapter 5

8.3.1 Weight changes in WT and TREM2-/- 28 d following BCAS and sham surgeries in cohort 1 (mixed coil).

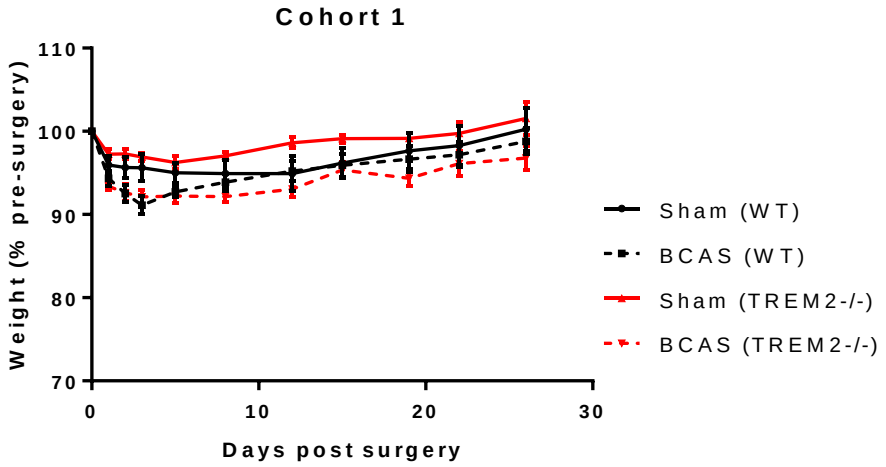

Figure S8.6: Weight change (% of pre-surgery weight) in WT and TREM2-/- mice following sham and BCAS surgeries (cohort 1) . BCAS caused a maximal 9.9 % and 8.9 % loss in weight in WT and TREM2-/- mice 3 d following surgery, respectively. Data show mean ±CAS caN = 6 - 7 independent animals per group.

8.3.2 Weight changes in WT and TREM2-/- 28 d following BCAS and sham surgeries in cohort 2 (2x 0.16 mm coils).

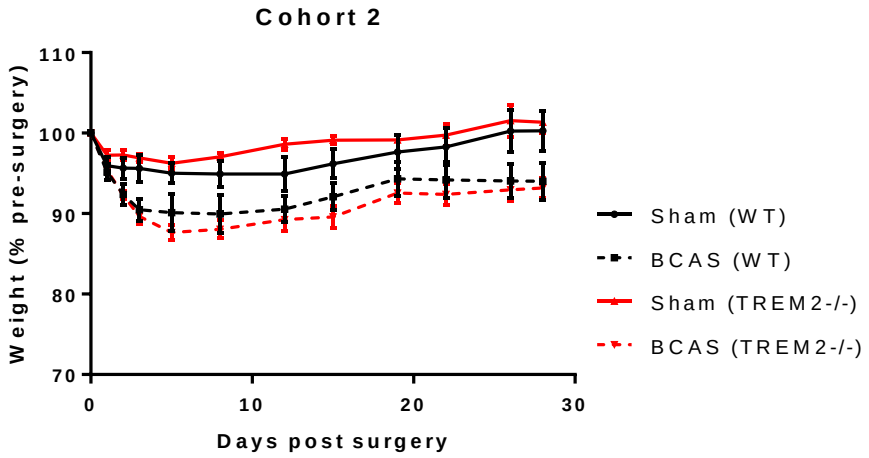

Figure S8.7: Weight change (% of pre-surgery weight) in WT and TREM2-/- mice 28 d post sham and BCAS surgeries. BCAS caused a maximal 9.9 % and 12.4 % loss in weight 5 d following surgery in WT and TREM2-/- mice, respectively. Data show mean ± SEM. N = 6 – 9 independent animals per group.

8.4 Appendix IV: Chapter 6:

Weight changes in WT and TREM2-/- mice 28 d following sham and BCAS surgeries.

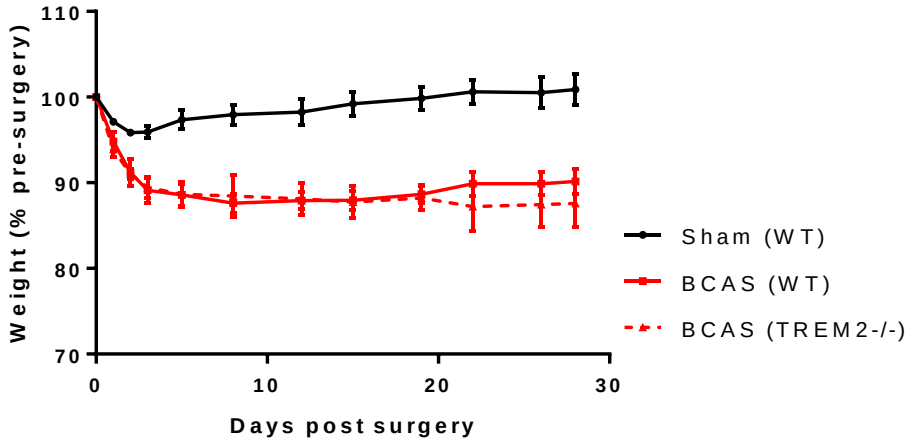

Figure S8.8: Weight change (% of pre-surgery weight) in WT and TREM2-/- mice 28 d post sham and BCAS surgeries. BCAS caused an average maximal 12.4 % loss of weight 8 d following surgery whilst TREM2-/- mice demonstrated an average maximal 12.8 % loss of weight 22 d following surgery. Data show mean ± SEM. N = 7 independent animals per group.

8.4.2 Yield and purity of RNA extracted from FACS-isolated microglia

8.4.2.1 White matter microglia

Treatment group	RNA (ng/ µl)	Total RNA yield (ng)	260/ 280 ratio
Sham	4.3	46.9	2.0
	7.8	85.7	2.0
	6.0	65.3	2.1
	7.7	84.2	2.3
	6.6	73.1	1.9
BCAS (WT)	13.1	144.8	1.8
	5.3	57.9	2.5
	14.2	156.0	1.9
	8.7	95.4	2.0
	9.4	103.6	2.3
BCAS (TREM2-/-)	8.6	94.6	2.3
	5.8	63.8	1.9
	6.4	69.9	2.5
	7.2	79.629	1.9
	12.3	135.1	2.4

Table S8.3: Yield and purity of RNA extracted from WT and TREM2-/- white matter microglia following sham and BCAS surgeries for future transcriptomic analysis.

8.4.2.2 Grey matter microglia

Treatment group	RNA (ng/ µl)	Total RNA yield (ng)	260/ 280 ratio
Sham	8.9	97.8	2.0
	9.4	103.6	1.9
	6.5	72.2	2.8
	10.6	116.3	2.1
	19.6	215.8	2.3
BCAS (WT)	16.6	182.1	1.9
	7.4	81.3	1.8
	13.5	148.8	2.1
	14.1	155.3	2.2
	10.9	119.4	1.9
BCAS (TREM2-/-)	12.7	139.7	1.8
	10.7	117.5	2.1
	11.3	124.7	2.1
	11.6	127.2	2.3
	9.1	99.6	2.4

Table S8.4: Yield and purity of RNA extracted from WT and TREM2-/- grey matter microglia following sham and BCAS surgeries for future transcriptomic analysis.

8.5 Appendix V: Buffer constituents

3.8% tri-sodium citrate: 3.8g tri-sodium citrate (Thermo Scientific) in 100 ml dH_20.

4 % PFA: 40 g paraformaldehyde (Sigma) in 1 l phosphate buffer, pH 7.4

Microglial media: DMEM/ F12 (1:1 mix) (Gibco), 10 % FBS.

Saline: 9 g NaCl in 1 l dH_20.

Tri-sodium citrate antigen retrieval buffer: 2.94 g tri-sodium citrate in 1X PBS, pH 6

FACS buffer: 0.5 g low endotoxin BSA (Sigma) in 500 ml PBS (-Ca^{2+}, -Mg^{2+}). For studies conducting FACS isolation of microglia this also contained 12.5mM HEPES.

Chapter 9:

Bibliography

Abbott, N. J., Patabendige, A. A. K., Dolman, D. E. M., Yusof, S. R. & Begley, D. J. 2010. Structure and function of the blood-brain barrier. Neurobiology of Disease, 37(1): pp.13-25.

Aboul-Enein, F., Rauschka, H., Kornek, B., Stadelmann, C., Stefferl, A., Bruck, W., Lucchinetti, C., Schmidbauer, M., Jellinger, K. & Lassmann, H. 2003. Preferential loss of myelin-associated glycoprotein reflects hypoxia-like white matter damage in stroke and inflammatory brain diseases. Journal of Neuropathology and Experimental Neurology, 62(1): pp.25-33.

Akiguchi, I., Tomimoto, H., Suenaga, T., Wakita, H. & Budka, H. 1998. Blood-brain barrier dysfunction in Binswanger's disease; an immunohistochemical study. Acta Neuropathologica, 95(1): pp.78-84.

Alafuzoff, I., Adolfsson, R., Grundkeiqbal, I. & Winblad, B. 1985. Perivascular deposits of serum-proteins in cerebral-cortex in vascular dementia. Acta Neuropathologica, 66(4): pp.292-298.

Arnett, H. A., Mason, J., Marino, M., Suzuki, K., Matsushima, G. K. & Ting, J. P. Y. 2001. TNF alpha promotes proliferation of oligodendrocyte progenitors and remyelination. Nature Neuroscience, 4(11): pp.1116-1122.

Askew, K., Li, K., Olmos-Alonso, A., Garcia-Moreno, F., Liang, Y., Richardson, P., Tipton, T., Chapman, M. A., Riecken, K., Beccari, S., Sierra, A., Molnar, Z., Cragg, M. S., Garaschuk, O., Perry, V. H. & Gomez-Nicola, D. 2017. Coupled Proliferation and Apoptosis Maintain the Rapid Turnover of Microglia in the Adult Brain. Cell Reports, 18(2): pp.391-405.

Back, S. A., Kroenke, C. D., Sherman, L. S., Lawrence, G., Gong, X., Taber, E. N., Sonnen, J. A., Larson, E. B. & Montine, T. J. 2011. White Matter Lesions Defined by Diffusion Tensor Imaging in Older Adults. Annals of Neurology, 70(3): pp.465-476.

Bailey, C. C., Devaux, L. B. & Farzan, M. 2015. The Triggering Receptor Expressed on Myeloid Cells 2 Binds Apolipoprotein E. Journal of Biological Chemistry, 290(43): pp.26033-26042.

Balestrini, S., Perozzi, C., Altamura, C., Vernieri, F., Luzzi, S., Bartolini, M., Provinciali, L. & Silvestrini, M. 2013. Severe carotid stenosis and impaired cerebral hemodynamics can influence cognitive deterioration. Neurology, 80(23): pp.2145-2150.

Barone, F. C., Knudsen, D. J., Nelson, A. H., Feuerstein, G. Z. & Willette, R. N. 1993. Mouse strain differences in susceptibility to cerebral-ischemia are related to cerebral vascular anatomy. Journal of Cerebral Blood Flow and Metabolism, 13(4): pp.683-692.

Beason-Held, L. L., Moghekar, A., Zonderman, A. B., Kraut, M. A. & Resnick, S. M. 2007. Longitudinal changes in cerebral blood flow in the older hypertensive brain. Stroke, 38(6): pp.1766-1773.

Bell, R. D., Winkler, E. A., Sagare, A. P., Singh, I., Larue, B., Deane, R. & Zlokovic, B. V. 2010. Pericytes Control Key Neurovascular Functions and Neuronal Phenotype in the Adult Brain and during Brain Aging. Neuron, 68(3): pp.409-427.

Benakis, C., Brea, D., Caballero, S., Faraco, G., Moore, J., Murphy, M., Sita, G., Racchumi, G., Lingo, L., Pamer, E. G., Iadecola, C. & Anrather, J. 2016. Commensal microbiota affects ischemic stroke outcome by regulating intestinal gamma delta T cells. Nature Medicine, 22(5): pp.516-523.

Bennett, M. L., Bennett, F. C., Liddelow, S. A., Ajami, B., Zamanian, J. L., Fernhoff, N. B., Mulinyawe, S. B., Bohlen, C. J., Adil, A., Tucker, A., Weissman, I. L., Chang, E. F., Li, G., Grant, G. A., Gephart, M. G. H. & Barres, B. A. 2016. New tools for studying microglia in the mouse and human CNS. Proceedings of the National Academy of Sciences of the United States of America, 113(12): pp.E1738-E1746.

Bennett, S. A. L., Tenniswood, M., Chen, J. H., Davidson, C. M., Keyes, M. T., Fortin, T. & Pappas, B. A. 1998. Chronic cerebral hypoperfusion elicits neuronal apoptosis and behavioral impairment. Neuroreport, 9(1): pp.161-166.

Bentourkia, M., Bol, A., Ivanoiu, A., Labar, D., Sibomana, M., Coppens, A., Michel, C., Cosnard, G. & De Volder, A. G. 2000. Comparison of regional cerebral blood flow and glucose metabolism in the normal brain: effect of aging. Journal of the Neurological Sciences, 181(1-2): pp.19-28.

Bernbaum, M., Menon, B. K., Fick, G., Smith, E. E., Goyal, M., Frayne, R. & Coutts, S. B. 2015. Reduced blood flow in normal white matter predicts development of leukoaraiosis. Journal of Cerebral Blood Flow and Metabolism, 35(10): pp.1610-1615.

Bianchin, M. M., Capella, H. M., Chaves, D. L., Steindel, M., Grisard, E. C., Ganev, G. G., Da Silva, J. P., Neto, E. S., Poffo, M. A., Walz, R., Carlotti, C. G. & Sakamoto, A. C. 2004. Nasu-Hakola disease (polycystic lipomembranous osteodysplasia with sclerosing leukoencephalopathy - PLOSL): A dementia associated with bone cystic lesions. From clinical to genetic and molecular aspects. Cellular and Molecular Neurobiology, 24(1): pp.1-24.

Bock, V., Botturi, A., Gaviani, P., Lamperti, E., Maccagnano, C., Piccio, L., Silvani, A. & Salmaggi, A. 2013. Polycystic Lipomembranous Osteodysplasia with Sclerosing Leukoencephalopathy (PLOSL): A new report of an Italian woman and review of the literature. Journal of the Neurological Sciences, 326(1-2): pp.115-119.

Boehm-Sturm, P., Fuechtemeier, M., Foddis, M., Mueller, S., Trueman, R. C., Zille, M., Rinnenthal, J. L., Kypraios, T., Shaw, L., Dirnagl, U. & Farr, T. D. 2017. Neuroimaging Biomarkers Predict Brain Structural Connectivity Change in a Mouse Model of Vascular Cognitive Impairment. Stroke, 48(2): pp.468-475.

Bouchon, A., Dietrich, J. & Colonna, M. 2000. Cutting edge: Inflammatory responses can be triggered by TREM-1, a novel receptor expressed on neutrophils and monocytes. Journal of Immunology, 164(10): pp.4991-4995.

Bouchon, A., Hernandez-Munain, C., Cella, M. & Colonna, M. 2001. A DAP12-mediated pathway regulates expression of CC chemokine receptor 7 and maturation of human dendritic cells. Journal of Experimental Medicine, 194(8): pp.1111-1122.

Brown, W. R. & Thore, C. R. 2011. Cerebral microvascular pathology in ageing and neurodegeneration. Neuropathology and Applied Neurobiology, 37(1): pp.56-74.

Bryant, C. D., Zhang, N. N., Sokoloff, G., Fanselow, M. S., Ennes, H. S., Palmer, A. A. & Mcroberts, J. A. 2008. Behavioral Differences among C57BL/6 Substrains: Implications for Transgenic and Knockout Studies. Journal of Neurogenetics, 22(4): pp.315-331.

Buntinx, M., Moreels, M., Vandenabeele, F., Lambrichts, I., Raus, J., Steels, P., Stinissen, P. & Ameloot, M. 2004. Cytokine-induced cell death in human oligodendroglial cell lines: I. Synergistic effects of IFN-gamma and TNF-alpha on apoptosis. Journal of Neuroscience Research, 76(6): pp.834-845.

Buratti, L., Balucani, C., Viticchi, G., Falsetti, L., Altamura, C., Avitabile, E., Provinciali, L., Vernieri, F. & Silvestrini, M. 2014. Cognitive Deterioration in Bilateral Asymptomatic Severe Carotid Stenosis. Stroke, 45(7): pp.2072-2077.

Butovsky, O., Jedrychowski, M. P., Moore, C. S., Cialic, R., Lanser, A. J., Gabriely, G., Koeglsperger, T., Dake, B., Wu, P. M., Doykan, C. E., Fanek, Z., Liu, L., Chen, Z., Rothstein, J. D., Ransohoffl, R. M., Gygi, S. P., Antel, J. P. & Weiner, H. L. 2014. Identification of a unique TGF-beta dependent molecular and functional signature in microglia. Nature Neuroscience, 17(1): pp.131-143.

Buttgereit, A., Lelios, I., Yu, X., Vrohlings, M., Krakoski, N. R., Gautier, E. L., Nishinakamura, R., Becher, B. & Greter, M. 2016. Sall1 is a transcriptional regulator defining microglia identity and function. Nature Immunology, 17(12): pp.1397-1406.

Caballero, M. A. A., Suarez-Calvet, M., Duering, M., Franzmeier, N., Benzinger, T., Fagan, A. M., Bateman, R. J., Jack, C. R., Levin, J., Dichgans, M., Jucker, M., Karch, C., Masters, C. L., Morris, J. C., Weiner, M., Rossor, M., Fox, N. C., Lee, J. H., Salloway, S., Danek, A., Goate, A., Yakushev, I., Hassenstab, J., Schofield, P. R., Haass, C., Ewers, M. & Dominantly Inherited, A. 2018. White matter diffusion alterations precede symptom onset in autosomal dominant Alzheimer's disease. Brain, 1413065-3080.

Cabezas, R., Avila, M., Gonzalez, J., El-Bacha, R. S., Baez, E., Garcia-Segura, L. M., Coronel, J. C. J., Capani, F., Cardona-Gomez, G. P. & Barreto, G. E. 2014. Astrocytic modulation of blood brain barrier: perspectives on parkinson's disease. Frontiers in Cellular Neuroscience, 8.

Cady, J., Koval, E. D., Benitez, B. A., Zaidman, C., Jockel-Balsarotti, J., Allred, P., Baloh, R. H., Ravits, J., Simpson, E., Appel, S. H., Pestronk, A., Goate, A. M., Miller, T. M., Cruchaga, C. & Harms, M. B. 2014. TREM2 Variant p.R47H as a Risk Factor for Sporadic Amyotrophic Lateral Sclerosis. Jama Neurology, 71(4): pp.449-453.

Candelario-Jalil, E., Thompson, J., Taheri, S., Grossetete, M., Adair, J. C., Edmonds, E., Prestopnik, J., Wills, J. & Rosenberg, G. A. 2011. Matrix Metalloproteinases Are Associated With Increased Blood-Brain Barrier Opening in Vascular Cognitive Impairment. Stroke, 42(5): pp.1345-1350.

Cannon, J. P., O'driscoll, M. & Litman, G. W. 2012. Specific lipid recognition is a general feature of CD300 and TREM molecules. Immunogenetics, 64(1): pp.39-47.

Cantoni, C., Bollman, B., Licastro, D., Xie, M., Mikesell, R., Schmidt, R., Yuede, C. M., Galimberti, D., Olivecrona, G., Klein, R. S., Cross, A. H., Otero, K. & Piccio, L. 2015. TREM2 regulates microglial cell activation in response to demyelination in vivo. Acta Neuropathologica, 129(3): pp.429-447.

Capone, C., Cognat, E., Ghezali, L., Baron-Menguy, C., Aubin, D., Mesnard, L., Stohr, H., Domenga-Denier, V., Nelson, M. T. & Joutel, A. 2016. Reducing Timp3 or Vitronectin Ameliorates Disease Manifestations in CADASIL Mice. Annals of Neurology, 79(3): pp.387-403.

Carbajosa, G., Malki, K., Lawless, N., Wang, H., Ryder, J. W., Wozniak, E., Wood, K., Mein, C. A., Dobson, R. J. B., Collier, D. A., O'neill, M. J., Hodges, A. K. & Newhouse, S. J. 2018. Loss of Trem2 in microglia leads to widespread disruption of cell coexpression networks in mouse brain. Neurobiology of Aging, 69151-166.

Chao, L. L., Buckley, S. T., Kornak, J., Schuff, N., Madison, C., Yaffe, K., Miller, B. L., Kramer, J. H. & Weiner, M. W. 2010. ASL Perfusion MRI Predicts Cognitive Decline and Conversion From MCI to Dementia. Alzheimer Disease & Associated Disorders, 24(1): pp.19-27.

Chen, Q., Zhang, K., Jin, Y., Zhu, T., Cheng, B., Shu, Q. & Fang, X. 2013. Triggering Receptor Expressed on Myeloid Cells-2 Protects against Polymicrobial Sepsis by Enhancing Bacterial Clearance. American Journal of Respiratory and Critical Care Medicine, 188(2): pp.201-212.

Chertoff, M., Shrivastava, K., Gonzalez, B., Acarin, L. & Gimenez-Llort, L. 2013. Differential Modulation of TREM2 Protein during Postnatal Brain Development in Mice. Plos One, 8(8): pp.

Chiu, I. M., Morimoto, E. T. A., Goodarzi, H., Liao, J. T., O'keeffe, S., Phatnani, H. P., Muratet, M., Carroll, M. C., Levy, S., Tavazoie, S., Myers, R. M. & Maniatis, T. 2013. A Neurodegeneration-Specific Gene-Expression Signature of Acutely Isolated Microglia from an Amyotrophic Lateral Sclerosis Mouse Model. Cell Reports, 4(2): pp.385-401.

Cho, K. O., La, H. O., Cho, Y. J., Sung, K. W. & Kim, S. Y. 2006. Minocycline attenuates white matter damage in a rat model of chronic cerebral hypoperfusion. Journal of Neuroscience Research, 83(2): pp.285-291.

Cipolla MJ. 2009. The Cerebral Circulation. San Rafael (CA): Morgan & Claypool Life Sciences. Chapter 5, Control of Cerebral Blood Flow. Retrieved from: http://www.ncbi.nlm.nih.gov/books/NBK53082/

Clark D. D. & Sokoloff, L. (1999) in Basic Neurochemistry: Molecular, Cellular and Medical Aspects, eds. Siegel, G. J., Agranoff, B. W., Albers, R. W., Fisher, S. K. & Uhler, M. D. (Lippincott, Philadelphia), pp. 637–670.

Cognat, E., Cleophax, S., Domenga-Denier, V. & Joutel, A. 2014. Early white matter changes in CADASIL: evidence of segmental intramyelinic oedema in a pre-clinical mouse model. Acta Neuropathologica Communications, 2.

Colonna, M. & Wang, Y. 2016. TREM2 variants: new keys to decipher Alzheimer disease pathogenesis. Nature Reviews Neuroscience, 17(4): pp.201-207.

Coltman, R., Spain, A., Tsenkina, Y., Fowler, J. H., Smith, J., Scullion, G., Allerhand, M., Scott, F., Kalaria, R. N., Ihara, M., Daumas, S., Deary, I. J., Wood, E., Mcculloch, J. & Horsburgh, K. 2011. Selective white matter pathology induces a specific impairment in spatial working memory. Neurobiology of Aging, 32(12): pp.

Correale, C., Genua, M., Vetrano, S., Mazzini, E., Martinoli, C., Spinelli, A., Arena, V., Peyrin-Biroulet, L., Caprioli, F., Passini, N., Panina-Bordignon, P., Repici, A., Malesci, A., Rutella, S., Rescigno, M. & Danese, S. 2013. Bacterial Sensor Triggering Receptor Expressed on Myeloid Cells-2 Regulates the Mucosal Inflammatory Response. Gastroenterology, 144(2): pp.346-+.

Cunningham, C. L., Martinez-Cerdeno, V. & Noctor, S. C. 2013. Microglia Regulate the Number of Neural Precursor Cells in the Developing Cerebral Cortex. Journal of Neuroscience, 33(10): pp.4216-4233.

Daws, M. R., Sullam, P. M., Niemi, E. C., Chen, T. T., Tchao, N. K. & Seaman, W. E. 2003. Pattern recognition by TREM-2: Binding of anionic ligands. Journal of Immunology, 171(2): pp.594-599.

Deary, I. J., Leaper, S. A., Murray, A. D., Staff, R. T. & Whalley, L. J. 2003. Cerebral white matter abnormalities and lifetime cognitive change: A 67-year follow-up of the Scottish mental survey of 1932. Psychology and Aging, 18(1): pp.140-148.

Deczkowska, A., Keren-Shaul, H., Weiner, A., Colonna, M., Schwartz, M. & Amit, I. 2018. Disease-Associated Microglia: A Universal Immune Sensor of Neurodegeneration. Cell, 173(5): pp.1073-1081.

Dichgans, M. & Leys, D. 2017. Vascular Cognitive Impairment. Circulation Research, 120(3): pp.573-591.

Difrancesco, J. C., Novara, F., Zuffardi, O., Forlino, A., Gioia, R., Cossu, F., Bolognesi, M., Andreoni, S., Saracchi, E., Frigeni, B., Stellato, T., Tolnay, M., Winkler, D. T.,

Remida, P., Isimbaldi, G. & Ferrarese, C. 2015. TREX1 C-terminal frameshift mutations in the systemic variant of retinal vasculopathy with cerebral leukodystrophy. Neurological Sciences, 36(2): pp.323-330.

Dong, Y.-F., Kataoka, K., Toyama, K., Sueta, D., Koibuchi, N., Yamamoto, E., Yata, K., Tomimoto, H., Ogawa, H. & Kim-Mitsuyama, S. 2011. Attenuation of Brain Damage and Cognitive Impairment by Direct Renin Inhibition in Mice With Chronic Cerebral Hypoperfusion. Hypertension, 58(4): pp.635-U247.

Dulken, B., Buckley, M. T., Negredo, P. N., Saligrama, N., Cayrol, R., Leeman, D. S., George, B. M., Boutet, S. C., Hebestreit, K., Pluvinage, J. V., Wyss-Coray, T., Weissman, I. L., Vogel, H., Davis, M. M. & Brunet, A. 2019. Single-cell analysis reveals T cell infiltration in old neurogenic niches. Nature, 571(7764): pp.205-+.

Erblich, B., Zhu, L., Etgen, A. M., Dobrenis, K. & Pollard, J. W. 2011. Absence of Colony Stimulation Factor-1 Receptor Results in Loss of Microglia, Disrupted Brain Development and Olfactory Deficits. Plos One, 6(10): pp.

Esiri, M. M., Nagy, Z., Smith, M. Z., Barnetson, L. & Smith, A. D. 1999. Cerebrovascular disease and threshold for dementia in the early stages of Alzheimer's disease. Lancet, 354(9182): pp.919-920.

Fantin, A., Vieira, J. M., Gestri, G., Denti, L., Schwarz, Q., Prykhozhij, S., Peri, F., Wilson, S. W. & Ruhrberg, C. 2010. Tissue macrophages act as cellular chaperones for vascular anastomosis downstream of VEGF-mediated endothelial tip cell induction. Blood, 116(5): pp.829-840.

Faraco, G., Park, L., Anrather, J. & Iadecola, C. 2017. Brain perivascular macrophages: characterization and functional roles in health and disease. Journal of Molecular Medicine-Jmm, 95(11): pp.1143-1152.

Farkas, E., Institoris, A., Domoki, F., Mihaly, A. & Bari, F. 2006. The effect of pre- and posttreatment with diazoxide on the early phase of chronic cerebral hypoperfusion in the rat. Brain Research, 1087168-174.

Farooq, M. U. & Gorelick, P. B. 2013. Vascular Cognitive Impairment. Current Atherosclerosis Reports, 15(6): pp.

Farrall, A. J. & Wardlaw, J. M. 2009. Blood-brain barrier: Ageing and microvascular disease-systematic review and meta-analysis. Neurobiology of Aging, 30(3): pp.337-352.

Fernando, M. S., Simpson, J. E., Matthews, F., Brayne, C., Lewis, C. E., Barber, R., Kalaria, R. N., Forster, G., Esteves, F., Wharton, S. B., Shaw, P. J., O'brien, J. T., Ince, P. G., Function, M. R. C. C. & Ageing Neuropathology Study, G. 2006. White matter lesions in an unselected cohort of the elderly - Molecular pathology suggests origin from chronic hypoperfusion injury. Stroke, 37(6): pp.1391-1398.

Feuerbach, D., Schindler, P., Barske, C., Joller, S., Beng-Louka, E., Worringer, K. A., Kommineni, S., Kaykas, A., Ho, D. J., Ye, C., Welzenbach, K., Elain, G., Klein, L., Brzak, I., Mir, A. K., Farady, C. J., Aichholz, R., Popp, S., George, N. & Neumann, U.

2017. ADAM17 is the main sheddase for the generation of human triggering receptor expressed in myeloid cells (hTREM2) ectodomain and cleaves TREM2 after Histidine 157. Neuroscience Letters, 660109-114.

Filipello, F., Morini, R., Corradini, I., Zerbi, V., Canzi, A., Michalski, B., Erreni, M., Markicevic, M., Starvaggi-Cucuzza, C., Otero, K., Piccio, L., Cignarella, F., Perrucci, F., Tamborini, M., Genua, M., Rajendran, L., Menna, E., Vetrano, S., Fahnestock, M., Paolicelli, R. C. & Matteoli, M. 2018. The Microglial Innate Immune Receptor TREM2 Is Required for Synapse Elimination and Normal Brain Connectivity. Immunity, 48(5): pp.979-+.

Fontaine, D. A. & Davis, D. B. 2016. Attention to Background Strain Is Essential for Metabolic Research: C57BL/6 and the International Knockout Mouse Consortium. Diabetes, 65(1): pp.25-33.

Forabosco, P., Ramasamy, A., Trabzuni, D., Walker, R., Smith, C., Bras, J., Levine, A. P., Hardy, J., Pocock, J. M., Guerreiro, R., Weale, M. E. & Ryten, M. 2013. Insights into TREM2 biology by network analysis of human brain gene expression data. Neurobiology of Aging, 34(12): pp.2699-2714.

Ford, J. W. & Mcvicar, D. W. 2009. TREM and TREM-like receptors in inflammation and disease. Current Opinion in Immunology, 21(1): pp.38-46.

Fowler, J. H., Mcqueen, J., Holland, P. R., Manso, Y., Marangoni, M., Scott, F., Chisholm, E., Scannevin, R. H., Hardingham, G. E. & Horsburgh, K. 2018. Dimethyl fumarate improves white matter function following severe hypoperfusion: Involvement of microglia/macrophages and inflammatory mediators. Journal of Cerebral Blood Flow and Metabolism, 38(8): pp.1354-1370.

Fredriksson, K., Auer, R. N., Kalimo, H., Nordborg, C., Olsson, Y. & Johansson, B. B. 1985. Cerebrovascular lesions in stroke-prone spontaneously hypertensive rats. Acta Neuropathologica, 68(4): pp.284-294.

Friedman, B. A., Srinivasan, K., Ayalon, G., Meilandt, W. J., Lin, H., Huntley, M. A., Cao, Y., Lee, S.-H., Haddick, P. C. G., Ngu, H., Modrusan, Z., Larson, J. L., Kaminker, J. S., Van Der Brug, M. P. & Hansen, D. V. 2018. Diverse Brain Myeloid Expression Profiles Reveal Distinct Microglial Activation States and Aspects of Alzheimer's Disease Not Evident in Mouse Models. Cell Reports, 22(3): pp.832-847.

Fuechtemeier, M., Brinckmann, M. P., Foddis, M., Kunz, A., Po, C., Curato, C., Dirnagl, U. & Farr, T. D. 2015. Vascular change and opposing effects of the angiotensin type 2 receptor in a mouse model of vascular cognitive impairment. Journal of Cerebral Blood Flow and Metabolism, 35(3): pp.476-484.

Fueger, P., Hefendehl, J. K., Veeraraghavalu, K., Wendeln, A.-C., Schlosser, C., Obermueller, U., Wegenast-Braun, B. M., Neher, J. J., Martus, P., Kohsaka, S., Thunemann, M., Feil, R., Sisodia, S. S., Skodras, A. & Jucker, M. 2017. Microglia

turnover with aging and in an Alzheimer's model via long-term in vivo single-cell imaging. Nature Neuroscience, 20(10): pp.1371-+.

Gaidhani, N., Sun, F., Schreihofer, D. & Uteshev, V. V. 2017. Duration of isoflurane-based surgical anesthesia determines severity of brain injury and neurological deficits after a transient focal ischemia in young adult rats. Brain Research Bulletin, 134168-176.

Ghani, M., Sato, C., Kakhki, E. G., Gibbs, J. R., Traynor, B., St George-Hyslop, P. & Rogaeva, E. 2016. Mutation analysis of the MS4A and TREM gene clusters in a case-control Alzheimer's disease data set. Neurobiology of Aging, 42.

Ghosh, M., Balbi, M., Hellal, F., Dichgans, M., Lindauer, U. & Plesnila, N. 2015. Pericytes Are Involved in the Pathogenesis of Cerebral Autosomal Dominant Arteriopathy with Subcortical Infarcts and Leukoencephalopathy. Annals of Neurology, 78(6): pp.887-900.

Ginhoux, F., Greter, M., Leboeuf, M., Nandi, S., See, P., Gokhan, S., Mehler, M. F., Conway, S. J., Ng, L. G., Stanley, E. R., Samokhvalov, I. M. & Merad, M. 2010. Fate Mapping Analysis Reveals That Adult Microglia Derive from Primitive Macrophages. Science, 330(6005): pp.841-845.

Giraldo, M., Lopera, F., Siniard, A. L., Corneveaux, J. J., Schrauwen, I., Carvajal, J., Munoz, C., Ramirez-Restrepo, M., Gaiteri, C., Myers, A. J., Caselli, R. J., Kosik, K. S., Reiman, E. M. & Huentelman, M. J. 2013. Variants in triggering receptor expressed on myeloid cells 2 are associated with both behavioral variant frontotemporal lobar degeneration and Alzheimer's disease. Neurobiology of Aging, 34(8): pp.

Glebov, K., Wunderlich, P., Karaca, I. & Walter, J. 2016. Functional involvement of gamma-secretase in signaling of the triggering receptor expressed on myeloid cells-2 (TREM2). Journal of Neuroinflammation, 13.

Goldstein, E. Z., Church, J. S., Hesp, Z. C., Popovich, P. G. & Mctigue, D. M. 2016. A silver lining of neuroinflammation: Beneficial effects on myelination. Experimental Neurology, 283550-559.

Gordon, G. R. J., Howarth, C. & Macvicar, B. A. 2016. Bidirectional Control of Blood Flow by Astrocytes: A Role for Tissue Oxygen and Other Metabolic Factors. Hypoxia: Translation in Progress, 903209-219.

Grabert, K. & Mccoll, B. W. 2018. Isolation and Phenotyping of Adult Mouse Microglial Cells. Macrophages: Methods and Protocols, 178477-86.

Grabert, K., Michoel, T., Karavolos, M. H., Clohisey, S., Baillie, J. K., Stevens, M. P., Freeman, T. C., Summers, K. M. & Mccoll, B. W. 2016. Microglial brain region-dependent diversity and selective regional sensitivities to aging. Nature Neuroscience, 19(3): pp.504-+.

Guerreiro, R., Wojtas, A., Bras, J., Carrasquillo, M., Rogaeva, E., Majounie, E., Cruchaga, C., Sassi, C., Kauwe, J. S. K., Lupton, M. K., Ryten, M., Brown, K., Lowe, J., Ridge, P. G., Hammer, M. B., Wakutani, Y., Proitsi, P., Newhouse, S., Lohmann, E.,

Erginel-Unaltuna, N., Medway, C., Hanagasi, H., Troakes, C., Gurvit, H., Bilgic, B., Al-Sarraj, S., Benitez, B., Cooper, B., Carrell, D., Emre, M., Zou, F., Ma, L., Murray, M. E., Dickson, D. W., Younkin, S., Hazrati, L., Petersen, R. C., Corcoran, C. D., Cai, Y., Oliveira, C., Ribeiro, M. H., Santana, I., Tschanz, J. T., Gibbs, J. R., Norton, M. C., Kloszewska, I., Mecocci, P., Soininen, H., Tsolaki, M., Vellas, B., Munger, R. G., Mann, D. M. A., Pickering-Brown, S., Lovestone, S., Beck, J., Mead, S., Collinge, J., Parsons, L., Pocock, J., Morris, J. C., Revesz, T., Lashley, T., Fox, N. C., Rossor, M. N., Grenier-Boley, B., Bellenguez, C., Moskvina, V., Sims, R., Harold, D., Williams, J., Lambert, J.-C., Amouyel, P., Graff-Radford, N., Goate, A., Rademakers, R., Morgan, K., Powell, J., St George-Hyslop, P., Singleton, A., Hardy, J., Consortium, E., Consortium, G., Consortium, U. & Alzheimer Genetic Anal, G. 2013a. TREM2 Variants in Alzheimer's Disease. New England Journal of Medicine, 368(2): pp.117-127.

Guerreiro, R. J., Lohmann, E., Bras, J. M., Gibbs, J. R., Rohrer, J. D., Gurunlian, N., Dursun, B., Bilgic, B., Hanagasi, H., Gurvit, H., Emre, M., Singleton, A. & Hardy, J. 2013b. Using Exome Sequencing to Reveal Mutations in TREM2 Presenting as a Frontotemporal Dementia-like Syndrome Without Bone Involvement. Jama Neurology, 70(1): pp.78-84.

Haelewyn, B., David, H. N., Rouillon, C., Chazalviel, L., Lecocq, M., Risso, J.-J., Lemaire, M. & Abraini, J. H. 2008. Neuroprotection by nitrous oxide: Facts and evidence. Critical Care Medicine, 36(9): pp.2651-2659.

Hagemeyer, N., Hanft, K.-M., Akriditou, M.-A., Unger, N., Park, E. S., Stanley, E. R., Staszewski, O., Dimou, L. & Prinz, M. 2017. Microglia contribute to normal myelinogenesis and to oligodendrocyte progenitor maintenance during adulthood. Acta Neuropathologica, 134(3): pp.441-458.

Haimon, Z., Volaski, A., Orthgiess, J., Boura-Halfon, S., Varol, D., Shemer, A., Yona, S., Zuckerman, B., David, E., Chappell-Maor, L., Bechmann, I., Gericke, M., Ulitsky, I. & Jung, S. 2018. Re-evaluating microglia expression profiles using RiboTag and cell isolation strategies. Nature Immunology, 19(6): pp.636-+.

Hakola, H. P. 1972. Neuropsychiatric and genetic aspects of a new hereditary disease characterized by progressive dementia and lipomembranous polycystic osteodysplasia. Acta psychiatrica Scandinavica. Supplementum, 2321-173.

Hamel, E. 2006. Perivascular nerves and the regulation of cerebrovascular tone. Journal of Applied Physiology, 100(3): pp.1059-1064.

Hamerman, J. A., Jarjoura, V. R., Humphrey, M. B., Nakamura, M. C., Seaman, W. E. & Lanier, L. L. 2006. Cutting edge: Inhibition of TLR and FcR responses in macrophages by triggering receptor expressed on myeloid cells (TREM)-2 and DAP12. Journal of Immunology, 177(4): pp.2051-2055.

Hammond, T. R., Dufort, C., Dissing-Olesen, L., Giera, S., Young, A., Wysoker, A., Walker, A. J., Gergits, F., Segel, M., Nemesh, J., Marsh, S. E., Saunders, A., Macosko, E., Ginhoux, F., Chen, J., Franklin, R. J. M., Piao, X., Mccarroll, S. A. & Stevens, B. 2019. Single-Cell RNA Sequencing of Microglia throughout the Mouse Lifespan and in the Injured Brain Reveals Complex Cell-State Changes. Immunity, 50(1): pp.253-+.

Hart, A. D., Wyttenbach, A., Perry, V. H. & Teeling, J. L. 2012. Age related changes in microglial phenotype vary between CNS regions: Grey versus white matter differences. Brain Behavior and Immunity, 26(5): pp.754-765.

Hart, M. N., Heistad, D. D. & Brody, M. J. 1980. Effect of chronic hypertension and sympathetic denervation on wall-lumen ratio of cerebral vessels. Hypertension, 2(4): pp.419-423.

Hase, Y., Craggs, L., Hase, M., Stevenson, W., Slade, J., Lopez, D., Mehta, R., Chen, A., Liang, D., Oakley, A., Ihara, M., Horsburgh, K. & Kalaria, R. N. 2017. Effects of environmental enrichment on white matter glial responses in a mouse model of chronic cerebral hypoperfusion. Journal of Neuroinflammation, 14.

Hattori, Y., Enmi, J., Iguchi, S., Saito, S., Yamamoto, Y., Tsuji, M., Nagatsuka, K., Kalaria, R. N., Iida, H. & Ihara, M. 2016a. Gradual Carotid Artery Stenosis in Mice Closely Replicates Hypoperfusive Vascular Dementia in Humans. Journal of the American Heart Association, 5(2): pp.

Hattori, Y., Enmi, J., Kitamura, A., Yamamoto, Y., Saito, S., Takahashi, Y., Iguchi, S., Tsuji, M., Yamahara, K., Nagatsuka, K., Iida, H. & Ihara, M. 2015. A Novel Mouse Model of Subcortical Infarcts with Dementia. Journal of Neuroscience, 35(9): pp.3915-3928.

Hattori, Y., Enmi, J.-I., Iguchi, S., Saito, S., Yamamoto, Y., Nagatsuka, K., Iida, H. & Ihara, M. 2016b. Substantial Reduction of Parenchymal Cerebral Blood Flow in Mice with Bilateral Common Carotid Artery Stenosis. Scientific Reports, 6.

Hawkes, C. A. & Mclaurin, J. 2009. Selective targeting of perivascular macrophages for clearance of beta-amyloid in cerebral amyloid angiopathy. Proceedings of the National Academy of Sciences of the United States of America, 106(4): pp.1261-1266.

Hoeffel, G., Chen, J., Lavin, Y., Low, D., Almeida, F. F., See, P., Beaudin, A. E., Lum, J., Low, I., Forsberg, E. C., Poidinger, M., Zolezzi, F., Larbi, A., Ng, L. G., Chan, J. K. Y., Greter, M., Becher, B., Samokhvalov, I. M., Merad, M. & Ginhoux, F. 2015. C-Myb(+) Erythro-Myeloid Progenitor-Derived Fetal Monocytes Give Rise to Adult Tissue-Resident Macrophages. Immunity, 42(4): pp.665-678.

Holland, P. R., Searcy, J. L., Salvadores, N., Scullion, G., Chen, G., Lawson, G., Scott, F., Bastin, M. E., Ihara, M., Kalaria, R., Wood, E. R., Smith, C., Wardlaw, J. M. & Horsburgh, K. 2015. Gliovascular disruption and cognitive deficits in a mouse model

with features of small vessel disease. Journal of Cerebral Blood Flow and Metabolism, 35(6): pp.1005-1014.

Hsieh, C. L., Koike, M., Spusta, S. C., Niemi, E. C., Yenari, M., Nakamura, M. C. & Seaman, W. E. 2009. A role for TREM2 ligands in the phagocytosis of apoptotic neuronal cells by microglia. Journal of Neurochemistry, 109(4): pp.1144-1156.

Huebner, E. A. & Strittmatter, S. M. 2009. Axon Regeneration in the Peripheral and Central Nervous Systems. Cell Biology of the Axon, 48339-351.

Iadecola, C. 2010. The overlap between neurodegenerative and vascular factors in the pathogenesis of dementia. Acta Neuropathologica, 120(3): pp.287-296.

Iadecola, C. 2013. The Pathobiology of Vascular Dementia. Neuron, 80(4): pp.844-866.

Ihara, M., Tomimoto, H., Kinoshita, M., Oh, J., Noda, M., Wakita, H., Akiguchi, I. & Shibasaki, H. 2001. Chronic cerebral hypoperfusion induces MMP-2 but not MMP-9 expression in the microglia and vascular endothelium of white matter. Journal of Cerebral Blood Flow and Metabolism, 21(7): pp.828-834.

Ito, H. & Hamerman, J. A. 2012. TREM-2, triggering receptor expressed on myeloid cell-2, negatively regulates TLR responses in dendritic cells. European Journal of Immunology, 42(1): pp.176-185.

Iturria-Medina, Y., Sotero, R. C., Toussaint, P. J., Mateos-Perez, J. M., Evans, A. C. & Alzheimer's Dis, N. 2016. Early role of vascular dysregulation on late-onset Alzheimer's disease based on multifactorial data-driven analysis. Nature Communications, 7.

Jay, T. R., Hirsch, A. M., Broihier, M. L., Miller, C. M., Neilson, L. E., Ransohoff, R. M., Lamb, B. T. & Landreth, G. E. 2017. Disease Progression-Dependent Effects of TREM2 Deficiency in a Mouse Model of Alzheimer's Disease. Journal of Neuroscience, 37(3): pp.637-647.

Jay, T. R., Miller, C. M., Cheng, P. J., Graham, L. C., Bemiller, S., Broihier, M. L., Xu, G., Margevicius, D., Karlo, J. C., Sousa, G. L., Cotleur, A. C., Butovsky, O., Bekris, L., Staugaitis, S. M., Leverenz, J. B., Pimplikar, S. W., Landreth, G. E., Howell, G. R., Ransohoff, R. M. & Lamb, B. T. 2015. TREM2 deficiency eliminates TREM2(+) inflammatory macrophages and ameliorates pathology in Alzheimer's disease mouse models. Journal of Experimental Medicine, 212(3): pp.287-295.

Jendresen, C., Arskog, V., Daws, M. R. & Nilsson, L. N. G. 2017. The Alzheimer's disease risk factors apolipoprotein E and TREM2 are linked in a receptor signaling pathway. Journal of Neuroinflammation, 14.

Jiang, M., Sun, L., Feng, D.-X., Yu, Z.-Q., Gao, R., Sun, Y.-Z. & Chen, G. 2017a. Neuroprotection provided by isoflurane pre-conditioning and post-conditioning. Medical Gas Research, 7(1): pp.48-55.

Jiang, T., Tan, L., Chen, Q., Tan, M.-S., Zhou, J.-S., Zhu, X.-C., Lu, H., Wang, H.-F., Zhang, Y.-D. & Yu, J.-T. 2016a. A rare coding variant in TREM2 increases risk for Alzheimer's disease in Han Chinese. Neurobiology of Aging, 42.

Jiang, T., Tan, L., Zhu, X.-C., Zhang, Q.-Q., Cao, L., Tan, M.-S., Gus, L.-Z., Wang, H.-F., Ding, Z.-Z., Zhang, Y.-D. & Yu, J.-T. 2014a. Upregulation of TREM2 Ameliorates Neuropathology and Rescues Spatial Cognitive Impairment in a Transgenic Mouse Model of Alzheimer's Disease. Neuropsychopharmacology, 39(13): pp.2949-2962.

Jiang, T., Wan, Y., Zhang, Y. D., Zhou, J. S., Gao, Q., Zhu, X. C., Shi, J. Q., Lu, H., Tan, L. & Yu, J. T. 2017b. TREM2 Overexpression has No Improvement on Neuropathology and Cognitive Impairment in Aging APPswe/PS1dE9 Mice. Molecular Neurobiology, 54(2): pp.855-865.

Jiang, T., Yu, J.-T., Zhu, X.-C., Tan, M.-S., Gu, L.-Z., Zhang, Y.-D. & Tan, L. 2014b. Triggering receptor expressed on myeloid cells 2 knockdown exacerbates aging-related neuroinflammation and cognitive deficiency in senescence-accelerated mouse prone 8 mice. Neurobiology of Aging, 35(6): pp.1243-1251.

Jiang, T., Zhang, Y.-D., Chen, Q., Gao, Q., Zhu, X.-C., Zhou, J.-S., Shi, J.-Q., Lu, H., Tan, L. & Yu, J.-T. 2016b. TREM2 modifies microglial phenotype and provides neuroprotection in P301S tau transgenic mice. Neuropharmacology, 105196-206.

Jin, S. C., Benitez, B. A., Karch, C. M., Cooper, B., Skorupa, T., Carrell, D., Norton, J. B., Hsu, S., Harari, O., Cai, Y., Bertelsen, S., Goate, A. M. & Cruchaga, C. 2014. Coding variants in TREM2 increase risk for Alzheimer's disease. Human Molecular Genetics, 23(21): pp.5838-5846.

Jin, W. N., Shi, S. X. Y., Li, Z. G., Li, M. S., Wood, K., Gonzales, R. J. & Liu, Q. 2017. Depletion of microglia exacerbates postischemic inflammation and brain injury. Journal of Cerebral Blood Flow and Metabolism, 37(6): pp.2224-2236.

Jonsson, T., Stefansson, H., Steinberg, S., Jonsdottir, I., Jonsson, P. V., Snaedal, J., Bjornsson, S., Huttenlocher, J., Levey, A. I., Lah, J. J., Rujescu, D., Hampel, H., Giegling, I., Andreassen, O. A., Engedal, K., Ulstein, I., Djurovic, S., Ibrahim-Verbaas, C., Hofman, A., Ikram, M. A., Van Duijn, C. M., Thorsteinsdottir, U., Kong, A. & Stefansson, K. 2013. Variant of TREM2 Associated with the Risk of Alzheimer's Disease. New England Journal of Medicine, 368(2): pp.107-116.

Joutel, A., Monet-Lepretre, M., Gosele, C., Baron-Menguy, C., Hammes, A., Schmidt, S., Lemaire-Carrette, B., Domenga, V., Schedl, A., Lacombe, P. & Hubner, N. 2010. Cerebrovascular dysfunction and microcirculation rarefaction precede white matter lesions in a mouse genetic model of cerebral ischemic small vessel disease. Journal of Clinical Investigation, 120(2): pp.433-445.

Kakae, M., Tobori, S., Morishima, M., Nagayasu, K., Shirakawa, H. & Kaneko, S. 2019. Depletion of microglia ameliorates white matter injury and cognitive impairment in a

mouse chronic cerebral hypoperfusion model. Biochemical and Biophysical Research Communications, 514(4): pp.1040-1044.

Kaneko, M., Sano, K., Nakayama, J. & Amano, N. 2010. Nasu-Hakola disease: The first case reported by Nasu and review. Neuropathology, 30(5): pp.463-470.

Kang, S. S., Ebbert, M. T. W., Baker, K. E., Cook, C., Wang, X. W., Sens, J. P., Kocher, J. P., Petrucelli, L. & Fryer, J. D. 2018. Microglial translational profiling reveals a convergent APOE pathway from aging, amyloid, and tau. Journal of Experimental Medicine, 215(9): pp.2235-2245.

Kang, S. S., Kurti, A., Baker, K. E., Liu, C. C., Colonna, M., Ulrich, J. D., Holtzman, D. M., Bu, G. J. & Fryer, J. D. 2018. Behavioral and transcriptomic analysis of Trem2-null mice: not all knockout mice are created equal. Human Molecular Genetics, 27(2)**:** pp.211-223.

Karch, C. M. & Goate, A. M. 2015. Alzheimer's Disease Risk Genes and Mechanisms of Disease Pathogenesis. Biological Psychiatry, 77(1): pp.43-51.

Kawabori, M., Kacimi, R., Kauppinen, T., Calosing, C., Kim, J. Y., Hsieh, C. L., Nakamura, M. C. & Yenari, M. A. 2015. Triggering Receptor Expressed on Myeloid Cells 2 (TREM2) Deficiency Attenuates Phagocytic Activities of Microglia and Exacerbates Ischemic Damage in Experimental Stroke. Journal of Neuroscience, 35(8): pp.3384-3396.

Keren-Shaul, H., Spinrad, A., Weiner, A., Matcovitch-Natan, O., Dvir-Szternfeld, R., Ulland, T. K., David, E., Baruch, K., Lara-Astaiso, D., Toth, B., Itzkovitz, S., Colonna, M., Schwartz, M. & Amit, I. 2017. A Unique Microglia Type Associated with Restricting Development of Alzheimer's Disease. Cell, 169(7): pp.1276-+.

Khan, M. B., Hoda, M. N., Vaibhav, K., Giri, S., Wang, P., Waller, J. L., Ergul, A., Dhandapani, K. M., Fagan, S. C. & Hess, D. C. 2015. Remote Ischemic Postconditioning: Harnessing Endogenous Protection in a Murine Model of Vascular Cognitive Impairment. Translational Stroke Research, 6(1): pp.69-77.

Kierdorf, K., Erny, D., Goldmann, T., Sander, V., Schulz, C., Perdiguero, E. G., Wieghofer, P., Heinrich, A., Riemke, P., Hoelscher, C., Mueller, D. N., Luckow, B., Brocker, T., Debowski, K., Fritz, G., Opdenakker, G., Diefenbach, A., Biber, K., Heikenwalder, M., Geissmann, F., Rosenbauer, F. & Prinz, M. 2013. Microglia emerge from erythromyeloid precursors via Pu.1- and Irf8-dependent pathways. Nature Neuroscience, 16(3): pp.273-280.

Kim, C. C., Nakamura, M. C. & Hsieh, C. L. 2016. Brain trauma elicits non-canonical macrophage activation states. Journal of Neuroinflammation, 13.

Kim, Y., Sato, K., Asagiri, M., Morita, I., Soma, K. & Takayanagi, H. 2005. Contribution of nuclear factor of activated T cells c1 to the transcriptional control of immunoreceptor osteoclast-associated receptor but not triggering receptor expressed by myeloid

cells-2 during osteoclastogenesis. Journal of Biological Chemistry, 280(38): pp.32905-32913.

Kim, Y. S., Immink, R. V., Stok, W. J., Karemaker, J. M., Secher, N. H. & Van Lieshout, J. J. 2008. Dynamic cerebral autoregulatory capacity is affected early in Type 2 diabetes. Clinical Science, 115(7-8): pp.255-262.

Kitagawa, K., Matsumoto, M., Yang, G. M., Mabuchi, T., Yagita, Y., Hori, M. & Yanagihara, T. 1998. Cerebral ischemia after bilateral carotid artery occlusion and intraluminal suture occlusion in mice: Evaluation of the patency of the posterior communicating artery. Journal of Cerebral Blood Flow and Metabolism, 18(5): pp.570-579.

Kitamura, A., Fujita, Y., Oishi, N., Kalaria, R. N., Washida, K., Maki, T., Okamoto, Y., Hase, Y., Yamada, M., Takahashi, J., Ito, H., Tomimoto, H., Fukuyama, H., Takahashi, R. & Ihara, M. 2012. Selective white matter abnormalities in a novel rat model of vascular dementia. Neurobiology of Aging, 33(5): pp.

Kitamura, A., Manso, Y., Duncombe, J., Searcy, J., Koudelka, J., Binnie, M., Webster, S., Lennen, R., Jansen, M., Marshall, I., Ihara, M., Kalaria, R. N. & Horsburgh, K. 2017. Long-term cilostazol treatment reduces gliovascular damage and memory impairment in a mouse model of chronic cerebral hypoperfusion. Scientific Reports, 7.

Kleinberger, G., Brendel, M., Mracsko, E., Wefers, B., Groeneweg, L., Xiang, X., Focke, C., Deussing, M., Suarez-Calvet, M., Mazaheri, F., Parhizkar, S., Pettkus, N., Wurst, W., Feederle, R., Bartenstein, P., Mueggler, T., Arzberger, T., Knuesel, I., Rominger, A. & Haass, C. 2017. The FTD-like syndrome causing TREM2 T66M mutation impairs microglia function, brain perfusion, and glucose metabolism. Embo Journal, 36(13): pp.1837-1853.

Kleinberger, G., Yamanishi, Y., Suarez-Calvet, M., Czirr, E., Lohmann, E., Cuyvers, E., Struyfs, H., Pettkus, N., Wenninger-Weinzierl, A., Mazaheri, F., Tahirovic, S., Lleo, A., Alcolea, D., Fortea, J., Willem, M., Lammich, S., Molinuevo, J. L., Sanchez-Valle, R., Antonell, A., Ramirez, A., Heneka, M. T., Sleegers, K., Van Der Zee, J., Martin, J.-J., Engelborghs, S., Demirtas-Tatlidede, A., Zetterberg, H., Van Broeckhoven, C., Gurvit, H., Wyss-Coray, T., Hardy, J., Colonna, M. & Haass, C. 2014. TREM2 mutations implicated in neurodegeneration impair cell surface transport and phagocytosis. Science Translational Medicine, 6(243): pp.

Klunemann, H., Ridha, B. H., Magy, L., Wherrett, J. R., Hemelsoet, D. M., Keen, R. W., Debleecker, J. L., Rossor, M. N., Marienhagen, J., Klein, H. E., Peltonen, L. & Paloneva, J. 2006. The genetic causes of basal ganglia calcification, dementia, and bone cysts: DAP12 and TREM2 - Reply. Neurology, 66(4): pp.616-616.

Kober, D. L., Alexander-Brett, J. M., Karch, C. M., Cruchaga, C., Colonna, M., Holtzman, M. J. & Brett, T. J. 2016. Neurodegenerative disease mutations in TREM2 reveal a functional surface and distinct loss-of-function mechanisms. Elife, 5.

Kober, D. L. & Brett, T. J. 2017. TREM2-Ligand Interactions in Health and Disease. Journal of Molecular Biology, 429(11): pp.1607-1629.

Koizumi, K., Hattori, Y., Ahn, S. J., Buendia, I., Ciacciarelli, A., Uekawa, K., Wang, G., Hiller, A., Zhao, L., Voss, H. U., Paul, S. M., Schaffer, C., Park, L. & Iadecola, C. 2018. Apo epsilon 4 disrupts neurovascular regulation and undermines white matter integrity and cognitive function. Nature Communications, 9.

Kondo, Y., Lemere, C. A. & Seabrook, T. J. 2007. Osteopetrotic (op/op) mice have reduced microglia, no A beta deposition, and no changes in dopaminergic neurons. Journal of Neuroinflammation, 4.

Korvatska, O., Leverenz, J. B., Jayadev, S., Mcmillan, P., Kurtz, I., Guo, X., Rumbaugh, M., Matsushita, M., Girirajan, S., Dorschner, M. O., Kiianitsa, K., Yu, C.-E., Brkanac, Z., Garden, G. A., Raskind, W. H. & Bird, T. D. 2015. R47H Variant of TREM2 Associated With Alzheimer Disease in a Large Late-Onset Family Clinical, Genetic, and Neuropathological Study. Jama Neurology, 72(8): pp.920-927.

Kotter, M. R., Li, W. W., Zhao, C. & Franklin, R. J. M. 2006. Myelin impairs CNS remyelination by inhibiting oligodendrocyte precursor cell differentiation. Journal of Neuroscience, 26(1): pp.328-332.

Krasemann, S., Madore, C., Cialic, R., Baufeld, C., Calcagno, N., El Fatimy, R., Beckers, L., O'loughlin, E., Xu, Y., Fanek, Z., Greco, D. J., Smith, S. T., Tweet, G., Humulock, Z., Zrzavy, T., Conde-Sanroman, P., Gacias, M., Weng, Z., Chen, H., Tjon, E., Mazaheri, F., Hartmann, K., Madi, A., Ulrich, J. D., Glatzel, M., Worthmann, A., Heeren, J., Budnik, B., Lemere, C., Ikezu, T., Heppner, F. L., Litvak, V., Holtzman, D. M., Lassmann, H., Weiner, H. L., Ochando, J., Haass, C. & Butovsky, O. 2017. The TREM2-APOE Pathway Drives the Transcriptional Phenotype of Dysfunctional Microglia in Neurodegenerative Diseases. Immunity, 47(3): pp.566-+.

Krishnan, S. M., Sobey, C. G., Latz, E., Mansell, A. & Drummond, G. R. 2014. IL-1 beta and IL-18: inflammatory markers or mediators of hypertension? British Journal of Pharmacology, 171(24): pp.5589-5602.

Kurisu, K., Zheng, Z., Kim, J. Y., Shi, J., Kanoke, A., Liu, J., Hsieh, C. L. & Yenari, M. A. 2018. Triggering receptor expressed on myeloid cells-2 expression in the brain is required for maximal phagocytic activity and improved neurological outcomes following experimental stroke. Journal of cerebral blood flow and metabolism : official journal of the International Society of Cerebral Blood Flow and Metabolism, 271678X18817282-271678X18817282.

Lampron, A., Larochelle, A., Laflamme, N., Prefontaine, P., Plante, M.-M., Sanchez, M. G., Yong, V. W., Stys, P. K., Tremblay, M.-E. & Rivest, S. 2015. Inefficient clearance of myelin debris by microglia impairs remyelinating processes. Journal of Experimental Medicine, 212(4): pp.481-495.

Langbaum, J. B. S., Chen, K. W., Launer, L. J., Fleisher, A. S., Lee, W., Liu, X. F., Protas, H. D., Reeder, S. A., Bandy, D., Yu, M. X., Caselli, R. J. & Reiman, E. M. 2012. Blood pressure is associated with higher brain amyloid burden and lower glucose metabolism in healthy late middle-age persons. Neurobiology of Aging, 33(4): pp.

Lawrence, A. J., Chung, A. W., Morris, R. G., Markus, H. S. & Barrick, T. R. 2014. Structural network efficiency is associated with cognitive impairment in small-vessel disease. Neurology, 83(4): pp.304-311.

Lawrence, A. J., Patel, B., Morris, R. G., Mackinnon, A. D., Rich, P. M., Barrick, T. R. & Markus, H. S. 2013. Mechanisms of Cognitive Impairment in Cerebral Small Vessel Disease: Multimodal MRI Results from the St George's Cognition and Neuroimaging in Stroke (SCANS) Study. Plos One, 8(4): pp.

Lawson, L. J., Perry, V. H., Dri, P. & Gordon, S. 1990. Heterogeneity in the distribution and morphology of microglia in the normal adult-mouse brain. Neuroscience, 39(1): pp.151-170.

Le Ber, I., De Septenville, A., Guerreiro, R., Bras, J., Camuzat, A., Caroppo, P., Lattante, S., Couarch, P., Kabashi, E., Bouya-Ahmed, K., Dubois, B. & Brice, A. 2014. Homozygous TREM2 mutation in a family with atypical frontotemporal dementia. Neurobiology of Aging, 35(10): pp.

Lee, H.-M., Kim, J.-J., Kim, H. J., Shong, M., Ku, B. J. & Jo, E.-K. 2013. Upregulated NLRP3 Inflammasome Activation in Patients With Type 2 Diabetes. Diabetes, 62(1): pp.194-204.

Lee, K. M., Bang, J., Kim, B. Y., Lee, I. S., Han, J.-S., Hwang, B. Y. & Jeon, W. K. 2015. Fructus mume alleviates chronic cerebral hypoperfusion-induced white matter and hippocampal damage via inhibition of inflammation and downregulation of TLR4 and p38 MAPK signaling. Bmc Complementary and Alternative Medicine, 15.

Lee, S., Viqar, F., Zimmerman, M. E., Narkhede, A., Tosto, G., Benzinger, T. L. S., Marcus, D. S., Fagan, A. M., Goate, A., Fox, N. C., Cairns, N. J., Holtzman, D. M., Buckles, V., Ghetti, B., Mcdade, E., Martins, R. N., Saykin, A. J., Masters, C. L., Ringman, J. M., Ryan, N. S., Forster, S., Laske, C., Schofield, P. R., Sperling, R. A., Salloway, S., Correia, S., Jack, C., Weiner, M., Bateman, R. J., Morris, J. C., Mayeux, R., Brickman, A. M. & Dominantly Inherited, A. 2016. White Matter Hyperintensities Are a Core Feature of Alzheimer's Disease: Evidence from the Dominantly Inherited Alzheimer Network. Annals of Neurology, 79(6): pp.929-939.

Leenders, K. L., Perani, D., Lammertsma, A. A., Heather, J. D., Buckingham, P., Healy, M. J. R., Gibbs, J. M., Wise, R. J. S., Hatazawa, J., Herold, S., Beaney, R. P., Brooks, D. J., Spinks, T., Rhodes, C., Frackowiak, R. S. J. & Jones, T. 1990. CEREBRAL Blood-flow, blood-volume and oxygen utilization - normal values and effect of age. Brain, 11327-47.

Leyns, C. E. G., Ulrich, J. D., Finn, M. B., Stewart, F. R., Koscal, L. J., Serrano, J. R., Robinson, G. O., Anderson, E., Colonna, M. & Holtzman, D. M. 2017. TREM2 deficiency attenuates neuroinflammation and protects against neurodegeneration in a mouse model of tauopathy. Proceedings of the National Academy of Sciences of the United States of America, 114(43): pp.11524-11529.

Liddelow, S. A., Guttenplan, K. A., Larke, L. E. C., Bennett, F. C., Bohlen, C. J., Schirmer, L., Bennett, M. L., Munch, A. E., Chung, W.-S., Peterson, T. C., Wilton, D. K., Frouin, A., Napier, B. A., Panicker, N., Kumar, M., Buckwalter, M. S., Rowitch, D. H., Dawson, V. L., Dawson, T. M., Stevens, B. & Barres, B. A. 2017. Neurotoxic reactive astrocytes are induced by activated microglia. Nature, 541(7638): pp.481-487.

Lin, W. S., Kemper, A., Dupree, J. L., Harding, H. P., Ron, D. & Popko, B. 2006. Interferon-gamma inhibits central nervous system remyelination through a process modulated by endoplasmic reticulum stress. Brain, 1291306-1318.

Lindahl, P., Johansson, B. R., Leveen, P. & Betsholtz, C. 1997. Pericyte loss and microaneurysm formation in PDGF-B-deficient mice. Science, 277(5323): pp.242-245.

Liu, C., Wu, C., Yang, Q., Gao, J., Li, L., Yang, D. & Luo, L. 2016. Macrophages Mediate the Repair of Brain Vascular Rupture through Direct Physical Adhesion and Mechanical Traction. Immunity, 44(5): pp.1162-1176.

Liu, Q. H., Radwanski, R., Babadjouni, R., Patel, A., Hodis, D. M., Baumbacher, P., Zhao, Z., Zlokovic, B. & Mack, W. J. 2019. Experimental chronic cerebral hypoperfusion results in decreased pericyte coverage and increased blood-brain barrier permeability in the corpus callosum. Journal of Cerebral Blood Flow and Metabolism, 39(2): pp.240-250.

Liu, Y., Wu, X.-M., Luo, Q.-Q., Huang, S., Yang, Q.-W. Q., Wang, F.-X., Ke, Y. & Qian, Z.-M. 2015. CX3CL1/CX3CR1-mediated microglia activation plays a detrimental role in ischemic mice brain via p38MAPK/PKC pathway. Journal of Cerebral Blood Flow and Metabolism, 35(10): pp.1623-1631.

Lloyd, A., Miron, V. 2019. The pro-remyelination properties of microglia in the central nervous system. Nature reviews neurology. https://doi.org/10.1038/s41582-019-0184-2

Lopert, P. & Patel, M. 2014. Nicotinamide Nucleotide Transhydrogenase (Nnt) Links the Substrate Requirement in Brain Mitochondria for Hydrogen Peroxide Removal to the Thioredoxin/Peroxiredoxin (Trx/Prx) System. Journal of Biological Chemistry, 289(22): pp.15611-15620.

Lucin, K. M., O'brien, C. E., Bieri, G., Czirr, E., Mosher, K. I., Abbey, R. J., Mastroeni, D. F., Rogers, J., Spencer, B., Masliah, E. & Wyss-Coray, T. 2013. Microglial Beclin 1 Regulates Retromer Trafficking and Phagocytosis and Is Impaired in Alzheimer's Disease. Neuron, 79(5): pp.873-886.

Mabbott, N. A., Baillie, J. K., Hume, D. A. & Freeman, T. C. 2010. Meta-analysis of lineage-specific gene expression signatures in mouse leukocyte populations. Immunobiology, 215(9-10): pp.724-736.

Madigan, J. B., Wilcock, D. M. & Hainsworth, A. H. 2016. Vascular Contributions to Cognitive Impairment and Dementia Topical Review of Animal Models. Stroke, 47(7): pp.1953-1959.

Maillard, P., Carmichael, O., Fletcher, E., Reed, B., Mungas, D. & Decarli, C. 2012. Coevolution of white matter hyperintensities and cognition in the elderly. Neurology, 79(5): pp.442-448.

Maniega, S. M., Chappell, F. M., Hernandez, M. C. V., Armitage, P. A., Makin, S. D., Heye, A. K., Thrippleton, M. J., Sakka, E., Shuler, K., Dennis, M. S. & Wardlaw, J. M. 2017. Integrity of normal-appearing white matter: Influence of age, visible lesion burden and hypertension in patients with small-vessel disease. Journal of Cerebral Blood Flow and Metabolism, 37(2): pp.644-656.

Manso, Y., Holland, P. R., Kitamura, A., Szymkowiak, S., Duncombe, J., Hennessy, E., Searcy, J. L., Marangoni, M., Randall, A. D., Brown, J. T., Mccoll, B. W. & Horsburgh, K. 2018. Minocycline reduces microgliosis and improves subcortical white matter function in a model of cerebral vascular disease. Glia, 66(1): pp.34-46.

Mantovani, A., Sica, A., Sozzani, S., Allavena, P., Vecchi, A. & Locati, M. 2004. The chemokine system in diverse forms of macrophage activation and polarization. Trends in Immunology, 25(12): pp.677-686.

Marchal, G., Rioux, P., Petittaboue, M. C., Sette, G., Travere, J. M., Lepoec, C., Courtheoux, P., Derlon, J. M. & Baron, J. C. 1992. Regional cerebral oxygen-consumption, blood-flow, and blood-volume in healthy-human aging. Archives of Neurology, 49(10): pp.1013-1020

Marin-Teva, J. L., Dusart, I., Colin, C., Gervais, A., Van Rooijen, N. & Mallat, M. 2004. Microglia promote the death of developing Purkinje cells. Neuron, 41(4): pp.535-547.

Mark, K. S. & Miller, D. W. 1999. Increased permeability of primary cultured brain microvessel endothelial cell monolayers following TNF-alpha exposure. Life Sciences, 64(21): pp.1941-1953.

Mason, J. L., Suzuki, K., Chaplin, D. D. & Matsushima, G. K. 2001. Interleukin-1 beta promotes repair of the CNS. Journal of Neuroscience, 21(18): pp.7046-7052.

Masuda, T., Sankowski, R., Staszewski, O., Boettcher, C., Amann, L., Scheiwe, C., Nessler, S., Kunz, P., Van Loo, G., Coenen, V. A., Reinacher, P. C., Michel, A., Sure, U., Gold, R., Priller, J., Stadelmann, C. & Prinz, M. 2019. Spatial and temporal heterogeneity of mouse and human microglia at single-cell resolution. Nature, 566(7744): pp.388-392.

Matt, S. M. & Johnson, R. W. 2016. Neuro-immune dysfunction during brain aging: new insights in microglial cell regulation. Current Opinion in Pharmacology, 2696-101.

Mccoll, B. W., Carswell, H. V., Mcculloch, J. & Horsburgh, K. 2004. Extension of cerebral hypoperfusion and ischaemic pathology beyond MCA territory after intraluminal filament occlusion.in C57B1/6J mice. Brain Research, 997(1): pp.15-23.

Mcqueen, J., Reimer, M. M., Holland, P. R., Manso, Y., Mclaughlin, M., Fowler, J. H. & Horsburgh, K. 2014. Restoration of Oligodendrocyte Pools in a Mouse Model of Chronic Cerebral Hypoperfusion. Plos One, 9(2): pp.

Mekada, K., Abe, K., Murakami, A., Nakamura, S., Nakata, H., Moriwaki, K., Obata, Y. & Yoshiki, A. 2009. Genetic Differences among C57BL/6 Substrains. Experimental Animals, 58(2): pp.141-149.

Melchior, B., Garcia, A. E., Hsiung, B.-K., Lo, K. M., Doose, J. M., Thrash, J. C., Stalder, A. K., Staufenbiel, M., Neumann, H. & Carson, M. J. 2010. Dual induction of TREM2 and tolerance-related transcript, Tmem176b, in amyloid transgenic mice: implications for vaccine-based therapies for Alzheimer's disease. Asn Neuro, 2(3): pp.157-170.

Melchior, B., Puntambekar, S. S. & Carson, M. J. 2006. Microglia and the control of autoreactive T cell responses. Neurochemistry International, 49(2): pp.145-153.

Miki, K., Ishibashi, S., Sun, L. Y., Xu, H. Y., Ohashi, W., Kuroiwa, T. & Mizusawa, H. 2009. Intensity of Chronic Cerebral Hypoperfusion Determines White/Gray Matter Injury and Cognitive/Motor Dysfunction in Mice. Journal of Neuroscience Research, 87(5): pp.1270-1281.

Miron, V. E., Boyd, A., Zhao, J.-W., Yuen, T. J., Ruckh, J. M., Shadrach, J. L., Van Wijngaarden, P., Wagers, A. J., Williams, A., Franklin, R. J. M. & Ffrench-Constant, C. 2013. M2 microglia and macrophages drive oligodendrocyte differentiation during CNS remyelination. Nature Neuroscience, 16(9): pp.1211-U75.

Miyamoto, N., Maki, T., Pham, L.-D. D., Hayakawa, K., Seo, J. H., Mandeville, E. T., Mandeville, J. B., Kim, K.-W., Lo, E. H. & Arai, K. 2013. Oxidative Stress Interferes With White Matter Renewal After Prolonged Cerebral Hypoperfusion in Mice. Stroke, 44(12): pp.3516-3521.

Miyanohara, J., Kakae, M., Nagayasu, K., Nakagawa, T., Mori, Y., Arai, K., Shirakawa, H. & Kaneko, S. 2018. TRPM2 Channel Aggravates CNS Inflammation and Cognitive Impairment via Activation of Microglia in Chronic Cerebral Hypoperfusion. Journal of Neuroscience, 38(14): pp.3520-3533.

Moller, T., Bard, F., Bhattacharya, A., Biber, K., Campbell, B., Dale, E., Eder, C., Gan, L., Garden, G. A., Hughes, Z. A., Pearse, D. D., Staal, R. G. W., Sayed, F. A., Wes, P. D. & Boddeke, H. W. G. M. 2016. Critical Data-Based Re-Evaluation of Minocycline as a Putative Specific Microglia Inhibitor. Glia, 64(10): pp.1788-1794.

Montalbetti, L., Ratti, M. T., Greco, B., Aprile, C., Moglia, A. & Soragna, D. 2005. Neuropsychological tests and functional nuclear neuroimaging provide evidence of

subclinical impairment in Nasu-Hakola disease heterozygotes. Functional Neurology, 20(2): pp.71-75.

Morimoto, T., Enmi, J.-I., Hattori, Y., Iguchi, S., Saito, S., Harada, K. H., Okuda, H., Mineharu, Y., Takagi, Y., Youssefian, S., Iida, H., Miyamoto, S., Ihara, M., Kobayashi, H. & Koizumi, A. 2018. Dysregulation of RNF213 promotes cerebral hypoperfusion. Scientific Reports, 8.

Nakaji, K., Ihara, M., Takahashi, C., Itohara, S., Noda, M., Takahashi, R. & Tomimoto, H. 2006. Matrix metalloproteinase-2 plays a critical role in the pathogenesis of white matter lesions after chronic cerebral hypoperfusion in rodents. Stroke, 37(11): pp.2816-2823.

Naruse, M., Shibasaki, K., Shimauchi-Ohtaki, H. & Ishizaki, Y. 2018. Microglial Activation Induces Generation of Oligodendrocyte Progenitor Cells from the Subventricular Zone after Focal Demyelination in the Corpus Callosum. Developmental Neuroscience, 40(1): pp.54-63

Nasu, T., Tsukahara, Y. & Terayama, K. 1973. Lipid metabolic disease - membranous lipodystrophy - autopsy case demonstrating numerous peculiar membrane-structures composed of compound lipid in bone and bone-marrow and various adipose tissues. Acta Pathologica Japonica, 23(3): pp.539-558.

Nickel, A. G., Von Hardenberg, A., Hohl, M., Loeffler, J. R., Kohlhaas, M., Becker, J., Reil, J.-C., Kazakov, A., Bonnekoh, J., Stadelmaier, M., Puhl, S.-L., Wagner, M., Bogeski, I., Cortassa, S., Kappl, R., Pasieka, B., Lafontaine, M., Lancaster, C. R. D., Blacker, T. S., Hall, A. R., Duchen, M. R., Kaestner, L., Lipp, P., Zeller, T., Mueller, C., Knopp, A., Laufs, U., Boehm, M., Hoth, M. & Maack, C. 2015. Reversal of Mitochondrial Transhydrogenase Causes Oxidative Stress in Heart Failure. Cell Metabolism, 22(3): pp.472-484.

Nimmerjahn, A., Kirchhoff, F. & Helmchen, F. 2005. Resting microglial cells are highly dynamic surveillants of brain parenchyma in vivo. Science, 308(5726): pp.1314-1318.

Nishio, K., Ihara, M., Yamasaki, N., Kalaria, R. N., Maki, T., Fujita, Y., Ito, H., Oishi, N., Fukuyama, H., Miyakawa, T., Takahashi, R. & Tomimoto, H. 2010. A Mouse Model Characterizing Features of Vascular Dementia With Hippocampal Atrophy. Stroke, 41(6): pp.1278-1284.

Nitkunan, A., Barrick, T. R., Charlton, R. A., Clark, C. A. & Markus, H. S. 2008. Multimodal MRI in cerebral small vessel disease - Its relationship with cognition and sensitivity to change over time. Stroke, 39(7): pp.1999-2005.

Nitkunan, A., Lanfranconi, S., Charlton, R. A., Barrick, T. R. & Markus, H. S. 2011. Brain Atrophy and Cerebral Small Vessel Disease A Prospective Follow-Up Study. Stroke, 42(1): pp.133-138.

O'Brien, J.T. 2006. Vascular cognitive impairment. Am J Geriatr Psychiatry 14(9), 724-33.

O'sullivan, M., Lythgoe, D. J., Pereira, A. C., Summers, P. E., Jarosz, J. M., Williams, S. C. R. & Markus, H. S. 2002. Patterns of cerebral blood flow reduction in patients with ischemic leukoaraiosis. Neurology, 59(3): pp.321-326.

Ohtaki, H., Fujimoto, T., Sato, T., Kishimoto, K., Fujimoto, M., Moriya, M. & Shioda, S. 2006. Progressive expression of vascular endothelial growth factor (VEGF) and angiogenesis after chronic ischemic hypoperfusion in rat. Brain Edema Xiii, 96283-+.

Oide, T., Nakayama, H., Yanagawa, S., Ito, N., Ikeda, S. I. & Arima, K. 2008. Extensive loss of arterial medial smooth muscle cells and mural extracellular matrix in cerebral autosomal recessive arteriopathy with subcortical infarcts and leukoencephalopathy (CARASIL). Neuropathology, 28(2): pp.132-142.

Okamoto, K., Yamori, Y. & Nagaoka, A. 1974. Establishment of stroke-prone spontaneously hypertensive rat (SHR). Circulation Research, 34I143-I153.

Olson, J. K. & Miller, S. D. 2004. Microglia initiate central nervous system innate and adaptive immune responses through multiple TLRs. Journal of Immunology, 173(6): pp.3916-3924.

Otero, K., Shinohara, M., Zhao, H., Cella, M., Gilfillan, S., Colucci, A., Faccio, R., Ross, F. P., Teitelbaum, S. L., Takayanagi, H. & Colonna, M. 2012. TREM2 and beta-Catenin Regulate Bone Homeostasis by Controlling the Rate of Osteoclastogenesis. Journal of Immunology, 188(6): pp.2612-2621.

Otero, K., Turnbull, I. R., Poliani, P. L., Vermi, W., Cerutti, E., Aoshi, T., Tassi, I., Takai, T., Stanley, S. L., Miller, M., Shaw, A. S. & Colonna, M. 2009. Macrophage colony-stimulating factor induces the proliferation and survival of macrophages via a pathway involving DAP12 and beta-catenin. Nature Immunology, 10(7): pp.734-U90.

Otori, T., Katsumata, T., Muramatsu, H., Kashiwagi, F., Katayama, Y. & Terashi, A. 2003. Long-term measurement of cerebral blood flow and metabolism in a rat chronic hypoperfusion model. Clinical and Experimental Pharmacology and Physiology, 30(4): pp.266-272.

Owens, R., Grabert, K., Davies, C. L., Alfieri, A., Antel, J. P., Healy, L. M. & Mccoll, B. W. 2017. Divergent Neuroinflammatory Regulation of Microglial TREM Expression and Involvement of NF-kappa B. Frontiers in Cellular Neuroscience, 11.

Paloneva 2003. Mutations in two genes encoding different subunits of a receptor signaling complex result in an identical disease phenotype (vol 71, pg 656, 2002). American Journal of Human Genetics, 72(1): pp.225-225.

Pang, Y., Cai, Z. W. & Rhodes, P. G. 2003. Disturbance of oligodendrocyte development, hypomyelination and white matter injury in the neonatal rat brain after intracerebral injection of lipopolysaccharide. Developmental Brain Research, 140(2): pp.205-214.

Pang, Y., Fan, L.-W., Tien, L.-T., Dai, X., Zheng, B., Cai, Z., Lin, R. C. S. & Bhatt, A. 2013. Differential roles of astrocyte and microglia in supporting oligodendrocyte development and myelination in vitro. Brain and Behavior, 3(5): pp.503-514.

Paolicelli, R. C., Bolasco, G., Pagani, F., Maggi, L., Scianni, M., Panzanelli, P., Giustetto, M., Ferreira, T. A., Guiducci, E., Dumas, L., Ragozzino, D. & Gross, C. T. 2011. Synaptic Pruning by Microglia Is Necessary for Normal Brain Development. Science, 333(6048): pp.1456-1458.

Pappas, B. A., Delatorre, J. C., Davidson, C. M., Keyes, M. T. & Fortin, T. 1996. Chronic reduction of cerebral blood flow in the adult rat: Late-emerging CA1 cell loss and memory dysfunction. Brain Research, 708(1-2): pp.50-58.

Parkhurst, C. N., Yang, G., Ninan, I., Savas, J. N., Yates, J. R., Iii, Lafaille, J. J., Hempstead, B. L., Littman, D. R. & Gan, W.-B. 2013. Microglia Promote Learning-Dependent Synapse Formation through Brain-Derived Neurotrophic Factor. Cell, 155(7): pp.1596-1609.

Phongsisay, V., Iizasa, E. I., Hara, H. & Yoshida, H. 2015. Evidence for TLR4 and FcR gamma-CARD9 activation by cholera toxin B subunit and its direct bindings to TREM2 and LMIR5 receptors. Molecular Immunology, 66(2): pp.463-471.

Phongsisay, V., Ilizasa, E. I., Hara, H. & Yoshida, H. 2017. Pertussis toxin targets the innate immunity through DAP12, FcR gamma, and MyD88 adaptor proteins. Immunobiology, 222(4): pp.664-671.

Piccio, L., Buonsanti, C., Mariani, M., Cella, M., Gilfillan, S., Cross, A. H., Colonna, M. & Panina-Bordignon, P. 2007. Blockade of TREM-2 exacerbates experimental autoimmune encephalomyelitis. European Journal of Immunology, 37(5): pp.1290-1301.

Polfliet, M. M. J., Zwijnenburg, P. J. G., Van Furth, A. M., Van Der Poll, T., Dopp, E. A., De Lavalette, C. R., Van Kesteren-Hendrikx, E. M. L., Van Rooijen, N., Dijkstra, C. D. & Van Den Berg, T. K. 2001. Meningeal and perivascular macrophages of the central nervous system play a protective role during bacterial meningitis. Journal of Immunology, 167(8): pp.4644-4650.

Poliani, P. L., Wang, Y., Fontana, E., Robinette, M. L., Yamanish, Y., Gilfillan, S. & Colonna, M. 2015. TREM2 sustains microglial expansion during aging and response to demyelination. Journal of Clinical Investigation, 125(5): pp.2161-2170.

Prada, I., Ongania, G. N., Buonsanti, C., Panina-Bordignon, P. & Meldolesi, J. 2006. Triggering receptor expressed in myeloid cells 2 (TREM2) trafficking in microglial cells: Continuous shuttling to and from the plasma membrane regulated by cell stimulation. Neuroscience, 140(4): pp.1139-1148.

Primiani, C. T., Ryan, V. H., Rao, J. S., Cam, M. C., Ahn, K., Modi, H. R. & Rapoport, S. I. 2014. Coordinated Gene Expression of Neuroinflammatory and Cell Signaling Markers in Dorsolateral Prefrontal Cortex during Human Brain Development and Aging. Plos One, 9(10): pp.

Prins, N. D., Van Dijk, E. J., Den Heijer, T., Vermeer, S. E., Jolles, J., Koudstaal, P. J., Hofman, A. & Breteler, M. M. B. 2005. Cerebral small-vessel disease and decline in

information processing speed, executive function and memory. Brain, 1282034-2041.

Probert, L., Akassoglou, K., Pasparakis, M., Kontogeorgos, G. & Kollias, G. 1995. spontaneous inflammatory demyelinating disease in transgenic mice showing central nervous system-specific expression of tumor-necrosis-factor-alpha. Proceedings of the National Academy of Sciences of the United States of America, 92(24): pp.11294-11298.

Proebstl, D., Voisin, M. B., Woodfin, A., Whiteford, J., D'acquisto, F., Jones, G. E., Rowe, D. & Nourshargh, S. 2012. Pericytes support neutrophil subendothelial cell crawling and breaching of venular walls in vivo. Journal of Experimental Medicine, 209(6): pp.1219-1234.

Promjunyakul, N., Lahna, D., Kaye, J. A., Dodge, H. H., Erten-Lyons, D., Rooney, W. D. & Silbert, L. C. 2015. Characterizing the white matter hyperintensity penumbra with cerebral blood flow measures. Neuroimage-Clinical, 8224-229.

Rabin, J. S., Schultz, A. P., Hedden, T., Viswanathan, A., Marshall, G. A., Kilpatrick, E., Klein, H., Buckley, R. F., Yang, H. S., Properzi, M., Rao, V., Kirn, D. R., Papp, K. V., Rentz, D. M., Johnson, K. A., Sperling, R. A. & Chhatwal, J. P. 2018. Interactive Associations of Vascular Risk and beta-Amyloid Burden With Cognitive Decline in Clinically Normal Elderly Individuals Findings From the Harvard Aging Brain Study. Jama Neurology, 75(9): pp.1124-1131.

Rabin, J. S., Yang, H. S., Schultz, A. P., Hanseeuw, B. J., Hedden, T., Viswanathan, A., Gatchel, J. R., Marshall, G. A., Kilpatrick, E., Klein, H., Rao, V., Buckley, R. F., Yau, W. Y. W., Kirn, D. R., Rentz, D. M., Johnson, K. A., Sperling, R. A. & Chhatwal, J. P. 2019. Vascular Risk and beta-Amyloid Are Synergistically Associated with Cortical Tau. Annals of Neurology, 85(2): pp.272-279.

Raha, A. A., Henderson, J. W., Stott, S. R. W., Vuono, R., Foscarin, S., Friedland, R. P., Zaman, S. H. & Raha-Chowdhury, R. 2017. Neuroprotective Effect of TREM-2 in Aging and Alzheimer's Disease Model. Journal of Alzheimers Disease, 55(1): pp.199-217.

Raj, D., Yin, Z., Breur, M., Doorduin, J., Holtman, I. R., Olah, M., Mantingh-Otter, I. J., Van Dam, D., De Deyn, P. P., Den Dunnen, W., Eggen, B. J. L., Amor, S. & Boddeke, E. 2017. Increased White Matter Inflammation in Aging- and Alzheimer's Disease Brain. Frontiers in Molecular Neuroscience, 10.

Rajagopalan, P., Hibar, D. P. & Thompson, P. M. 2013. TREM2 and Neurodegenerative Disease. New England Journal of Medicine, 369(16): pp.1565-1567.

Rajani, R. M., Quick, S., Ruigrok, S. R., Graham, D., Harris, S. E., Verhaaren, B. F. J., Fornage, M., Seshadri, S., Atanur, S. S., Dominiczak, A. F., Smith, C., Wardlaw, J. M. & Williams, A. 2018. Reversal of endothelial dysfunction reduces white matter

vulnerability in cerebral small vessel disease in rats. Science Translational Medicine, 10(448): pp.

Ransohoff, R. M. 2016. A polarizing question: do M1 and M2 microglia exist? Nature Neuroscience, 19(8): pp.987-991.

Ransohoff, R. M. & Perry, V. H. 2009. Microglial Physiology: Unique Stimuli, Specialized Responses. Annual Review of Immunology, 27119-145.

Rayaprolu, S., Mullen, B., Baker, M., Lynch, T., Finger, E., Seeley, W. W., Hatanpaa, K. J., Lomen-Hoerth, C., Kertesz, A., Bigio, E. H., Lippa, C., Josephs, K. A., Knopman, D. S., White, C. L., Iii, Caselli, R., Mackenzie, I. R., Miller, B. L., Boczarska-Jedynak, M., Opala, G., Krygowska-Wajs, A., Barcikowska, M., Younkin, S. G., Petersen, R. C., Ertekin-Taner, N., Uitti, R. J., Meschia, J. F., Boylan, K. B., Boeve, B. F., Graff-Radford, N. R., Wszolek, Z. K., Dickson, D. W., Rademakers, R. & Ross, O. A. 2013. TREM2 in neurodegeneration: evidence for association of the p.R47H variant with frontotemporal dementia and Parkinson's disease. Molecular Neurodegeneration, 8.

Reimer, M. M., Mcqueen, J., Searcy, L., Scullion, G., Zonta, B., Desmazieres, A., Holland, P. R., Smith, J., Gliddon, C., Wood, E. R., Herzyk, P., Brophy, P. J., Mcculloch, J. & Horsburgh, K. 2011. Rapid Disruption of Axon-Glial Integrity in Response to Mild Cerebral Hypoperfusion. Journal of Neuroscience, 31(49): pp.18185-18194.

Ren, M., Guo, Y., Wei, X., Yan, S., Qin, Y., Zhang, X., Jiang, F. & Lou, H. 2018. TREM2 overexpression attenuates neuroinflammation and protects dopaminergic neurons in experimental models of Parkinson's disease. Experimental Neurology, 302205-213.

Rice, R. A., Pham, J., Lee, R. J., Najafi, A. R., West, B. L. & Green, K. N. 2017. Microglial repopulation resolves inflammation and promotes brain recovery after injury. Glia, 65(6): pp.931-944.

Riekse, R. G., Leverenz, J. B., Mccormick, W., Bowen, J. D., Teri, L., Nochlin, D., Simpson, K., Eugenio, C., Larson, E. B. & Tsuang, D. 2004. Effect of vascular lesions on cognition in Alzheimer's disease: A community-based study. Journal of the American Geriatrics Society, 52(9): pp.1442-1448.

Ronchi, J. A., Figueira, T. R., Ravagnani, F. G., Oliveira, H. C. F., Vercesi, A. E. & Castilho, R. F. 2013. A spontaneous mutation in the nicotinamide nucleotide transhydrogenase gene of C57BL/6J mice results in mitochondrial redox abnormalities. Free Radical Biology and Medicine, 63446-456.

Rosenberg, G. A., Sullivan, N. & Esiri, M. M. 2001. White matter damage is associated with matrix metalloproteinases in vascular dementia. Stroke, 32(5): pp.1162-1167.

Rosenthal, S. L., Bamne, M. N., Wang, X., Berman, S., Snitz, B. E., Klunk, W. E., Sweet, R. A., Demirci, F. Y., Lopez, O. L. & Kamboh, M. I. 2015. More evidence for association of a rare TREM2 mutation (R47H) with Alzheimer's disease risk. Neurobiology of Aging, 36(8): pp.

Ruitenberg, A., Den Heijer, T., Bakker, S. L. M., Van Swieten, J. C., Koudstaal, P. J., Hoftnan, A. & Breteler, M. M. B. 2005. Cerebral hypoperfusion and clinical onset of dementia: The Rotterdam study. Annals of Neurology, 57(6): pp.789-794.

Ruiz, A., Dols-Icardo, O., Bullido, M. J., Pastor, P., Rodriguez-Rodriguez, E., Lopez De Munain, A., De Pancorbo, M. M., Perez-Tur, J., Alvarez, V., Antonell, A., Lopez-Arrieta, J., Hernandez, I., Tarraga, L., Boada, M., Lleo, A., Blesa, R., Frank-Garcia, A., Sastre, I., Razquin, C., Ortega-Cubero, S., Lorenzo, E., Sanchez-Juan, P., Combarros, O., Moreno, F., Gorostidi, A., Elcoroaristizabal, X., Baquero, M., Coto, E., Sanchez-Valle, R., Clarimon, J. & Dementia Genetic Spanish, C. 2014. Assessing the role of the TREM2 p.R47H variant as a risk factor for Alzheimer's disease and frontotemporal dementia. Neurobiology of Aging, 35(2): pp.

Saber, M., Kokiko-Cochran, O., Puntambekar, S. S., Lathia, J. D. & Lamb, B. T. 2017. Triggering Receptor Expressed on Myeloid Cells 2 Deficiency Alters Acute Macrophage Distribution and Improves Recovery after Traumatic Brain Injury. Journal of Neurotrauma, 34(2): pp.423-+.

Safaiyan, S., Kannaiyan, N., Snaidero, N., Brioschi, S., Biber, K., Yona, S., Edinger, A. L., Jung, S., Rossner, M. J. & Simons, M. 2016. Age-related myelin degradation burdens the clearance function of microglia during aging. Nature Neuroscience, 19(8): pp.995-+.

Saggu, R., Schumacher, T., Gerich, F., Rakers, C., Tai, K., Delekate, A. & Petzold, G. C. 2016. Astroglial NF-kB contributes to white matter damage and cognitive impairment in a mouse model of vascular dementia. Acta Neuropathologica Communications, 4.

Sam, K., Conklin, J., Holmes, K. R., Sobczyk, O., Poublanc, J., Crawley, A. P., Mandell, D. M., Venkatraghavan, L., Duffin, J., Fisher, J. A., Black, S. E. & Mikulis, D. J. 2016. Impaired dynamic cerebrovascular response to hypercapnia predicts development of white matter hyperintensities. Neuroimage-Clinical, 11796-801.

Sayed, F. A., Telpoukhovskaia, M., Kodama, L., Li, Y., Zhou, Y., Le, D., Hauduc, A., Ludwig, C., Gao, F., Clelland, C., Zhan, L., Cooper, Y. A., Davalos, D., Akassoglou, K., Coppola, G. & Gan, L. 2018. Differential effects of partial and complete loss of TREM2 on microglial injury response and tauopathy. Proceedings of the National Academy of Sciences of the United States of America, 115(40): pp.10172-10177.

Schafer, D. P., Lehrman, E. K., Kautzman, A. G., Koyama, R., Mardinly, A. R., Yamasaki, R., Ransohoff, R. M., Greenberg, M. E., Barres, B. A. & Stevens, B. 2012. Microglia Sculpt Postnatal Neural Circuits in an Activity and Complement-Dependent Manner. Neuron, 74(4): pp.691-705.

Schmid, C. D., Sautkulis, L. N., Danielson, P. E., Cooper, J., Hasel, K. W., Hilbush, B. S., Sutcliffe, J. G. & Carson, M. J. 2002. Heterogeneous expression of the triggering receptor expressed on myeloid cells-2 on adult murine microglia. Journal of Neurochemistry, 83(6): pp.1309-1320.

Schuberth, M., Levin, J., Sawalhe, D., Schwarzkopf, R., Von Baumgarten, L., Ertl-Wagner, B., Rominger, A., Arzberger, T., Kretzschmar, H. A., Frobose, T., Diehl-Schmid, J., Biskup, S. & Danek, A. 2014. Hereditary diffuse leukencephalopathy with spheroids. A microgliopathy due to CSF1 receptor impairment. Nervenarzt, 85(4): pp.465-470.

Schuff, N., Matsumoto, S., Kmiecik, J., Studholme, C., Du, A. T., Ezekiel, F., Miller, B. L., Kramer, J. H., Jagust, W. J., Chui, H. C. & Weiner, M. W. 2009. Cerebral blood flow in ischemic vascular dementia and Alzheimer's disease, measured by arterial spin-labeling magnetic resonance imaging. Alzheimers & Dementia, 5(6): pp.454-462.

Seno, H., Miyoshi, H., Brown, S. L., Geske, M. J., Colonna, M. & Stappenbeck, T. S. 2009. Efficient colonic mucosal wound repair requires Trem2 signaling. Proceedings of the National Academy of Sciences of the United States of America, 106(1): pp.256-261.

Sharif, O., Gawish, R., Warszawska, J. M., Martins, R., Lakovits, K., Hladik, A., Doninger, B., Brunner, J., Korosec, A., Schwarzenbacher, R. E., Berg, T., Kralovics, R., Colinge, J., Mesteri, I., Gilfillan, S., Salmaggi, A., Verschoor, A., Colonna, M. & Knapp, S. 2014. The Triggering Receptor Expressed on Myeloid Cells 2 Inhibits Complement Component 1q Effector Mechanisms and Exerts Detrimental Effects during Pneumococcal Pneumonia. Plos Pathogens, 10(6): pp.

Sherwin, C. & Fern, R. 2005. Acute lipopolysaccharide-mediated injury in neonatal white matter glia: Role of TNF-alpha IL-1,beta and calcium. Journal of Immunology, 175(1): pp.155-161.

Shi, Y. L., Thrippleton, M. J., Makin, S. D., Marshall, I., Geerlings, M. I., De Craen, A. J. M., Van Buchem, M. A. & Wardlaw, J. M. 2016. Cerebral blood flow in small vessel disease: A systematic review and meta-analysis. Journal of Cerebral Blood Flow and Metabolism, 36(10): pp.1653-1667.

Shibata, M., Ohtani, R., Ihara, M. & Tomimoto, H. 2004. White matter lesions and glial activation in a novel mouse model of chronic cerebral hypoperfusion. Stroke, 35(11): pp.2598-2603.

Shibata, M., Yamasaki, N., Miyakawa, T., Kalaria, R. N., Fujita, Y., Ohtani, R., Ihara, M., Takahashi, R. & Tomimoto, H. 2007. Selective impairment of working memory in a mouse model of chronic cerebral hypoperfusion. Stroke, 38(10): pp.2826-2832.

Sieber, M. W., Jaenisch, N., Brehm, M., Guenther, M., Linnartz-Gerlach, B., Neumann, H., Witte, O. W. & Frahm, C. 2013. Attenuated Inflammatory Response in Triggering Receptor Expressed on Myeloid Cells 2 (TREM2) Knock-Out Mice following Stroke. Plos One, 8(1): pp.

Sierra, A., Encinas, J. M., Deudero, J. J. P., Chancey, J. H., Enikolopov, G., Overstreet-Wadiche, L. S., Tsirka, S. E. & Maletic-Savatic, M. 2010. Microglia Shape Adult Hippocampal Neurogenesis through Apoptosis-Coupled Phagocytosis. Cell Stem Cell, 7(4): pp.483-495.

Sigfridsson, E., Marangoni, M., Johnson, J. A., Hardingham, G. E., Fowler, J. H. & Horsburgh, K. 2018. Astrocyte-specific overexpression of Nrf2 protects against optic tract damage and behavioural alterations in a mouse model of cerebral hypoperfusion. Scientific Reports, 8.

Simon, M. M., Greenaway, S., White, J. K., Fuchs, H., Gailus-Durner, V., Wells, S., Sorg, T., Wong, K., Bedu, E., Cartwright, E. J., Dacquin, R., Djebali, S., Estabel, J., Graw, J., Ingham, N. J., Jackson, I. J., Lengeling, A., Mandillo, S., Marvel, J., Meziane, H., Preitner, F., Puk, O., Roux, M., Adams, D. J., Atkins, S., Ayadi, A., Becker, L., Blake, A., Brooker, D., Cater, H., Champy, M.-F., Combe, R., Danecek, P., Di Fenza, A., Gates, H., Gerdin, A.-K., Golini, E., Hancock, J. M., Hans, W., Hoelter, S. M., Hough, T., Jurdic, P., Keane, T. M., Morgan, H., Mueller, W., Neff, F., Nicholson, G., Pasche, B., Roberson, L.-A., Rozman, J., Sanderson, M., Santos, L., Selloum, M., Shannon, C., Southwell, A., Tocchini-Valentini, G. P., Vancollie, V. E., Westerberg, H., Wurst, W., Zi, M., Yalcin, B., Ramirez-Solis, R., Steel, K. P., Mallon, A.-M., De Angelis, M. H., Herault, Y. & Brown, S. D. M. 2013. A comparative phenotypic and genomic analysis of C57BL/6J and C57BL/6N mouse strains. Genome Biology, 14(7): pp.

Simpson, J. E., Fernando, M. S., Clark, L., Ince, P. G., Matthews, F., Forster, G., O'brien, J. T., Barber, R., Kalaria, R. N., Brayne, C., Shaw, P. J., Lewis, C. E., Wharton, S. B. & Grp, M. C. S. 2007. White matter lesions in an unselected cohort of the elderly: astrocytic, microglial and oligodendrocyte precursor cell responses. Neuropathology and Applied Neurobiology, 33(4): pp.410-419.

Slattery, C. F., Beck, J. A., Harper, L., Adamson, G., Abdi, Z., Uphill, J., Campbell, T., Druyeh, R., Mahoney, C. J., Rohrer, J. D., Kenny, J., Lowe, J., Leung, K. K., Barnes, J., Clegg, S. L., Blair, M., Nicholas, J. M., Guerreiro, R. J., Rowe, J. B., Ponto, C., Zerr, I., Kretzschmar, H., Gambetti, P., Crutch, S. J., Warren, J. D., Rossor, M. N., Fox, N. C., Collinge, J., Schott, J. M. & Mead, S. 2014. R47H TREM2 variant increases risk of typical early-onset Alzheimer's disease but not of prion or frontotemporal dementia. Alzheimers & Dementia, 10(6): pp.602-608.

Snowdon, D. A., Greiner, L. H., Mortimer, J. A., Riley, K. P., Greiner, P. A. & Markesbery, W. R. 1997. Brain infarction and the clinical expression of Alzheimer disease - The nun study. Jama-Journal of the American Medical Association, 277(10): pp.813-817.

Sondergaard, C. B., Nielsen, J. E., Hansen, C. K. & Christensen, H. 2017. Hereditary cerebral small vessel disease and stroke. Clinical Neurology and Neurosurgery, 15545-57.

Sopala, M. & Danysz, W. 2001. Chronic cerebral hypoperfusion in the rat enhances age-related deficits in spatial memory. Journal of Neural Transmission, 108(12): pp.1445-1456.

Soragna, D., Papi, L., Ratti, M. T., Sestini, R., Tupler, R. & Montalbetti, L. 2003. An Italian family affected by Nasu-Hakola disease with a novel genetic mutation in the TREM2 gene(vol 74, pg 825, 2003). Journal of Neurology Neurosurgery and Psychiatry, 74(8): pp.1165-1165.

Spangenberg, E. E., Lee, R. J., Najafi, A. R., Rice, R. A., Elmore, M. R. P., Blurton-Jones, M., West, B. L. & Green, K. N. 2016. Eliminating microglia in Alzheimer's mice prevents neuronal loss without modulating amyloid-beta pathology. Brain, 1391265-1281.

Stevens, B. 2008. The classical complement cascade mediates CNS synapse elimination. Journal of Neurochemistry, 104143-143.

Sudduth, T. L., Powell, D. K., Smith, C. D., Greenstein, A. & Wilcock, D. M. 2013. Induction of hyperhomocysteinemia models vascular dementia by induction of cerebral microhemorrhages and neuroinflammation. Journal of Cerebral Blood Flow and Metabolism, 33(5): pp.708-715.

Szalay, G., Martinecz, B., Lenart, N., Kornyei, Z., Orsolits, B., Judak, L., Csaszar, E., Fekete, R., West, B. L., Katona, G., Rozsa, B. & Denes, A. 2016. Microglia protect against brain injury and their selective elimination dysregulates neuronal network activity after stroke. Nature Communications, 7.

Takahashi, K., Prinz, M., Stagi, M., Chechneva, O. & Neumann, H. 2007. TREM2-transduced myeloid precursors mediate nervous tissue debris clearance and facilitate recovery in an animal model of multiple sclerosis. Plos Medicine, 4(4): pp.675-689.

Takahashi, K., Rochford, C. D. P. & Neumann, H. 2005. Clearance of apoptotic neurons without inflammation by microglial triggering receptor expressed on myeloid cells-2. Journal of Experimental Medicine, 201(4): pp.647-657.

Ter Telgte, A., Wiegertjes, K., Tuladhar, A. M., Noz, M. P., Marques, J. P., Gesierich, B., Huebner, M., Mutsaerts, H., Elias-Smale, S. E., Beelen, M. J., Ropele, S., Kessels, R. P. C., Riksen, N. P., Klijn, C. J. M., Norris, D. G., Duering, M. & De Leeuw, F. E. 2018. Investigating the origin and evolution of cerebral small vessel disease: The RUN DMC - InTENse study. European Stroke Journal, 3(4): pp.369-378.

Thorburne, S. K. & Juurlink, B. H. J. 1996. Low glutathione and high iron govern the susceptibility of oligodendroglial precursors to oxidative stress. Journal of Neurochemistry, 67(3): pp.1014-1022.

Thurgur, H. & Pinteaux, E. 2019. Microglia in the Neurovascular Unit: Blood-Brain Barrier-microglia Interactions After Central Nervous System Disorders. Neuroscience, 40555-67.

Toledo, J. B., Arnold, S. E., Raible, K., Brettschneider, J., Xie, S. X., Grossman, M., Monsell, S. E., Kukull, W. A. & Trojanowski, J. Q. 2013. Contribution of cerebrovascular

disease in autopsy confirmed neurodegenerative disease cases in the National Alzheimer's Coordinating Centre. Brain, 1362697-2706.

Tomimoto, H., Ihara, M., Wakita, H., Ohtani, R., Lin, J. X., Akiguchi, I., Kinoshita, M. & Shibasaki, H. 2003. Chronic cerebral hypoperfusion induces white matter lesions and loss of oligodendroglia with DNA fragmentation in the rat. Acta Neuropathologica, 106(6): pp.527-534.

Topakian, R., Barrick, T. R., Howe, F. A. & Markus, H. S. 2010. Blood-brain barrier permeability is increased in normal-appearing white matter in patients with lacunar stroke and leucoaraiosis. Journal of Neurology Neurosurgery and Psychiatry, 81(2): pp.192-197.

Tremblay, M.-E., Lowery, R. L. & Majewska, A. K. 2010. Microglial Interactions with Synapses Are Modulated by Visual Experience. Plos Biology, 8(11): pp.

Tsai, T.-H., Sun, C.-K., Su, C.-H., Sung, P.-H., Chua, S., Zhen, Y.-Y., Leu, S., Chang, H.-W., Yang, J.-L. & Yip, H.-K. 2015. Sitagliptin attenuated brain damage and cognitive impairment in mice with chronic cerebral hypo-perfusion through suppressing oxidative stress and inflammatory reaction. Journal of Hypertension, 33(5): pp.1001-1013.

Turnbull, I. R., Gilfillan, S., Cella, M., Aoshi, T., Miller, M., Piccio, L., Hernandez, M. & Colonna, M. 2006. Cutting edge: TREM-2 attenuates macrophage activation. Journal of Immunology, 177(6): pp.3520-3524.

Ueki, Y., Kohara, N., Oga, T., Fukuyama, H., Akiguchi, I., Kimura, J. & Shibasaki, H. 2000. Membranous lipodystrophy presenting with palilalia: a PET study of cerebral glucose metabolism. Acta Neurologica Scandinavica, 102(1): pp.60-64.

Ueno, Y., Zhang, N., Miyamoto, N., Tanaka, R., Hattori, N. & Urabe, T. 2009. Edaravone attenuates white matter lesions through endothelial protection in a rat chronic hypoperfusion model. Neuroscience, 162(2): pp.317-327.

Ulland, T. K., Song, W. M., Huang, S. C.-C., Ulrich, J. D., Sergushichev, A., Beatty, W. L., Loboda, A. A., Zhou, Y., Caims, N. J., Kambal, A., Loginicheva, E., Gilfillan, S., Cella, M., Virgin, H. W., Unanue, E. R., Wang, Y., Artyomov, M. N., Holtzman, D. M. & Colonna, M. 2017. TREM2 Maintains Microglial Metabolic Fitness in Alzheimer's Disease. Cell, 170(4): pp.649-+.

Ulrich, J. D., Finn, M. B., Wang, Y., Shen, A., Mahan, T. E., Jiang, H., Stewart, F. R., Piccio, L., Colonna, M. & Holtzman, D. M. 2014. Altered microglial response to A beta plaques in APPPS1-21 mice heterozygous for TREM2. Molecular Neurodegeneration, 9.

Van Beek, A., Claassen, J., Rikkert, M. & Jansen, R. 2008. Cerebral autoregulation: an overview of current concepts and methodology with special focus on the elderly. Journal of Cerebral Blood Flow and Metabolism, 28(6): pp.1071-1085.

Van Dalen, J. W., Mutsaerts, H., Nederveen, A. J., Vrenken, H., Steenwijk, M. D., Caan, M. W. A., Majoie, C., Van Gool, W. A. & Richard, E. 2016. White Matter Hyperintensity Volume and Cerebral Perfusion in Older Individuals with Hypertension Using Arterial Spin-Labeling. American Journal of Neuroradiology, 37(10): pp.1824-1830.

Van Der Veen, P. H., Muller, M., Vincken, K. L., Hendrikse, J., Mali, W., Van Der Graaf, Y., Geerlings, M. I. & Grp, S. S. 2015. Longitudinal Relationship Between Cerebral Small-Vessel Disease and Cerebral Blood Flow The Second Manifestations of Arterial Disease-Magnetic Resonance Study. Stroke, 46(5): pp.1233-1238.

Vemuri, P., Lesnick, T. G., Przybelski, S. A., Knopman, D. S., Lowe, V. J., Graff-Radford, J., Roberts, R. O., Mielke, M. M., Machulda, M. M., Petersen, R. C. & Jack, C. R. 2017. Age, vascular health, and Alzheimer disease biomarkers in an elderly sample. Annals of Neurology, 82(5): pp.706-718.

Vermeer, S. E., Prins, N. D., Den Heijer, T., Hofman, A., Koudstaal, P. J. & Breteler, M. M. B. 2003. Silent brain infarcts and the risk of dementia and cognitive decline. New England Journal of Medicine, 348(13): pp.1215-1222.

Vinters, H. V. & Gilbert, J. J. 1983. Cerebral amyloid angiopathy - incidence and complications in the aging brain .2. the distribution of amyloid vascular changes. Stroke, 14(6): pp.924-934.

Voss, E. V., Skuljec, J., Gudi, V., Skripuletz, T., Pul, R., Trebst, C. & Stangel, M. 2012. Characterisation of microglia during de- and remyelination: Can they create a repair promoting environment? Neurobiology of Disease, 45(1): pp.519-528.

Wake, H., Moorhouse, A. J., Jinno, S., Kohsaka, S. & Nabekura, J. 2009. Resting Microglia Directly Monitor the Functional State of Synapses In Vivo and Determine the Fate of Ischemic Terminals. Journal of Neuroscience, 29(13): pp.3974-3980.

Wakita, H., Tomimoto, H., Akiguchi, I. & Kimura, J. 1995. Protective effect of cyclosporine-a on white-matter changes in the rat-brain after chronic cerebral hypoperfusion. Stroke, 26(8): pp.1415-1422.

Wakita, H., Tomimoto, H., Akiguchi, I., Matsuo, A., Lin, J. X., Ihara, M. & Mcgeer, P. L. 2002. Axonal damage and demyelination in the white matter after chronic cerebral hypoperfusion in the rat. Brain Research, 924(1): pp.63-70.

Wakselman, S., Bechade, C., Roumier, A., Bernard, D., Triller, A. & Bessis, A. 2008. Developmental neuronal death in hippocampus requires the microglial CD11b integrin and DAP12 immunoreceptor. Journal of Neuroscience, 28(32): pp.8138-8143.

Walker, E. J. & Rosenberg, G. A. 2010. Divergent Role for MMP-2 in Myelin Breakdown and Oligodendrocyte Death Following Transient Global Ischemia. Journal of Neuroscience Research, 88(4): pp.764-773.

Wang, X.-Q., Tao, B.-B., Li, B., Wang, X.-H., Zhang, W.-C., Wan, L., Hua, X.-M. & Li, S.-T. 2016a. Overexpression of TREM2 enhances glioma cell proliferation and invasion: a therapeutic target in human glioma. Oncotarget, 7(3): pp.2354-2366.

Wang, Y., Cella, M., Mallinson, K., Ulrich, J. D., Young, K. L., Robinette, M. L., Gilfillan, S., Krishnan, G. M., Sudhakar, S., Zinselmeyer, B. H., Holtzman, D. M., Cirrito, J. R. & Colonna, M. 2015. TREM2 Lipid Sensing Sustains the Microglial Response in an Alzheimer's Disease Model. Cell, 160(6): pp.1061-1071.

Wang, Y. & Colonna, M. 2014. Interkeukin-34, a cytokine crucial for the differentiation and maintenance of tissue resident macrophages and Langerhans cells. European Journal of Immunology, 44(6): pp.1575-1581.

Wang, Y., Ulland, T. K., Ulrich, J. D., Song, W., Tzaferis, J. A., Hole, J. T., Yuan, P., Mahan, T. E., Shi, Y., Gilfillan, S., Cella, M., Grutzendler, J., Demattos, R. B., Cirrito, J. R., Holtzman, D. M. & Colonna, M. 2016b. TREM2-mediated early microglial response limits diffusion and toxicity of amyloid plaques. Journal of Experimental Medicine, 213(5): pp.667-675.

Wardlaw, J. M., Makin, S. J., Hernandez, M. C. V., Armitage, P. A., Heye, A. K., Chappell, F. M., Munoz-Maniega, S., Sakka, E., Shuler, K., Dennis, M. S. & Thrippleton, M. J. 2017. Blood-brain barrier failure as a core mechanism in cerebral small vessel disease and dementia: evidence from a cohort study. Alzheimers & Dementia, 13(6): pp.634-643.

Wardlaw, J. M., Smith, C. & Dichgans, M. 2013. Mechanisms of sporadic cerebral small vessel disease: insights from neuroimaging. Lancet Neurology, 12(5): pp.483-497.

Washida, K., Ihara, M., Nishio, K., Fujita, Y., Maki, T., Yamada, M., Takahashi, J., Wu, X., Kihara, T., Ito, H., Tomimoto, H. & Takahashi, R. 2010. Nonhypotensive Dose of Telmisartan Attenuates Cognitive Impairment Partially Due to Peroxisome Proliferator-Activated Receptor-gamma Activation in Mice With Chronic Cerebral Hypoperfusion. Stroke, 41(8): pp.1798-1806.

Wegiel, J., Wisniewski, H. M., Dziewiatkowski, J., Tarnawski, M., Kozielski, R., Trenkner, E. & Wiktor-Jedrzejczak, W. 1998. Reduced number and altered morphology of microglial cells in colony stimulating factor-1-deficient osteopetrotic op/op mice. Brain Research, 804(1): pp.135-139.

Wilkins, A., Majed, H., Layfield, R., Compston, A. & Chandran, S. 2003. Oligodendrocytes promote neuronal survival and axonal length by distinct intracellular mechanisms: A novel role for oligodendrocyte-derived glial cell line-derived neurotrophic factor. Journal of Neuroscience, 23(12): pp.4967-4974.

Winkler, E. A., Sagare, A. P. & Zlokovic, B. V. 2014. The Pericyte: A Forgotten Cell Type with Important Implications for Alzheimer's Disease? Brain Pathology, 24(4): pp.371-386.

Wolf, G., Lotan, A., Lifschytz, T., Ben-Ari, H., Merzel, T. K., Tatarskyy, P., Valitzky, M., Mernick, B., Avidan, E., Koroukhov, N. & Lerer, B. 2017. Differentially Severe Cognitive Effects of Compromised Cerebral Blood Flow in Aged Mice: Association with Myelin Degradation and Microglia Activation. Frontiers in Aging Neuroscience, 9.

Wong, D., Prameya, R. & Dorovini-Zis, K. 2007. Adhesion and migration of polymorphonuclear leukocytes across human brain microvessel endothelial cells are differentially regulated by endothelial cell adhesion molecules and modulate monolayer permeability. Journal of Neuroimmunology, 184(1-2): pp.136-148.

Wu, B., Ma, Q., Khatibi, N., Chen, W., Sozen, T., Cheng, O. & Tang, J. 2010. Ac-YVAD-CMK Decreases Blood-Brain Barrier Degradation by Inhibiting Caspase-1 Activation of Interleukin-1 beta in Intracerebral Hemorrhage Mouse Model. Translational Stroke Research, 1(1): pp.57-64.

Wu, K., Byers, D. E., Jin, X., Agapov, E., Alexander-Brett, J., Patel, A. C., Cella, M., Gilfilan, S., Colonna, M., Kober, D. L., Brett, T. J. & Holtzman, M. J. 2015. TREM-2 promotes macrophage survival and lung disease after respiratory viral infection. Journal of Experimental Medicine, 212(5): pp.681-697.

Wu, R., Li, X., Xu, P., Huang, L., Cheng, J., Huang, X., Jiang, J., Wu, L.-J. & Tang, Y. 2017. TREM2 protects against cerebral ischemia/reperfusion injury. Molecular Brain, 10.

Wunderlich, P., Glebov, K., Kemmerling, N., Tien, N. T., Neumann, H. & Walter, J. 2013. Sequential Proteolytic Processing of the Triggering Receptor Expressed on Myeloid Cells-2 (TREM2) Protein by Ectodomain Shedding and gamma-Secretase-dependent Intramembranous Cleavage. Journal of Biological Chemistry, 288(46): pp.33027-33036.

Xie, D., Shen, F., He, S., Chen, M., Han, Q., Fang, M., Zeng, H., Chen, C. & Deng, Y. 2016. IL-1 beta Induces Hypomyelination in the Periventricular White Matter Through Inhibition of Oligodendrocyte Progenitor Cell Maturation via FYN/MEK/ERK Signaling Pathway in Septic Neonatal Rats. Glia, 64(4): pp.583-602.

Yamagata, K., Tagami, M., Takenaga, F., Yamori, Y. & Itoh, S. 2004. Hypoxia-induced changes in tight junction permeability of brain capillary endothelial cells are associated with IL-1beta and nitric oxide. Neurobiology of Disease, 17(3): pp.491-499.

Yamazaki, K., Yoshino, Y., Mori, Y., Ochi, S., Yoshida, T., Lshimaru, T. & Ueno, S.-I. 2015. A Case of Nasu-Hakola Disease without Fractures or Consanguinity Diagnosed Using Exome Sequencing and Treated with Sodium Valproate. Clinical Psychopharmacology and Neuroscience, 13(3): pp.324-326.

Yamori, Y., Horie, R., Sato, M. & Fukase, M. 1976. Hypertension as an important factor for cerebrovascular atherogenesis in rats. Stroke, 7(2): pp.120-125.

Yang, G. M., Kitagawa, K., Matsushita, K., Mabuchi, T., Yagita, Y., Yanagihara, T. & Matsumoto, M. 1997. C57BL/6 strain is most susceptible to cerebral ischemia following bilateral common carotid occlusion among seven mouse strains: Selective neuronal death in the murine transient forebrain ischemia. Brain Research, 752(1-2): pp.209-218.

Yata, K., Nishimura, Y., Unekawa, M., Tomita, Y., Suzuki, N., Tanaka, T., Mizoguchi, A. & Tomimoto, H. 2014. In Vivo Imaging of the Mouse Neurovascular Unit Under Chronic Cerebral Hypoperfusion. Stroke, 45(12): pp.3698-+.

Yeh, F. L., Wang, Y., Tom, I., Gonzalez, L. C. & Sheng, M. 2016. TREM2 Binds to Apolipoproteins, Including APOE and CLU/APOJ, and Thereby Facilitates Uptake of Amyloid-Beta by Microglia. Neuron, 91(2): pp.328-340.

Yew, B., Nation, D. A. & Alzheimer's Dis, N. 2017. Cerebrovascular resistance: effects on cognitive decline, cortical atrophy, and progression to dementia. Brain, 1401987-2001.

Yin, J., Liu, X., He, Q., Zhou, L., Yuan, Z. & Zhao, S. 2016. Vps35-dependent recycling of Trem2 regulates microglial function. Traffic, 17(12): pp.1286-1296.

Yokoo, N., Sheng, H. X., Mixco, J., Homi, H. M., Pearlstein, R. D. & Warner, D. S. 2004. Intraischemic nitrous oxide alters neither neurologic nor histologic outcome: A comparison with dizocilpine. Anesthesia and Analgesia, 99(3): pp.896-903.

Yuan, P., Condello, C., Keene, C. D., Wang, Y., Bird, T. D., Paul, S. M., Luo, W., Colonna, M., Baddeley, D. & Grutzendler, J. 2016. TREM2 Haplodeficiency in Mice and Humans Impairs the Microglia Barrier Function Leading to Decreased Amyloid Compaction and Severe Axonal Dystrophy. Neuron, 90(4): pp.724-739.

Zeestraten, E. A., Lawrence, A. J., Lambert, C., Benjamin, P., Brookes, R. L., Mackinnon, A. D., Morris, R. G., Barrick, T. R. & Markus, H. S. 2017. Change in multimodal MRI markers predicts dementia risk in cerebral small vessel disease. Neurology, 89(18): pp.1869-1876.

Zhan, Y., Paolicelli, R. C., Sforazzini, F., Weinhard, L., Bolasco, G., Pagani, F., Vyssotski, A. L., Bifone, A., Gozzi, A., Ragozzino, D. & Gross, C. T. 2014. Deficient neuron-microglia signaling results in impaired functional brain connectivity and social behavior. Nature Neuroscience, 17(3): pp.400-406.

Zhang, G., Zhao, Z., Gao, L., Deng, J., Wang, B., Xu, D., Liu, B., Qu, Y., Yu, J., Li, J. & Gao, G. 2011a. Gypenoside attenuates white matter lesions induced by chronic cerebral hypoperfusion in rats. Pharmacology Biochemistry and Behavior, 99(1): pp.42-51.

Zhang, S.-L., Chen, T.-S., Xiao, L., Ye, Y., Xia, W. & Zhang, H. 2016. TREM2 siRNA inhibits cell proliferation of human liver cancer cell lines. International Journal of Clinical and Experimental Pathology, 9(4): pp.4318-4328.

Zhang, X., Surguladze, N., Slagle-Webb, B. & Connor, J. R. 2006. Cellular iron status influences the functional relationship between microglia and Oligodendrocytes. Glia, 54(8): pp.795-804.

Zhang, Z., Zhang, Z., Lu, H., Yang, Q., Wu, H. & Wang, J. 2017. Microglial Polarization and Inflammatory Mediators After Intracerebral Hemorrhage. Molecular Neurobiology, 54(3): pp.1874-1886.

Zhang, Z., Zhang, Z. Y., Schittenhelm, J., Wu, Y., Meyermann, R. & Schluesener, H. J. 2011b. Parenchymal accumulation of CD163(+) macrophages/microglia in multiple sclerosis brains. Journal of Neuroimmunology, 237(1-2): pp.73-79.

Zhao, L., Mulligan, M. K. & Nowak, T. S., Jr. 2019. Substrain- and sex-dependent differences in stroke vulnerability in C57BL/6 mice. Journal of Cerebral Blood Flow and Metabolism, 39(3): pp.426-438.

Zheng, H., Jia, L., Liu, C.-C., Rong, Z., Zhong, L., Yang, L., Chen, X.-F., Fryer, J. D., Wang, X., Zhang, Y.-W., Xu, H. & Bu, G. 2017. TREM2 Promotes Microglial Survival by Activating Wnt/beta-Catenin Pathway. Journal of Neuroscience, 37(7): pp.1772-1784.

Zhong, L., Chen, X.-F., Wang, T., Wang, Z., Liao, C., Wang, Z., Huang, R., Wang, D., Li, X., Wu, L., Jia, L., Zheng, H., Painter, M., Atagi, Y., Liu, C.-C., Zhang, Y.-W., Fryer, J. D., Xu, H. & Bu, G. 2017. Soluble TREM2 induces inflammatory responses and enhances microglial survival. Journal of Experimental Medicine, 214(3): pp.597-607.

Zhong, L., Chen, X.-F., Zhang, Z.-L., Wang, Z., Shi, X.-Z., Xu, K., Zhang, Y.-W., Xu, H. & Bu, G. 2015. DAP12 Stabilizes the C-terminal Fragment of the Triggering Receptor Expressed on Myeloid Cells-2 (TREM2) and Protects against LPS-induced Pro-inflammatory Response. Journal of Biological Chemistry, 290(25): pp.15866-15877.

Zhu, M., Li, D., Wu, Y., Huang, X. & Wu, M. 2014. TREM-2 Promotes Macrophage-Mediated Eradication of Pseudomonas aeruginosa via a PI3K/Akt Pathway. Scandinavian Journal of Immunology, 79(3): pp.187-196.